INFORMATION TO USERS

This manuscript has been reproduced from the microfilm master. UMI films the text directly from the original or copy submitted. Thus, some thesis and dissertation copies are in typewriter face, while others may be from any type of computer printer.

The quality of this reproduction is dependent upon the quality of the copy submitted. Broken or indistinct print, colored or poor quality illustrations and photographs, print bleedthrough, substandard margins, and improper alignment can adversely affect reproduction.

In the unlikely event that the author did not send UMI a complete manuscript and there are missing pages, these will be noted. Also, if unauthorized copyright material had to be removed, a note will indicate the deletion.

Oversize materials (e.g., maps, drawings, charts) are reproduced by sectioning the original, beginning at the upper left-hand corner and continuing from left to right in equal sections with small overlaps.

Photographs included in the original manuscript have been reproduced xerographically in this copy. Higher quality 6" x 9" black and white photographic prints are available for any photographs or illustrations appearing in this copy for an additional charge. Contact UMI directly to order.

Bell & Howell Information and Learning
300 North Zeeb Road, Ann Arbor, MI 48106-1346 USA
800-521-0600

UMI®

Elimination of Zinc from Synaptic Vesicles in the Intact Mouse Brain by Targeted Disruption of *ZnT3*

Toby B. Cole

A dissertation submitted in partial fulfillment
of the requirements for the degree of

Doctor of Philosophy

University of Washington

2000

Program Authorized to Offer Degree: Department of Biochemistry

UMI Number: 9975970

UMI Microform9975970

Bell & Howell Information and Learning Company
300 North Zeeb Road
P.O. Box 1346
Ann Arbor, MI 48106-1346

In presenting this dissertation in partial fulfillment of the requirements for the Doctoral degree at the University of Washington, I agree that the Library shall make its copies freely available for inspection. I further agree that extensive copying of the dissertation is allowable only for scholarly purposes, consistent with "fair use" as prescribed in the U.S. Copyright Law. Requests for copying or reproduction of this dissertation may be referred to Bell and Howell Information and Learning, 300 North Zeeb Road, Ann Arbor, MI 48106-1346, to whom the author has granted "the right to reproduce and sell (a) copies of the manuscript in microform and/or (b) printed copies of the manuscript made from microform."

Signature 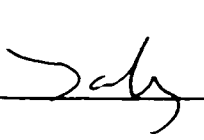

Date 5/30/00

University of Washington
Graduate School

This is to certify that I have examined this copy of a doctoral dissertation by

Toby B. Cole

And have found that it is complete and satisfactory in all respects, and that any and all revisions required by the final examining committee have been made.

Chair of Supervisory Committee:

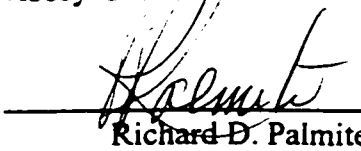

Richard D. Palmiter

Reading Committee:

Richard D. Palmiter

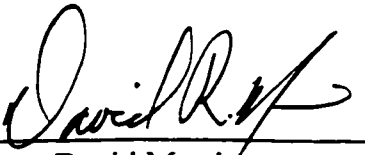

David Morris

Sandra Bajjalieh

Date: 5/30/00

University of Washington

Abstract

Elimination of Zinc from Synaptic Vesicles in the Intact Mouse Brain by Targeted Disruption of *ZnT3*

Toby B. Cole

Chairperson of the Supervisory Committee:
Professor Richard D. Palmiter
Department of Biochemistry

This dissertation demonstrates that zinc is taken up into synaptic vesicles by a mechanism that requires the zinc transporter, ZnT3, at the vesicle membrane and begins to address the physiological importance of synaptic vesicle zinc. *In situ* hybridization and immunohistochemistry showed that *ZnT3* expression is limited to zinc-containing neurons in the brain, and that ZnT3 protein resides on the membranes of zinc-rich synaptic vesicles in mouse, monkey, and human brain. A genetic approach was used to test whether ZnT3 was essential for vesicular zinc transport, by generating mice that were homozygous for a null mutation in the *ZnT3* gene. Histochemically-reactive zinc (i.e., zinc accessible to Timm and TSQ staining reagents) was undetectable in synaptic vesicles in the brains of these ZnT3-deficient mice, indicating that ZnT3 is required for vesicular zinc transport. Upon neuronal activation vesicular zinc is released into the synaptic cleft, where it has been proposed to modulate excitatory and inhibitory neurotransmitter receptors. In addition, synaptically-released zinc has been widely considered to be the source of the zinc that may kill neurons following seizures or ischemic insults. To assess the physiological importance of synaptic vesicle zinc, ZnT3-deficient mice were tested for deficits in sensorimotor functions, learning and memory, sensitivity to seizure-inducing drugs, and neuronal damage. Most of these functions were remarkably normal in the absence of vesicular zinc. ZnT3-deficient mice were more susceptible than wild-type mice to kainic acid-induced seizures, demonstrating that zinc has a net inhibitory effect on seizures. Despite the lack of histochemically reactive zinc in synaptic vesicles

in the ZnT3-deficient brain, zinc accumulated in the cytosol of postsynaptic neurons following seizures, and this zinc accumulation was associated with extensive neuronal death. Thus, the histochemically reactive zinc found in synaptic vesicles is not the major source of toxic zinc accumulation following seizures.

TABLE OF CONTENTS

LIST OF FIGURES

ACKNOWLEDGMENTS

I wish to thank Jürgen Wenzel for his contributions to this work. He was instrumental in demonstrating the presence of ZnT3 on vesicle membranes, and performed all of the ultrastructural analyses. His attention to detail produces the histology of an artisan. Philip Schwartzkroin and the members of his lab were extremely helpful with the aspects of this work pertaining to seizures and mossy fiber sprouting. Carol Robbins implanted the electrodes and directed me in their analysis. Valeri Lopantsev patiently taught me how to make recordings from hippocampal slices and took on the task of characterizing the electrophysiology of the *ZnT3-/-* hippocampus. Donald Born provided the epileptic human brain. Sidney Strickland and Keith Crutcher performed the zymography assays and NGF assays, respectively. The test of the zinc translocation hypothesis was part of a collaborative effort with Joo-Yong Lee and Jae-Young Koh at the University of Ulsan in Korea.

In the Palmiter lab, Carol Quaife assisted in determining the expression patterns of *ZnT3* and tested ZnT3 antiserum on tissues. Glenda Froelick frequently provided expertise in histology and cut many sections for me. Tim Dawe, Russell Cherne, and Grant Miura assisted with genotyping. Amy Martyanova performed the passive avoidance test and several of the sensorimotor tests on the mice. Past and present members of the Palmiter, McKnight, Kapur, and Perlmutter labs provided valuable input during lab meetings.

I would like to thank the members of my committee, Sandra Bajjalieh, Stephen Hauschka, David Morris, Richard Palmiter, David Gretch, and Leroy Hood.

I would especially like to thank Dr. Richard Palmiter for serving as my mentor. His enthusiasm for science, constant input of ideas, and ready availability for questions, whether practical or theoretical, made my doctoral research interesting and productive.

DEDICATION

Completion of this dissertation would not have been possible without the encouragement and constant support of my wife, Jean, whose patience, love, and cheerfulness were a constant source of inspiration to me. I dedicate this work to her and to Henry.

INTRODUCTION

I. Vesicular zinc

Zinc is an abundant element in the brain (150-200 μM in grey matter; Frederickson, 1989). In the mammalian brain, 10 to 20% of this zinc is sequestered in synaptic vesicles along with glutamate (Frederickson and Danscher, 1990). In contrast to metabolic zinc that is tightly bound to proteins, this vesicular zinc is free or relatively weakly bound, and is thus accessible to histochemical staining reagents like the Timm or selenium autometallographic stains (Danscher, 1982; Danscher et al., 1985), or to the zinc-selective fluorescent dyes TSQ (Frederickson et al., 1987) or TFL-Zn (Budde et al., 1997). These stains also detect histochemically reactive zinc in the pancreas (Maske 1957; Zalewski 1994), salivary gland (Frederickson et al., 1987), pituitary gland (Thorlacius-Ussing 1987), and testis (Vera-Gil, 1991).

Neurons that contain histochemically reactive zinc in synaptic vesicles have been termed "zinc-containing", and with the exception of some terminals in the spinal cord (Jo et al., 2000b), represent a subset of glutamatergic (i.e., excitatory) neurons (Frederickson, 1989). Zinc-containing neurons are found in the dorsal and ventral horns of the spinal cord and a number of brain regions, including the hippocampus, amygdala, entorhinal cortex, caudate putamen, neocortex, pyriform cortex, olfactory bulb, and cochlear nucleus (See Fig. 1) (Frederickson, 1989; Frederickson and Danscher, 1990; Jo et al., 2000a-c). Zinc staining is especially prominent in the hippocampal formation, where zinc-containing projections are found throughout the primary excitatory circuitry, including (*i*) perforant path projections from the entorhinal cortex to the outer molecular layer of the dentate gyrus, (*ii*) mossy fiber (MF) projections from granule cells in the dentate gyrus to hilar neurons and pyramidal cells in the CA3 region, (*iii*) Schaffer collateral projections from CA3 pyramidal neurons to pyramidal neurons in the CA1 region, and (*iv*) projections from CA1 to subiculum (Figs. 1, 2 A)(Slomianka, 1992; Frederickson, 1989).

Figure 1. Zinc-rich regions of the brain.

(A-D) Different regions of the mouse brain, stained with the Timm stain for vesicular zinc (black staining) and counterstained with cresyl violet (purple staining). (A) Sagittal section illustrating Timm stain in the hippocampus (HPC), neocortex (NCx), caudate putamen (CPu), stria terminalis (st), bed nucleus of the stria terminalis (BST), olfactory tubercle (OT), accessory olfactory bulb (AO), and olfactory bulb (OB). (B) Coronal section through the hippocampus. Staining is evident in projection fields throughout the primary excitatory circuitry, including the outer molecular layer (oml) of the dentate gyrus (DG), the hilus (hi), mossy fibers (mf) projecting to stratum (s.) lucidum and s. oriens of the CA3 subregion, and Schaffer collaterals projecting to s. oriens and s. radiatum of subregion CA1. This section was stained for a long time (90 min) in order to illustrate Timm stain in the oml. (C) Coronal section through the cochlear nucleus, illustrating Timm stain in the dorsal (DCN) but not ventral (VCN) nucleus. Cb = cerebellum. (D) Coronal section through the olfactory bulb. AOB, accessory olfactory bulb; Gl, glomerular layer; Pl, plexiform layer; Gr, granular layer. Arrows point to regions reactive with Timm stain. Scale bars: 1000 μm (A); 500 μm (B-D).

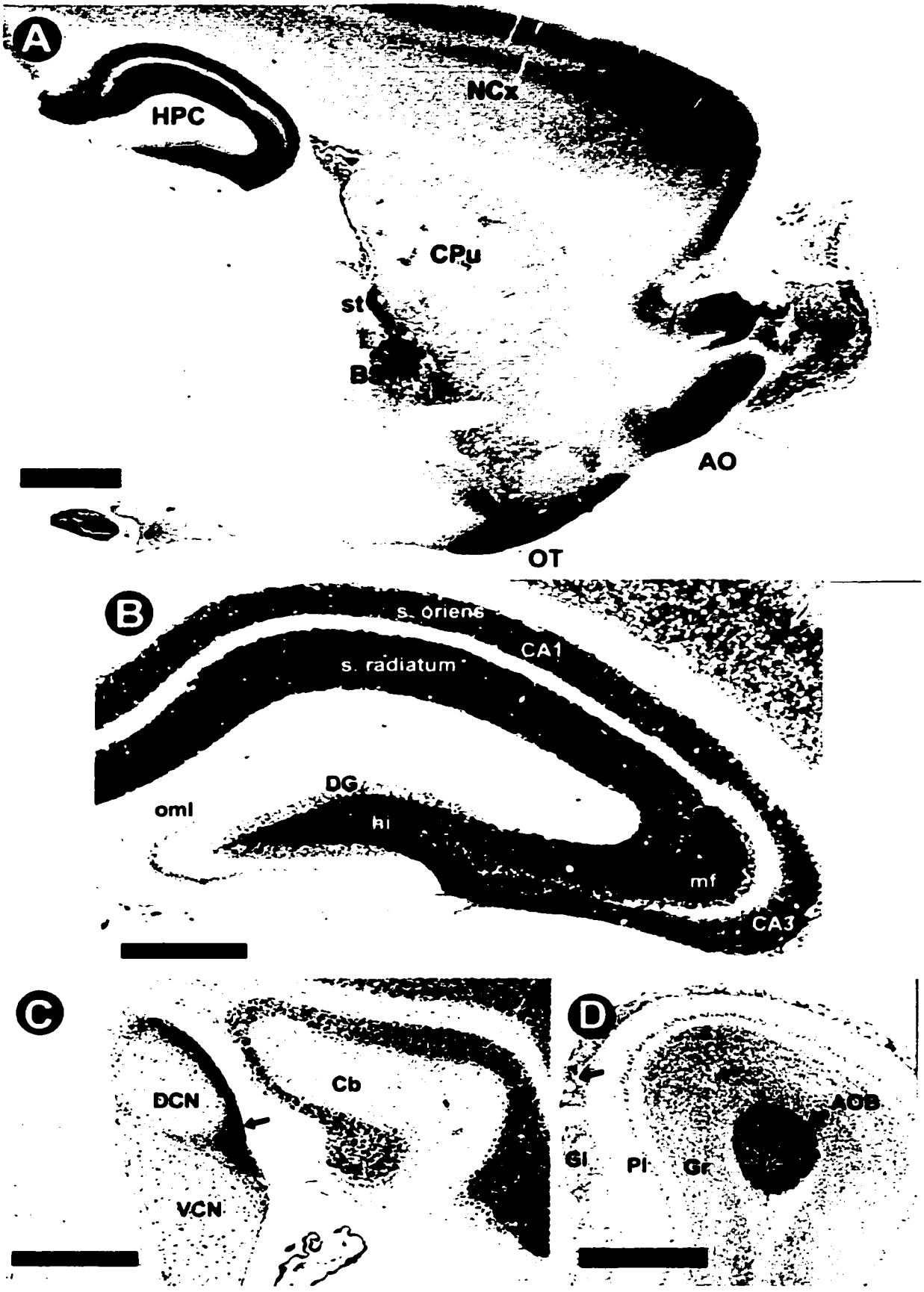
A
HPC
NCx
CPu
st
B
AO
OT
B
s. oriens
CA1
s. radiatum
DG
oml
hi
mf
CA3
C
DCN
Cb
VCN
D
AOB
Gl
Pl
Gr

The function of vesicular zinc is not well understood. Zinc may facilitate storage of glutamate or macromolecules within synaptic vesicles (Frederickson, 1989), in a manner analogous to its role in the storage of insulin in pancreatic β cells (Epand et al., 1985) or NGF in the salivary gland (Pattison and Dunn, 1976). Alternatively, zinc could serve extracellular functions as a neuromodulator upon its release into the synaptic cleft.

Several lines of evidence suggest that the histochemically reactive pool of synaptic vesicle zinc is released into the synaptic cleft upon neuronal activation. Activation of neurons either *in vivo* or in live hippocampal slices depletes histochemically reactive zinc from mossy fiber terminals in the hippocampus (Sloviter, 1986; Frederickson et al., 1988; Budde et al., 1997). In hippocampal slices, zinc is released into the extracellular space upon neuronal excitation produced by addition of K^+ or kainic acid, or by direct electrical stimulation of the mossy fiber bundle (Assaf and Chung, 1984; Howell et al., 1984). In rats, electrical stimulation of the perforant path or addition of K^+ through a push-pull cannula evoked significant release of zinc (100-300 μM; 200 times higher than normal CSF zinc concentrations) in the CA3 region of the hippocampus, and release was dependent on intact mossy fibers (Charton et al., 1985; Aniksztejn et al., 1987). Taken together, these observations suggest that neuronal activation releases zinc into the synaptic cleft by exocytosis of the zinc-rich synaptic vesicles.

Upon release, zinc could modulate the activity of multiple ligand- and voltage-gated ion channels (Fig. 2 B; reviewed in Harrison and Gibbons, 1994; Smart et al., 1994). Potential roles for synaptically-released zinc include inhibition of NMDA receptors (Peters et al., 1987; Westbrook and Mayer, 1987; Christine and Choi, 1990), potentiation of AMPA receptor responses (Rassendren et al., 1990), and antagonism of voltage-gated calcium channels (Winegar and Lansman, 1990). If zinc can diffuse away from its site of release, it could affect inhibitory (GABAergic) terminals as well (Fig. 2 B). Zinc inhibits $GABA_A$ receptors that lack γ subunits (Westbrook and Mayer, 1987; Draguhn et al., 1990; Legendre and Westbrook, 1991; Celentano et al., 1991; Smart et al., 1991). In hippocampal slices, zinc application causes giant depolarizing potentials that are probably due to zinc-induced synchronization of GABA release (Xie and Smart, 1991).

Figure 2. Hippocampal circuitry and potential zinc effects.

(A) Simplified diagram of the hippocampal circuitry, illustrating some of the major excitatory zincergic neuronal pathways (circles represent cell bodies and triangles represent terminals). The neurons diagrammed in white contain both zinc and glutamate in their terminals, and represent the primary excitatory pathway through the hippocampus. Perforant path projections (pp) extend from the entorhinal cortex (ECx) to make contacts with dendrites of dentate granule cells (DG) and CA3 pyramidal cells. In turn, dentate granule cells extend zinc-rich mossy fiber projections to the CA3 region, where they form synaptic contacts with inhibitory interneurons (diagrammed in black) and with dendrites of excitatory CA3 pyramidal cells. CA3 pyramidal cells extend axons back across the pyramidal cell layer, where they form Schaffer Collaterals (sc) that make contacts with dendrites of CA1 pyramidal cells, and Commissural / Associational fibers (ca) that make contacts with the dendrites of other CA3 pyramidal cells. CA1 pyramidal cells project to the subiculum (Sub). CA3 pyramidal cells and the inhibitory interneurons that contact them are the major targets of the zinc-rich mossy fibers. In addition, CA3 pyramidal cells receive excitatory, zincergic inputs from the perforant path and commissural / associational fibers. CA3 and CA1 pyramidal cells are especially prone to seizure- and ischemia-related neuronal damage.

(B) Potential zinc effects in the CA3 region of the hippocampus. A CA3 pyramidal cell dendrite or dendritic spine is depicted in the center, receiving inputs from mossy fiber (MF), commissural / associational (CA), and inhibitory terminals. Zinc is presumably released along with glutamate from MF, CA, and perforant path terminals. Upon release, it may have inhibitory (-) or potentiating (+) effects on various neurotransmitter receptors, including ionotropic glutamate receptors (KA, AMPA, and NMDA receptors) on the CA3 pyramidal cell or, with diffusion away from the release site, pre- or post-synaptic GABA or KA receptors at inhibitory terminals. After seizures, zinc may also enter post-synaptic neurons through AMPA or NMDA channels following seizures, where it may be toxic. ZnT3, as demonstrated in this dissertation, resides on synaptic vesicles and is required for accumulation of histochemically reactive zinc.

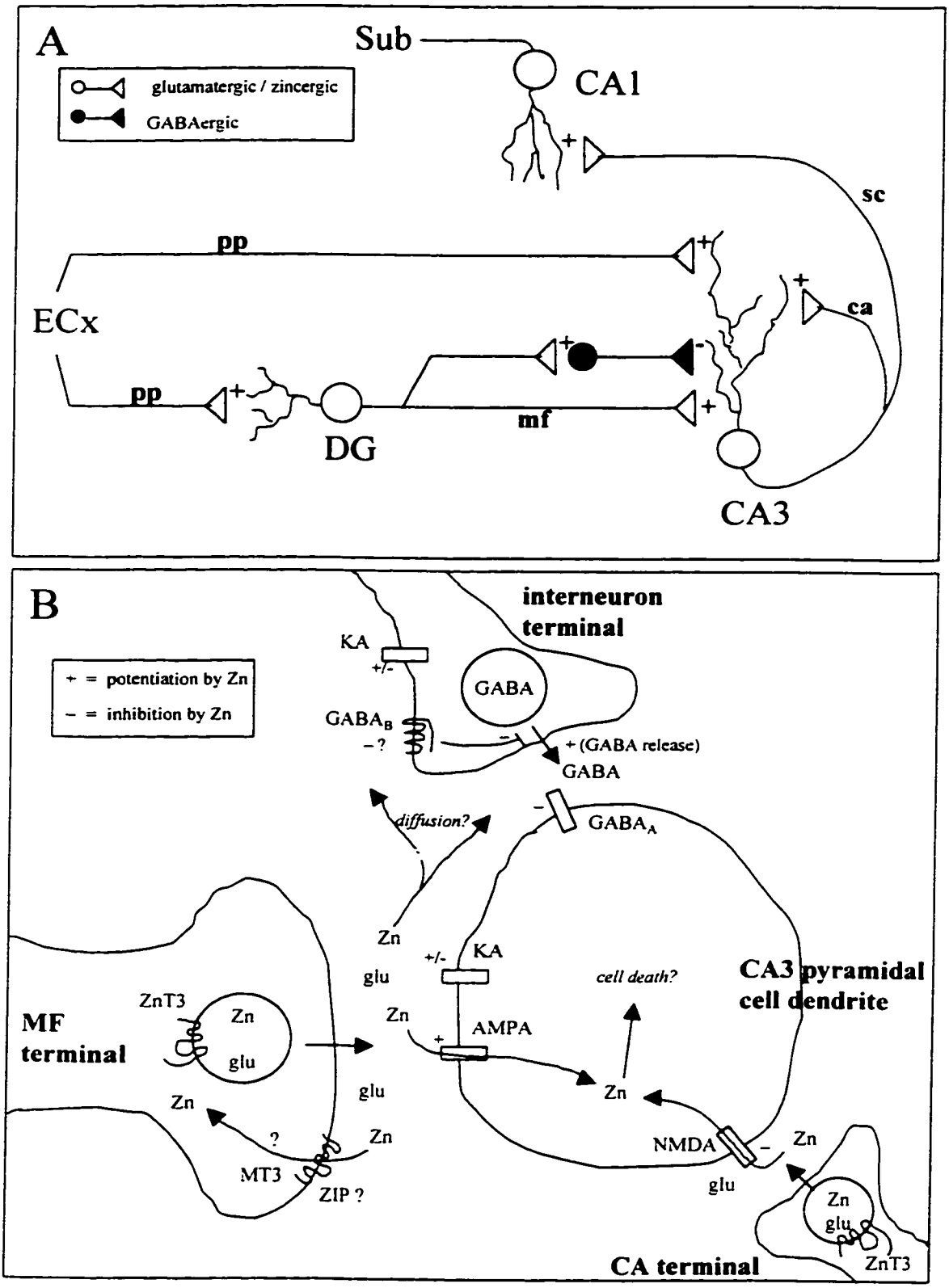
A
Sub
CA1
glutamatergic / zincergic
GABAergic
sc
pp
ECx
ca
pp
mf
DG
CA3
B
interneuron terminal
KA
+/-
GABA
GABA$_B$
-?
+ (GABA release)
GABA
diffusion?
GABA$_A$
Zn
+/-
KA
glu
cell death?
CA3 pyramidal cell dendrite
ZnT3
Zn
MF terminal
glu
Zn
+
AMPA
glu
Zn
Zn
?
Zn
NMDA
-
Zn
MT3
ZIP ?
glu
Zn
glu
ZnT3
CA terminal
+ = potentiation by Zn
- = inhibition by Zn

Such neuromodulatory effects of zinc have been thought to be important for appropriate function of the brain regions where zinc-containing neurons are present. Because zinc-containing neurons are prevalent throughout the limbic system and zinc is capable of exerting neuromodulatory effects on both glutamate receptors and GABA receptors *in vitro*, synaptically-released zinc has been considered to play an important role in memory formation, as well as in the control of limbic seizures. Likewise, the presence of histochemically reactive zinc in the striatum, olfactory bulb, cochlear nucleus, and spinal cord suggested that the neuromodulatory effects of zinc are important for motor coordination, olfaction, processing of auditory stimuli, and nociception, respectively. With respect to seizures, zinc is capable of exerting effects *in vitro* that could either inhibit or promote neuronal excitability, suggesting the possibility of both pro- and anti-convulsant effects. Many studies have attempted to determine which of these effects predominate *in vivo* in the initiation or propagation of seizures. Some of these studies suggest that the net neuromodulatory effect of zinc *in vivo* is to exacerbate seizures, whereas others support a net inhibitory effect of zinc on neuronal excitability (see Appendix D).

In addition to modulating neuronal transmission, zinc may contribute to neuronal injury. Zinc can bind with high affinity to the amyloid β protein and promote its aggregation, suggesting that it may contribute to the neuronal death associated with Alzheimer's disease (Bush et al, 1994). Zinc can also be toxic to neurons (Choi and Koh, 1998). The translocation of zinc from presynaptic terminals to postsynaptic cell bodies has been suggested to be responsible for much of the neuronal degeneration seen after prolonged seizures (Sloviter, 1985; Frederickson et al., 1989), ischemia (Tonder et al., 1990; Koh et al., 1996), or trauma (Suh et al., 2000).

II. Zinc transporters and metal homeostasis in the brain

Prior to the work described in this dissertation, the mechanism by which zinc accumulates in synaptic vesicles was not known. Indeed, despite tight regulation of zinc levels in mammalian cells, only recently have the mechanisms controlling zinc

homeostasis begun to be worked out. Neurons, like other mammalian cells, are likely to control zinc concentrations by influx and efflux across the plasma membrane, sequestration of zinc in intracellular compartments, and binding of zinc in the cytosol. In the past decade, some of the proteins involved in these processes have been identified, allowing investigators to begin to address their more precise functions in specific tissues.

Among these proteins are the metallothioneins (MTs), a family of small, cysteine-rich proteins that serve to detoxify or regulate the availability of zinc and other metal ions by high affinity binding (Käji, 1993; Bremner, 1993). Four MT isoforms have been identified in the mouse. *MT-I* and *MT-II* are coordinately and ubiquitously expressed (Käji , 1993), whereas *MT-III* expression is limited to the CNS (Palmiter et al., 1992) and *MT-IV* is expressed in stratified squamous epithelia (Quaife et al., 1994). In the brain, *MT-III* is expressed in zinc-containing neurons, where it may aid in distributing or buffering zinc in the cytosol, or recycling zinc from the synapse back into synaptic vesicles (Fig. 2 B; Masters et al., 1994; Erickson et al., 1997). *MT-III*-deficient mice had decreased concentrations of zinc in the brain and displayed greater susceptibility to seizure-related neuronal damage, suggesting a neuroprotective role for MT3 that may be related to to its ability to bind zinc (Erickson et al., 1997).

In addition, membrane-bound zinc transporters of the ZnT and ZIP families have recently been identified (Eng et al., 1998; Huang and Gitschier, 1997; Palmiter and Findley, 1995; Palmiter et al., 1996; Appendix A). Zrt/Irt-related protein (ZIP) transporters are involved in zinc uptake into cells (Eng et al., 1998; Gaither and Eide, 2000), and ZnT transporters appear to be involved in efflux of zinc either across the plasma membrane (Palmiter and Findley, 1995) or into vesicular compartments (Palmiter et al., 1996; Murgia et al., 1999). Like the yeast transporters ZRC1 (Kamizono et al., 1989; Conklin et al., 1994) and COT1 (Conklin et al., 1992; Conklin et al., 1994), the four members of the ZnT family of metal transporters are predicted to have six membrane spanning domains, a histidine rich cytoplasmic loop, and a long C-terminal tail, with both the amino and carboxy termini predicted to lie on the cytoplasmic side of the membrane (for ZnT3, see Fig. 3)(reviewed in McMahon and Cousins, 1998). The mechanisms by

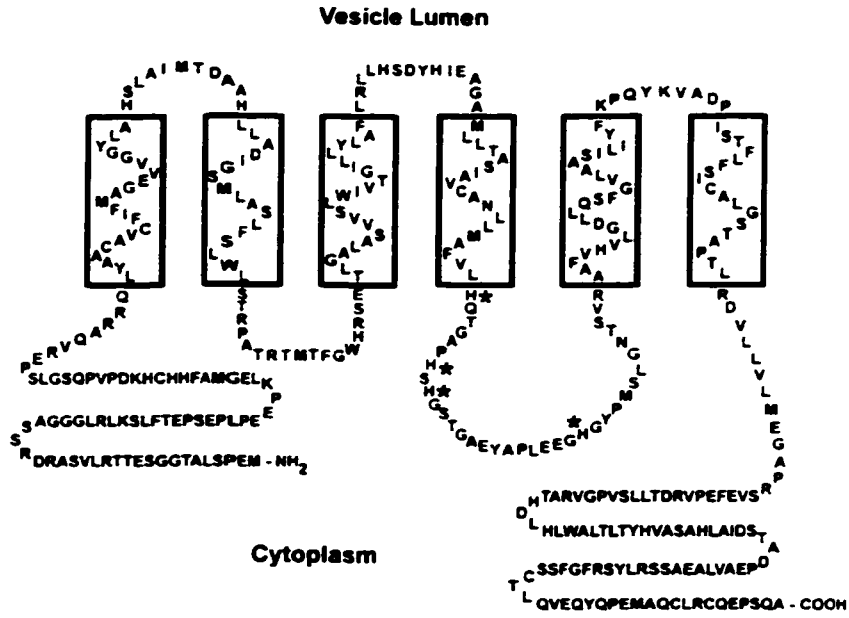

Figure 3. Predicted transmembrane structure of ZnT3.

Predicted amino acid sequence is depicted according to insertion topology within the membrane bilayer, following the "positive inside" rule of von Heijne (1994). Like the other members of the ZnT family, ZnT3 has 6 membrane-spanning domains (boxes), with both the amino and carboxy termini on the cytoplasmic side of the membrane. Asterisks mark histidines that may bind zinc in the cytoplasmic loop.

which these proteins transport zinc across membranes is not known. The cytoplasmic loop between the fourth and fifth transmembrane domains contains variable numbers of histidines which, in the case of ZnT1 (our unpublished data) and ZnT4 (Murgia et al., 1999), are capable of binding zinc. In transfected baby hamster kidney (BHK) cells, ZnT1 spans the plasma membrane, where it protects against zinc toxicity by effluxing zinc (Palmiter and Findley 1995), whereas ZnT2 and ZnT4 protect against zinc toxicity by transporting zinc into vesicles (Palmiter et al., 1996; Huang and Gitschier, 1997; Murgia et al., 1999). ZnT1, ZnT3, and ZnT4 are expressed in the brain (Appendix A; Murgia et al., 1999). ZnT1 is expressed ubiquitously (Appendix A), and is induced in the hippocampus following ischemic insult (Tsuda et al., 1997). ZnT4, in addition to its expression in peripheral tissues (Huang and Gitschier, 1997, Murgia et al., 1999), is expressed in zinc-containing neurons in the hippocampus (J. Gitschier, unpublished data). However, histochemically reactive zinc in the brains of *lethal milk* (*LM*) mice, which have a spontaneous mutation in *ZnT4* (Huang and Gitschier, 1997), is unaffected (our unpublished data).

The work presented in this dissertation was aimed at determining the function of the putative zinc transporter, ZnT3. *ZnT3* was cloned from a mouse brain cDNA library on the basis of its homology to *ZnT2* (Palmiter et al., 1996; Appendix A). In contrast to *ZnT1* and *ZnT2*, expressing *ZnT3* in BHK cells resulted in no obvious phenotype related to metal homeostasis. Similarly, while ZnT1 resides on the plasma membrane and ZnT2 and ZnT4 reside on vesicle membranes (Palmiter et al., 1996; Murgia et al., 1999), the subcellular localization of ZnT3 was not known. This dissertation demonstrates that *ZnT3* expression is limited to zinc-containing neurons in the brain and spinal cord. ZnT3 is shown to reside on the membranes of zinc-rich synaptic vesicles, and targeted disruption of *ZnT3* in mice is used to demonstrate that ZnT3 is required for the transport of zinc into synaptic vesicles. The lack of histochemically reactive zinc in synaptic vesicles in these mice allowed us to begin to elucidate the roles that synaptically-released zinc plays in the CNS.

RESULTS

I. ZnT3 is localized to the projections of zinc-containing neurons

A. *ZnT3* is expressed in zinc-containing neurons

RT-PCR, *in situ* hybridization, western blotting, and immunohistochemistry were used to determine the expression pattern of ZnT3 (Appendix A). To determine where *ZnT1*, *ZnT2*, and *ZnT3* are expressed *in vivo*, total RNA from various mouse organs was isolated then subjected to reverse transcription followed by PCR. ZnT1 mRNA was present in all tissues tested, whereas ZnT2 and ZnT3 showed a more restricted distribution, with ZnT3 mRNA present only in the brain and testis (Appendix A, Fig. 3). *In situ* hybridization with antisense RNA probes for mouse ZnT3 was used to determine which cells in brain and testis express *ZnT3*. In the testis, hybridization was confined to germ cells, primarily pachytene spermatocytes and round spermatids. In the brain, hybridization was evident in the hippocampal formation, pyriform cortex, amygdala, paraventricular thalamic nucleus, zona inserta, and several layers of the neocortex (Fig. 4A). Within the hippocampus, hybridization was evident in the dentate gyrus and stratum (s.) pyramidale of subregions CA3 and CA1 (Fig. 4B). Examination of sagittal sections of mouse brain revealed hybridization in the entorhinal cortex and cochlear nucleus (data not shown). No specific hybridization to either brain or testis sections was observed with a ZnT3 sense probe (data not shown).

A rabbit polyclonal antibody was raised against the C-terminal cytoplasmic tail of mouse ZnT3 and purified by affinity chromatography. The specificity of this antibody was assessed by Western blots of total cell proteins from BHK cells that were stably transfected with constructs expressing ZnT1, ZnT2, or ZnT3. Only BHK cells expressing *ZnT3* reacted with this antibody, indicating that it does not react with the homologous proteins (Appendix A, Fig. 5). An immunoreactive band of approximately the same size (~40 kDa) was detected in brain samples, but no protein was detected in either the testis or kidney samples (Appendix A, Fig. 5). Consistent with the absence of ZnT3

Figure 4. *ZnT3* is expressed in zinc-containing neurons.

Localization of ZnT3 mRNA, ZnT3 protein, and histochemically reactive zinc in the brain. Coronal sections of mouse brain were subjected to *in situ* hybridization with a ^{33}P-labeled probe complementary to mouse ZnT3 mRNA (A and B), immunohistochemistry with affinity-purified antisera raised against the C-terminal tail of ZnT3 (C and D), and Timm stain for vesicular zinc (E and F). ZnT3 colocalizes with Timm stain throughout the brain. In the hippocampus (B,D,F), ZnT3 mRNA is present in the cell bodies of dentate granule (DG) cells, and ZnT3 protein is abundant in the zinc-rich mossy fiber (mf) projections emanating from these neurons. A, amygdala (lateral nucleus); H, hippocampus; NCx, neocortex; PCx, piriform cortex; PV, paraventricular thalamic nucleus; ZI, zona inserta; DG, dentate gyrus; hi, hilus; mf, mossy fibers. Scale bars: 1000 μm (A); 200 μm (B).

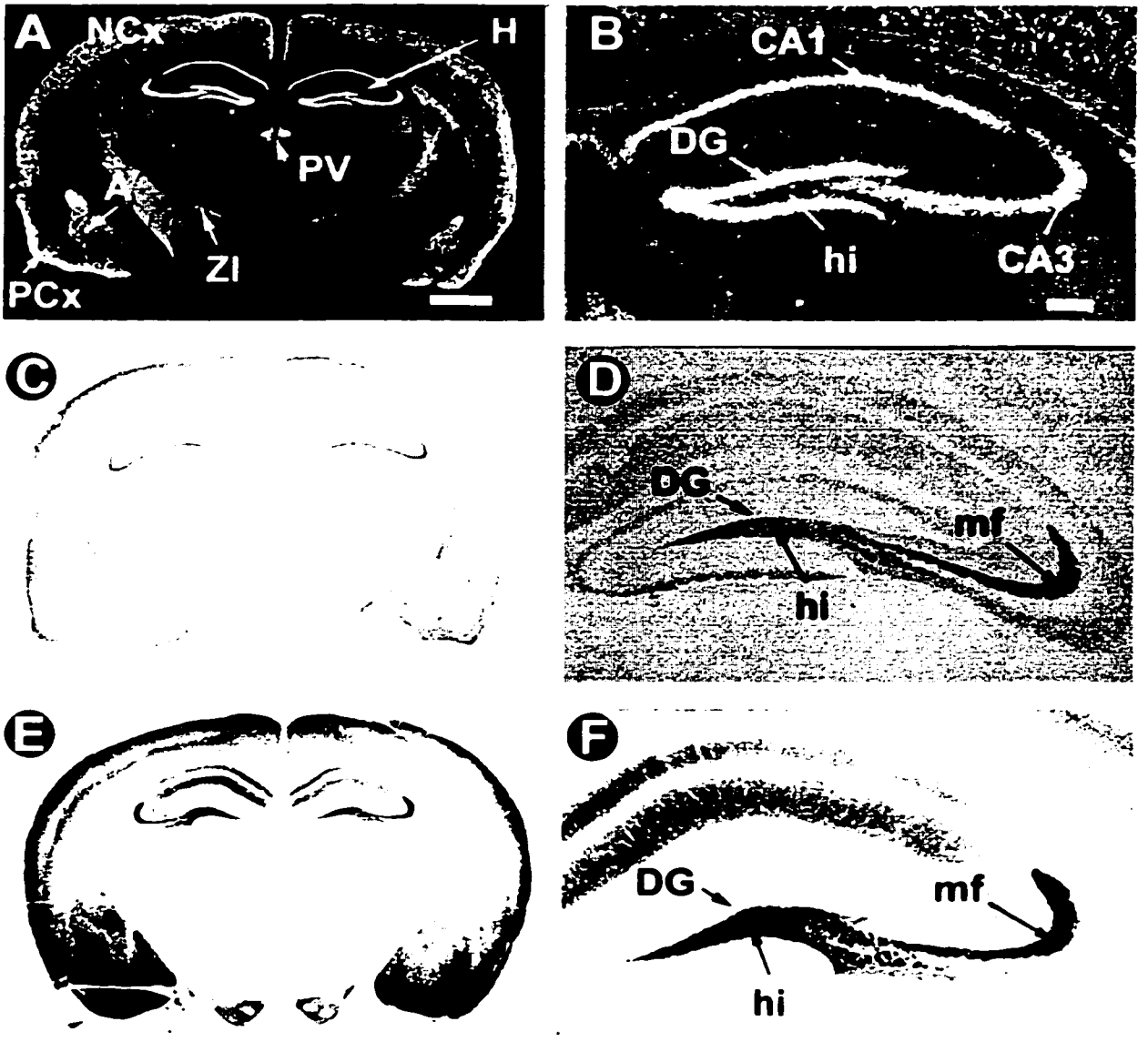
A
NCx
H
PV
A
ZI
PCx
B
CA1
DG
hi
CA3
C
D
DG
mf
hi
E
F
DG
mf
hi

immunoreactivity in the testis, polysome analysis of testis RNA separated by sucrose fractionation revealed that ZnT3 mRNA was associated primarily with the monosome fraction, indicating that ZnT3 mRNA in the testis is transcribed but not efficiently translated.

When the ZnT3 antibody was applied to brain sections, the most intense staining was observed over the mossy fiber projections emanating from granule cell neurons in the dentate gyrus (Fig. 4D). ZnT3 immunoreactivity was also evident in the pyriform cortex, amygdala, and neocortex (Fig. 4C). In the hippocampus, in addition to the mossy fiber staining seen in stratum (s.) lucidum and s. oriens of the CA3 region, staining was observed in s. oriens and s. radiatum of the CA1 region, probably representing Schaffer collateral projections from CA3 pyramidal cells, and in the outer molecular layer of the dentate gyrus, probably representing perforant path projections from the entorhinal cortex (Fig. 4D). The antibody staining pattern in the brain was very similar to the histochemical localization of zinc by the Timm reaction, which detects loosely bound vesicular zinc (compare Fig. 4D and F). Longer development times than shown here for the Timm reaction reveal zinc staining in the outer molecular layer of the dentate gyrus as well. Control sections not exposed to the ZnT3 antibody showed no immunoreactivity. Thus, ZnT3 mRNA is present in the cell bodies of zinc-containing neurons, and ZnT3 protein is present in the projections from those neurons. These observations, together with its similarity to the vesicular zinc transporter, ZnT2, suggested that ZnT3 was involved in the transport of zinc into synaptic vesicles.

B. ZnT3 resides on the membranes of zinc-rich synaptic vesicles

To test whether ZnT3 resides on synaptic vesicles, ZnT3 immunoreactivity was assessed at the electron microscopic level in the mouse and monkey hippocampus (Appendix B). In mice, ZnT3 immunoreactivity was observed in mossy fiber boutons (MFB's) within the hilus and the CA3 subregion (Appendix B, Figure 1D and F). The intense ZnT3 immunoreactivity corresponded exclusively to MFB's; synaptic vesicles of interneurons in the same sections were not stained (Appendix B, Figure 1D). Electron

micrographs of MFB's at higher magnification (Appendix B, Fig. 1F) revealed that ZnT3 immunoreactivity was localized uniformly to the membranes of spherical, clear synaptic vesicles. ZnT3 immunoreactivity associated with round clear synaptic vesicles was similar in both the small boutons on dendritic shafts (Appendix B, Fig. 3B) and large boutons associated with complex spines (Appendix B, Figs. 1F and 3A). MFB's sampled from different locations in the hilus and the CA3 subregion showed no difference in the pattern or intensity of ZnT3 immunoreactivity. In the outer molecular layer of the dentate gyrus, less intense ZnT3 immunoreactivity was observed on synaptic vesicles in some axon terminals (Appendix B, Fig. 3D). Electron microscopy of Timm-stained hippocampal sections revealed Timm silver precipitate in regions corresponding to the MFB's (Appendix B, Fig. 1C). At higher magnification, it was apparent that up to 60-80% of the synaptic vesicles of MFB's contain silver granules (Appendix B, Fig. 1E). In experiments in which immunocytochemical staining for ZnT3 was carried out in Timm-stained ultrathin sections, the ZnT3-associated gold particles were found exclusively over Timm-positive MFB's (Appendix B, Fig. 3G). Glutamate immunoreactivity was also evident in these MFB's (Appendix B, Fig. 3H).

In the monkey hippocampus, patterns of ZnT3 immunoreactivity and Timm stain were somewhat different to that seen in mice. Prominent staining for both was evident in the inner molecular layer of the dentate gyrus, and neither ZnT3 immunoreactivity nor Timm stain were detected in the dentate outer molecular layer (Appendix B, Fig. 2). As in the mouse, electron microscopy revealed Timm stain and ZnT3 immunoreactivity on clear spherical synaptic vesicles in MFB's (Appendix B, Fig. 2C-F).

C. ZnT3 and mossy fiber sprouting in the epileptic human and mouse hippocampus.

In the epileptic human brain and in many animal models of epilepsy, recurrent seizures are associated with aberrantly-sprouted mossy fiber axons emanating from dentate granule cells in the hippocampus and projecting back across the granule cell layer into the dentate inner molecular layer (IML), where the dendritic fields of these neurons

reside (Babb et al., 1991; Franck et al., 1995; Represa et al., 1994). It is not known whether these newly sprouted axon terminals are a cause or consequence of epilepsy, but some evidence suggests that zinc found in these sprouted terminals might be implicated in the establishment of epilepsy (Buhl et al., 1996). To examine whether ZnT3 in present in these newly-formed terminals, and to determine which cells the sprouted axons contact, we stained hippocampi from epileptic human brain (autopsy tissue provided by D. Born) and from the brains of Kv1.1 knockout mice, which have frequent spontaneous seizures (Smart et al., 1998), with Timm stain or ZnT3 immunohistochemistry. In the brains of epileptic mouse (Fig. 5) and human (Fig. 6), Timm stain and ZnT3 immunoreactivity were present in the dentate IML, indicating mossy fiber sprouting (Compare Fig. 5 A with Fig. 4 F). Ultrastructurally, ZnT3 immunoreactivity and Timm precipitate were localized to synaptic vesicles within the newly-formed mossy fiber boutons (MFB's)(Fig. 5 B-E; Fig 5 C, D). In the brain of the Kv1.1 mouse, ZnT3-immunoreactive MFB's in the IML made contact with the dendrites and dendritic spines of excitatory granule cells (Fig. 5 B, C) and with inhibitory basket cells (Fig. 5D). Thus, ZnT3 colocalizes with vesicular zinc in aberrant neuronal projections associated with epilepsy as well as in normal zinc-containing neurons. The presence of zinc in terminals that make contact with both excitatory and inhibitory neurons could have important implications for the propagation of seizures in epilepsy, as these contacts could form local excitatory or inhibitory feedback loops within the dentate gyrus.

Figure 5. ZnT3 on terminals of sprouted mossy fiber axons in the mouse.

Light (A) and electron (B-E) micrographs demonstrating Timm stain (A,E) and ZnT3 immunoreactivity (B-D) in newly sprouted axon terminals in the inner molecular layer (IML) of the dentate gyrus of a Kv1.1 knockout mouse, which displays frequent spontaneous seizures. In addition to the normal Timm stain seen in the hilus (H), newly sprouted axons in the IML stain with Timm (Compare (A) with Fig. 4F). GC, Granule cell layer. (B,C) Mossy fiber boutons (MFB) of newly sprouted axons in the IML, making asymmetric contacts with a dendrite (D) and dendritic spines (S) of excitatory dentate granule cells. (D) Lower power electron micrograph showing multiple MFBs (arrows) in the IML making synaptic contacts (arrowheads) with an inhibitory basket cell (BC). (E) Individual MFB in the IML stained with Timm, illustrating zinc within synaptic vesicles of the new terminals.

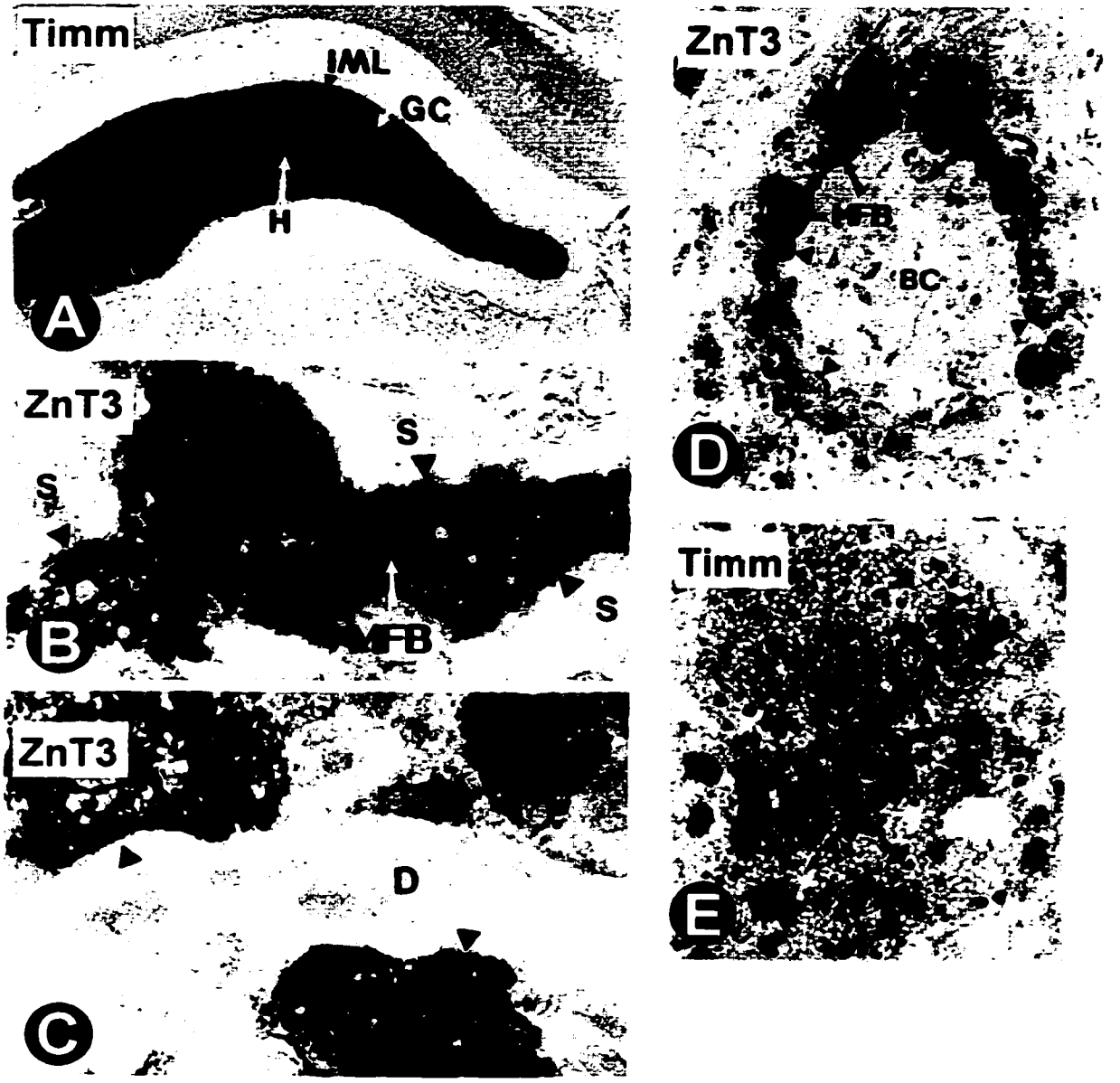
Timm
IML
GC
H
A
ZnT3
S
S
FB
S
B
ZnT3
D
C
ZnT3
FB
BC
D
Timm
E

Figure 6. ZnT3 on terminals of sprouted axons in the epileptic human brain.

Hippocampal section from a 33 year old female patient with epilepsy. (A) Combined Timm and cresyl violet stain. Timm stain is reduced relative to normal human brain (not shown) in the hilus (H) and CA3 region, and is abnormally present in the dentate inner molecular layer (IML, arrows), indicating mossy fiber sprouting. (B) ZnT3 immunoreactivity in a hippocampal section from the same patient. ZnT3 immunoreactivity is present in the hilus, CA3, and IML (arrows) in a pattern similar to that of the Timm stain. (C) Electron micrograph from the boxed area in (A), showing histochemically reactive zinc in synaptic vesicles of small mossy fiber boutons (MFB) in sprouted terminals of the IML. (D) Electron micrograph of a newly sprouted MFB in the IML, showing ZnT3 immunoreactivity on synaptic vesicles. S, dendritic spines.

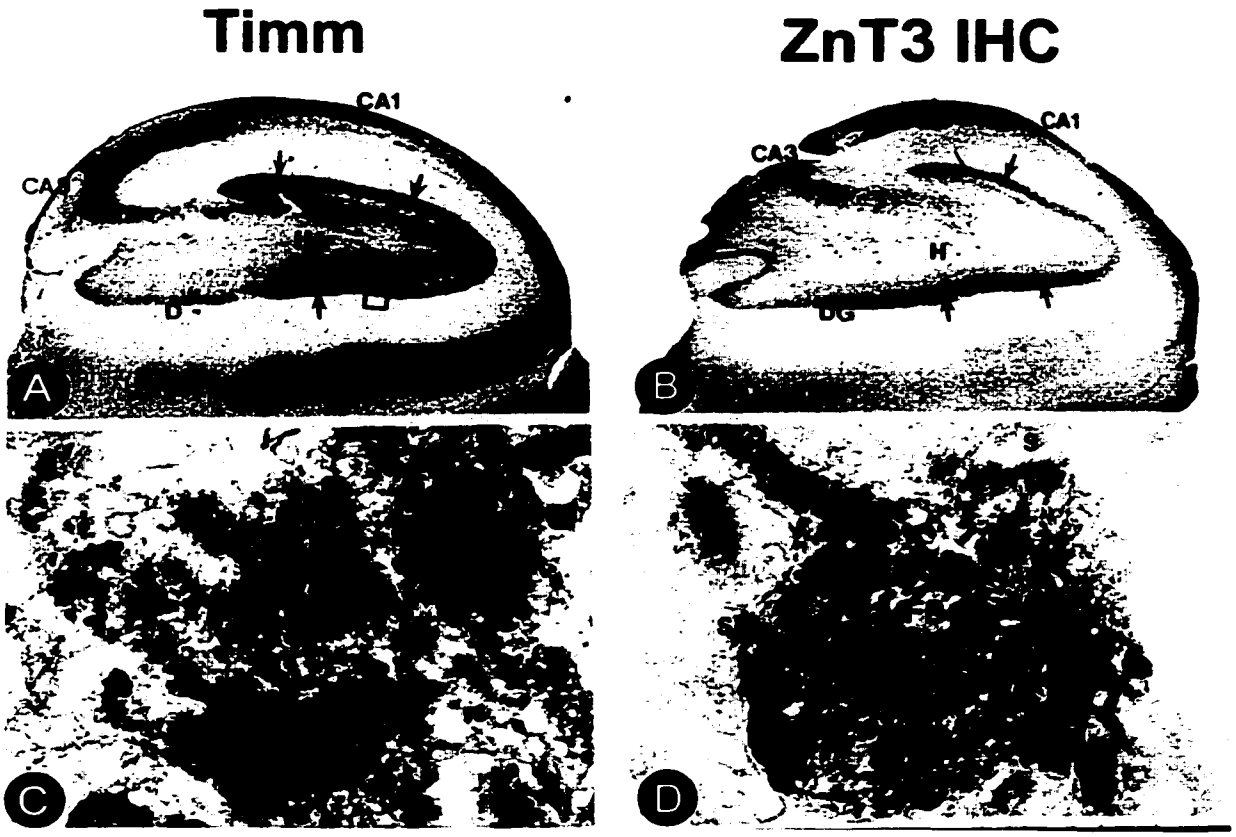
Timm
ZnT3 IHC
CA1
CA3
H
DG
A
B
C
D

II. ZnT3 transports zinc into synaptic vesicles

A. Targeted disruption of the murine *ZnT3* gene

The hypothesis that ZnT3 is required for zinc transport into synaptic vesicles was tested by targeted disruption of *ZnT3* in mice (Appendix C). The first four exons of *ZnT3* were replaced by a cassette that included *nlacZ* and *neo*^{r} (Appendix C, Fig. 1A). This construct was electroporated into embryonic stem cells. PCR analysis of 60 clones revealed three that underwent homologous recombination appropriately. One of these produced chimeras that transmitted the targeted allele through the germ line. F1 heterozygotes were generated by crossing the chimeras with C57Bl/6 females. The F2 progeny from these mice, genotyped by DNA dot hybridization, Southern blot analysis (Appendix C, Fig. 1B), or PCR, were born in the expected Mendelian ratio. ZnT3 protein, assessed by Western blot analysis of brain homogenates, was reduced in the brains of mice with one copy of the mutant allele (*ZnT3*$^{+/-}$ mice) and undetectable in the brains of homozygous mutant mice (*ZnT3*$^{-/-}$ mice)(Appendix C, Fig. 1C).

Insertion of *nlacZ* into the *ZnT3* locus confirmed the patterns of *ZnT3* expression seen previously by *in situ* hybridization, including expression in granule cells of the dentate gyrus, pyramidal cells of the CA3 and CA1 regions, and the amygdala, neocortex, and piriform and entorhinal cortices (Appendix C, Fig. 2). In addition, *nlacZ* expression was detected in the cochlear nucleus, laminae I-IV of the dorsal horn of the spinal cord (Appendix C, Fig. 2), and the testis (not shown), where ZnT3 mRNA is abundant but not translated into protein. ZnT3 mRNA, isolated from the brains of wild-type embryos or pups and quantified by solution hybridization, was negligible at birth, then increased linearly, reaching a maximum at about 3 weeks postpartum (Appendix C, Fig. 2).

B. Vesicular zinc is eliminated from the brains of ZnT3 knockout mice

To determine whether the levels of zinc or other metals were altered upon disruption of *ZnT3*, metal content was measured by plasma emission spectroscopy (Appendix C). In the hippocampus and cortex, regions that contain abundant vesicular zinc, total zinc was

reduced in the *ZnT3*$^{-/-}$ mice by 20% ($P < 0.001$, Student's t-test) and 23% ($P < 0.01$), respectively, whereas the cerebellum and other (primarily hypothalamus and thalamus) regions without appreciable levels of vesicular zinc were unaffected (Appendix C, Fig. 3). Total zinc levels in the hippocampus and cortex of *ZnT3*$^{+/-}$ mice were reduced by 10% ($P < 0.05$, Student's t-test)(Appendix C, Fig. 3). None of the other 11 elements tested (Al, As, B, Ca, Cu, Fe, K, Mg, Na, P, and Si) showed any change in abundance. Ag, Ba, Cd, Co, Cr, Mn, Ni, Pb, Se, and V were below detectable levels.

To test whether vesicular zinc was altered in these mice, we used two stains for histochemically reactive zinc, Timm stain and *N*-(6-Methoxy-8-quinolyl)-*p*-Toluene-Sulfonamide (TSQ) fluorescence (Appendix C). Timm stain was reduced in the brains of *ZnT3*$^{+/-}$ mice and eliminated from the brains of *ZnT3*$^{-/-}$ mice, including the staining normally seen in the hippocampus, neocortex, piriform cortex, amygdala (Appendix C, Fig. 4), entorhinal cortex, striatum, olfactory bulb, and cochlear nucleus (not shown). In the hippocampus, Timm stain was reduced (*ZnT3*$^{+/-}$) or undetectable (*ZnT3*$^{-/-}$) in the mossy fibers projecting from dentate granule neurons to the hilus and s. lucidum and s. oriens of the CA3 region, and in projections to s. radiatum and s. oriens of the CA1 region (Appendix C, Fig. 4). Timm stain was undetectable in the *ZnT3*$^{-/-}$ brain even after long histochemical development times (> 90 min) that normally produce intense staining in CA1 and prominent staining in the inner and outer molecular layers of the dentate gyrus (not shown). In contrast, Timm stain was readily detectable in the choroid plexus (Appendix C, Fig. 4), as well as islet cells of the pancreas and convoluted tubule cells of the submandibular salivary gland (Fig. 7). At the ultrastructural level, Timm reaction product was present within synaptic vesicles of MFB's in the wild-type (*ZnT3*$^{+/+}$) brain, whereas the number of Timm-positive vesicles in *ZnT3*$^{+/-}$ boutons was reduced, and no Timm-staining was detected within synaptic vesicles of *ZnT3*$^{-/-}$ boutons (Appendix C, Fig. 4 H, I, J), indicating that histochemically reactive zinc is eliminated from synaptic vesicles in the brains of *ZnT3*$^{-/-}$ mice.

Figure 7. Timm stain is not perturbed in the *ZnT3*$^{-/-}$ pancreas or submandibular gland.

Sections were stained with Timm (black stain, arrows) and counterstained with hematoxylin and eosin. (A) Section of pancreas from a *ZnT3*$^{-/-}$ mouse. The arrow points to one of the Islets of Langerhans, comprised of beta cells that store insulin in zinc-rich secretory granules. (B) Section of the submandibular gland of a male *ZnT3*$^{-/-}$ mouse, illustrating Timm stain in secretory granules of convoluted tubule cells. Timm stain in both of these organs was similar to that seen in wild-type mice. Scale bars: 200 μm.

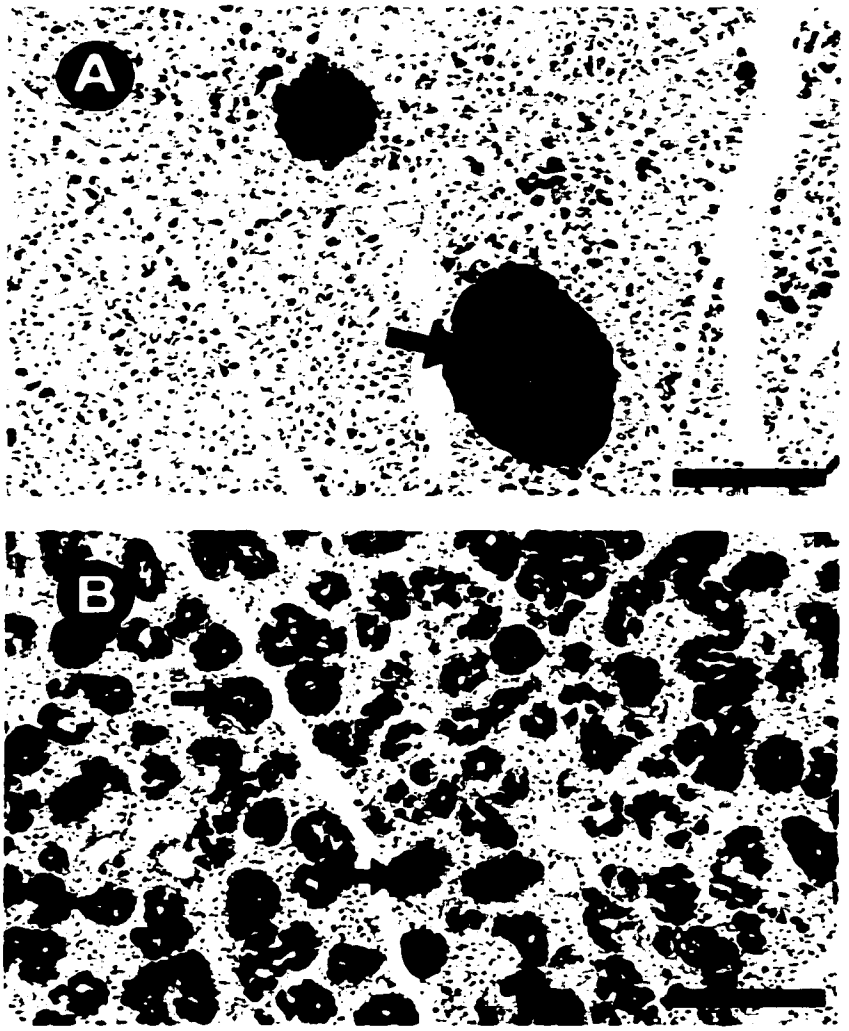
A
B

C. Vesicular zinc content is determined by the abundance of ZnT3 on synaptic vesicle membranes.

To investigate whether the amount of ZnT3 present on vesicle membranes was reduced in the *ZnT3*$^{+/-}$ brain, we assessed ZnT3 immunoreactivity in the brains of *ZnT3*$^{+/+}$, *ZnT3*$^{+/-}$, and *ZnT3*$^{-/-}$ mice at the light microscopic and electron microscopic levels (Appendix C). In the mutant brain, ZnT3 immunoreactivity was reduced (*ZnT3*$^{+/-}$) or undetectable (*ZnT3*$^{-/-}$), including the amygdala, cortex, and hippocampus (for hippocampus, see Appendix C, Fig. 5; other regions, data not shown). At the ultrastructural level, ZnT3 immunoreactivity was present on all synaptic vesicles within *ZnT3*$^{+/-}$ MFB's, similarly as in *ZnT3*$^{+/+}$ MFB's, but the intensity of ZnT3 immunoreactivity was reduced (compare Appendix C, Fig. 5 B and D). TSQ fluorescence, a specific indicator of vesicular zinc, was used to corroborate the results seen with the Timm stain and to provide a quantitative comparison of vesicular zinc levels in the hippocampi of *ZnT3*$^{+/+}$, *ZnT3*$^{+/-}$, and *ZnT3*$^{-/-}$ mice. TSQ fluorescence was undetectable in the *ZnT3*$^{-/-}$ hippocampus (Fig. 8 A), but still abundant in differentiating spermatids of the testis and in β-islet cells of the pancreas (Fig. 8 C, D). TSQ fluorescence was quantified, using computer-assisted laser cytometry, from several regions of the hippocampus and a small region within the dorsomedial thalamus (Fig. 8 B). Average fluorescence was plotted as a percentage of the maximal fluorescence, which was seen in the wild-type hilus. TSQ fluorescence in the hilus and regions CA3 and CA1 was absent in the *ZnT3*$^{-/-}$ hippocampus ($P < 0.0001$, Student's t-test), where it was even lower than the background fluorescence, i.e., that seen in the thalamus or corpus callosum (Fig. 8 A). TSQ fluorescence in the *ZnT3*$^{+/-}$ hippocampus was reduced by 47% in the hilus, 39% in region CA3, and 50% in region CA1 ($P < 0.0001$ for all regions, Student's t-test)(Fig. 8 B).

Figure 8. TSQ fluorescence is undetectable in the brains of *ZnT3*$^{-/-}$ mice.

(A) Computer-generated images of TSQ fluorescence (color coded as follows: red > yellow > green > blue) in the hippocampi of *ZnT3*$^{+/+}$ (left panel), *ZnT3*$^{+/-}$ (middle panel), and *ZnT3*$^{-/-}$ (right panel) mice. The bright fluorescence in the hilus, s oriens and s lucidum of CA3, and s oriens and s radiatum of CA1 was reduced in the *ZnT3*$^{+/-}$ hippocampus and undetectable in the *ZnT3*$^{-/-}$ hippocampus. TSQ staining was also reduced in the neocortex. TSQ fluorescence in the hippocampus of the mutants was less than the autofluorescence of the overlying corpus callosum. (B) Quantification of TSQ fluorescence in regions within the hippocampus, by computer-assisted laser cytometry. Data are expressed as mean ± SEM (n = 5). (C) TSQ-stained section of a single seminiferous tubule from the testis of a *ZnT3*$^{-/-}$ mouse. Spermatids poised at the lumen of the tubule fluoresced with TSQ, similar to wild-type spermatids (not shown). (D) TSQ-stained pancreas from a *ZnT3*$^{-/-}$ mouse, illustrating a single Islet of Langerhans. Scale bars: 50 μm (C); 100 μm (D).

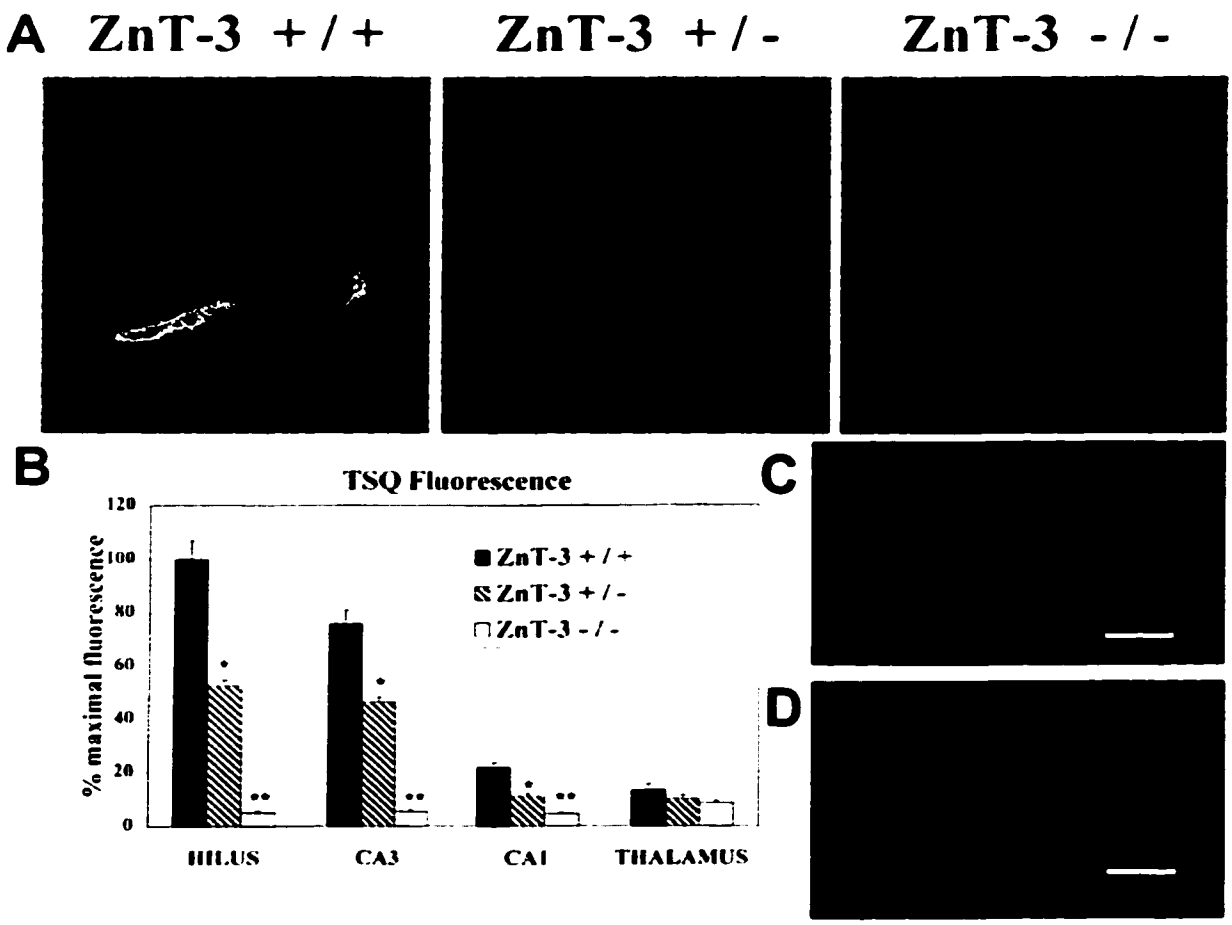
A
ZnT-3 + / +
ZnT-3 + / -
ZnT-3 - / -
B
TSQ Fluorescence
% maximal fluorescence
120
100
80
60
40
20
0
ZnT-3 + / +
ZnT-3 + / -
ZnT-3 - / -
*
**
HILUS
CA3
CA1
THALAMUS
C
D

III. Consequences of removing zinc from synaptic vesicles: the phenotype of the ZnT3 knockout mouse

A. General description and gross morphology

ZnT3$^{+/-}$ and *ZnT3*$^{-/-}$ mice showed no obvious phenotypic differences from their wild-type littermates. Body weight, lifespan, fertility, and litter size were normal, and the mice showed no obvious morphological abnormalities. Examination of the brains of adult *ZnT3*$^{-/-}$ mice by light microscopy revealed no grossly aberrant morphology. In the hippocampus, stratum (s.) granulosum of the dentate gyrus and s. pyramidale, s. oriens, and s. radiatum of the CA3 and CA1 regions were normal in appearance, and mossy fiber projections, as detected by dynorphin immunoreactivity, were evident in s. lucidum and s. oriens of CA3 (not shown). Ultrastructural analysis revealed the *ZnT3*$^{-/-}$ hippocampus to be normal with respect to the number, distribution, and size of MFB's in the hilus and s. lucidum (Fig. 9 A, B), as well as the number of asymmetric synaptic contacts made with dendritic spines (Fig. 9 C-F), and the presence of glutamate immunoreactivity (Fig. 9 E, F). MFB's in the *ZnT3*$^{-/-}$ hippocampus showed normal characteristic ultrastructure, with densely packed clear, round synaptic vesicles, a few dense core vesicles, and numerous mitochondria (Fig. 9 C-F), lacking only histochemically reactive zinc within the synaptic vesicles.

In the pancreas and salivary gland, vesicular zinc is packaged with insulin and NGF, respectively, and is thought to stabilize these proteins during storage (Maske, 1957; Epand et al., 1985; Frederickson et al., 1987; Pattison and Dunn, 1975; Ross et al., 1997). We tested the possibility that zinc may be serving a similar role in synaptic vesicles in the brain by measuring NGF in the zinc-rich hippocampus and, as a control, in the cerebellum, where vesicular zinc is not normally present. NGF levels were normal in the *ZnT3*$^{-/-}$ hippocampus (Fig. 10 B). Zinc is a potent inhibitor of tissue plasminogen activator (tPA), which causes excitotoxic neuronal death in the hippocampus by generating plasmin (Tsirka et al., 1995; Tsirka et al., 1997). To assess whether zinc

Figure 9. Mossy fiber boutons in the *ZnT3*$^{-/-}$ hippocampus show normal ultrastructure.

Electron micrographs of mossy fiber boutons (MB) in stratum lucidum of the CA3 region, taken from a *ZnT3*$^{+/+}$ (A,C,E) and *ZnT3*$^{-/-}$ (B,D,F) mouse. (A,B) Lower magnification electron micrographs showing normal size, shape and density of MB's. (C,D) Higher magnification of a single MB from each genotype. *ZnT3*$^{-/-}$ MB's were normal with respect to their size, the approximate number of small, clear synaptic vesicles contained within them, the numbers and types of synaptic contacts made with dendritic spines (S), and the presence of mitochondria. A, terminals of inhibitory interneurons. (E,F) MB's immunoreacted with an antibody against glutamate (gold particles, arrows).

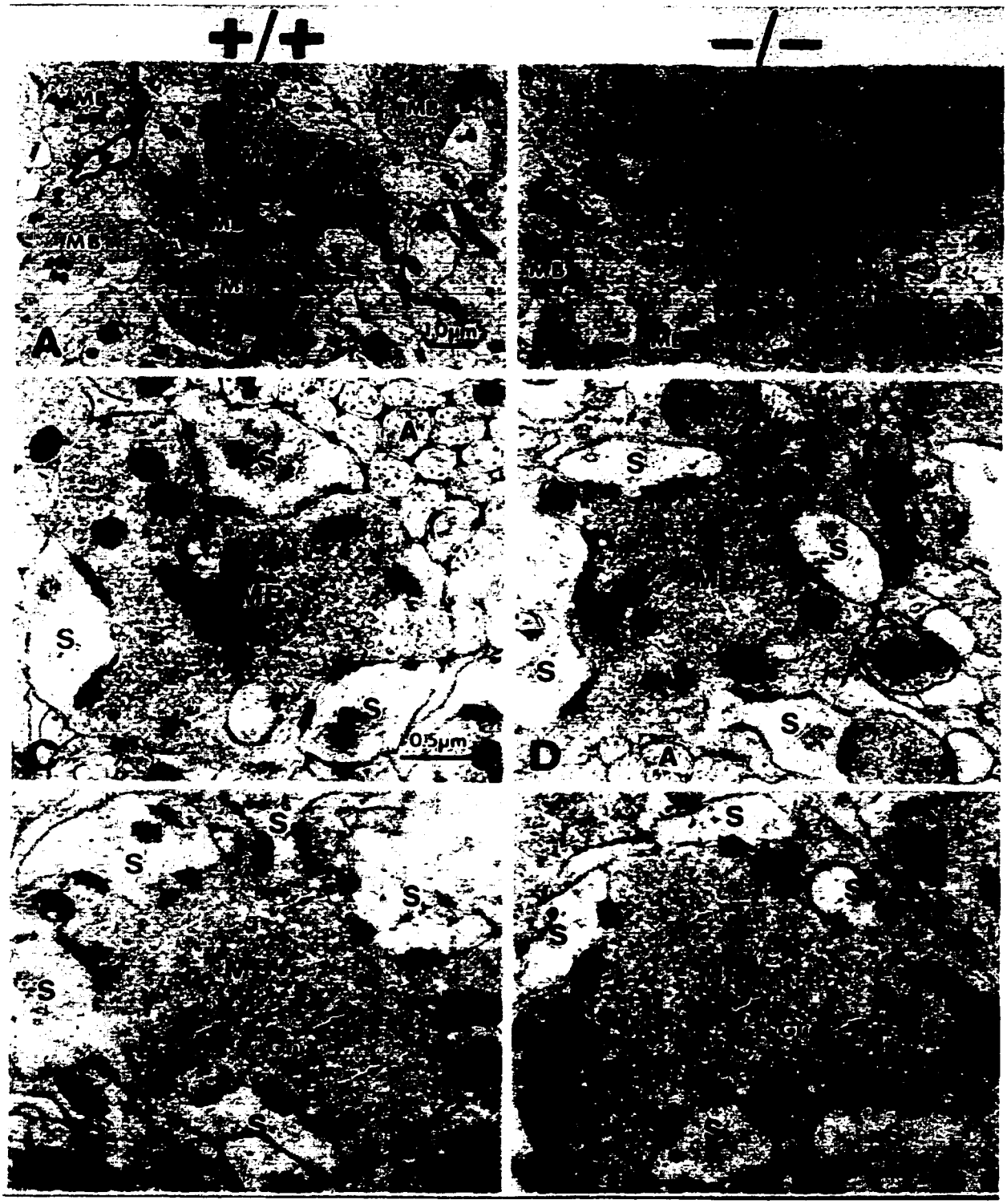
+/+
−/−
MB
MB
MB
MB
A
1.0μm
A
S
S
MB
S
S
C
0.5μm
S
S
S
S
S
S
S
D
A

Figure 10. Normal NGF levels and TPA activity in the *ZnT3*$^{-/-}$ hippocampus.

(A) Plasminogen overlay assay for TPA activity in a coronal section of mouse brain. TPA activity was detected as a "plaque" (absence of milk proteins; white arrow), for which the intensity was similar in *ZnT3*$^{-/-}$ and *ZnT3*$^{+/+}$ mice. (B) NGF levels in the hippocampus and cerebellum, assessed by ELISA assay with an anti-NGF antibody.

A

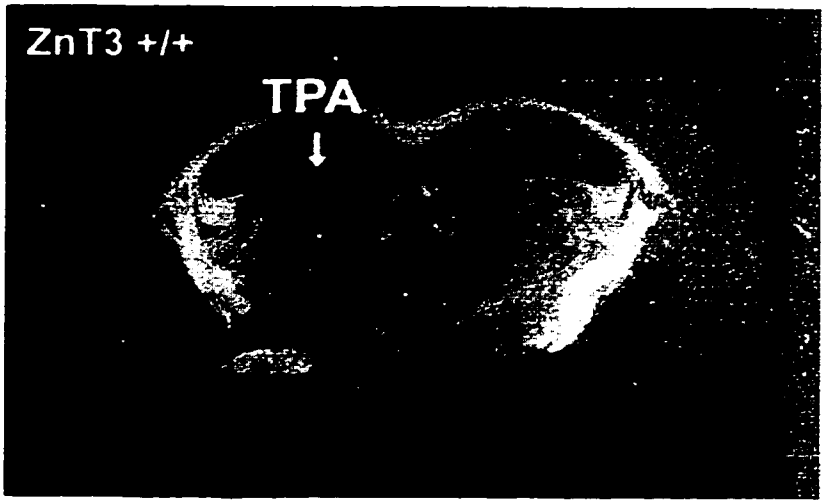
ZnT3 +/+
TPA

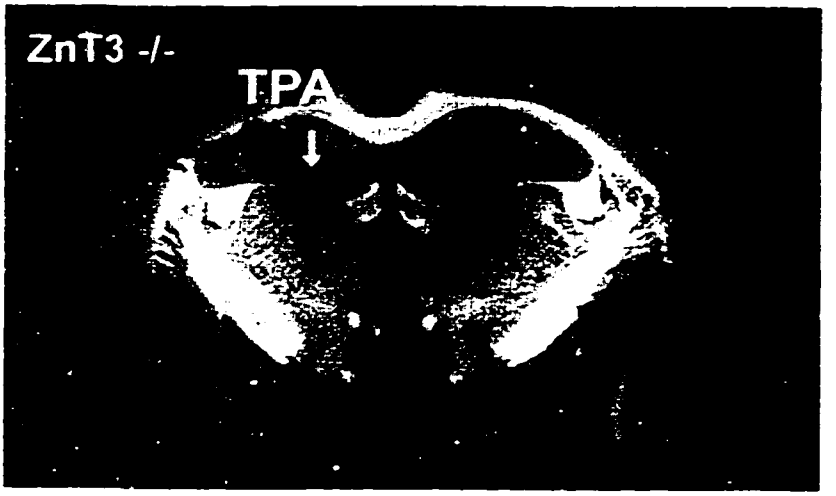
ZnT3 -/-
TPA

B

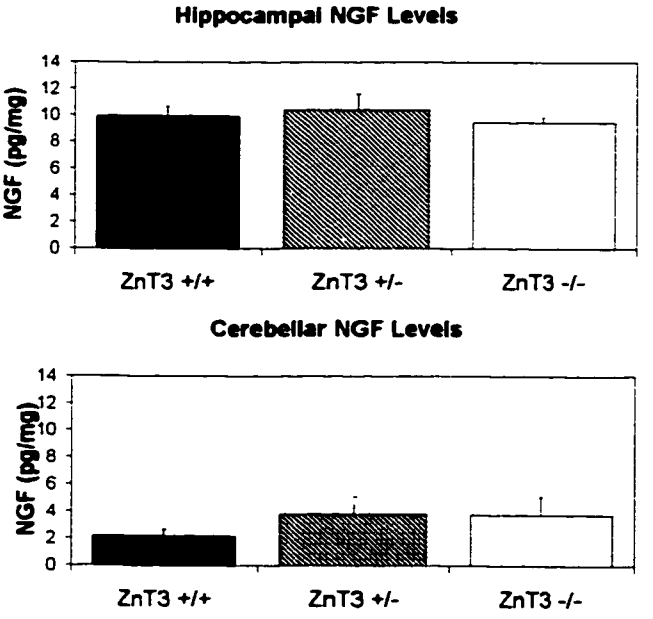
Hippocampal NGF Levels
NGF (pg/mg)
14
12
10
8
6
4
2
0
ZnT3 +/+
ZnT3 +/-
ZnT3 -/-
Cerebellar NGF Levels
NGF (pg/mg)
14
12
10
8
6
4
2
0
ZnT3 +/+
ZnT3 +/-
ZnT3 -/-

inhibition of tPA occurs under normal conditions in the mouse brain, tPA activity was assessed in *ZnT3*$^{+/+}$ and *ZnT3*$^{-/-}$ mice by zymography using a plasminogen overlay assay on coronal brain sections. TPA in the section generates active plasmin from plasminogen in the overlay. Casein in the overlay is digested by plasmin, generating a dark zone over areas of tPA activity (Tsirka et al., 1997). TPA activity was prominent over the hilus and CA3 subregions of both *ZnT3*$^{+/+}$ and *ZnT3*$^{-/-}$ hippocampi (Fig. 10 A) in a pattern similar to that described by Tsirka et al. (1997). The extent of the dark zone of casein dissolution was similar between *ZnT3*$^{+/+}$ and *ZnT3*$^{-/-}$ mice (Fig. 10 A), indicating similar tPA activity under normal brain activity. Thus, tPA activity was similar regardless of the presence of zinc as an inhibitor.

B. Sensorimotor functions

Zinc is present in terminals of cortical projections to the striatum (Frederickson, 1989; Vincent and Semba, 1989), where it may be capable of modulating dopamine receptors (Schetz et al., 1999). Motor coordination was measured in the *ZnT3*$^{-/-}$ mice using the rotarod (Thomas and Palmiter, 1997), the pole test (Ogawa et al., 1985) and the cagetop test. In the rotarod test (Fig. 11 A), mice were placed on a stationary cylinder (rotarod; San Diego Instruments). After 3 sec, the rotarod was switched on to a speed of 4 rpm, and the mice were timed until they fell, with a maximum cutoff of 90 sec. Mice were tested for 4 trials in succession, with 1 min between trials. There were no significant differences in latency to fall from the rotarod (Fig. 11 A). The trend of poor performance for the naïve *ZnT3*$^{-/-}$ mice was not statistically significant. Coordination was also tested in this same group of mice by placing the mice head-upward at the top of a rough-surfaced vertical metal pole (~1 cm diameter; 55 cm height), and recording the latency to reach the bottom of the pole (Pole test, Fig. 11 B). At the start of testing, mice explored the base of the pole for 20 sec, then mice were tested for 3 trials in succession, with a 20 sec reward period between trials. Mice that remained at the top of the pole for the duration of the test (60 sec) were assigned a latency of 60 sec. There were no significant differences in pole descent latency between *ZnT3*$^{+/+}$ and *ZnT3*$^{-/-}$ mice (Fig. 11

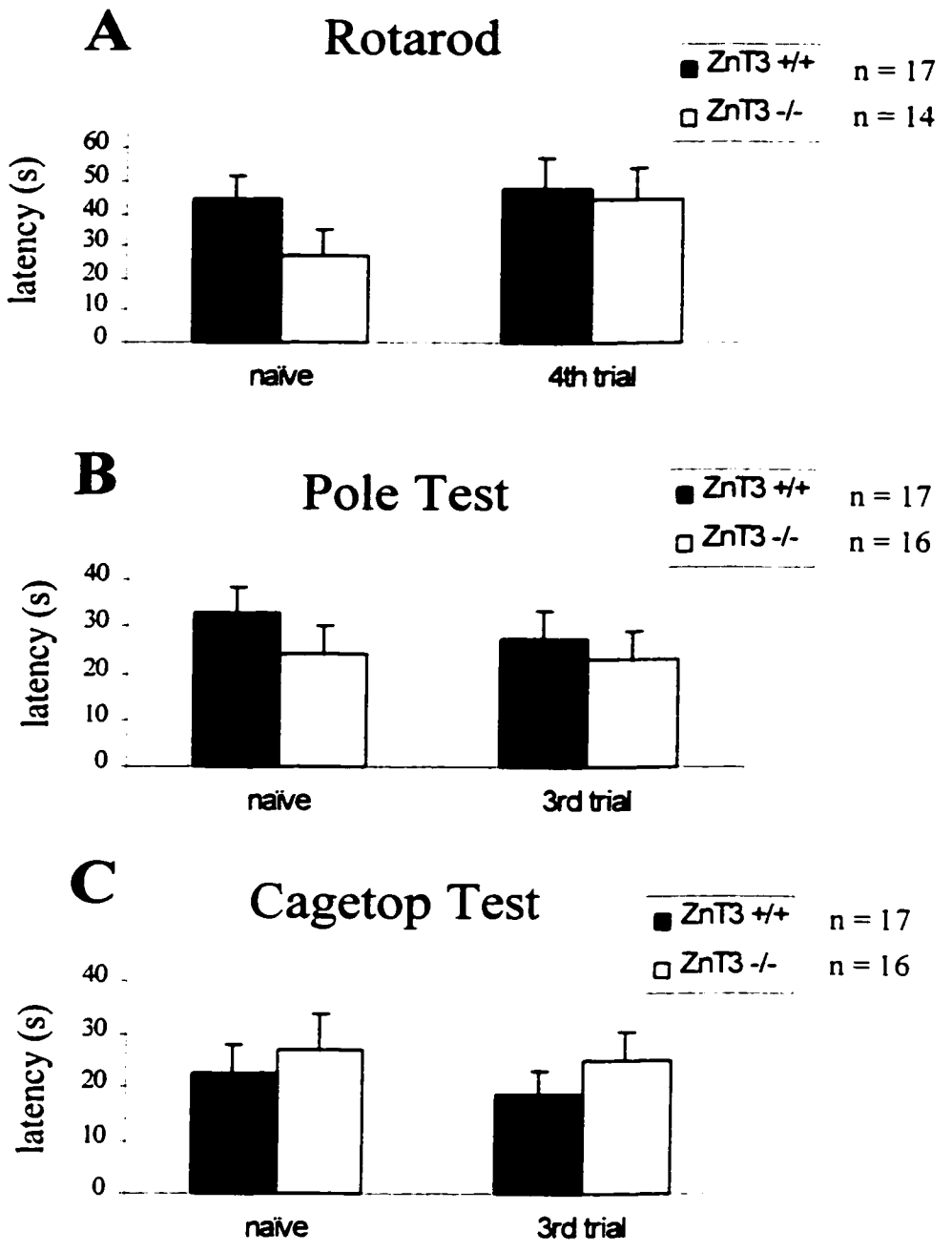

Figure 11. Motor coordination is normal in *ZnT3*$^{-/-}$ mice.

Latencies to fall off of the rotarod (A), descend a pole (B), or descend from the cagetop (C) were similar to those for wild-type mice. Mice were tested for several trials in succession. Neither naïve mice (trial 1) nor trained mice (trials 3 or 4) showed any significant differences relative to wild-type controls.

B). Finally, motor coordination was tested using a motor task that is commonly observed in the home cage, descent from the cagetop to the bottom of the cage. Mice were placed upside down on the bottom of the wire cagetop of their cage, and the latency to climb down to their cage was measured (Fig. 11 C). Mice were tested 3 times in succession, with about 30 sec between trials. There were no significant differences in cagetop descent latency between *ZnT3*$^{+/+}$ and *ZnT3*$^{-/-}$ mice (Fig. 11 C).

Many behavioral tests are dependent on the assumption that experimental and control groups display similar levels of anxiety. Anxiety was tested using the elevated plus maze (Lister, 1987) and by measuring activity in a novel environment. The elevated plus maze consists of two "closed" (walled) and two "open" (unwalled) arms connected by a central platform elevated 39 cm above the floor. Mice were placed in the center of the maze, and the amount of time the mice spent in the open versus the closed arms was measured. Mice with higher levels of anxiety spend a greater percentage of time in the closed arms than the open arms, presumably reflecting the innate tendency of mice to seek out enclosed spaces. *ZnT3*$^{-/-}$ mice spent an equivalent amount of time as *ZnT3*$^{+/+}$ mice in the exposed open arms (Fig. 12 A), indicating that anxiety is similar among mice of both genotypes. Open field activity was examined to assess behaviors that are dictated by a combination of anxiety, curiosity, and locomotor drive. In the first test of open field activity, mice were placed in a novel rat cage and ambulations were measured as successive light-beam breaks in a photobeam activity chamber (San Diego Instruments)(Fig. 12 B). Data were collected in 5-min bins for 60 min. Although *ZnT3*$^{-/-}$ mice appeared to ambulate less frequently shortly following introduction into the chamber, which might reflect heightened anxiety, the number of ambulations was not significantly different from the number of ambulations made by *ZnT3*$^{+/+}$ mice (Fig. 12 B). In a different group of mice, activity in the open field was monitored using a computerized tracking system that allowed measurement of the time spent in the most exposed portion of the open field, the center, versus the outer edge. Mice were placed in a white box (48 cm by 48 cm) for 30 min, and movements were tracked with the Polytrack system (San Diego Instruments). Both *ZnT3*$^{+/+}$ and *ZnT3*$^{-/-}$ mice had latencies

Figure 12. Exploratory behavior and anxiety are normal in *ZnT3*$^{-/-}$ mice.

(A) Elevated plus maze. *ZnT3*$^{-/-}$ mice spent the same percentage of time in the exposed open arms as wild-type mice. (B) Ambulatory activity. Ambulations were counted as successive light-beam breaks following introduction into a novel environment (a rat cage with novel bedding). Although *ZnT3*$^{-/-}$ mice had a tendency to ambulate less frequently following introduction into the chamber, this tendency was not statistically significant. (C-E) Open field behavior. Mice were placed in a brightly lit open field, and movements were tracked by software-assisted contrast detection. (C) Latency to enter center area of the open field. (D) # entries into center area. (E) Dwell time in center area. There were no significant differences between *ZnT3*$^{-/-}$ and *ZnT3*$^{+/+}$ mice.

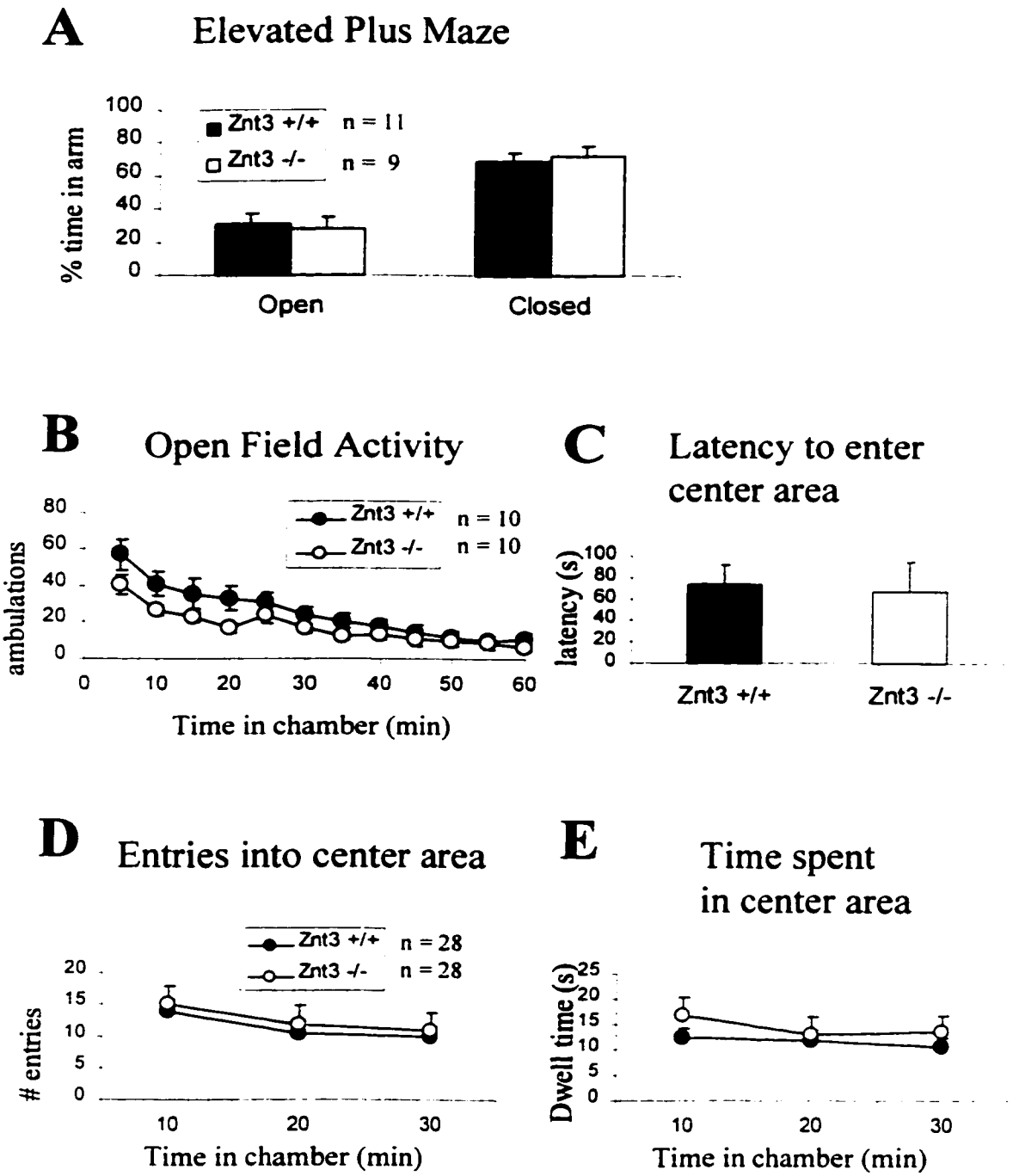
A
Elevated Plus Maze
% time in arm
100
80
60
40
20
0
Znt3 +/+ n = 11
Znt3 -/- n = 9
Open
Closed
B
Open Field Activity
ambulations
80
60
40
20
0
Znt3 +/+ n = 10
Znt3 -/- n = 10
0
10
20
30
40
50
60
Time in chamber (min)
C
Latency to enter center area
latency (s)
100
80
60
40
20
0
Znt3 +/+
Znt3 -/-
D
Entries into center area
entries
20
15
10
5
0
Znt3 +/+ n = 28
Znt3 -/- n = 28
10
20
30
Time in chamber (min)
E
Time spent in center area
Dwell time (s)
25
20
15
10
5
0
10
20
30
Time in chamber (min)

of 60 to 70 sec on average to enter the center area (25 cm x 25 cm)(Fig. 12 C). Total number of entries into the center area, and dwell time in the center area were measured in three 10 min bins (Fig. 12 D, E). There were no significant differences in any of these behaviors between *ZnT3*$^{+/+}$ and *ZnT3*$^{-/-}$ mice.

Zinc and ZnT3 are present in excitatory terminals of the dorsal cochlear nucleus (Frederickson, 1989; Rubio and Juiz, 1998; Cole et al., 1999), suggesting that the absence of zinc might affect hearing. Prepulse inhibition, a commonly used test of schizophrenic behavior in both humans and rodents (Swerdlow et al., 1998; Sallinen et al., 1998), has also been used to assess hearing loss in mice by adjusting the intensity of the prepulse or pulse (Willott et al., 1994). Auditory startle threshold and threshold for prepulse inhibition of the startle response were assessed with a startle reflex box (San Diego Instruments), similarly as described (Willott et al., 1994). For both tests, mice were placed into a small cylindrical chamber (4 cm by 10 cm) small enough to restrict movement but large enough that the mice could still turn around within it. The chamber was attached to a plexiglass platform with a piezoelectric sensor mounted to the bottom to measure the startle response to an auditory stimulus. The platform was placed inside a soundproof box with a 2 inch speaker mounted 15 cm above the enclosure. Mice were allowed to habituate for 2 min, then a series of auditory stimuli (40-msec pulses of white noise) were presented to the mice in random order, with 5 to 30 sec between pulses. For assessing startle threshold, pulse intensities ranging from 0 to 125 dB were presented in random order, with each intensity of pulse repeated at least 4 times. Startle response was measured only within the first 100 msec following the pulse to reduce contamination by background movement of the mouse. The threshold pulse intensity sufficient to produce a startle response was between 50 and 70 dB for both *ZnT3*$^{+/+}$ and *ZnT3*$^{-/-}$ mice (Fig. 13 A). Prepulse inhibition was tested in a similar manner, except the startle pulse was always 115 dB, and it was preceded by a prepulse of varying intensity, with a 100 msec interval between prepulse and pulse. Prepulse intensities were presented in random order throughout testing, with each intensity used at least 4 times. For controls, the pulse was given alone (0 dB prepulse), or startle was recorded in the absence of any audio stimulus

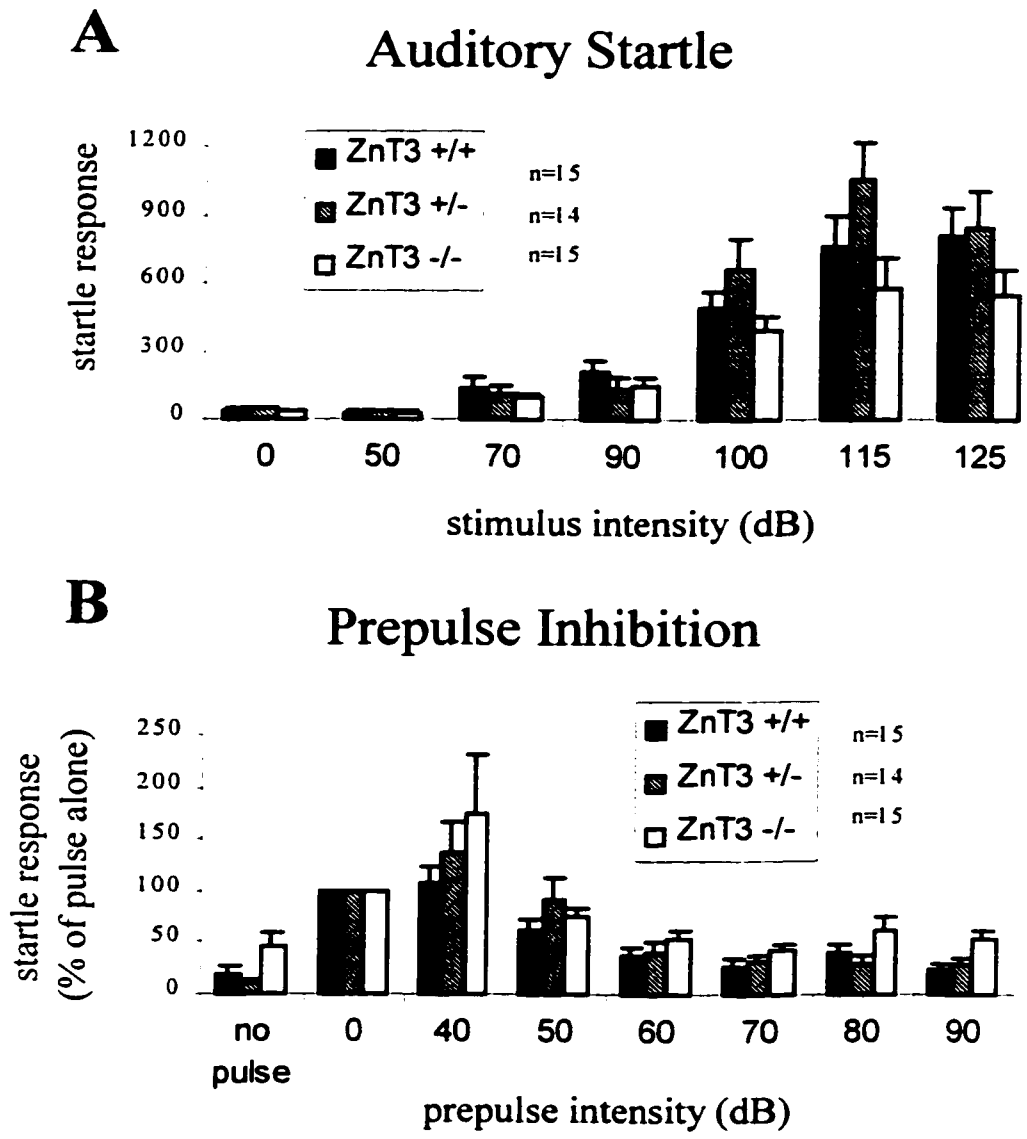

Figure 13. Auditory threshold is normal in *ZnT3*$^{-/-}$ mice.

Auditory startle threshold and threshold for prepulse inhibition of the startle response were tested with a startle reflex box. (A) Auditory startle threshold. *ZnT3*$^{-/-}$ mice showed a similar startle response curve to increasing intensities of auditory stimuli as *ZnT3*$^{+/+}$ mice. (B) Prepulse inhibition. In *ZnT3*$^{-/-}$ and *ZnT3*$^{+/+}$ mice, equivalent prepulse intensities inhibited the subsequent startle response to the 115 dB pulse to a similar extent. Startle response in (B) is plotted as % of the startle response to the pulse alone. For both genotypes, the threshold for prepulse inhibition (50-70 dB) was similar to the threshold for auditory startle.

(no pulse). The threshold prepulse intensity that was sufficient to allow inhibition of the subsequent startle response to the pulse was similar for *ZnT3*$^{-/-}$ and *ZnT3*$^{-/-}$ mice (Fig. 13 B). Data are presented relative to the startle response to the 115 dB pulse alone. Thus, auditory threshold (and sensorimotor gating) is normal in *ZnT3*$^{-/-}$ mice.

ZnT3 and histochemically reactive zinc are present in terminals of neurons in the granule cell layer, periglomerular layer, and glomerular layer of the olfactory bulb (Friedman and Price, 1984; Jo et al., 2000a), where zinc has been suggested to act as a neuromodulator (Trombley and Shepherd, 1993). Olfaction was tested in the *ZnT3-/-* mice in two ways. Gross deficits in olfaction were tested by measuring the latency to find food that was hidden underneath the bedding. Mice were food-deprived for 18 hr, then placed in a cage (~ 50 cm by 50 cm) containing 2 inches of wood-chip bedding, under which a food pellet (regular mouse chow) was hidden. Latency to discover the food (drag it out of the bedding) was measured in three separate trials, with a 5-min, inter-trial interval. *ZnT3*$^{-/-}$ mice had similar food-recovery latencies as *ZnT3*$^{+/+}$ mice (Fig. 14 A). Olfactory threshold was tested with a conditioning paradigm that required the mice to associate a non-noxious odor (peppermint oil) with an aversive stimulus (quinine) in their drinking water. Mice were water-deprived for 18 hr, then given water bottles containing quinine and peppermint oil for three days, with fresh water given in addition two times daily. Mice were then given 10 practice trials in a two-choice paradigm (water versus quinine-peppermint). Mice were then tested every other day, following 18-hr water-deprivation, for preference in the two-bottle paradigm, with various concentrations (serial dilutions presented in random order) of peppermint oil, Each concentration was presented at least four times over all of the testing days. Mice were given fresh water daily for 30 min in the afternoon. Odorant was diluted for each mouse until the threshold odorant concentration sufficient to allow avoidance of the quinine-containing water was reached (i.e., choice of quinine-containing water 50% of the time). For *ZnT3*$^{-/-}$ and *ZnT3*$^{+/+}$ mice, olfactory threshold was similar (50% correct choice was attained at a similar concentration of peppermint oil, Fig. 14 B).

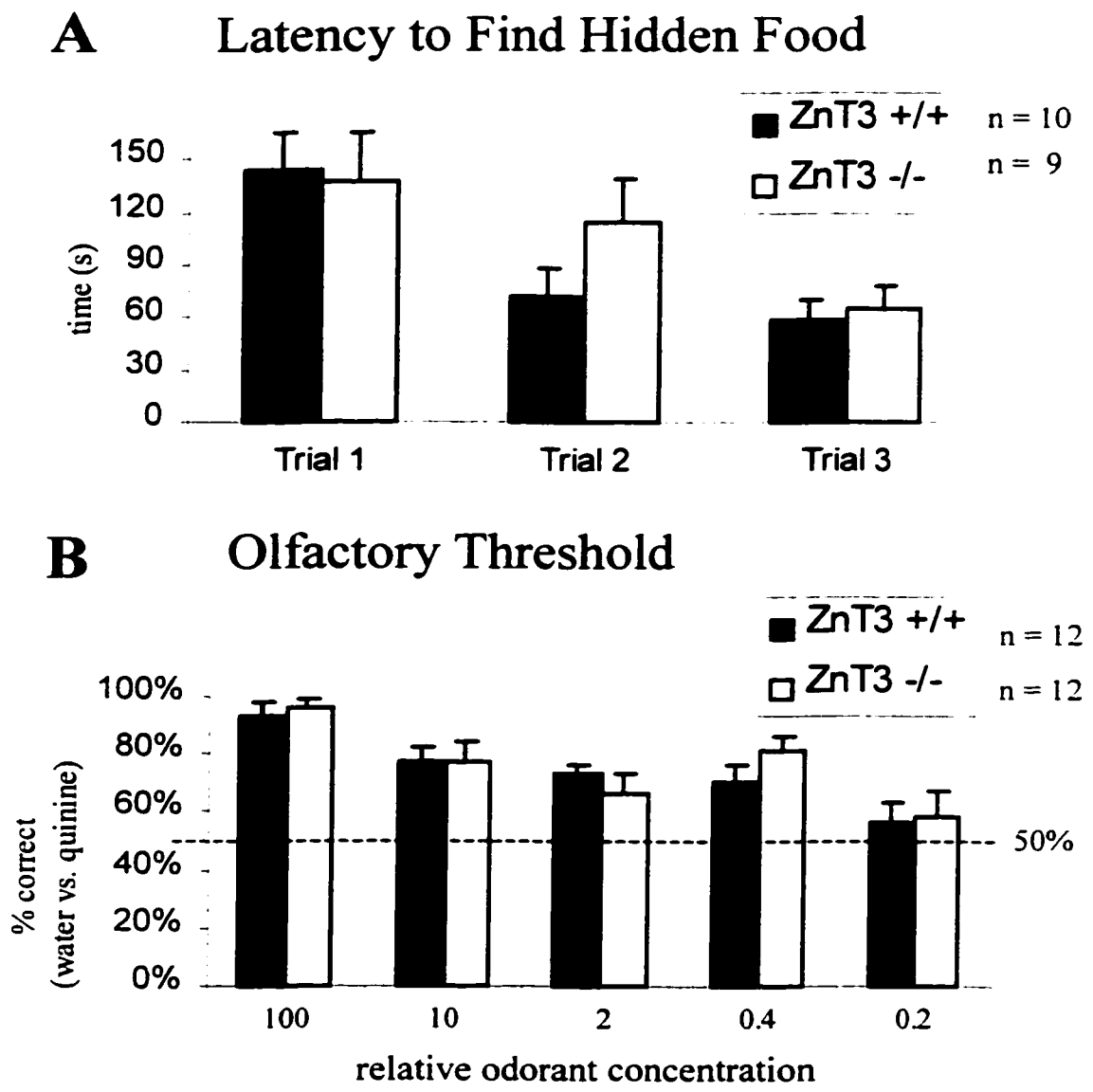

Figure 14. Olfactory threshold is normal in *ZnT3*$^{-/-}$ mice.

(A) Latency to recover food hidden beneath the bedding was similar for food-deprived *ZnT3*$^{+/+}$ and *ZnT3*$^{-/-}$ mice. (B) Olfactory threshold. Odorant (peppermint oil) was paired with an aversive stimulus (quinine) in a two-water-bottle choice paradigm. Following 10 training trials, mice were tested for 4 trials, scoring whether they chose water (correct) or quinine (incorrect). Over subsequent days, mice were tested with randomized dilutions of odorant to determine the threshold odorant concentration sufficient to allow avoidance of the quinine-containing water (i.e., 50% correct). *ZnT3*$^{+/+}$ and *ZnT3*$^{-/-}$ mice had similar olfactory threshold curves.

ZnT3 and zinc are present in both excitatory and inhibitory terminals in the dorsal and ventral horns of mouse spinal cord (Danscher, 1982; Jo et al., 2000b,c), and injection of zinc or zinc chelators has been shown to alter nociceptive activity in mice (Larson and Kitto, 1997; 1999). We assessed nociception in *ZnT3*$^{-/-}$ mice by measuring tail-flick latency in response to a heat lamp, and separately by measuring latency to respond to thermal stimulation from a hot plate (Mogil et al., 1999). For the tail-flick assay, mice were restrained in a plastic tube and the tail was exposed to the heat lamp of a tail-flick apparatus. Latency to remove the tail from the heat was used as a measure of thermal nociception. *ZnT3*$^{-/-}$ mice had significantly longer latencies to remove their tail from the heat lamp, suggesting that nociception is impaired in these mice. However, the 129/SvJ strain of mice, from which the *ZnT3*$^{-/-}$ mice were derived, also have higher tail-flick latencies than C57Bl/6 mice (Mogil et al., 1999), suggesting that this effect could be due to a 129/SvJ allele closely linked to the targeted mutation, rather than an effect of the gene disruption itself. The difference in tail-flick latency between 129/SvJ and C57Bl/6 mice disappears if the mice are allowed to acclimate to the restraint tube (G. Terman, unpublished observations), and is perhaps related to heightened anxiety in the 129/SvJ mice. When *ZnT3*$^{-/-}$ mice were allowed to acclimate for 1 hr to the restraint tube, there was no difference in tail-flick latency compared to *ZnT3*$^{+/+}$ mice. Thus, the difference in tail-flick latency seen in the absence of acclimation to the tube is not a difference in nociception, but probably reflects a behavioral difference due to a "hitchhiking" 129/SvJ allele. A different group of mice were tested in the hot plate test, another paradigm for assessing thermal nociception. Mice were placed on a 51° C hot plate, surrounded by a plexiglass cylinder that gave the mouse room to move, groom and jump. Upon the first behavior indicative of thermal discomfort (licking of hindpaws or jumping), the mouse was removed from the hot plate and the latency to this first response was recorded as a measure of thermal nociception. Latency to first response was similar for *ZnT3*$^{+/+}$ and *ZnT3*$^{-/-}$ mice (Fig. 15 B), confirming that thermal nociception is normal in the absence of vesicular zinc.

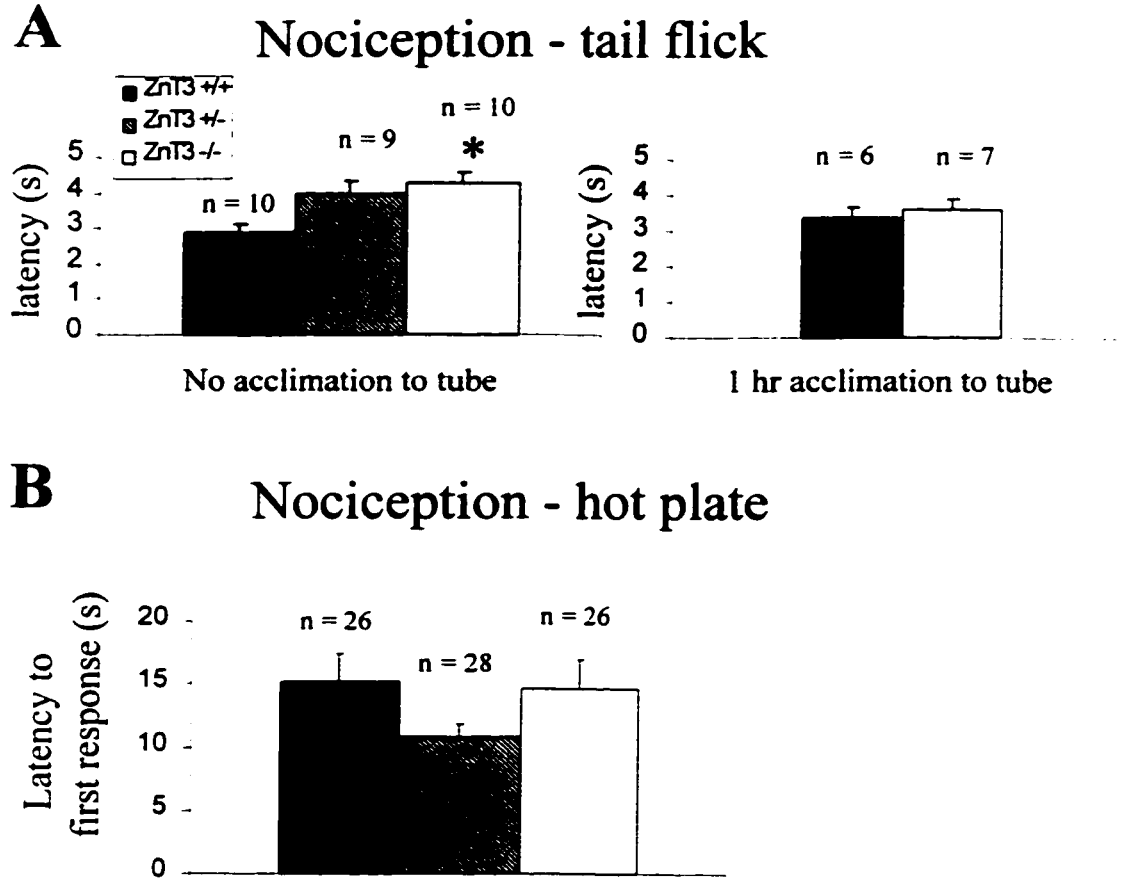

Figure 15. Nociception is normal in *ZnT3*$^{-/-}$ mice.

(A) Tail-flick assay. *ZnT3*$^{-/-}$ mice had significantly longer latencies to remove their tail from the heat lamp ($p < 0.005$, Student's t-test), suggesting impaired nociception. However, 1 hr acclimation to the restraint tube abrogated the difference in tail-flick latency between *ZnT3*$^{+/+}$ and *ZnT3*$^{-/-}$ mice, indicating that the difference seen in the absence of acclimation was not due to a difference in nociception. A similar phenomenon has been reported for the 129sv/J vs. C57Bl/6 strains of mice, suggesting that the difference is strain-related rather than an effect of specific gene disruption. (B) Hot plate assay. Latency to first response (hindpaw licking or jumping) after being placed on a 51°C hot plate was similar in *ZnT3*$^{-/-}$ and *ZnT3*$^{+/+}$ mice.

C. Learning and memory

ZnT3 and zinc are present in terminals throughout the limbic circuitry (Crawford and Connor, 1972; Zimmer and Haug, 1978; Appendices A and B), and zinc or zinc chelators can exert effects on neuronal excitability and long term potentiation in hippocampal slices (Smart et al., 1994; Weiss et al., 1989). Reference memory and working memory were tested in the *ZnT3*$^{-/-}$ mice using several different paradigms that required the mouse to learn different kinds of tasks varying in complexity and information content. Passive inhibitory avoidance (Thomas and Palmiter, 1997) was used as a test of the ability to make a simple association between an aversive stimulus (footshock) and entry into a dark chamber. One chamber of a shuttle box (Coulbourn Instruments) was lined with black plastic, while the other chamber remained well-lit. Mice were placed in the lighted chamber and the latency to enter the dark chamber through an inter-connecting door was recorded. The door was lowered and a 0.7 mA shock was delivered through the floor bars for 1 sec, using a grid-scanning shocker (Coulbourn Instruments). After 10 sec, the mice were returned to their home cage. Testing was identical to training except no shock was delivered after the mouse entered the dark chamber. Mice were tested 2 hr, 1 day, 7 days, and 28 days after training. *ZnT3*$^{+/+}$ and *ZnT3*$^{-/-}$ mice learned to avoid the dark chamber, and had similar retention up to 28 days post-training (Fig. 16).

Contextual fear conditioning was used to test learning that involves the hippocampus and amygdala (reviewed in McGaugh et al., 1996). Mice were placed in one chamber of a shuttle box (Coulbourn Instruments), and movements were monitored every 8 sec, scoring behavior as "freezing" (absence of any movement except respiration) or "no freezing". Freezing behavior was used as a measure of fear associated with an aversive stimulus (footshock). Training was conducted by placing the mouse in the shock box for 2 min, then delivering 3 tone-shock pairs at 1 min intervals, with each tone-shock pair consisting of a 30-sec tone (2 kHz; 80 dB) paired with a 0.7 mA footshock (delivered during the last 2 sec of the tone). After the final tone-shock pair, mice were monitored for 1 min, then removed to their home cage. *ZnT3*$^{+/+}$ and *ZnT3*$^{-/-}$ mice both spent a higher

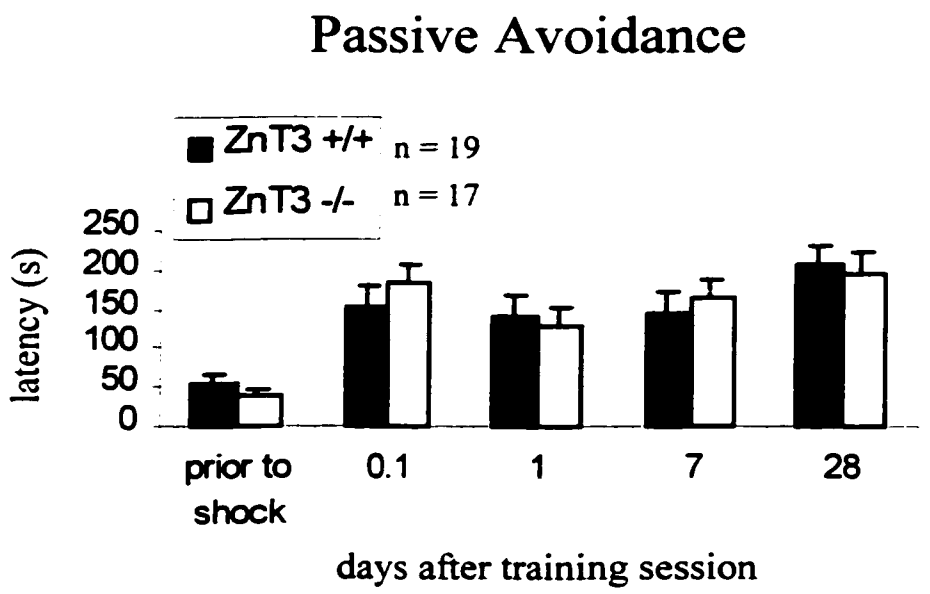

Figure 16. Passive inhibitory avoidance.

The latency to re-enter the dark chamber of a shuttle box after receiving a shock in that chamber was recorded as a measure of simple associative learning. *ZnT3*$^{+/+}$ and *ZnT3*$^{-/-}$ mice learned to avoid the dark chamber after receiving the shock, and retained the association for at least 28 days following training.

percentage of the time freezing as training progressed, whereas control mice that received the identical training in the absence of a footshock were unaffected (Fig. 17 A). Mice were tested the next day for fear conditioning to the context (hippocampus- and amygdala-dependent learning) by placing them back in the shock box for 6 min, without delivering a shock. *ZnT3*$^{+/+}$ and *ZnT3*$^{-/-}$ mice that received shocks in the training trial spent a significant percentage of time freezing upon exposure to the context of the shock box, and decay of the freezing response over the 6-min recording period was similar between *ZnT3*$^{+/+}$ and *ZnT3*$^{-/-}$ mice (Fig. 17 B). On the second day after training, mice were tested for fear conditioning to the auditory cue by placing them in a novel cage (a rat cage with corn cob bedding) in a different room from the training room, to reduce the possibility of fear conditioning to context. After 2 min in the novel cage, the same auditory cue used during training was presented for 4 min, and freezing was monitored as a measure of fear conditioning to the cue (hippocampus-independent learning). *ZnT3*$^{+/+}$ and *ZnT3*$^{-/-}$ mice actively explored the new cage for the first 2 min, and presentation of the cue caused mice of both genotypes to spend an equivalent percentage of time freezing, with equivalent decay times for freezing behavior as the cue continued to be presented (Fig. 17 C). Control mice that did not receive a shock during training continued to actively explore the cage upon presentation of the cue. Thus, *ZnT3*$^{-/-}$ mice do not show any deficits in this form of aversive conditioning.

Spatial learning, reversal, and retention were tested using the Morris water maze (Morris, 1984; Thomas and Palmiter, 1997). A steel circular water tank 59.5 cm high and 115 cm in diameter, painted white and filled with water plus 4 gallons of whole milk, to a level of 36 cm was used. A circular platform 10 cm in diameter was submerged 1 cm below the surface of the water in the middle of one quadrant, and prominent visual cues were placed outside the tank. A video camera was mounted above the tank and mouse movements were tracked with a computerized videotracking device (Polytrack system, San Diego Instruments). Mice were placed in the pool between quadrants, with the drop location changing for each trial but the platform location remaining constant. For each trial mice were allowed to search for the platform for 60 sec, then they were dragged to

Figure 17. Contextual and cued fear conditioning.

Spatial (contextual) and associative (cued) learning were tested in $ZnT3^{+/+}$ and $ZnT3^{-/-}$ mice with a fear conditioning paradigm. Mice were placed in a shock box and movements were monitored every 8 seconds, scoring freezing as + (no movement besides respiration) or – (any movement). (A) Training consisted of 3 tone-shock pairs (30 sec tone; 2 sec shock) delivered at 1 min intervals. Percent time freezing increased with training for all $ZnT3^{+/+}$ and $ZnT3^{-/-}$ mice that received a shock. (B) 24 hr later, mice were placed back in the shock box and freezing behavior was scored for 6 min to measure fear response to the context of the box (hippocampus- and amygdala-dependent learning). (C) 48 hr after training, mice were placed in a novel rat cage in a different room. Freezing was scored for 6 min, with presentation of the auditory cue for the last 4 min, to test associative learning (amygdala-dependent learning). No differences were detected between $ZnT3^{+/+}$ and $ZnT3^{-/-}$ mice.

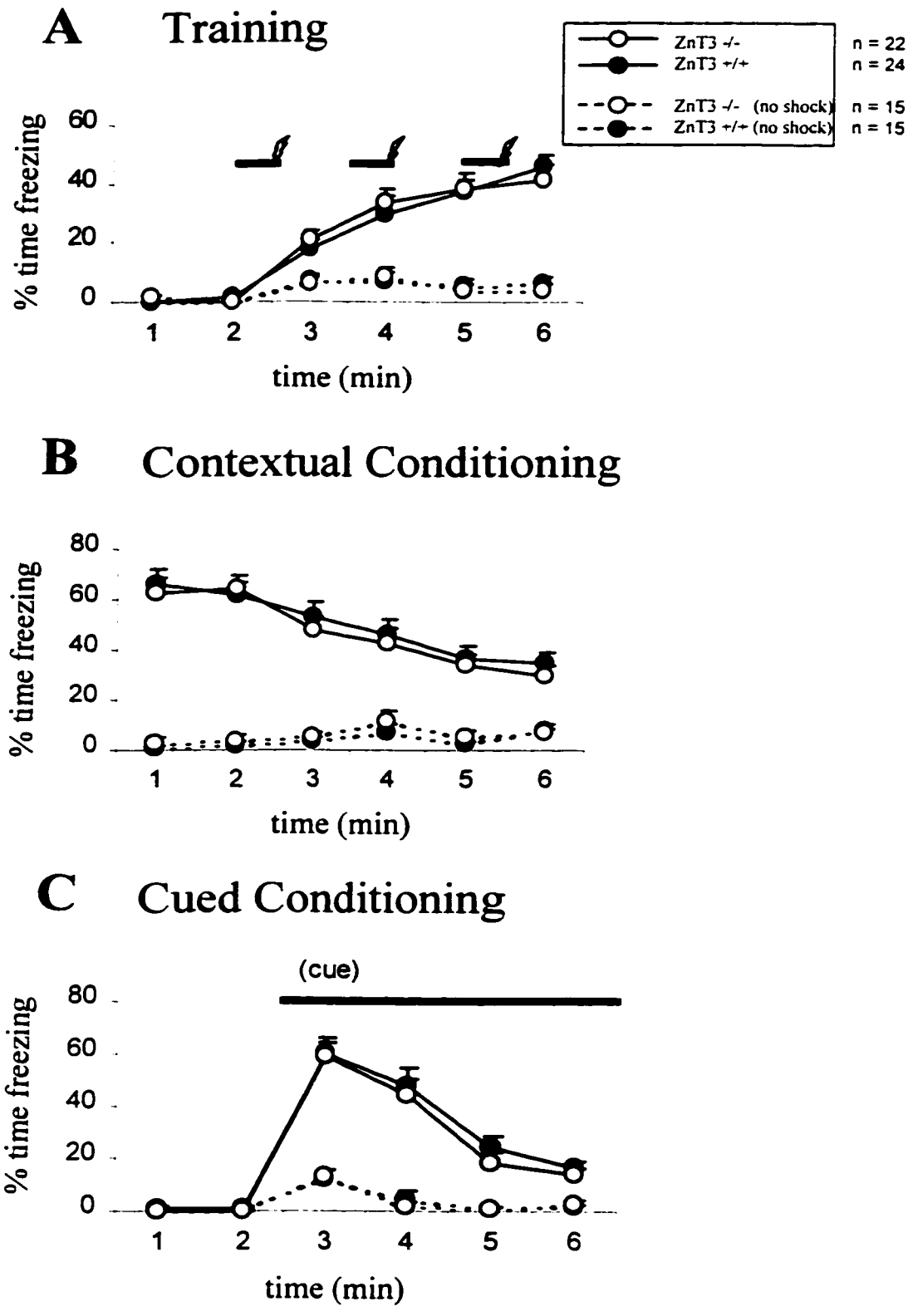
A
Training
ZnT3 -/-
ZnT3 +/+
ZnT3 -/- (no shock)
ZnT3 +/+ (no shock)
n = 22
n = 24
n = 15
n = 15
% time freezing
60
40
20
0
1
2
3
4
5
6
time (min)
B
Contextual Conditioning
% time freezing
80
60
40
20
0
1
2
3
4
5
6
time (min)
C
Cued Conditioning
(cue)
% time freezing
80
60
40
20
0
1
2
3
4
5
6
time (min)

the platform if they did not locate it themselves. After remaining on the platform for 10 sec, the mice were dried off and removed to a warm cage. Mice were trained for 3 trials (1 session) per day for 7 days, with trials for each mouse separated by about 2 hr. *ZnT3*$^{+/+}$ and *ZnT3*$^{-/-}$ mice learned the task equivalently, since latency to find the platform decreased over the training sessions (not shown), and they traversed a shorter distance (path length) before finding the platform (Fig. 18 A). For half of the mice trained in this task, reversal of spatial learning was tested by placing the platform in the opposite quadrant from where it had previously been located and testing the mice for extinction of the old platform location and learning of the new location over 9 additional trials (3 sessions)(Fig. 18 B). *ZnT3*$^{+/+}$ and *ZnT3*$^{-/-}$ mice learned the new platform location within 3 or 4 trials, but *ZnT3*$^{-/-}$ mice required 1 more trial to acquire the new platform location (i.e., path length to the platform was significantly greater in trial 2; Fig. 18 B). This same group of mice was then tested with a platform made visible with a local cue (the platform was raised just above the level of the water and a black ping-pong ball was attached to the platform) to test the mice in a simpler learning paradigm that does not require the hippocampus. Path length to the visible platform was equivalent for the two genotypes (Fig. 18 C). The other half of the mice trained in the Morris water maze task were not tested for reversal of spatial learning. With these mice, retention of platform location was tested immediately following training (Fig. 18 D). Retention was tested in probe trials at 1, 7, 14, 21, and 28 days post-training by removing the platform from the maze and allowing mice to search the maze for 60 sec. The percentage of time spent searching in the correct quadrant (the quadrant where the platform had been located) versus the opposite quadrant was recorded as a measure of spatial memory retention. *ZnT3*$^{+/+}$ and *ZnT3*$^{-/-}$ mice had similar long-term retention of the platform location (Fig. 18 D). Swim speed was similar for *ZnT3*$^{+/+}$ and *ZnT3*$^{-/-}$ mice (Fig. 18 E).

Zinc chelators disrupt spatial working memory, but not reference memory, in rats tested in a delayed-matching-to-sample variant of the Morris water maze (Frederickson et al., 1990). This test was adapted to test working memory in the *ZnT3*$^{+/+}$ and *ZnT3*$^{-/-}$ mice. For the delayed-matching-to-sample variant of the Morris water maze, a different group

Figure 18. Morris Water Maze: Learning, retention, reversal, and delayed-match-to-sample.

(A) Mice were trained for 7 sessions (21 trials) over a 7-day period, with the submerged platform always in the same location, but the start location changing with each trial. By the 7th session, *ZnT3*$^{+/+}$ and *ZnT3*$^{-/-}$ mice traversed a shorter path length than in earlier sessions to locate the platform, indicating successful acquisition of the task. (B) For half of the mice of each genotype, the platform location was reversed (changed to the opposite quadrant), and extinction/relearning was assessed for 3 more sessions (9 trials). *ZnT3*$^{-/-}$ mice required 1 more trial than *ZnT3*$^{+/+}$ mice to acquire the new platform location (the path length for trial #2 was significantly greater for *ZnT3*$^{-/-}$ mice; $p < 0.005$, Student's *t*-test). (C) For the same group of mice tested in (B), the platform was then made visible by raising it above the surface of the water and attaching a prominent cue (a dark ping-pong ball). Path length to the platform, recorded for 6 more trials, was similar between *ZnT3*$^{+/+}$ and *ZnT3*$^{-/-}$ mice. (D) Retention was tested at 1, 7, 14, 21 and 28 days post-training in the remainder of mice trained in (A) by removing the platform and monitoring the amount of time spent searching in the region where the platform had been located. *ZnT3*$^{+/+}$ and *ZnT3*$^{-/-}$ mice both spent about 40% of the time in the quadrant where the platform had been previously located (correct), and about 15% of the time in the opposite quadrant, and retained the spatial information equally well for at least 28 days. (E) Swim speed was similar between the 2 genotypes. (F) To test working memory, a delayed-matching-to-sample variant of the Morris Water Maze was used with a different group of mice ($n = 12$ each genotype). Mice were tested for 14 sessions over 14 days, with each session consisting of 2 trials separated by a 10 sec interval. Platform location changed for each session, but remained the same for both trials within a session, allowing mice to utilize working memory to locate the platform on the 2nd trial of each session. Percent reduction in latency from the 1st to 2nd trial of each session was used as a measure of working memory. As shown in (F), even the wild-type mice do not appear to be capable of learning this task, as on average, the 2nd trial latency was longer than the 1st trial latency.

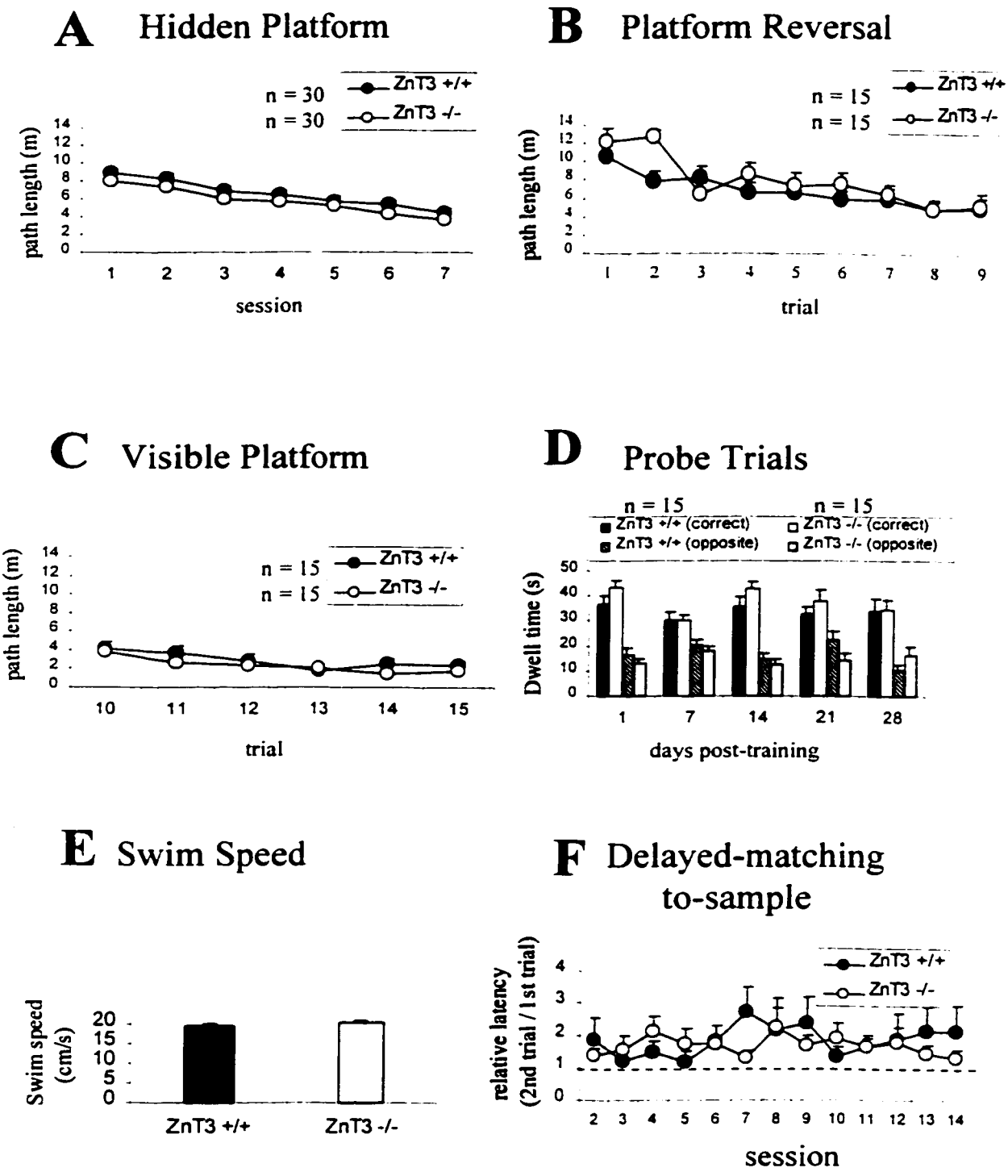
A Hidden Platform
n = 30
n = 30
ZnT3 +/+
ZnT3 -/-
path length (m)
session
B Platform Reversal
n = 15
n = 15
ZnT3 +/+
ZnT3 -/-
path length (m)
trial
C Visible Platform
n = 15
n = 15
ZnT3 +/+
ZnT3 -/-
path length (m)
trial
D Probe Trials
n = 15
n = 15
ZnT3 +/+ (correct)
ZnT3 +/+ (opposite)
ZnT3 -/- (correct)
ZnT3 -/- (opposite)
Dwell time (s)
days post-training
E Swim Speed
Swim speed (cm/s)
ZnT3 +/+
ZnT3 -/-
F Delayed-matching to-sample
relative latency (2nd trial / 1st trial)
ZnT3 +/+
ZnT3 -/-
session

of mice was tested for 14 sessions over 7 days, with each session consisting of 2 trials separated by a 10-sec interval. Platform location changed for each session, but remained the same for both trials within a session, allowing mice to utilize working memory to locate the platform on the second trial of each session. Since the latency to find the platform in the second trial of each session should be less than that in the first trial of each session, the reduction in latency from the first to second trial of each session is used as a measure of working memory. In contrast to rats, mice do not appear to be capable of learning this task; for both $ZnT3^{+/+}$ and $ZnT3^{-/-}$ mice, the second trial latency was longer than the first trial latency, indicating no improvement in performance in the second trial (Fig. 18 F). Therefore, working memory could not be compared between $ZnT3^{+/+}$ and $ZnT3^{-/-}$ mice using this test.

As an alternative test of working memory, a water version of the radial arm maze was used (Fig. 19 A; Hyde et al., 1998). The maze was constructed of galvanized steel with 8 removable arms (23.1 cm long by 12.8 cm wide) radiating from a central area 48.7 cm in diameter, and was immersed in water so the distance to the top of the maze was about 15 cm. Extra-maze cues were displayed prominently just outside the perimeter of the maze. Hidden escape platforms (7.5 cm by 11 cm) were placed at the ends of 4 of the arms, 1 cm below the surface of the water, while the other 4 arms remained empty. Platform locations were different for each mouse, and remained fixed throughout the experiment. Platform locations were semi-randomly determined, with no more than two platforms in adjacent arms. For each trial, the mouse was released into the maze facing the end of the start arm. Mice were allowed to swim until they located one of the four platforms, or for a maximum time of 2 min, at which time they were dragged to the nearest platform. After remaining on the platform for 20 sec, they were removed to a warm cage under a heat lamp, and the platform located in that trial was removed. Each session consisted of four trials separated by 90 sec inter-trial intervals, requiring the mice to find all four platforms in succession (Fig. 19 A). Mice underwent one training session per day for 12 days, during which time they were required to (1) remember and avoid entering arms that never contained platforms (reference memory); (2) remember and enter the arms that

Figure 19. Radial arm maze: experimental design.

(A) Mice were tested in a water version of the 8-arm radial arm maze. 4 arms contained platforms (platform arms) and 4 arms were always empty (reference arms). For each trial, mice were allowed to swim in the maze until they located a platform, then the mouse and the platform found in that trial were removed from the maze. Each session consisted of 4 trials, with a 90 sec inter-trial interval, requiring mice to locate all 4 platforms in succession. Mice were trained for 12 sessions over 12 days, then retention was tested at 1 wk, 2 wks, and 4 wks, recording the latency to find each platform, the number of working memory errors (reentries into previously-visited arms) and the number of reference memory errors (entries into reference arms). (B-E) Latency to find the platform in each trial. Latencies decreased with training in both $ZnT3^{+/+}$ and $ZnT3^{-/-}$ mice. With increasing task difficulty (increased memory load, eg. in trial 4), the mice took longer to locate a platform initially but latencies still decreased significantly over time.

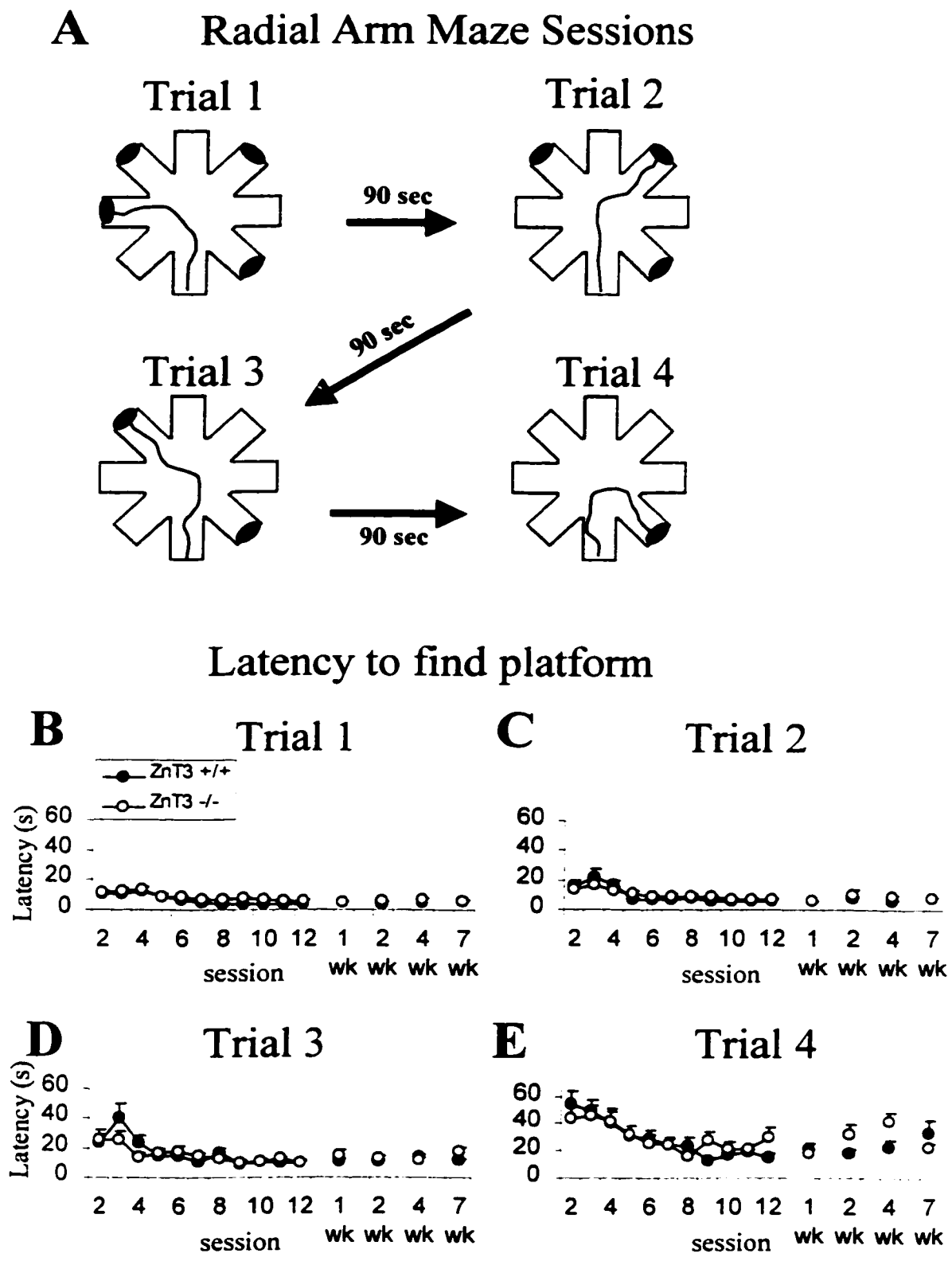
A
Radial Arm Maze Sessions
Trial 1
Trial 2
90 sec
90 sec
Trial 3
Trial 4
90 sec
Latency to find platform
B
Trial 1
ZnT3 +/+
ZnT3 -/-
Latency (s)
60
40
20
0
2 4 6 8 10 12 1 2 4 7
session
wk wk wk wk
C
Trial 2
60
40
20
0
2 4 6 8 10 12 1 2 4 7
session
wk wk wk wk
D
Trial 3
Latency (s)
60
40
20
0
2 4 6 8 10 12 1 2 4 7
session
wk wk wk wk
E
Trial 4
60
40
20
0
2 4 6 8 10 12 1 2 4 7
session
wk wk wk wk

should have platforms (reference memory); and (3) remember not to reenter an arm which had previously contained a platform in that session (working memory). For each trial, latency to find a platform was recorded, and the numbers of working memory errors and reference memory errors were determined. Working memory errors were defined as entries into any arm the mice had previously entered within that session. Reference memory errors were defined as entries or reentries into arms that never contained a platform (reference arms). The increasing difficulty of the task from Trial 1 to Trial 4 allowed assessment of working memory and reference memory under different memory loads. Following the 12 training sessions, working memory and reference memory were tested at 1 wk, 2 wk, 4 wk, and 7 wk, to test long-term retention of the task.

Latency to find a platform decreased with training for both *ZnT3*$^{+/+}$ and *ZnT3*$^{-/-}$ mice for all trials (Fig. 19 B-E), indicating that the mice learned an effective strategy for finding platforms in each of the four trials. Within each session, increased memory load (i.e., trials 3 and 4 versus trials 1 and 2) was associated with longer latency to locate a platform (compare Fig. 19 B and E). At 1, 2, 4 and 7 wk following training, mice of both genotypes continued to have short platform-localization latencies in the first three trials (Fig. 19 B-D). However, in the fourth trial (the trial with the highest memory load) *ZnT3*$^{-/-}$ mice had longer latencies than *ZnT3*$^{+/+}$ mice at 4 wks post-training (Fig. 19 E). Fourth trial latencies were similar between *ZnT3*$^{+/+}$ mice and *ZnT3*$^{-/-}$ mice at 1, 2, and 7 wk post-training.

The numbers of reference memory errors and working memory errors also decreased with training for both *ZnT3*$^{+/+}$ and *ZnT3*$^{-/-}$ mice (Fig. 20). Within each session, the number of working memory errors was higher in trials 3 and 4 than in trial 2 (Fig. 20 C, E, G), consistent with the increased memory load inherent in the later trials of each session. Within each session, the number of reference memory errors was also higher in the later trials (Fig. 20 D, F, H). Since reference memory load should not change within a session, this result suggests that working memory errors are probably interfering with assessment of reference memory. At 1, 2, 4, and 7 wk after training, the number of reference memory errors was similar for *ZnT3*$^{+/+}$ and *ZnT3*$^{-/-}$ mice (Fig. 20 B, D, F, H).

Figure 20. Radial arm maze: working memory and reference memory errors.

Total number of working memory errors (A,C,E,G) and reference memory errors (B,D,F,H). Working memory errors were defined as reentries into any arm previously visited in that session, and reference memory errors were defined as entries (or reentries) into reference arms. (A,B) Total number of working or reference memory errors summed for all 4 trials. (C-H) Number of working or reference memory errors in Trials 2, 3, or 4. The numbers of both working and reference memory errors decreased over the 12 training days for all trials. Within each session, the number of working memory errors increased with each trial (compare C, E, and G), probably reflecting the increased memory load involved in Trials 3 and 4. Unexpectedly, the number of reference memory errors also increased with each trial (compare D,F, and H). There were no differences between $ZnT3^{+/+}$ and $ZnT3^{-/-}$ mice in the numbers of working or reference memory errors made during the 12 training sessions. One, two, four and seven weeks after training, $ZnT3^{+/+}$ and $ZnT3^{-/-}$ mice had similar retention of the locations of reference arms (B, D, F, H). $ZnT3^{-/-}$ mice made a similar number of working memory errors as $ZnT3^{+/+}$ mice at most of these time points (A, C, E, G). In Trial 4, $ZnT3^{-/-}$ mice made significantly more working memory errors than $ZnT3^{+/+}$ mice at 4 wk post-training ($P < 0.05$ Student's t-test), but not at 1 wk, 2 wk, or 7 wk post-training (G).

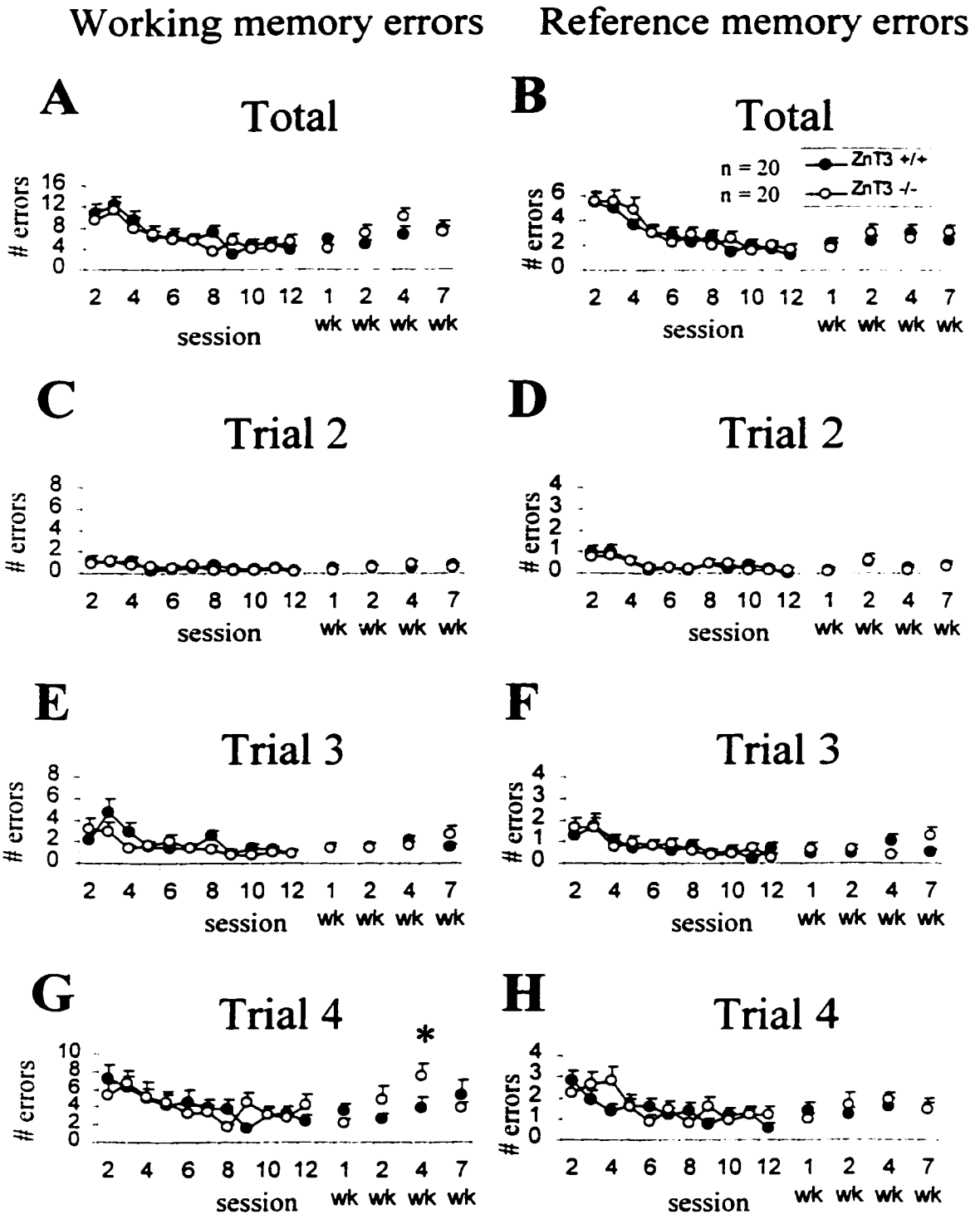
Working memory errors
Reference memory errors
A
Total
B
Total
n = 20
n = 20
ZnT3 +/+
ZnT3 -/-
errors
session
2 4 6 8 10 12 1 2 4 7
wk wk wk wk
C
Trial 2
D
Trial 2
E
Trial 3
F
Trial 3
G
Trial 4
*
H
Trial 4

Figure 21. Radial arm maze: working memory errors (same-trial vs. inter-trial).

Types of working memory errors made by *ZnT3*$^{+/+}$ and *ZnT3*$^{-/-}$ mice during training and retention testing. (A) Number of reentries into arms visited within the same trial (i.e., Type 1 errors). (B) Number of entries into arms visited in the previous trial (~ 1.5 min prior) (i.e., Type 2 errors). (C) Number of entries into arms visited 2 trials ago (~3.5 min prior) (i.e., Type 3 errors). (D) Number of entries into arms visited 3 trials ago (5-7 min prior) (i.e., Type 4 errors). For (B), (C), and (D), only the first entry into a previously visited arm was counted (i.e., same trial reentries were not included). At 4 wks post-training, most of the working memory errors made by *ZnT3*$^{-/-}$ mice were same trial reentries (compare A with B-D). Compared to *ZnT3*$^{+/+}$ mice, at 4 weeks post-training *ZnT3*$^{-/-}$ mice made more same-trial reentries and more Type 4 errors. Most of these errors were made in Trial 4 (see Fig. 19).

Working memory errors

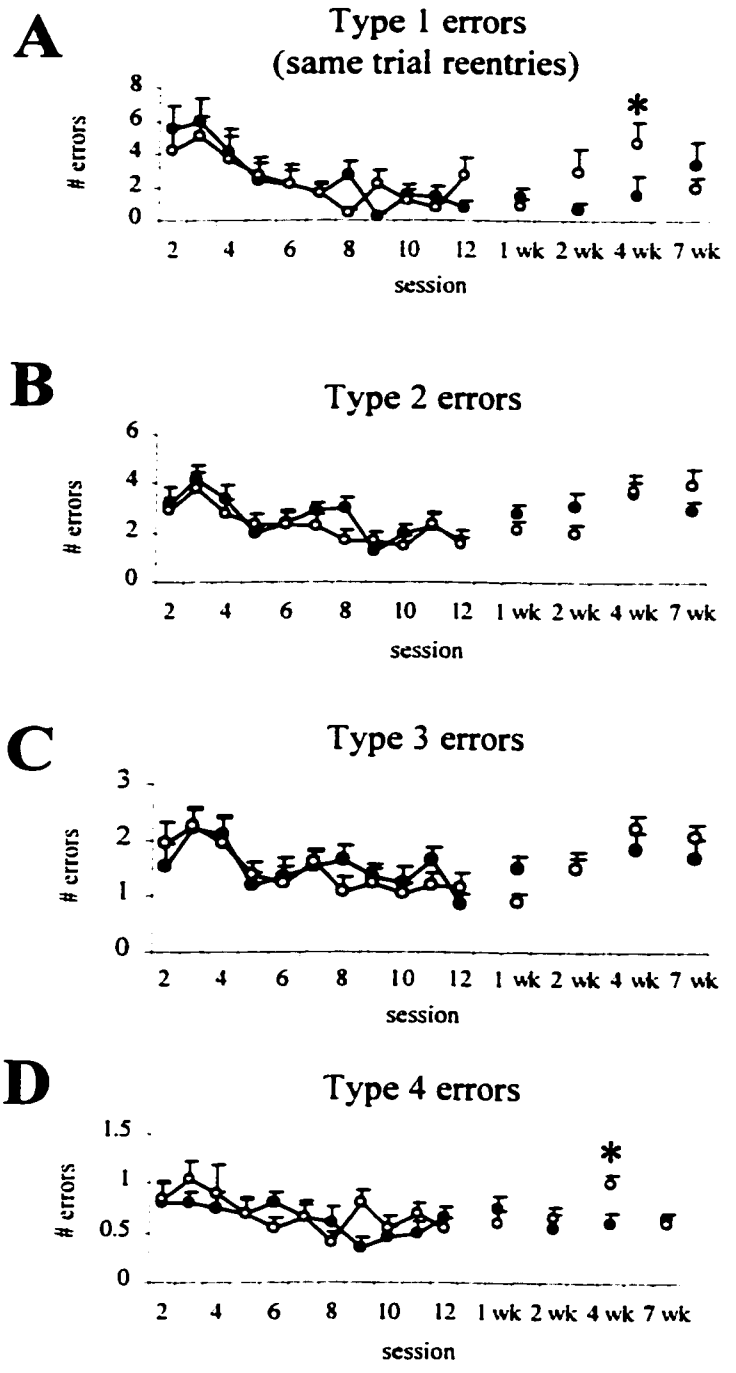

At 4 wks post-training, *ZnT3*$^{-/-}$ mice made significantly more working memory errors than *ZnT3*$^{+/+}$ mice in the fourth trial (Fig. 20 G), suggesting that *ZnT3*$^{-/-}$ mice have poorer retention of complex tasks. However, *ZnT3*$^{-/-}$ mice made a similar number of working memory errors as *ZnT3*$^{+/+}$ mice in the fourth trial at 1, 2, and 7 wk post-training, and the number of working memory errors in the second and third trials at 1, 2, 4, and 7 wk was similar between *ZnT3*$^{+/+}$ and *ZnT3*$^{-/-}$ mice (Fig. 20 C, E). Thus, the higher number of fourth trial working memory errors seen in the mice at 4 wk probably represents variability inherent in the task, rather than a difference between genotypes.

To determine what types of working memory errors *ZnT3*$^{-/-}$ mice made, working memory errors were separated into four types: (1) entries into arms previously visited within the same trial; (2) entries into arms visited in the immediately previous trial; (3) entries into arms visited two trials ago; and (4) entries into arms visited three trials ago. Same-trial reentries (i.e., type 1 working memory errors) occur within seconds of each other, whereas type 2, type 3, and type 4 working memory errors involve 1.5 min, 3.5 min, and 5-7 min intervals, respectively. Type 1 errors can occur in any trial, whereas type 2 errors are limited to trials 2, 3, and 4. Type 3 errors are limited to trials 3 and 4, and type 4 errors are limited to trial 4. At 2 and 4 wk post-training, most of the working memory errors made by *ZnT3*$^{-/-}$ mice were type 1 errors (same-trial reentries) (compare Fig. 21 B-E), whereas *ZnT3*$^{+/+}$ mice made mostly type 2 errors. At 4 wk (but not at 1, 2, or 7 wk), *ZnT3*$^{-/-}$ mice made significantly more type 1 and type 2 errors (Fig. 21 B, E) than *ZnT3*$^{+/+}$ mice. Most of these errors occurred in trial 4.

D. Seizures

To determine whether the net effect of zinc release during prolonged neuronal firing is excitatory or inhibitory, we tested seizure susceptibility of *ZnT3*$^{-/-}$ mice in a number of seizure-induction protocols (Appendix D). *ZnT3*$^{-/-}$ mice do not display spontaneous hyperexcitability, nor were they any more susceptible than *ZnT3*$^{+/+}$ mice to audiogenic seizures or seizures induced by flurothyl, pentylenetetrazol, or bicuculline (Appendix D, Figs. 1, 2, 3; Appendix D, Table 2). *ZnT3*$^{-/-}$ mice were somewhat less sensitive than

ZnT3$^{+/+}$ to mild seizures (e.g., myoclonic jerks) induced by low doses of the $GABA_A$ receptor antagonist, bicuculline, whereas higher doses of bicuculline produced seizures of equivalent severity (e.g., limb clonus; loss of posture) in *ZnT3*$^{+/+}$ and *ZnT3*$^{-/-}$ mice (Appendix D, Fig. 3; Appendix D, Table 2).

ZnT3$^{-/-}$ mice were more susceptible than *ZnT3*$^{+/+}$ mice to seizures induced by kainic acid (Appendix D, Fig. 4), with an ED_{90} for tonic/clonic seizure of about 15 mg/kg, compared to about 20 mg/kg for *ZnT3*$^{+/+}$ mice (Appendix D, Table 2). Monitoring electrographic activity with cortical electrodes during kainate-induced seizures revealed shorter latency to electrographic seizure, longer electrographic seizure episodes, and a greater percent time spent in electrographic seizures for *ZnT3*$^{-/-}$ mice compared to *ZnT3*$^{+/+}$ mice (Appendix D, Fig. 5), suggesting that zinc may be important for controlling either the initial seizure induction or maintenance of seizures after they have begun. In many cases, electrographic status epilepticus was observed in *ZnT3*$^{-/-}$ mice, whereas *ZnT3*$^{+/+}$ mice typically had discrete electrographic seizure episodes (Appendix D, Fig. 5).

E. Neuronal damage

Zinc is released from synaptic vesicles upon neuronal excitation (Assaf and Chung, 1984; Howell et al., 1984), and subsequent accumulation of zinc in the cytosol of post-synaptic neurons has been shown to correlate very well with neuronal damage associated with seizures, ischemia, and trauma (Frederickson et al., 1988; Tonder et al., 1990; Koh et al., 1996; Suh et al., 2000). The zinc translocation hypothesis proposes that histochemically reactive zinc in synaptic vesicles is released into the synaptic cleft following brain insults; synaptically-released zinc then translocates to the cytosol of post-synaptic target neurons by passage through ionotropic glutamate receptors or other ion channels, where its accumulation is thought to be responsible for much of the damage to these neurons (Frederickson et al., 1989; Choi and Koh, 1998; Lee et al., 1999). According to this hypothesis, the *ZnT3*$^{-/-}$ brain should show less seizure-induced neuronal damage than the *ZnT3*$^{+/+}$ brain in regions where zinc is normally released, since histochemically reactive zinc is no longer available for release into the synapse.

Surprisingly, the opposite occurred; neuronal damage following kainate-induced seizures was much higher in *ZnT3*$^{-/-}$ mice than *ZnT3*$^{+/+}$ mice, especially in CA1 pyramidal cells (Appendix D, Fig. 6), even when behavioral seizure severity was equivalent.

In a direct test of the zinc translocation hypothesis, we asked whether zinc still accumulated in the cytosol of post-synaptic neurons after seizures in the *ZnT3*$^{-/-}$ brain, where histochemically reactive zinc is no longer present in synaptic vesicles. Intraperitoneal injection of a high dose of kainate (40 mg/kg) produced severe seizures in both *ZnT3*$^{+/+}$ (n = 5) and *ZnT3*$^{-/-}$ (n = 5) mice, as well as *ZnT3*$^{-/-}$ mice that were injected intracerebroventricularly (icv) with 2 µl of 300 mM CaEDTA, a specific zinc chelator, 30 min prior to kainic acid injection (n = 5)(Fig. 22 E). Two hr after kainate injection, seizures were halted by intraperitoneal injection of sodium phenytoin (50 mg/kg). Twenty-four hr later, the brain was harvested, cryosections were cut, and the zinc-specific fluorescent indicator, TFL-Zn (Budde et al., 1997) was added to the unfixed sections for 90 sec. After washing with saline, TFL-Zn stained sections were examined under a fluorescence microscope and photographed (Fig. 22). To identify cell death in the sections, TUNEL staining was performed with the in situ cell death detection kit (Boehringer Mannheim), according to the manufacturer's instructions. In the hippocampus of *ZnT3*$^{+/+}$ mice injected with saline, TFL-Zn staining was similar to that seen with the TSQ or Timm stains, with staining evident in the hilus, CA3 region, and CA1 region (Fig. 22 A). Twenty-four hr after kainate-induced seizures, TFL-stainable zinc was present in the cytosol of neurons in the CA3 and CA1 pyramidal cell layers, and TUNEL stained neurons were detectable in CA1 (Fig. 22 C). *ZnT3*$^{-/-}$ mice injected with saline had no detectable TFL-stainable zinc (Fig. 22 B). Twenty-four hr after kainate-induced seizure, TFL-stainable zinc was present in the cytosol of neurons in the CA3 and CA1 pyramidal cell layers of the *ZnT3*$^{-/-}$ hippocampus, and TUNEL stained neurons were especially abundant in the CA1 region (Fig. 22 D). The number of TFL-stained neurons in the CA1 region of the *ZnT3*$^{-/-}$ hippocampus was much greater than that seen in the *ZnT3*$^{+/+}$ hippocampus, as were the number of TUNEL-stained neurons (Fig. 22 C, D). Prior icv injection of the zinc chelator CaEDTA significantly reduced both the cytosolic

Figure 22. Vesicle zinc not the sole source of toxic zinc accumulation following seizures.

Hippocampi from *ZnT3*$^{+/+}$ (A, C) and *ZnT3*$^{-/-}$ (B, D, F) mice, stained with TFL-Zn (blue staining) or TUNEL (insets) before (A,B) or 24 hr after (C, D, F) kainate-induced seizures. Mice were injected with kainate (40 mg/kg, ip) and seizures were scored on the basis of behavior, as in Appendix D, Table I. Two hr later, seizures were halted by injection of sodium phenytoin (50 mg/kg). (E) *ZnT3*$^{+/+}$ mice (triangles), *ZnT3*$^{-/-}$ mice (black ovals) and *ZnT3*$^{-/-}$ mice injected icv with CaEDTA (white ovals) had similar seizure severities. Before seizures, TFL-Zn stain was present in the mossy fibers and schaffer collaterals of the *ZnT3*$^{+/+}$ (A), but not *ZnT3*$^{-/-}$ (B) hippocampus. After seizures, TFL-Zn staining appeared in CA3 and CA1 pyramidal cell bodies (black arrows) in both *ZnT3*$^{+/+}$ (C) and *ZnT3*$^{-/-}$ (D) hippocampus, and TUNEL-stain was evident in CA1 pyramidal cells (insets). Zinc accumulation and neuronal death were greater in the *ZnT3*$^{-/-}$ mice (D) than in *ZnT3*$^{+/+}$ mice (C), and in the *ZnT3*$^{-/-}$ hippocampus, CA1 cell death and zinc accumulation were markedly attenuated by icv injection of 2 μl of 300 mM CaEDTA (F).

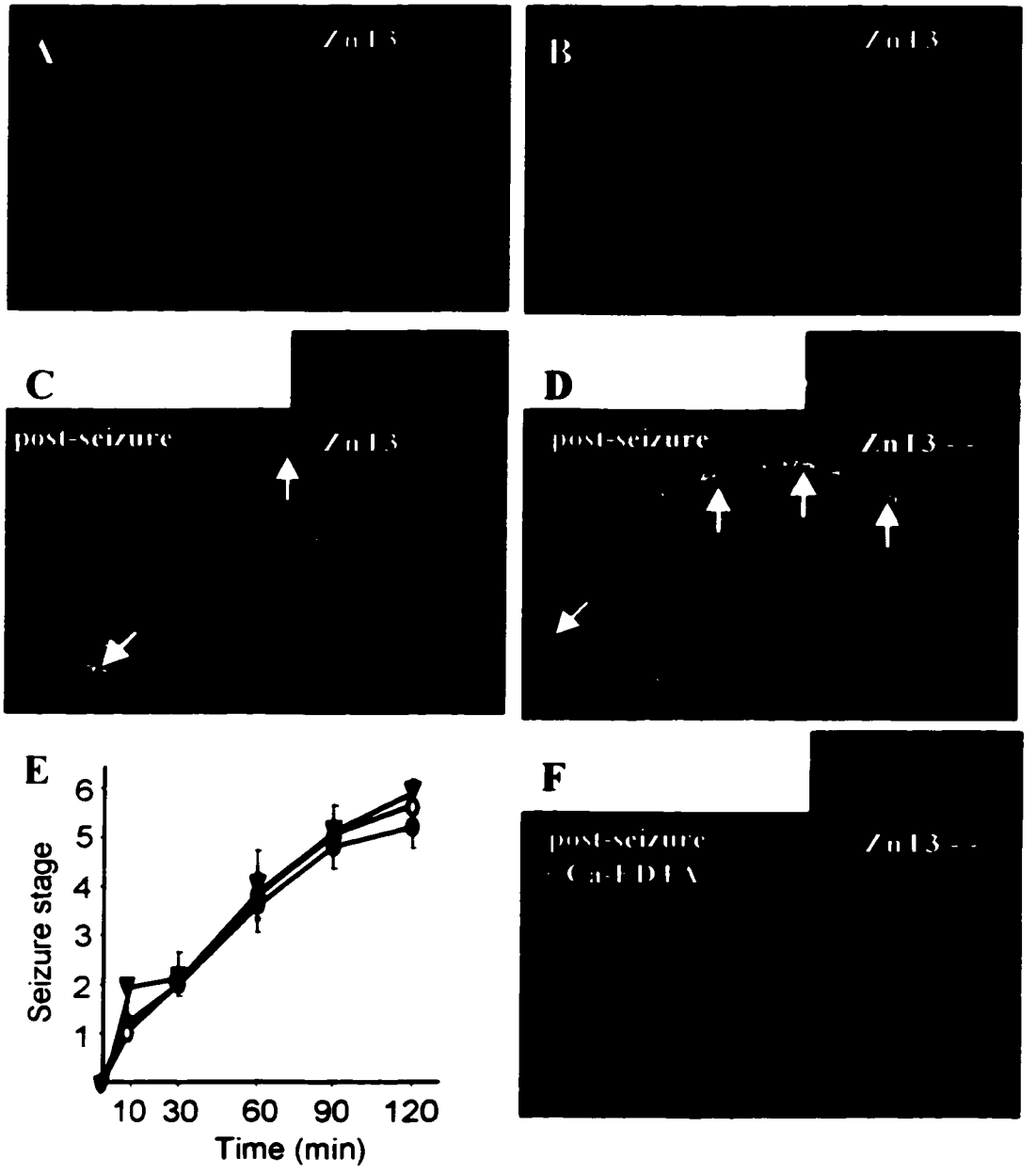
A
Zn13
B
Zn13
C
post-seizure
Zn13
D
post-seizure
Zn13
E
Seizure stage
6
5
4
3
2
1
10 30 60 90 120
Time (min)
F
post-seizure
Zn13

zinc accumulation and the number of TUNEL-stained neurons (Fig. 22 F), whereas seizure severity was unaffected (Fig. 22 E). Thus, zinc still accumulates in the cytosol of CA3 and CA1 pyramidal cells despite the lack of histochemically reactive zinc in the terminals of mossy fibers or schaffer collaterals. Prevention of staining by the extracellular zinc chelator CaEDTA indicates that the zinc is derived from an extracellular source. The higher neuronal damage seen in the *ZnT3*$^{-/-}$ hippocampus versus the *ZnT3*$^{+/+}$ hippocampus suggests that ZnT3 is neuroprotective for these neurons. Zinc accumulation in the cytosol correlated well with neuronal damage (Fig. 22 C, D), and zinc chelation significantly reduced neuronal damage in the *ZnT3*$^{-/-}$ hippocampus (Fig. 22 F), as it does in wild-type mice (Koh et al., 1996), consistent with a toxic role for cytosolic zinc accumulation following seizures.

DISCUSSION

This dissertation demonstrates that zinc is taken up into synaptic vesicles by a mechanism that requires ZnT3 at the vesicle membrane. ZnT3 mRNA is present in the cell bodies of zinc-containing neurons, and ZnT3 immunoreactivity is present on the membranes of zinc-rich synaptic vesicles in the projections of those neurons. Removal of ZnT3 prevents histochemically reactive zinc from accumulating in synaptic vesicles in all of the zinc-containing regions of the brain and spinal cord we have examined. These results, together with its homology to the zinc transporters, ZnT2 and ZnT4, suggest that ZnT3 transports zinc across the synaptic vesicle membrane. *ZnT3*$^{+/-}$ mice have reduced ZnT3 immunoreactivity on vesicle membranes and a corresponding reduction in vesicular zinc, indicating that the amount of zinc within synaptic vesicles is limited by the abundance of ZnT3 on the vesicle membrane. This is consistent with a steady-state model for the regulation of vesicular zinc content, where vesicular zinc content is determined by steady-state balance between influx and efflux, rather than a predetermined "set point" (Williams, 1997).

As with the other members of this family, the mechanism of zinc transport is unknown. Compared to the other members of the family, ZnT3 has a smaller cytoplasmic loop between the fourth and fifth transmembrane domains, and this loop contains fewer histidines (see Fig. 3; Palmiter and Findley, 1995; Palmiter et al., 1996). Other proteins may be involved, because ZnT3 does not have any nucleotide binding sites and zinc is transported into the vesicle against a strong concentration gradient. Alternatively, zinc transport could be coupled to the energetically favorable transport of another ion or solute, perhaps in an exchange reaction. ZnT3 depends on the vesicular chaperone, AP-3, for appropriate cellular localization, as ZnT3 immunoreactivity is reduced in *mocha* mutant mice, which lack the δ-subunit of AP-3 and consequently exhibit reduced levels of synaptic vesicle zinc (Kantheti et al., 1998). The phenotype of *mocha* mutant mice, which includes hypersynchronized theta rhythms, spontaneous bursts of epileptiform activity, and loss of hearing, in addition to reduced vesicular zinc

(Noebels and Sidman, 1989), is much more severe than that seen in *ZnT3*$^{-/-}$ mice, as would be expected if AP-3 is involved in the assembly of many vesicular components.

Disrupting *ZnT3* prevented histochemically reactive zinc from accumulating in synaptic vesicles. The remaining 80% of total brain zinc represents zinc that is inaccessible to Timm stain or TSQ, presumably due to its tight association with metalloproteins in other parts of the cell. In the absence of ZnT3-mediated zinc sequestration, one might expect aberrant zinc homeostasis in other parts of the cell or in the extracellular space (i.e., CSF). However, total zinc levels in the hippocampus and cortex are only reduced by about 20%, which corresponds closely with literature estimates of the relative contribution of vesicular zinc to total zinc in those regions (Frederickson, 1989). Undoubtedly, there are efficient mechanisms that control zinc concentrations in the cytosol and CSF, since zinc levels need to be maintained within a narrow window to avoid the detrimental effects of zinc deficiency or toxicity. Thus, the protein-bound zinc pools in the cytosol and CSF are probably unaltered in the absence of ZnT3.

ZnT3 protein appears to be limited to the CNS. *ZnT3* mRNA was also detected in germ cells in the testis, but neither Western blots nor immunohistochemistry revealed any ZnT3 protein in the testis, and histochemically reactive zinc was unperturbed in this organ. Normal levels of histochemically reactive zinc were also found in the pancreas and salivary gland, indicating that ZnT3 is not responsible for zinc sequestration in those organs. Other members of the ZnT family are likely candidates for regulation of these peripheral pools of histochemically reactive zinc.

Because ZnT3 colocalizes with vesicular zinc and is required for the accumulation of zinc in synaptic vesicles throughout the CNS, ZnT3 is a defining feature of the zinc-containing neuron. Detection of ZnT3 mRNA in neuronal somata and ZnT3 immunoreactivity in projection terminals is useful for mapping zinc-containing pathways in the CNS, which in the past has relied on autometallographic methods that are not intrinsically specific for zinc or fluorescent compounds that do not give good cellular resolution. This may be especially valuable for examining mossy fiber sprouting or other

morphological rearrangements in post-mortem samples of epileptic human brain, which often are not amenable to autometallography. As we demonstrated, ZnT3 immunoreactivity is detectable in the human brain, even at the ultrastructural level.

ZnT3$^{-/-}$ mice should not be capable of releasing zinc into the synaptic cleft, since they no longer have detectable zinc in synaptic vesicles. However, our experiments examining zinc translocation following seizures demonstrate that substantial increases in extracellular zinc concentrations are possible following neuronal activation, even in the absence of histochemically reactive zinc in synaptic vesicles. Indeed, in the absence of ZnT3, extracellular zinc concentrations are probably even higher than in the wild-type hippocampus. The source of this transient rise in extracellular zinc is unknown; our experiments demonstrate that the major source of this zinc is not release of histochemically reactive zinc from synaptic vesicles. Perhaps a histochemically invisible pool of zinc is present in synaptic vesicles, and the zinc in these vesicles is released upon neuronal activation. Consistent with this possibility, only a subset of vesicles within individual mossy fiber boutons contains Timm stain (20-70% of vesicles). However, since the percentage of Timm-positive vesicles varies with fixation and staining conditions, we interpreted this absence of Timm stain in some vesicles to be due to a lack of sensitivity of the procedure, rather than an accurate reflection of their zinc content. Furthermore, ZnT3 immunoreactivity is present on all of the small clear round synaptic vesicles in the bouton, suggesting that all of these vesicles have the capability of accumulating histochemically reactive zinc. It seems unlikely that a synaptic vesicle would be capable of independently regulating a histochemically reactive and histochemically invisible pool of zinc. However, the invisible pool of zinc could reside in a different compartment, e.g., protein-containing vesicles derived from the secretory pathway.

When *ZnT3*$^{-/-}$ mice were used to assess the physiological importance of synaptic vesicle zinc, most of the functions tested in these mice were remarkably normal. The brain developed normally, with the hippocampus displaying normal ultrastructure. Thus, despite its early presence during brain development (e.g., Vincent and Semba, 1989)

vesicular zinc is not required for assembly of the neuronal architecture. Because *ZnT3*$^{-/-}$ mice are indistinguishable from *ZnT3*$^{+/+}$ mice in most of the behavioral tests described here, and because these behaviors undoubtedly depend on glutamate as a neurotransmitter, it seems unlikely that glutamate storage or release are altered in the absence of histochemically reactive zinc. Consistent with this, glutamate immunoreactivity over mossy fiber boutons was normal in *ZnT3*$^{-/-}$ mice, and preliminary electrophysiological studies of hippocampal slices from these mice have not revealed any differences in glutamate-mediated responses (V. Lopantsev, unpublished data).

Tests of motor coordination, anxiety, hearing, olfaction, and nociception revealed no differences between *ZnT3*$^{-/-}$ and *ZnT3*$^{+/+}$ mice. Similarly, most of the tests of learning and memory revealed no differences. However, in the platform reversal test of the Morris water maze, *ZnT3*$^{-/-}$ mice required one additional trial to extinguish the memory of the previous platform location and learn the new platform location, indicating a possible involvement of synaptic vesicle zinc in memory extinction or relearning. When required to retain a simple association between a dark chamber and aversive stimulus in the passive avoidance paradigm, *ZnT3*$^{-/-}$ mice performed similarly as *ZnT3*$^{+/+}$ mice. *ZnT3*$^{-/-}$ mice also demonstrated normal spatial memory in the Morris water maze and normal working memory and reference memory in the radial arm maze. While *ZnT3*$^{-/-}$ mice made more working memory errors in trial 4 than *ZnT3*$^{+/+}$ mice at 4 wk post-training, their performance at 1, 2, and 7 wk post-training was similar to that of the *ZnT3*$^{+/+}$ mice, suggesting that this difference was due to week-to-week variability in performance in the task rather than a difference due to genotype.

Removing ZnT3 caused mice to be more susceptible to kainic acid-induced seizures, indicating that the net effect of having zinc in synaptic vesicles is inhibitory for neuronal excitability. Because *ZnT3*$^{+/-}$ mice had intermediate levels of vesicular zinc and intermediate seizure severities (relative to *ZnT3*$^{+/+}$ and *ZnT3*$^{-/-}$ mice), the enhanced seizure sensitivity in these mice is likely to be due to dose-dependent removal of zinc from synaptic vesicles. Inhibitory effects of zinc that could be relevant for its dampening effect on seizures include antagonism of NMDA receptors (Peters et al., 1987; Westbrook

and Mayer, 1987; Christine and Choi, 1990) and enhancement of GABA release, perhaps via blockade of presynaptic $GABA_B$ receptors (see Fig. 2 B)(Ben-Ari and Cherubini, 1991; Xie and Smart, 1991). Additionally, potentiation of AMPA receptor responses by zinc (Rassendren et al., 1990) could result in an increased excitatory drive onto inhibitory interneurons in the CA3 region (Fig. 2 A). Finally, kainate (KA) receptors are inhibited by zinc in a subunit- and pH-dependent manner (D. Mott and R. Dingledine, personal communication). Thus, in the *ZnT3*$^{-/-}$ mice, loss of zinc inhibition could result in enhanced KA receptor-induced depolarization as the pH declines during seizures.

While *ZnT3*$^{-/-}$ mice exhibited a very striking susceptibility to seizures elicited by kainic acid, they showed similar sensitivities as *ZnT3*$^{+/+}$ mice to other epileptogenic drugs, and they were less sensitive than *ZnT3*$^{+/+}$ mice to bicuculline-induced seizures. These other drugs all produce seizures, at least in part, by blocking $GABA_A$-mediated inhibition, suggesting that functional $GABA_A$ receptors need to be present to reveal an effect of zinc on seizure susceptibility. This suggests that the predominant dampening actions of zinc on seizures may be due to enhancement of GABA-mediated inhibition, rather than direct inhibition of post-synaptic glutamate receptors. KA is thought to inhibit GABA release by inhibitory interneurons, and may also act directly on post-synaptic glutamate receptors on pyramidal cells (Lerma, 1997). In the absence of zinc, which normally would enhance GABA release and antagonize NMDA receptors, these effects of KA would be even more pronounced. Finally, it is possible that the resistance of *ZnT3*$^{-/-}$ mice to bicuculline-induced seizures is due to compensatory upregulation of GABA neurotransmission, i.e., *ZnT3*$^{-/-}$ mice have compensated for the inhibitory effects of synaptic vesicle zinc by enhancing inhibition in some other way.

In the epileptic human brain and in many animal models of epilepsy, zinc-rich mossy fibers sprout back across the dentate granule cell layer into the inner molecular layer of the dentate gyrus (Babb et al., 1991; Franck et al., 1995; Represa et al., 1994). Their aberrant terminal localization and their proximity to GABA receptors have prompted investigators to postulate a role for zinc in the breakdown of inhibition that is associated with seizure generation in epileptic hippocampus (Buhl et al., 1996). In the epileptic

human and mouse brain, we observed ZnT3 immunoreactivity and histochemically reactive zinc in newly sprouted terminals that made contacts with both inhibitory basket cells and granule cell dendrites, consistent with such a disinhibitory role for zinc. If mossy fiber sprouting can occur in the *ZnT3*$^{-/-}$ hippocampus, it will be interesting to see if the absence of zinc in the new terminals allows them to augment inhibition (by increasing the excitatory drive onto inhibitory interneurons) and thus control further seizures.

Synaptically-released zinc is thought to mediate much of the damage to neurons that occurs following brain insults (Frederickson et al, 1988; Tonder et al, 1990; Koh et al., 1996; Choi and Koh, 1998; Suh et al., 2000). In a direct test of the zinc translocation hypothesis, we asked whether zinc still accumulated in the cytosol of CA3 or CA1 pyramidal cells of the *ZnT3*$^{-/-}$ hippocampus after seizures, and whether removal of synaptic vesicle zinc was neuroprotective. We demonstrated that zinc still accumulates after seizures in the cytosol of CA3 and CA1 pyramidal cells in the *ZnT3*$^{-/-}$ hippocampus, even though no detectable zinc is present prior to seizure in the mossy fiber or Schaffer collateral terminals. We also discovered that severe neuronal damage is possible in the absence of synaptic vesicle zinc. Indeed, zinc accumulation and neuronal damage were more prevalent in the *ZnT3*$^{-/-}$ hippocampus than in the *ZnT3*$^{+/+}$ hippocampus, suggesting that zinc levels in the extracellular space might be even higher in the absence of ZnT3. Perhaps by sequestering zinc in vesicles, ZnT3 facilitates clearance of zinc from the synaptic cleft, thus keeping extracellular zinc concentrations low after neuronal insults. Alternatively, the increased post-synaptic zinc accumulation and increased neuronal damage could be due simply to more extensive electrographic activity in the *ZnT3*$^{-/-}$ hippocampus during seizures. Although *ZnT3*$^{+/+}$ and *ZnT3*$^{-/-}$ mice had similar behavioral seizure severities, our EEG recordings indicate that behavioral scoring is not a sensitive indicator of electrographic seizure severity.

CaEDTA, an extracellular zinc chelator, prevented cytosolic zinc uptake in the *ZnT3*$^{-/-}$ hippocampus, suggesting that the source of toxic zinc uptake is a transient rise in extracellular zinc levels. Our experiments demonstrate that this increase in extracellular zinc is not due to the release of histochemically reactive zinc from synaptic vesicles.

Alternative sources of zinc release into the extracellular space might include: (1) release of a histochemically invisible pool of zinc from vesicles in the presynaptic terminal; (2) increased efflux of zinc from the cytosol of the post-synaptic cell by either ZnT1, which is induced following ischemia in the gerbil (Tsuda et al., 1997), or by reverse operation of a ZIP (zinc uptake) transporter; or (3) efflux of zinc from glial cells or other cells in the vicinity (see Fig. 23). Whatever its source, this zinc is invisible to histochemical staining reagents prior to seizure, indicating that before the seizure it is bound tightly enough to render it inaccessible to TFL-Zn, Timm, or TSQ.

Interestingly, mice deficient in MT3 are also more susceptible to seizures induced by kainic acid, and also show increased seizure-related damage (Erickson et al., 1997). Furthermore, removal of synaptic vesicle zinc from the MT3-deficient brain by making ZnT3/MT3 double knockout mice does not increase neuronal damage any further than that seen in the absence of MT3 alone, suggesting that the neuroprotective effects of MT3 are related to its ability to bind zinc (Appendix D). Our results with seizure-related damage in the *ZnT3*$^{-/-}$ mice are also consistent with a toxic role for extracellular zinc. Post-synaptic zinc accumulation correlated with neuronal death assessed by TUNEL staining, and CaEDTA blocked both zinc accumulation and cell death, indicating that zinc is involved in neuronal death. Because neuronal death is often delayed following seizures or ischemia, lowering the levels of zinc in the extracellular space within 24 hours of insult may be an effective way to reduce neuronal damage.

Figure 23. Zinc release and uptake during brain insults.

Diagram of a zinc-containing terminal making contact with its target cell in the CA3 or CA1 hippocampal subregion, illustrating possible routes of zinc release and uptake following a brain insult such as a seizure. The top panel illustrates the zinc translocation hypothesis, which predicted the major source of toxic zinc to be the histochemically reactive zinc in synaptic vesicles. Because our experiments demonstrated that synaptic vesicle zinc is not the major source of toxic zinc, alternative sources are depicted in the bottom panel.

(Top panel): The zinc translocation hypothesis suggests that zinc is released into the synaptic cleft upon neuronal activation (histochemically reactive zinc is depleted from synaptic vesicles, with concomitant increases in extracellular zinc). Under conditions of excessive neuronal activity, zinc released into the synaptic cleft passes through ion channels into the cytosol of the postsynaptic neuron, where zinc overload might contribute to cell death. Presumably, zinc is taken back up into the presynaptic terminal as well, through an unknown mechanism possibly involving zinc uptake by a ZIP transporter and binding of zinc by MT3. MT3 knockout mice exhibit more severe damage than wild-type mice in response to seizures, consistent with the possibility that MT3 recycles toxic zinc out of the extracellular space.

(Bottom panel): Zinc translocation is not the major source of toxic zinc accumulation after seizures. Our experiments demonstrate that zinc accumulates in CA3 and CA1 target neurons even in the absence of synaptic vesicle zinc. Because an extracellular zinc chelator prevented seizure-related zinc accumulation and cell death, this toxic pool of zinc must have arisen from a transient increase in extracellular zinc levels. Illustrated are several possible sources of extracellular zinc: (1) increased efflux of zinc from the cell by either ZnT1, which is known to be induced during ischemia, or reverse operation of a ZIP (zinc uptake) transporter; (2) release of a histochemically invisible pool of vesicular zinc from the presynaptic terminal (perhaps regulated by ZnT4); and (3) release of zinc from glial cells in the vicinity. In any case, prior to its accumulation in the cytosol, this zinc is invisible to histochemical staining reagents (histochemically invisible zinc is depicted in italics).

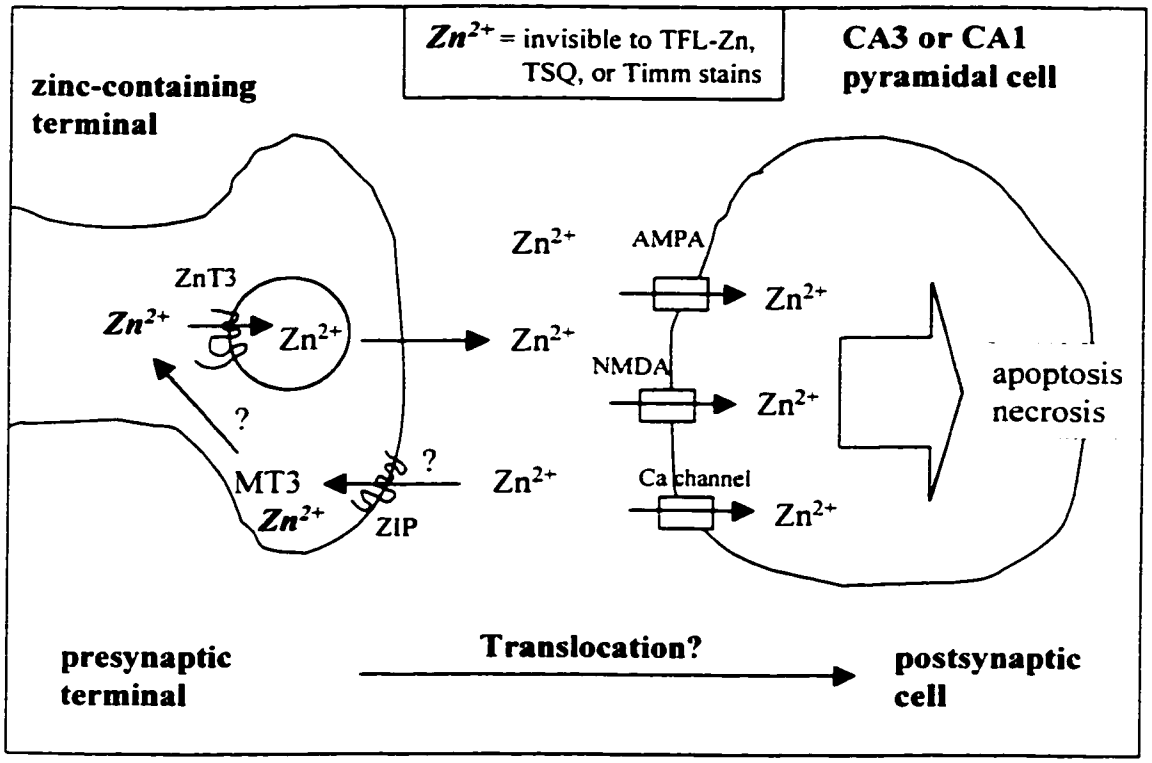
Zn^{2+} = invisible to TFL-Zn, TSQ, or Timm stains
zinc-containing terminal
CA3 or CA1 pyramidal cell
ZnT3
Zn^{2+}
Zn^{2+}
Zn^{2+}
Zn^{2+}
AMPA
Zn^{2+}
NMDA
Zn^{2+}
apoptosis
necrosis
?
?
MT3
Zn^{2+}
ZIP
Zn^{2+}
Ca channel
Zn^{2+}
presynaptic terminal
Translocation?
postsynaptic cell

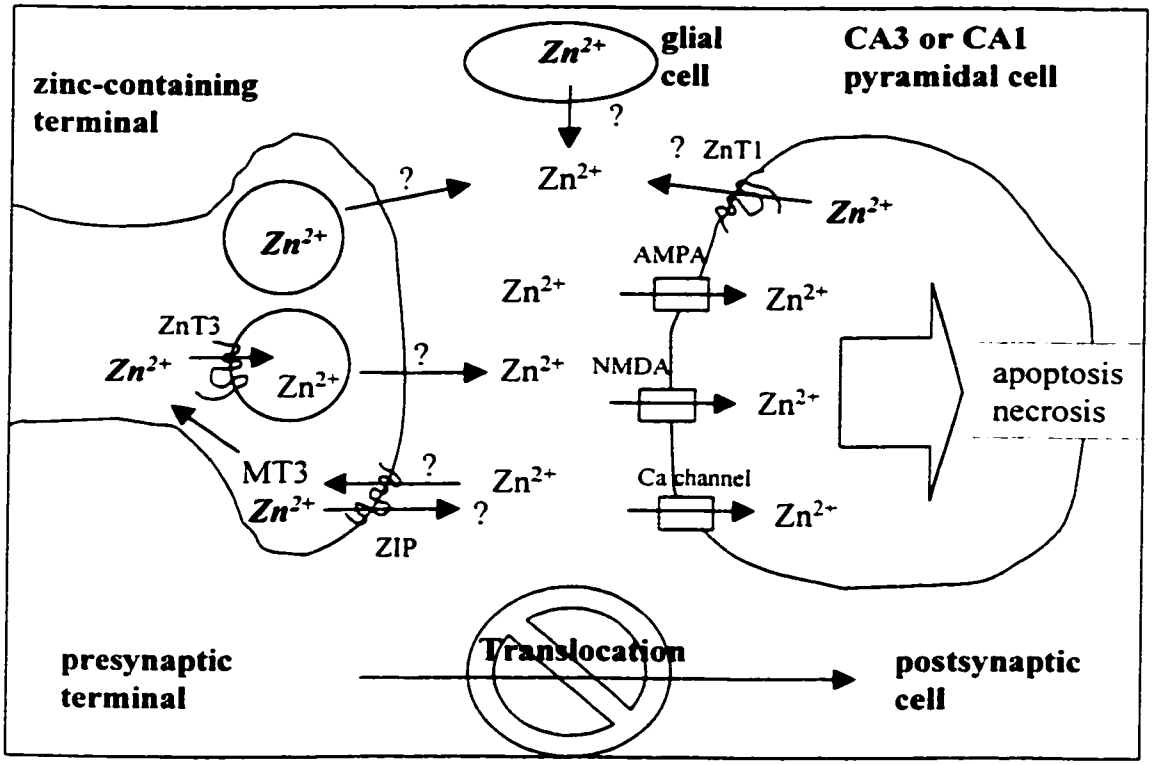
zinc-containing terminal
Zn^{2+}
glial cell
CA3 or CA1 pyramidal cell
?
?
Zn^{2+}
? ZnT1
Zn^{2+}
Zn^{2+}
AMPA
Zn^{2+}
ZnT3
Zn^{2+}
Zn^{2+}
?
Zn^{2+}
NMDA
Zn^{2+}
apoptosis
necrosis
MT3
?
Zn^{2+}
Ca channel
Zn^{2+}
Zn^{2+}
?
ZIP
presynaptic terminal
Translocation
postsynaptic cell

FUTURE DIRECTIONS

ZnT3$^{-/-}$ mice should not be capable of releasing zinc into the synaptic cleft, since they no longer have detectable zinc in synaptic vesicles. However, this hypothesis has yet to be directly tested. It will be important to determine how zinc release and reuptake are affected by the removal of ZnT3. Zinc release and uptake in the *ZnT3*$^{-/-}$ brain could be assessed in hippocampal slice preparations by stimulating dentate granule cells and measuring zinc released into the perfusate or taken up into the mossy fiber region (Assaf and Chung, 1984; Howell et al., 1984). However, robust neuronal activation (e.g., tetanic stimulation or addition of kainic acid) is necessary in order to liberate detectable levels of zinc. Under these conditions, vesicular release may not be the only possible source of extracellular zinc. Alternatively, we have preliminary evidence (J. Wenzel, unpublished data) suggesting that at the ultrastructural level, Timm stain accumulates over synaptic contacts in the wild-type hippocampus after brief periods of anoxia or neuronal activity. This may be due to release of zinc from the presynaptic terminal. Examining Timm stain in the hippocampus of *ZnT3*$^{-/-}$ mice during anoxic conditions will determine whether the source of this zinc accumulation over synaptic contacts is the Timm-stainable zinc normally found in synaptic vesicles.

Given the involvement of zinc in seizure-related neurodegeneration, high priority should be given to identifying the source of the extracellular toxic zinc. Mice that lack specific metallothioneins or zinc transporters (e.g., MT3 or ZnT4) could be tested for zinc accumulation and neuronal damage following seizures. It will be interesting to see whether the induction or function of ZIP or ZnT transporters or MTs are affected during brain insults. The observations made here should be extended to address the involvement of zinc in the neurodegeneration associated with ischemia and trauma. Further investigation of how cytosolic zinc accumulation might trigger apoptotic or necrotic mechanisms will be critical for identifying possible ways to ameliorate zinc-induced neuronal damage following insults to the brain.

Given the possible role that zinc in newly sprouted mossy fibers plays in the breakdown of inhibition associated with epilepsy (Buhl et al., 1996), it will be important to see if mossy fiber sprouting occurs in the *ZnT3*$^{-/-}$ hippocampus, and especially whether the absence of zinc in the new terminals allows them to increase the excitatory drive onto inhibitory neurons and thus augment inhibition. This is especially relevant given our suggestion that the effects of zinc on GABAergic neurotransmission may be more important than its inhibitory effects on glutamate receptors for the control of seizures.

Interpretation of the behavioral data presented here is complicated by the possibility of developmental compensation. The decreased sensitivity of *ZnT3*$^{-/-}$ mice to low doses of bicuculline is consistent with a compensatory increase in GABAergic neurotransmission. Further substantiation of this compensatory increase in inhibition would be useful, especially by examining changes in the abundance of specific receptors or receptor subunits that are known to determine zinc sensitivity *in vitro*, such as the gamma subunit of the $GABA_A$ receptor. For the same purpose, electrophysiology would be useful to examine responses mediated by $GABA_A$, AMPA, or NMDA receptors. ZnT3 is an ideal candidate for inducible knockout strategies, such as those that use tetracycline to shut off expression in the adult, to bypass the problem of compensation during development.

The mechanism by which ZnT3 transports zinc across the vesicle membrane is unknown. It may act as part of a complex of proteins that could be identified by yeast two-hybrid or crosslinking approaches. Disrupting ZnT3 lays the groundwork for future experiments in mice, where functional domains or motifs of ZnT3 could be selectively disrupted, or the expression of other genes could be directed to neurons where ZnT3 is normally expressed. Removal of ZnT3 did not affect histochemically reactive zinc in other organs outside of the CNS. Now that several ZnT and ZIP family members have been identified, it will be straightforward to determine which of these proteins regulates the specific pools of zinc found in the testis, pancreas, salivary gland, lung, intestine, or other organs by examining their expression patterns and selectively disrupting the genes encoding these transporters in mice.

Bibliography

Aniksztejn, L., Charton, G., Ben-Ari, Y., 1987. Selective release of endogenous zinc from the hippocampal mossy fibers in situ. Brain Res. 404, 58-64.

Assaf, S.Y., Chung, S.H., 1984. Release of endogenous Zn2+ from brain tissue during activity. Nature 308, 734-736.

Babb, T.L., Kupfer, W.R., Pretorius, J.K., Crandall, P.H., Levesque, M.F., 1991. Synaptic reorganization by mossy fibers in human epileptic fascia dentata. Neuroscience 42, 351-363.

Bremner, I., 1993. Involvement of metallothionein in the regulation of mineral metabolism. In: Metallothionein III: Biological roles and medical implications (Suzuki, K.T., Imura, N., Kimura, M., eds.), pp. 111-124. Birkhäuser Verlag, Bäsel, Switzerland.

Budde, T., Minta, A., White, J.A., Kay, A.R., 1997. Imaging free zinc in synaptic terminals in live hippocampal slices. Neuroscience 79, 347-358.

Buhl, E.H., Otis, T.S., Mody, I., 1996. Zinc-induced collapse of augmented inhibition by GABA in a temporal lobe epilepsy model. Science 271, 369-373.

Bush, A.I., Pettingell, W.H., Multhaup, G., Paradis, M., Vonsattel, J.P., Gusella, J.F., Beyreuther, K., Masters, C.L., Tanzi, R.E., 1994. Rapid induction of Alzheimer Aβ amyloid formation by zinc. Science 265, 1464-1467.

Celentano, J.J., Gyenes, M., Gibbs, T.T., Farb, D.H., 1991. Negative modulation of the gamma-aminobutyric acid response by extracellular zinc. Mol. Pharmacol. 40, 766-773.

Charton, G., Rovira, C., Ben-Ari, Y., Leviel, V., 1985. Spontaneous and evoked release of endogenous Zn2+ in the hippocampal mossy fiber zone of the rat in situ. Exp. Brain Res. 58, 202-205.

Choi, D.W., Koh, J.Y., 1998. Zinc and brain injury. Annu. Rev. Neurosci. 21, 347-375.

Christine, C.W., Choi, D.W., 1990. Effect of zinc on NMDA receptor-mediated channel currents in cortical neurons. J. Neurosci. 10, 108-116.

Conklin, D.S., Culbertson, M.R., Kung, C., 1994. Interactions between gene products involved in divalent cation transport in *Saccharomyces cerevisae*. Mol. Gen. Genet. 244, 303-311.

Conklin, D.S., McMaster, J.A., Culbertson, M.R., Kung, C., 1992. COT1, a gene involved in cobalt accumulation in *Saccharomyces cerevisae*. Mol. Cell Biol. 12, 3678-3688.

Crawford, I.L., Connor, J.D., 1972. Zinc in maturing rat brain: hippocampal concentration and localization. J. Neurochem. 19, 1451-1458.

Danscher, G., 1982. Exogenous selenium in the brain. A histochemical technique for light and electron microscopal localization of catalytic selenium bonds. Histochemistry 76, 281-293.

Danscher, G., Howell, G., Perez-Clausell, J., Hertel, N., 1985. The dithizone, Timm's sulphide silver and selenium methods demonstrate a chelatable pool of zinc in the CNS. Histochemistry 83, 419-422.

Draguhn, A., Verdorn, T.A., Ewert, M., Seeburg, P.H., Sakmann, B., 1990. Functional and molecular distinction between recombinant rat $GABA_A$ receptor subtypes by Zn2+. Neuron 5, 781-788.

Eng, B.H., Guerinot, M.L., Eide, D., Saier, M.H. Jr., 1998. Sequence analyses and phylogenetic characterization of the ZIP family of metal ion transport proteins. J. Membrane Biol. 166, 1-7.

Epand, R.M., Stafford, A.R., Tyers, M., Nieboer, E., 1985. Mechanism of action of diabetogenic zinc-chelating agents. Mol. Pharmacol. 27, 366-374.

Erickson, J.C., Hollopeter, G., Thomas, S.A., Froelick, G.J., Palmiter, R.D., 1997. Disruption of the metallothionein-III gene in mice: analysis of brain zinc, behavior, and neuron vulnerability to metals, aging and seizures. J. Neurosci. 17, 1271-1281.

Franck, J.E., Pokorny, J., Kunkel, D.D., Schwartzkroin, P.A. 1995. Physiologic and morphologic characteristics of granule cell circuitry in human epileptic hippocampus. Epilepsia 36, 543-558.

Frederickson, C.J., Perez-Clausell, J., Danscher, G., 1987. Zinc-containing 7S-NGF complex: Evidence from zinc histochemistry for localization in salivary secretory granules. J. Histochem. Cytochem. 35, 579-583.

Frederickson, C.J., 1989. Neurobiology of zinc and zinc-containing neurons. Int. Rev. Neurobiol. 31, 145-238.

Frederickson, C.J., Danscher, G., 1990. Zinc-containing neurons in hippocampus and related CNS structures. Prog. Brain Res. 83, 71-84.

Frederickson, R.E., Frederickson, C.J., Danscher, G. 1990. In situ binding of bouton zinc reversibly disrupts performance on a spatial memory task. Behavioral Brain Res. 38, 25-33.

Frederickson, C.J., Hernandez, M.D., Goik, S.A., Morton, J.D., McGinty, J.F., 1988. Loss of zinc staining from hippocampal mossy fibers during kainic acid induced seizures: a histofluorescence study. Brain Res. 446, 383-386.

Frederickson, C.J., Hernandez, M.D., McGinty, J.F., 1989. Translocation of zinc may contribute to seizure-induced death of neurons. Brain Res. 480, 317-321.

Frederickson, C.J., Kasarskis, E.J., Ringo, D., Frederickson, R.E., 1987. A quinoline fluorescence method for visualizing and assaying the histochemically reactive zinc (bouton zinc) in the brain. J. Neurosci. Methods 20, 91-103.

Friedman, B., Price, J.L., 1984. Fiber systems in the olfactory bulb and cortex: a study in adult and developing rats, using the timm method and the light and electron microscope. J. Comp. Neurol. 223, 88-109.

Gaither, L.A., Eide, D.J., 2000. Functional expression of the human hZIP2 zinc transporter. J. Biol. Chem. 275, 5560-5564.

Harrison, N.L., Gibbons, S.J., 1994. Zn2+: an endogenous modulator of ligand- and voltage-gated ion channels. Neuropharmacology 33, 935-952.

von Heijne, G., 1994. Membrane proteins: from sequence to structure. Annu. Rev. Biophys. Biomol. Struct. 23, 167-192.

Howell, G.A., Welch, M.G., Frederickson, C.J., 1984. Stimulation-induced uptake and release of zinc in hippocampal slices. Nature 308, 736-738.

Huang, L., Gitschier, J., 1997. A novel gene involved in zinc transport is deficient in the lethal milk mouse. Nat. Genet. 17, 292-297.

Hyde, L.A., Hoplight, B.J., Denenberg, V.H., 1998. Water version of the radial-arm maze: learning in three inbred strains of mice. Brain Res. 785, 236-244.

Jo, S.M., Won, M.H., Cole, T.B., Jensen, M.S., Danscher, G., 2000a. Zinc enriched (ZEN) terminals in mouse olfactory bulb. Brain Res. (In Press).

Jo, S.M., Danscher, G., Schroder, H.D., Cole, T.B., 2000b. Inhibitory zinc enriched terminals in mouse spinal cord. Brain Res. (manuscript in preparation).

Jo, S.M., Danscher, G., Won, M.H., Cole, T.B., Jensen, M.S., Schroder, H.D., 2000c. Zinc enriched (ZEN) terminals in mouse spinal cord: a light microscopical autometallographic study. Brain Res. (In press).

Käji, J.H.R., 1993. Evolution, structure, and chemical activity of class I metallothioneins: an overview. In: Metallothionein III: Biological roles and medical implications (Suzuki, K.T., Imura, N., Kimura, M., eds.), pp. 29-55. Birkhäuser Verlag, Bäsel, Switzerland.

Kamizono, A., Nishizawa, M., Teranishi, Y., Murata, K., Kimura, A., 1989. Identification of a gene conferring resistance to zinc and cadmium ions in the yeast *Saccharomyces cerevisae*. Mol. Cell Genet. 219, 161-167.

Kantheti, P., Qiao, X., Diaz, M.E., Peden, A.A., Meyer, G.E., Carskadon, S.L., Kapfhamer, D., Sufalko, D., Robinson, M.S., Noebels, J.L., Burmeister, M., 1998. Mutation in AP-3 delta in the mocha mouse links endosomal transport to storage deficiency in platelets, melanosomes, and synaptic vesicles. Neuron 21, 111-122.

Koh, J.Y., Suh, S.W., Gwag, B.J., He, Y.Y., Hsu, C.Y., Choi, D.W., 1996. The role of zinc in selective neuronal death after transient global cerebral ischemia. Science 272,1013-1016.

Larson, A.A., Kitto, K.F., 1997. Manipulations of zinc in the spinal cord, by intrathecal injection of zinc chloride, disodium-calcium-EDTA, or picolinic acid, alter nociceptive activity in mice. J. Pharmacol. Exp. Therap. 282, 1319-1325.

Larson, A.A., Kitto, K.F., 1999. Chelation of zinc in the extracellular area of the spinal cord, using EDTA disodium-calcium salt or dipicolinic acid, inhibits the antinociceptive effect of capsaicin in adult mice. J. Pharmacol. Exp. Therap. 288, 759-765.

Lee, J.M., Zipfel, G.J., Choi, D.W., 1999. The changing landscape of ischaemic brain injury mechanisms. Nature, 399, A7-14.

Lee, J.Y., Cole, T.B., Palmiter, R.D., Koh, J.Y., 2000. Accumulation of zinc in degenerating hippocampal neurons of ZnT3-null mice following seizures: evidence against synaptic vesicle origin. J. Neurosci. 20, RC79:1-5.

Legendre, P., Westbrook, G.L., 1991. Noncompetitive inhibition of gamma-aminobutyric $acid_A$ channels by Zn. Mol. Pharmacol. 39, 267-274.

Lister, R.G., 1987. The use of a plus-maze to measure anxiety in the mouse. Psychopharmacol. 92, 180-185.

Maske, H., 1957. Interaction between insulin and zinc in the islets of Langerhans. Diabetes 10, 367.

Masters, B.A., Quaife, C.J., Erickson, J.C., Kelly, E.J., Froelick, G.J., Zambrowicz, B.P., Brinster, R.L., Palmiter, R.D., 1994. Metallothionein-III is expressed in neurons that sequester zinc in synaptic vesicles. J. Neurosci. 14, 5844-5857.

McGaugh, J.L., Cahill, L., Roozendaal, B., 1996. Involvement of the amygdala in memory storage: interaction with other brain systems. Proc. Natl. Acad. Sci. USA 93, 13508-13514.

McMahon, R.J., Cousins, R.J., 1998. Mammalian zinc transporters. J. Nutr. 128, 667-670.

Mogil, J.S., Wilson, S.G., Bon, K., Lee, S.E., Chung, K., Raber, P., Pieper, J.O., Hain, H.S., Belknap, J.K., Hubert, L., Elmer, G.I., Chung, J.M., Devor, M., 1999. Heritability of nociception I: responses of 11 inbred mouse strains on 12 measures of nociception. Pain, 80, 67-82.

Morris, R., 1984. Developments of a water-maze procedure for studying spatial learning in the rat. J. Neurosci. Methods 11, 47-60.

Murgia, C., Vespignani, I., Cerase, J., Nobili, F., Perozzi, G., 1999. Cloning, expression, and vesicular localization of zinc transporter Dri 27/ZnT4 in intestinal tissue and cells. J. Pharmacol. Exp. Ther. 277, G1231-G1239.

Noebels, J.L., Sidman, R.L., 1989. Persistent hypersynchronization of neocortical neurons in the mocha mutant of mouse. J. Neurogenet. 6, 53-56.

Ogawa, N., Hirose, Y., Ohara, S., Ono, T., Watanabe, Y., 1985. A simple quantitative bradykinesia test in MPTP-treated mice. Res. Commun. Chem. Pathol. Pharmacol. 50, 435-441.

Palmiter, R.D., Cole, T.B., Findley, S.D., 1996. ZnT-2, a mammalian protein that confers resistance to zinc by facilitating vesicular sequestration. EMBO J. 15, 1784-1791.

Palmiter, R.D., Findley, S.D., 1995. Cloning and functional characterization of a mammalian zinc transporter that confers resistance to zinc. EMBO J. 14, 639-649.

Palmiter, R.D., Findley, S.D., Whitmore, T.E., Durnam, D.M., 1992. MT-III, a brain-specific member of the metallothionein gene family. Proc. Natl. Acad. Sci. USA 89, 6333-6337.

Pattison, S.E., Dunn, M.F., 1975. On the relationship of zinc ion to the structure and function of the 7S nerve growth factor protein. Biochemistry 14, 2733-2739.

Peters, S., Koh, J., Choi, D.W., 1987. Zinc selectively blocks the action of *N*-methyl-D-aspartate on cortical neurons. Science, 236, 589-593.

Quaife, C.J., Findley, S.D., Erickson, J.C., Froelick, G.J., Kelly, E.J., Zambrowicz, B.P., Palmiter, R.D., 1994. Induction of a new metallothionein isoform (MT-IV) occurs during differentiation of stratified squamous epithelia. Biochemistry 33, 7250-7259.

Rassendren, F.A., Lory, P., Pin, J.P., Nargeot, J., 1990. Zinc has opposite effects on NMDA and non-NMDA receptors expressed in *Xenopus* oocytes. Neuron 4, 733-740.

Represa, A., Niquet, J., Pollard, H., Khrestchatisky, M., Ben-Ari, Y., 1994. From seizures to neo-synaptogenesis: intrinsic and extrinsic determinants of mossy fiber sprouting in the adult hippocampus. Hippocampus 4, 270-274.

Ross, G.M., Shamovsky, I.L., Lawrance, G., Solc, M., Dostaler, S.M., Jimmo, S.L., Weaver, D.F., Riopelle, R.J., 1997. Zinc alters conformation and inhibits biological activities of nerve growth factor and related neurotrophins. Nature Med. 3, 872-878.

Rubio, M.E., Juiz, J.M., 1998. Chemical anatomy of excitatory endings in the dorsal cochlear nucleus of the rat: differential synaptic distribution of aspartate aminotransferase, glutamate, and vesicular zinc. J. Comp. Neurol. 399, 341-358.

Sallinen, J., Haapalinna, A., Viitamaa, T., Kobilka, B.K., Scheinin, M., 1998. Adrenergic a2c receptors modulate the acoustic startle reflex, prepulse inhibition, and aggression in mice. J. Neurosci. 18, 3035-3042.

Schetz, J.A., Chu, A., Sibley, D.R., 1999. Zinc modulates antagonist interactions with D2-like dopamine receptors through distinct molecular mechanisms. J. Pharmacol. Exp. Ther. 289, 956-964.

Slomianka, L., 1992. Neurons of origin of zinc-containing pathways and the distribution of zinc-containing boutons in the hippocampal region of the rat. Neuroscience 48, 325-352.

Sloviter, R.S., 1985. A selective loss of hippocampal mossy fiber Timm stain accompanies granule cell seizure activity induced by perforant path stimulation. Brain Res. 330, 150-153.

Smart, S.L., Lopantsev, V., Zhang, C.L., Robbins, C.A., Wang, H., Chiu, S.Y., Schwartzkroin, P.A., Messing, A., Tempel, B.L., 1998. Deletion of the K(V)1.1 potassium channel causes epilepsy in mice. Neuron 4, 809-819.

Smart, T.G., Moss, S.J., Xie, X., Huganir, R.L., 1991. GABAA receptors are differentially sensitive to zinc: dependence on subunit composition. Br. J. Pharmacol. 103, 1837-1839.

Smart, T.G., Xie, X., Krishek, B.J., 1994. Modulation of inhibitory and excitatory amino acid receptor ion channels by zinc. Prog. Neurobiol. 42, 393-441.

Suh, S.W., Chen, J.W., Motamedi, M., Bell, B., Listiak, K., Pons, N.F., Danscher, G., Frederickson, C.J., 2000. Evidence that synaptically-released zinc contributes to neuronal injury after traumatic brain injury. Brain Res. 852, 268-273.

Swerdlow, N.R., Geyer, M.A., 1998. Using an animal model of deficient sensorimotor gating to study the pathophysiology and new treatments of schizophrenia. Schizophrenia Bulletin 24, 285-301.

Thomas, S.A., Palmiter, R.D., 1997. Disruption of the dopamine beta-hydroxylase gene in mice suggests roles for norepinephrine in motor function, learning, and memory. Behav. Neurosci. 111, 579-589.

Thorlacius-Ussing, O., 1987. Zinc in the anterior pituitary of the rat: a histochemical and analytical work. Neuroendocrinology 45, 233-242.

Tonder, N., Johansen, F.F., Frederickson, C.J., Zimmer, J., Diemer, N.H., 1990. Possible role of zinc in the selective degeneration of dentate hilar neurons after cerebral ischemia in the adult rat. Neurosci. Lett. 109, 247-252.

Trombley, P.Q., Shepherd, G.M., 1993. Synaptic transmission and modulation in the olfactory bulb. Curr. Opin. Neurobiol. 3, 540-547.

Tsirka, S., Gualandris, A., Amaral, D.G., Strickland, S., 1995. Excitotoxin induced neuronal degeneration and seizure are mediated by tissue plasminogen activator. Nature 377, 340-344.

Tsirka, S., Rogove, A.D., Bugge, T.H., Degen, J.L., Strickland, S., 1997. An extracellular proteolytic cascade promotes neuronal degeneration in the mouse hippocampus. J. Neurosci. 17, 543-552.

Tsuda, M., Imaizumi, K., Katayama, T., Kitagawa, K., Wanaka, A., Tohyama, M., Takagi, T., 1997. Expression of zinc transporter gene, ZnT-1, is induced after transient forebrain ischemia in the gerbil. J. Neurosci. 17, 6678-6684.

Weiss, J.H., Koh, J.Y., Christine, C.W., Choi, D.W., 1989. Zinc and LTP. Nature 338, 212.

Westbrook, G.L., Mayer, M.L., 1987. Micromolar concentrations of Zn2+ antagonize NMDA and GABA responses of hippocampal neurons. Nature 328, 640-643.

Williams, J., 1997. How does a vesicle know it is full? Neuron 18, 683-686.

Willott, J.F., Carlson, S., Chen, H., 1994. Prepulse inhibition of the startle response in mice: relationship to hearing loss and auditory system plasticity. Behavioral Neurosci. 108, 703-713.

Vera-Gil, A., Perez-Castejon, M.C., Barral, M.J., Recreo, P., Perez-Castejon, M.J., 1991. Location of zinc in the testicle of the rat. Acta Anat. 141, 70-73.

Vincent, S.R., Semba, K., 1989. A heavy metal marker of the developing striatal mosaic. Development. Brain Res. 45, 155-159.

Xie, X.M., Smart, T.G., 1991. A physiological role for endogenous zinc in rat hippocampal synaptic neurotransmission. Nature 349, 521-524.

Zalewski, P.D., Millard, S.H., Forbes, I.J., Kapaniris, O., Slavotinek, A., Betts, W.H., Ward, A.D., Lincoln, S.F., Mahadevan, I., 1994. Video image analysis of labile zinc in viable pancreatic islet cells using a specific fluorescent probe for zinc. J. Histochem. Cytochem. 42, 877-884.

Zimmer, J., Haug, F.M.S., 1978. Laminar differentiation of the hippocampus, fascia dentata, and subiculum in developing rats, observed with the timm sulphide silver method. J. Comp. Neurol. 179, 581-618.

APPENDIX A

ZnT3, a putative transporter of zinc into synaptic vesicles.

Palmiter, R.D., Cole, T.B., Quaife, C.J., Findley, S.D., (1996) *Proc. Natl. Acad. Sci. USA* 93, 14934-14939.

Proc. Natl. Acad. Sci. USA
Vol. 93, pp. 14934–14939, December 1996
Neurobiology

ZnT-3, a putative transporter of zinc into synaptic vesicles

RICHARD D. PALMITER*, TOBY B. COLE, CAROL J. QUAIFE, AND SETH D. FINDLEY

Howard Hughes Medical Institute and Department of Biochemistry, University of Washington, Box 357370, Seattle, WA 98195

Contributed by Richard D. Palmiter, September 23, 1996

ABSTRACT **The murine *ZnT3* gene was cloned by virtue of its homology to the *ZnT2* gene, which encodes a membrane protein that facilitates sequestration of zinc in endosomal vesicles. ZnT-3 protein is predicted to have six transmembrane domains and shares 52% amino acid identity with ZnT-2, with the homology extending throughout the two sequences. Human ZnT-3 cDNAs were also cloned; the amino acid sequence is 86% identical to murine ZnT-3. The mouse *ZnT3* gene has 8 exons and maps to chromosome 5. Northern blot and reverse transcriptase–PCR analyses demonstrate that murine ZnT-3 expression is restricted to the brain and testis. *In situ* hybridization reveals that within the brain, ZnT-3 mRNA is most abundant in the hippocampus and cerebral cortex. Antibodies raised against the C-terminal tail of mouse ZnT-3 react with the projections from these neurons and produce a pattern similar to that obtained with Timm's reaction, which reveals histochemically reactive zinc within synaptic vesicles. We propose that ZnT-3 facilitates the accumulation of zinc in synaptic vesicles.**

Cytoplasmic zinc concentration is maintained within a narrow range in mammalian cells (1). Zinc is required for the maintenance and activity of numerous metalloproteins where it plays either a structural role (e.g., in zinc-finger proteins) or catalytic function as part of the active site of various metalloenzymes (2). Cells can tolerate slight increases in zinc over the amount required to fulfill metalloprotein needs, but beyond that excess, zinc becomes toxic unless cells can induce protective mechanisms (1). One protective mechanism involves the induction of metallothioneins that can sequester the excess zinc (3). However, another important mode of zinc regulation is likely to be at the level of transporters that facilitate zinc influx during deficiency and efflux during excess. Some of the molecules involved in zinc transport have been cloned recently. ZRT1 is a yeast protein with eight predicted transmembrane domains that mediates high-affinity uptake of zinc and is inducible by zinc limitation (4). A related low-affinity zinc uptake transporter (ZRT2) has also been cloned from yeast (5). Zinc efflux in mammalian cells is mediated by ZnT-1, a protein predicted to span the membrane six times. ZnT-1 is activated by excess zinc (1).

Zinc can also be concentrated in organelles in some cell types. Vesicular zinc has been visualized in pancreas, salivary gland, testis, and brain with the Timm's sulfide–silver staining procedure (6), as well as with the fluorescent probes 6-methoxy-8-*p*-toluene sulfonamide quinoline (TSQ) and zinquin (7, 8). These probes do not react appreciably with cytoplasmic zinc, suggesting that vesicular zinc is not tightly complexed with proteins. In pancreatic beta cells and male salivary glands, the detectable zinc is in secretory granules (7, 8), whereas in the brain the staining is predominantly in synaptic vesicles of neuronal axons (7). Neurons containing histochemically detectable zinc are particularly abundant in the hippocampal formation and cerebral cortex. The most intense Timm's or TSQ staining is seen in the "mossy fibers" that project from the granule cells of the dentate gyrus to the CA3 region of the hippocampus (9–12). Other regions of the hippocampus, cortex, and amygdala are also reactive. These neurons are thought to be excitatory glutamatergic neurons (7). Specific transporters are probably essential to concentrate zinc in various vesicular compartments.

We cloned a gene encoding a zinc transporter (ZnT-2) that facilitates accumulation of zinc in endosomal vesicles and confers resistance to zinc toxicity by complementation of a zinc-sensitive baby hamster kidney (BHK) cell line (13). This transporter is homologous to ZnT-1, but it is localized on endosomal vesicles instead of the plasma membrane. BHK cells expressing ZnT-2 accumulate detectable levels of zinc in endosomes only when they are exposed to elevated levels of extracellular zinc.

In the process of screening a mouse genomic λ library with rat ZnT-2 cDNA, a homologous gene was cloned. Herein we characterize that gene, which we call *ZnT3*, and show that its mRNA is abundant in the hippocampus and cortex. The ZnT-3 protein is detected immunologically in the mossy fibers, where zinc-containing vesicles are most abundant. Overall, the pattern of ZnT-3 expression resembles that observed with the Timm's stain or TSQ. Because the zinc in synaptic vesicles is coreleased with glutamate in response to high-frequency stimulation (14, 15) and can modulate the activity of various receptors *in vitro*, including ionotropic glutamate receptors and γ-aminobutyric acid receptors (16–23), zinc has been postulated to function as a neuromodulator (7, 24, 25). We propose that ZnT-3 is an essential component of the complex that sequesters zinc in synaptic vesicles, enabling it to serve as a neuromodulator.

MATERIALS AND METHODS

Cloning and Sequencing. A mouse (strain 129) genomic λ library was screened using rat ZnT-2 cDNA as a probe at reduced stringency. Eight clones were purified; four overlapping clones corresponded to mouse ZnT-2, whereas the other four overlapping clones represented a related gene. Most of the hybridization to the related gene was confined to a 2-kb *Eco*RI fragment that was isolated and sequenced. That *Eco*RI fragment was then used as a probe in a screen of a mouse brain cDNA library (Stratagene). The clone with the longest insert was sequenced. An oligonucleotide probe based on the 5′ end of the cDNA sequence was used to find the corresponding exon in the genomic DNA, which was then subcloned and sequenced. DNA sequencing was by the dideoxynucleotide method, using 7-deaza-dATP and 7-deaza-dGTP when necessary to resolve ambiguities. The cDNA was sequenced on both strands but the genomic DNA was only sequenced on one strand. The human ZnT-3 cDNA

The publication costs of this article were defrayed in part by page charge payment. This article must therefore be hereby marked "*advertisement*" in accordance with 18 U.S.C. §1734 solely to indicate this fact.

Abbreviations: TSQ, 6-methoxy-8-*p*-toluene sulfonamide quinoline; BHK, baby hamster kidney.

Data deposition: The sequences reported in this paper have been deposited in the GenBank data base (accession nos. U76007 for mouse ZnT3 cDNA, U76008 and U76009 for mouse ZnT3 genomic, and U76010 for human ZnT3 cDNA sequences).

*To whom reprint requests should be addressed. e-mail: palmiter@u.washington.edu.

was isolated from a brain temporal cortex library (Stratagene) and sequenced on both strands.

Immunological Techniques. DNA corresponding to the C-terminal 93 amino acids of ZnT-3 was amplified by PCR and inserted, in-frame, downstream of the maltose binding protein in pMAL-CR1 (New England Biolabs). The fusion protein was purified from *Escherichia coli* on amylose resin and used to immunize two rabbits (R & R Rabbitry, Stanwood, WA). The immunoglobulin fraction was isolated by ammonium sulfate precipitation and affinity-purified by passing it through a column containing the same C-terminal tail of ZnT-3 fused to a biotinylated peptide (PinPoint vector, Promega). The concentration of the purified antibody was 65 μg/ml.

For Western blots, cell pellets or solid tissues were homogenized in 8 vol of sample buffer (2% sodium dodecyl sulfate/5% 2-mercapoethanol/50 mM Tris·HCl, pH 7/10% glycerol/0.01% bromophenol blue) and boiled, and aliquots were electrophoresed on a 0.1% sodium dodecyl sulfate/10% polyacrylamide gel. The proteins were electrophoretically transferred to Hybond-C (Amersham). The nitrocellulose was soaked in 5% Blotto [PBS (138 mM NaCl/2.7 mM KCl/10 mM phosphate, pH 7.4) containing 5% nonfat powdered milk and 0.1% Tween-20] overnight at 4°C and then exposed to the purified antibody (diluted 1:100 in 1% Blotto) overnight at 4°C. The filter was washed three times in 1% Blotto and then incubated 1 hr with peroxidase-linked donkey anti-rabbit IgG (Amersham) that was diluted 1:3000 in 1% Blotto. This was followed by three washes in PBS/0.1% Tween-20, and the bound antibody was visualized using the Renaissance Western Blot Chemiluminescence reagents (DuPont/NEN) and exposed to X-Omat AR film (Eastman Kodak).

For immunocytochemistry, tissues were quickly removed from CO_2-asphyxiated C57BL/6 mice into ice-cold isopentane for 20 sec and then stored at −80°C prior to cutting 10-μm sections. The sections were air-dried, fixed in 4% paraformaldehyde in PBS, rinsed twice in PBS, and then boiled for 8 min in 10 mM citric acid using a microwave oven. The sections were returned to PBS and exposed to 3% H_2O_2 for 15 min, washed in PBS, and incubated overnight at 4°C with the primary antibody (1:100 dilution) in PBS containing 1% bovine serum albumin and 3% goat serum. After washing, the sections were incubated for 1 hr at 4°C with biotinylated anti-rabbit IgG, diluted 1:200 in PBS (Vector Laboratories). The reaction product was detected with streptavidin-peroxidase (1:20 dilution) using the AEC reagents from Zymed.

Timm's Staining. A modification of the Timm's staining procedure (26) was performed as described by Masters *et al.* (27).

RNA Detection. Total RNA was isolated from various organs of adult C57BL/6 mice using TRIzol reagent (BRL/GIBCO). Complementary DNA was prepared from 2 μg of total RNA using reverse transcriptase with oligo(dT) as a primer. Aliquots of the cDNA were then amplified by 35 cycles of PCR (94°C for 30 sec; 72°C for 90 sec) using the following oligonucleotide primers from genomic ZnT-1 sequence (1) [5′ primer, GGCCAACACCAGCAATTCCAACG (1011); 3′ primer, AAGGCATTCACGACCACGATCACG (2470)], from the mouse ZnT-2 cDNA sequence (13) [5′ primer, GTTGAGCTGGCTGTCCAGAGCAACC (133); 3′ primer, GCCGAAGTTCATGGTCTTGGTGGC (411)], from the mouse ZnT-3 cDNA sequence (this paper) [5′ primer, GGCCAACACCAGCAATTCCAACG (371); 3′ primer, AAGGCATTCACGACCACGATCACG (821)]. As a control for RNA integrity, primers for elongation factor 1α (EF1α) cDNA (2S) were used at 94°C for 30 sec, 55°C for 30 sec, and 72°C for 60 sec [5′ primer, ACATTAAGAAAATTGGCTAC (589); 3′ primer, ATTGAAGCCCACATTGTCCC (992)]. The number brackets refers to the location of the first base of the oligonucleotide on the published sequence. All of the primer pairs lie in separate exons to obviate any amplification due to DNA contamination. The products were visualized by ethidium bromide staining after electrophoresis through 0.8% agarose/2% NuSieve GTG agarose (FMC).

***In Situ* Hybridization.** *In situ* hybridization was performed essentially as described by Marks *et al.* (29). Tissues from C57BL/6 mice were prepared as described above. Frozen coronal sections (10 μm) were cut and placed on Superfrost/Plus microscope slides (Fisher Scientific). The sections were heated to 50°C for 2 min, air-dried 30 min, and stored at −80°C. The dried sections were fixed in 4% paraformaldehyde in PBS for 10 min at 4°C. After rinsing for two 5-min periods in PBS, the brain sections were dehydrated through a graded ethanol series to 70% ethanol, delipidated in chloroform for 5 min, rehydrated through the graded ethanol series, and rinsed in PBS for 5 min. Testis sections were not delipidated. To decrease nonspecific binding, the sections were treated with 0.25% acetic anhydride in 0.1 M triethanolamine (pH 9.5) for 10 min. After a brief rinse in PBS, the sections were incubated in 100 μl of hybridization mixture [50% formamide/1× Denhardt's solution/10% dextran sulfate/0.6 M NaCl/10 mM NaOAc/0.1% Tween 20/50 mM dithiothreitol (DTT)/heparin sodium (Fisher Scientific) (50 μg/ml)/yeast RNA (0.5 mg/ml)/herring sperm DNA (0.1 mg/ml)] for 3 hr at 50°C under a coverslip.

For the production of RNA probes, 1 μg of linearized template DNA [ZnT3 cDNA (1956 bp) in Bluescript (Stratagene)] was added to a 20-μl reaction mixture containing 2 μl of 10× transcription buffer (Boehringer Mannheim), 500 μM ATP, 500 μM GTP, 500 μM CTP, 5 μl (3 μM) of [^{33}P]UTP (Andotek, Irvine, CA), 40 units of RNAguard (Pharmacia), and 50 units of T3 or T7 RNA polymerase and incubated for 3 hr at 37°C. To destroy the template, the transcription reaction was diluted to 40 μl with H_2O and incubated with 1 μl (10 units) RNase-free DNase I (Boehringer Mannheim) for 30 min at 37°C. RNA was precipitated with 0.8 M LiCl and 3 vol of ethanol and resuspended in 50 μl of 0.2× SET (2 mM Tris/1 mM EDTA/0.2% SDS). This procedure gave a yield of 15,000 cpm/ng of RNA. The probe was diluted into fresh hybridization mixture (2 ng of RNA per μl). The coverslips were floated off the sections in PBS and rinsed briefly in PBS, 25 μl of the probe solution was applied, and a coverslip was sealed in place with a 1:1 mixture of petroleum ether and rubber cement. The sections were incubated for ≈16 hr at 50°C, after which the sealant was removed, the coverslips were floated off in 4× SSC (1× SSC = 150 mM NaCl/15 mM sodium citrate, pH 7.5), rinsed for 10 min in 2× SSC with 2 mM DTT, then treated with RNase A solution (RNase A at 20 μg/ml in 0.5 M NaCl/10 mM Tris, pH 8.0/10 mM DTT) for 30 min at 37°C. This was followed by a series of washes: 2× SSC/50% formamide/10 mM DTT at 60°C for 30 min; 1× SSC/50% formamide/10 mM DTT at 60°C (for brain) or 50°C (for testis) for 30 min; 0.1× SSC at 37°C for 30 min. The sections were then dehydrated through a graded ethanol series, air-dried for about 16 hr, and coated with emulsion (NTB-3, Eastman Kodak). Coated slides were exposed to emulsion for various times (4–17 days) at 4°C. After developing the sections, silver grains were visualized and photographed in dark field, using a Nikon Microphot FX microscope.

Chromosomal Mapping. ZnT-3 was mapped to chromosome 5 as described (13). The approved designation for its gene locus is *Znt3*. The chromosomal map location is available on the World Wide Web at http://www.jax.org/resources/documents/cmddata.

Expression of ZnT-3 in BHK Cells. The ZnT-3 cDNA was inserted into the cloning site of pcDNA1 that had been modified to carry a dihydrofolate reductase gene driven by simian virus 40 promoter/enhancer. This construct was transfected into a zinc-sensitive BHK cell line (32S6–S-S) and cells resistant to methotrexate were cloned (1). A clone with the highest level of ZnT-3 mRNA was selected for further studies.

A derivative, ZnT-3:GFP, with the green fluorescent protein (containing alanine at position 65) fused at the C terminus of ZnT-3 was also prepared in this vector.

RESULTS

Cloning and Characterization of Mouse *ZnT3* Gene and cDNA. Four overlapping mouse genomic clones were isolated from a λ library by screening with rat ZnT-2 cDNA. Restriction mapping revealed that most of the hybridization signal corresponded to a 2-kb *Eco*RI fragment that was subcloned and sequenced. It contained several putative exons with homology to ZnT-2. The *Eco*RI fragment was then used to screen a mouse brain cDNA library. The longest cDNA clone was sequenced; it contained an open reading frame encoding a protein of 388 amino acids that is 52% identical to rat ZnT-2 (Fig. 1). We call the new protein ZnT-3 (*Zinc Transporter-3*) because of its similarity to ZnT-2. The two proteins are predicted to have similar membrane topology with six transmembrane domains and both N and C termini on the cytoplasmic side of the membrane.

Seven exons encoding most of ZnT-3 were located in the λ clones and sequenced. About 800 nt corresponding to the 3′ end of the cDNA were not included in any of the λ clones; however, PCR of mouse genomic DNA with opposing primers from each end of the missing 800 nt gave a product with the same size as that obtained from the cDNA, indicating that they reside within one exon. This exon, number 8, which includes the C-terminal 50 amino acids and 3′ untranslated region, is located ≈1.05 kb downstream of exon 7, as determined by restriction mapping. A composite map of the mouse *ZnT3* gene is shown in Fig. 2*B*; the locations of the introns are indicated in Fig. 2*A*. Because the genomic sequence upstream of the 5′ end of the cDNA is G+C-rich and lacks potential splice acceptor sites, we assume that this is the first exon; however, no obvious TATA box was discerned and the transcription start site has not been mapped. Although the mouse *ZnT2* gene has not been completely characterized, its genomic organization appears to be similar to that of *ZnT3*; both of these genes are more complex than *ZnT1*, which has only two exons.

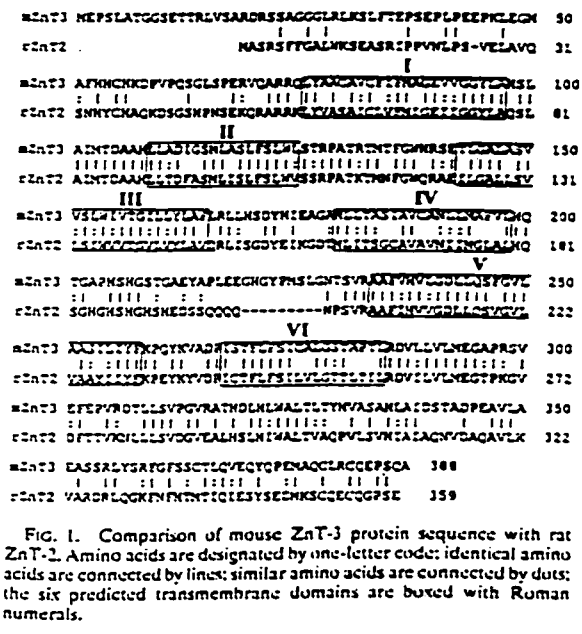

FIG. 1. Comparison of mouse ZnT-3 protein sequence with rat ZnT-2. Amino acids are designated by one-letter code; identical amino acids are connected by lines; similar amino acids are connected by dots; the six predicted transmembrane domains are boxed with Roman numerals.

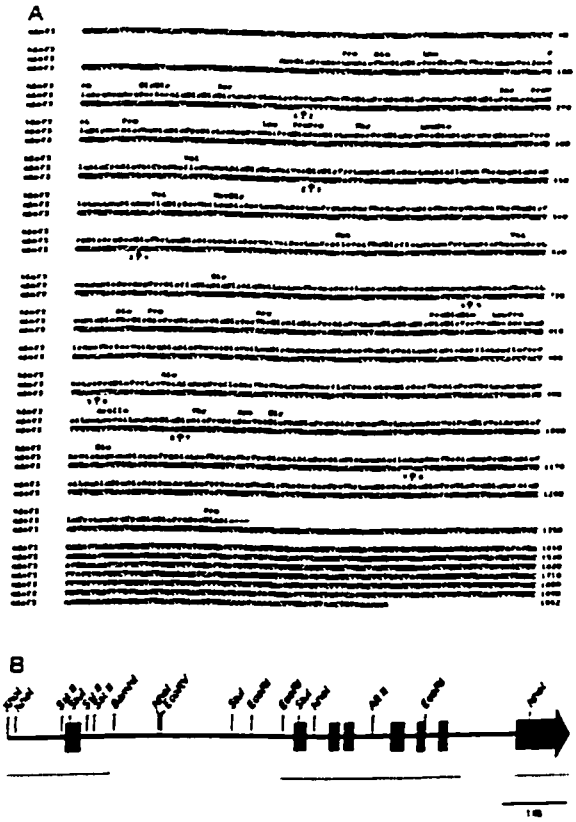

FIG. 2. Sequence of mouse ZnT-3 cDNA, comparison of mouse and human ZnT-3 protein sequences, and mouse ZnT-3 genomic organization. (*A*) Mouse ZnT-3 cDNA sequence with amino acid sequence in three-letter code above. Differences between human and mouse ZnT-3 are indicated above the mouse protein sequence. Arrows indicate the location of introns and numbers designate the flanking exons. (*B*) A map of the mouse ZnT-3 genomic DNA showing the location of 8 exons. The regions that have been sequenced are indicated with a dotted line.

Cloning Human ZnT-3 cDNA. The human counterpart of mouse ZnT-3 was cloned from a human temporal cortex cDNA library in a λ ZAP vector. Twenty-four clones were identified by hybridization to mouse ZnT-3 at low stringency; sequencing revealed that they all represented parts of the same cDNA. Two overlapping clones were sequenced to produce the complete open reading frame, which encodes a protein of 388 amino acids that is 86% identical to mouse ZnT-3; the amino acid differences are shown in Fig. 2*A*.

Chromosomal Mapping of ZnT-3. Genomic DNAs from C57BL/6J and *Mus spretus* were digested with 10 different enzymes, electrophoresed on agarose, and transferred to nitrocellulose, and the blots were probed with the mouse ZnT-3 cDNA. Polymorphisms were apparent for *Bgl*II, *Eco*RI, and *Msp*I. The *Bgl*II polymorphism was chosen to screen 94 segregants of the Jackson Laboratory BSS backcross panel (30) using Southern blot filters provided by the Jackson Laboratory BC Panel Map Service. This analysis indicated that *ZnT3* cosegregates with *Nos3*, *Pep1b*, and *Plk* on mouse chromosome 5 near the engrailed (*En*) locus. Human ZnT-3

was not mapped, but the syntenic region is on human chromosome 7. *ZnT3* is on a different chromosome than *ZnT2*, which resides on mouse chromosome 4 (10).

Expression of ZnT-3 in BHK Cells. Because the *ZnT3* gene was cloned by virtue of its homology to *ZnT2*, it was tested for its ability to confer resistance to metals in zinc-sensitive BHK cells. The ZnT-3 cDNA was inserted into an expression vector with a *DHFR*-selectable gene, transfected into BHK cells and a stable clones were isolated after growth in 20 μM methotrexate. Solution hybridization with an oligonucleotide complementary to ZnT-3 mRNA was used to identify clones with the highest levels of ZnT-3 mRNA. Western blots revealed a protein of the expected size in these cells (see below). Fluorescence with zinquin was not observed in the transfected BHK cells regardless of whether they were incubated in normal medium or in medium containing up to the maximum amount of zinc they could tolerate. These cells were also compared with the parental cells for their resistance to zinc, cadmium, cobalt, and copper toxicity. No resistance to the toxic effects of any of these metals was observed (data not shown). We conclude that expression of ZnT-3 in BHK cells has no discernible effect on their phenotype, in contrast to the pronounced effects of ZnT-1 or ZnT-2 expression in these cells (1, 13).

Expression of ZnT-3 *in Vivo*. To determine where ZnT-3 is expressed *in vivo*, total RNA was isolated from various mouse organs and converted to cDNA with reverse transcriptase using oligo(dT) as a primer. Aliquots were then subjected to PCR using primers in exons 2 and 5 (see Fig. 2). A product was detected by ethidium bromide staining with RNA from brain and testis but not the other organs indicated in Fig. 3. In contrast, ZnT-1 is expressed in most organs and ZnT-2 is expressed in intestine, kidney, seminal vesicles, and testis.

In situ hybridization with antisense RNA probes to mouse ZnT-3 was used to determine which cells in brain and testis express ZnT-3. Fig. 4*A* shows a coronal section of a mouse brain, revealing hybridization to the hippocampal formation, piriform cortex, and lateral amygdala, as well as several layers of the neocortex. Hybridization was also detectable in the paraventricular thalamic nucleus and the zona inserta. In the hippocampus (Fig. 4*B*), ZnT-3 mRNA is evident in granule cell neurons of the dentate gyrus and in pyramidal cells in the CA3 and CA1 regions. This hybridization pattern corresponds closely to the cell bodies of neurons that sequester zinc in synaptic vesicles (compare Fig. 4 *D* and *F*). Examination of sagittal sections of mouse brain revealed the presence of ZnT-3 mRNA in the entorhinal cortex as well, whereas there was none in olfactory bulb, cerebellum, or hypothalamus (data not shown). In the testis, hybridization was confined to germ cells and was most intense in pachytene spermatocytes and round spermatids (data not shown). No specific hybridization to either brain or testis sections was observed with a ZnT-3 sense probe (data not shown).

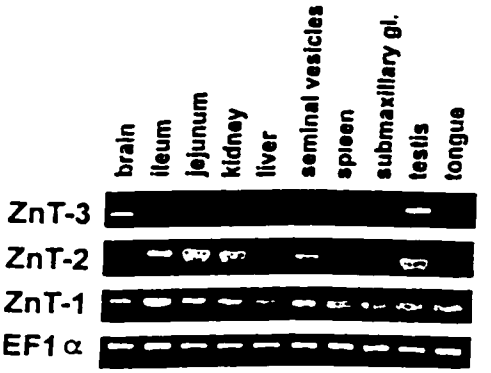

FIG. 3. Organ distribution of ZnT-3, ZnT-2, and ZnT-1 mRNAs. Total RNA from the indicated organs was prepared and subjected to reverse transcription followed by PCR. The products were electrophoresed through 2.3% agarose and stained with ethidium bromide.

ZnT-3 Protein Is Present in the Mossy Fibers of the Hippocampus That Sequester Zinc in Synaptic Terminals. A rabbit polyclonal antibody was raised against the C-terminal cytoplasmic tail of mouse ZnT-3 and purified by affinity chromatography. The specificity of this antibody was assessed by Western blots of total cell proteins from control BHK cells and BHK cells that were stably transfected with constructs expressing ZnT-1 (1), ZnT-2 (12), or ZnT-3 (described above). Only BHK cells expressing ZnT-3 reacted with this antibody, indicating that it does not react with the homologous proteins (Fig. 5). The specific band detected in the BHK cells has an apparent molecular weight of ≈40 kDa. An immunoreactive protein of similar size was detected in brain samples, but no protein of this size was detected in either the kidney or testis samples (Fig. 5). A faint band of lower molecular weight was evident in testis after longer development times.

When this antibody was applied to brain sections, the most intense immunostaining was observed over the mossy fiber projections emanating from the granule cell neurons in the dentate gyrus (Fig. 4 *C* and *D*). Projections from pyramidal cells of the hippocampus and in the cortex also stained with this antibody but not with preimmune serum (data not shown). The antibody staining pattern in the brain is very similar to the histochemical localization of zinc by the Timm's reaction, which detects loosely bound synaptic zinc (compare Fig. 4 *C* and *E* with *D* and *F*). The only exception being the dendritic field of the dentate granule cells that react with the antibody but not with Timm's staining procedure (compare Fig. 4 *D* and *F*).

Neither Western blots of total testis proteins (Fig. 5) nor immunohistochemistry on sections of adult testis using the purified antibody (data not shown) gave a reaction under conditions that worked well for detection of ZnT-3 protein in the brain.

DISCUSSION

We have cloned mouse and human ZnT-3 cDNAs encoding membrane proteins that are homologous to the mammalian zinc transporters, ZnT-1 and ZnT-2, as well as two yeast proteins, ZRC and COT1, that confer resistance to zinc and cobalt, respectively. All of these proteins are predicted to have six transmembrane domains with the N and C termini located in the cytoplasm (1). The cytoplasmic loop connecting the transmembrane domains IV and V is relatively short in ZnT-3 and lacks the characteristic histidines of ZnT-1 and ZnT-2. The transmembrane domains and C-terminal tail of ZnT-3 (≈150 amino acids) are similar to ZnT-2. Furthermore, the exon–intron structures of the ZnT-2 and ZnT-3 genes are similar, but unlike ZnT-1, which has only one intron. The low-stringency screen of the human brain cDNA library only produced the human counterpart of mouse ZnT-3, suggesting that if there are other members of this gene family, they are either too divergent from ZnT-3 to hybridize or are not expressed in temporal cortex.

The best clues for the function of ZnT-3 arise from its expression pattern and its homology to ZnT-2, which facilitates accumulation of zinc into vesicles in BHK cells. ZnT-3 mRNA is detected only in brain and testis when measured by reverse transcriptase–PCR or Northern blot analysis. ZnT-3 mRNA is readily detected in the hippocampus and cortex by *in situ* hybridization. Within the hippocampal formation, the cell bodies of the granule cells in the dentate gyrus produce the most intense hybridization signal, while pyramidal cells in the CA3 and CA1 regions also give strong signals. All of these

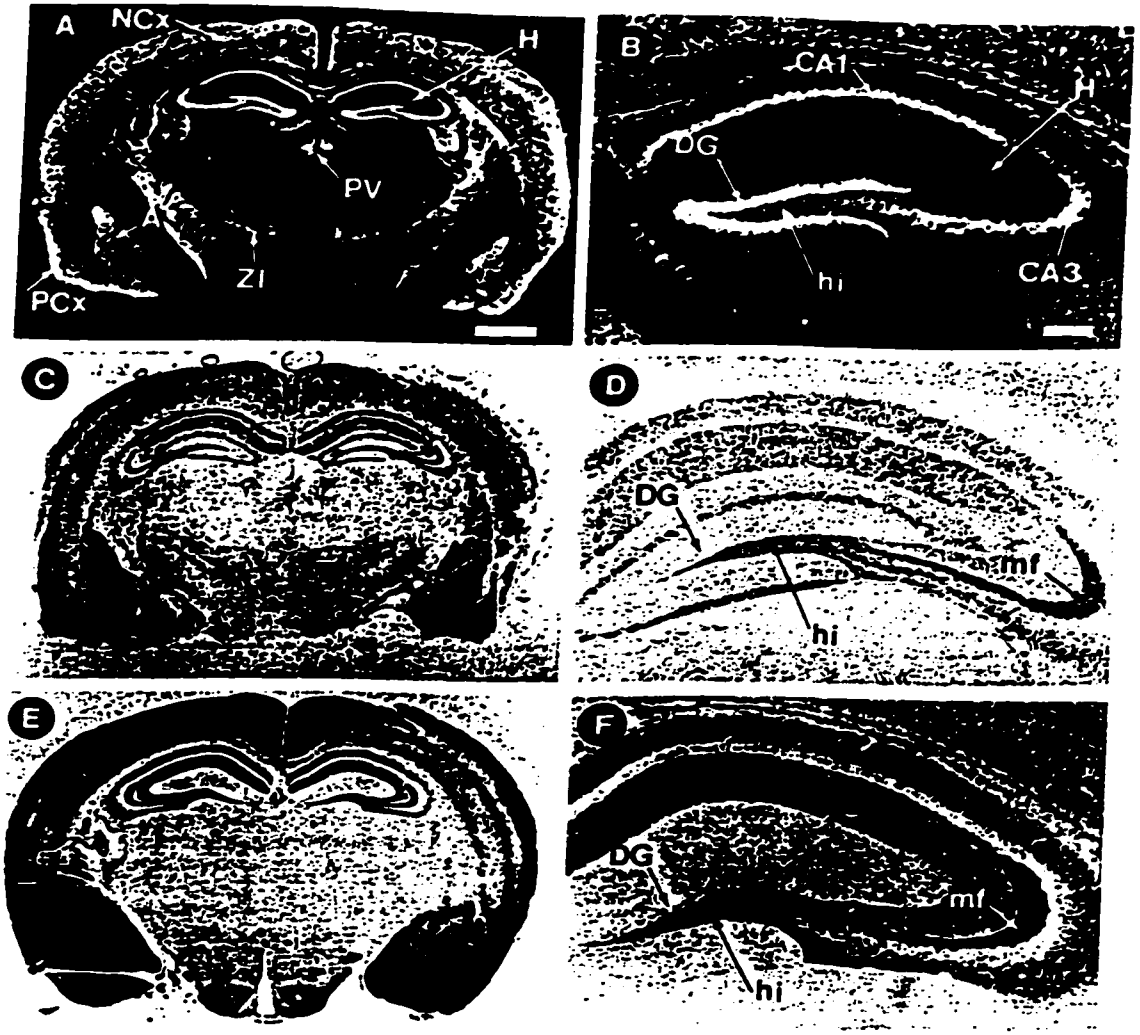

FIG. 4. Localization of ZnT-3 mRNA, protein, and histochemically reactive zinc in the brain. Coronal sections of mouse brain were subjected to *in situ* hybridization with a ^{33}P-labeled probe complementary to mouse ZnT-3 mRNA (*A* and *B*), immunocytochemistry with affinity-purified antisera raised against the C-terminal tail of ZnT-3 (*C* and *D*), and Timm's staining procedure for vesicular zinc (*E* and *F*). (*B*, *D*, and *F*, ×2.3; *A*, *C*, and *E*, ×0.7). In the hippocampus, ZnT-3 mRNA is present in the cell bodies of dentate granule cells, and ZnT-3 protein is abundant in the zinc-rich mossy fiber projections emanating from these neurons. A, amygdala (lateral nucleus); H, hippocampus; NCx, neocortex; PCx, piriform cortex; PV, paraventricular thalamic nucleus; ZI, zona inserta; GC, granule cell neurons of the dentate gyrus; hi, hilus; mf, mossy fibers. [Bars = 1000 μm (*A*) and 200 μm (*B*).]

glutamatergic neurons have processes containing vesicular zinc as revealed by a variety of histochemical techniques (9–12). The mossy fiber projections of granule cells produce the most intense staining for histochemically reactive zinc with the sulfide/silver or TSQ fluorescence methods. The mossy fibers also give the most intense reaction with the antibody against ZnT-3, suggesting that ZnT-3 is transported down the axons of granule cells in association with zinc. We also note *in situ* hybridization signals and immunostaining in many regions of the cerebral cortex that resemble the Timm's staining pattern; however, because the cellular architecture of the cortex is complex, we cannot be certain that ZnT-3 is localized exclusively in neurons that sequester zinc.

Because ZnT-3 is homologous to ZnT-2, which has been localized to endosomes of BHK cells and facilitates accumulation of zinc in those vesicles (13), we predict that ZnT-3 might also be localized to the membranes of a cellular organelle. An attractive possibility is that ZnT-3 is one component of a complex involved in transport of zinc into synaptic vesicles. In the hippocampus, the ZnT-3 protein is most abundant where zinc-laden synaptic vesicles reside, which is consistent with it being a membrane component of those vesicles. However, it is also possible that other organelles are transported down the axons of those neurons and ZnT-3 may be associated with them. Electron microscopy of immunogold-labeled sections after Timm's staining should answer the question of whether ZnT-3 is on the same vesicles that accumulate zinc in the mossy fibers and elsewhere in the brain.

We have no direct evidence that ZnT-3 transports zinc; however, its homology to other zinc transporters and its

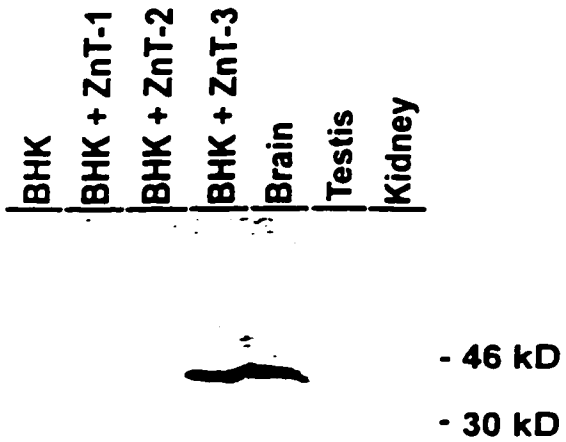

FIG. 5. Western blot analysis of ZnT-3 protein. Lanes 1–4 represent equivalent amounts of protein isolated from confluent BHK cells: untransfected cells (lane 1), cells expressing ZnT-1 (lane 2), cells expressing ZnT-2 (lane 3), and cells expressing ZnT-3 (lane 4). Lanes 5–7 represent total protein from brain (lane 5), testis (lane 6), and kidney (lane 7). The amount of protein in all lanes was similar by Coomassie blue 250 staining of a replicate gel. Affinity-purified antibody to ZnT-3 was detected with a peroxidase-linked secondary antibody by chemiluminescence.

association with vesicular zinc in the brain lends credence to this hypothesis. Unlike ZnT-2 (13), expression of ZnT-3 in BHK cells does not protect against zinc toxicity, does not result in accumulation of zinc, and does not produce zinquin fluorescence when the cells are grown in normal or zinc-supplemented medium. We tested whether ZnT-3 might provide resistance to other heavy metals (copper, cobalt, or cadmium) in cell culture, but none was detected. The mechanism of metal transport by members of this gene family are unknown. Presumably other components must be involved because these proteins do not have obvious ATP-binding domains. Thus, one possible explanation for the lack of ZnT-3 function in BHK cells may be that it normally functions as part of a protein complex and critical components of that complex may be missing in BHK cells. BHK cells expressing ZnT-3 were transfected with brain-derived cDNA expression libraries, followed by selection for zinc resistance; however, no cDNAs that could complement ZnT-3 were identified in this screen.

ZnT-3 mRNA, as detected by Northern blot and reverse transcriptase–PCR, is more abundant in adult testis than in brain and *in situ* hybridization reveals that ZnT-3 mRNA is in developing germ cells. However, neither Western blots nor immunocytochemistry of testis sections revealed any ZnT-3 protein. Northern blots of polysomal preparations from testis indicated that the ZnT-3 transcripts were abundant on ribonucleoprotein particles that sedimented slower than monoribosomes, rather than in the polysome region, suggesting that this mRNA may not be translated efficiently (data not shown). A small amount of translation at a late stage in spermiogenesis might be undetectable by the techniques used.

The cloning of the mouse ZnT-3 gene provides an opportunity to inactivate it by homologous recombination. This could provide definitive evidence regarding the role of this gene product in zinc sequestration. If inactivation of ZnT-3 prevents the accumulation of zinc in synaptic vesicles, as we predict, it will provide a unique opportunity to explore the function of this vesicular pool of zinc in neuronal function, learning, and memory, as well as its contribution to various disease processes.

We thank Glenda Froelick for preparing the histological sections, Mark Fajardo for sharing the testis polysome Northern blots, and our colleagues for valuable discussions during the course of this work and preparation of the manuscript.

1. Palmiter, R. D. & Findley, S. D. (1995) *EMBO J.* **14**, 639–649.
2. Vallee, B. L. & Falchuk, K. H. (1993) *Physiol. Rev.* **73**, 79–117.
3. Palmiter, R. D. (1987) *Experientia* **52**, Suppl., 63–80.
4. Zhao, H. & Eide, D. (1996) *Proc. Natl. Acad. Sci. USA* **93**, 2454–2458.
5. Zhao, H. & Eide, D. (1996) *J. Biol. Chem.* **271**, 23203–23210.
6. Timm, F. (1958) *Dtsch. Z. Ges. Gericht. Med.* **46**, 706–711.
7. Frederickson, C. J. & Moncrieff, D. D. (1994) *Biol. Signals* **3**, 127–139.
8. Zalewski, P. D., Millard, S. H., Forbes, I. J., Kapaniris, O., Slavotinek, A., Betts, W. H., Ward, D., Lincoln, S. F. & Mahadevan, I. (1994) *J. Histochem. Cytochem.* **42**, 877–884.
9. Danscher, G. (1981) *Histochemistry* **71**, 1–16.
10. Frederickson, C. J. (1989) *Int. Rev. Neurobiol.* **31**, 145–238.
11. Frederickson, C. J. & Danscher, G. (1990) *Prog. Brain Res.* **83**, 71–84.
12. Slomianka, L. (1992) *Neuroscience* **48**, 325–352.
13. Palmiter, R. D., Cole, T. B. & Findley, S. D. (1996) *EMBO J.* **15**, 1784–1791.
14. Assaf, S. & Chung, S. (1984) *Nature (London)* **308**, 734–738.
15. Howell, G. A., Welch, M. G. & Frederickson, C. J. (1984) *Nature (London)* **308**, 736–738.
16. Westbrook, G. L. & Mayer, M. L. (1987) *Nature (London)* **328**, 640–643.
17. Aniksztejn, L., Charton, G. & Ben-Ari, Y. (1987) *Brain Res.* **404**, 58–64.
18. Mayer, M. L., Vyklicky, L., Jr., & Westbrook, G. L. (1989) *J. Physiol. (London)* **415**, 329–350.
19. Christine, C. W. & Choi, D. W. (1990) *J. Neurosci.* **10**, 108–116.
20. Rassendren, F. A., Lory, P., Pin, J. P. & Nargeot, J. (1990) *Neuron* **10**, 943–954.
21. Xie, X. & Smart, T. G. (1991) *Nature (London)* **349**, 521–524.
22. Smart, T. G. (1992) *J. Physiol. (London)* **447**, 587–625.
23. Hollman, M., Boulter, J., Mason, C., Beasly, L., Sullivan, J., Pechet, G., Heinemann, S. (1993) *Neuron* **4**, 733–739.
24. Smart, T. G., Xie, X. & Krishek, B. J. (1994) *Prog. Neurobiol.* **42**, 393–441.
25. Harrison, N. L. & Gibbons, S. J. (1994) *Neuropharmacology* **33**, 935–952.
26. Sloviter, R. S. (1982) *Brain Res. Bull.* **8**, 771–774.
27. Masters, B. A., Quaife, C. J., Erickson, J. C., Kelly, E. J., Froelick, G. J., Zambrowicz, B. P., Brinster, R. L. & Palmiter, R. D. (1994) *J. Neurosci.* **14**, 5844–5857.
28. Reddy, N. S., Roth, W. W., Bragg, P. W. & Wahba, A. J. (1988) *Gene* **70**, 231–243.
29. Marks, D. L., Wienman, J. N., Burton, K. A., Lent, K. L., Clifton, D. K. & Steiner, R. A. (1992) *Mol. Cell. Neurosci.* **3**, 395–401.
30. Rowe, L. B., Nadeau, J. H., Turner, R., Frankel, W. N., Letts, V. A., Eppig, J. T., Ko, M. S. H., Thurston, S. J. & Birkenmeier, E. H. (1994) *Mamm. Genome* **5**, 253–274.

APPENDIX B

Ultrastructural localization of zinc transporter-3 (ZnT3) to synaptic vesicle membranes within mossy fiber boutons in the hippocampus of mouse and monkey.

Wenzel, H.J., Cole, T.B., Born, D.E., Palmiter, R.D., Schwartzkroin, P.A., (1997) *Proc. Natl. Acad. Sci. USA* 94, 12676-12681.

Proc. Natl. Acad. Sci. USA
Vol. 94, pp. 12676–12681, November 1997
Neurobiology

Ultrastructural localization of zinc transporter-3 (ZnT-3) to synaptic vesicle membranes within mossy fiber boutons in the hippocampus of mouse and monkey

H. JÜRGEN WENZEL*, TOBY B. COLE†, DONALD E. BORN‡, PHILIP A. SCHWARTZKROIN*§, AND RICHARD D. PALMITER†¶

Departments of *Neurological Surgery, ‡Pathology, §Physiology/Biophysics, and †Biochemistry and ¶Howard Hughes Medical Institute, Box 357370, University of Washington, Seattle, WA 98195

Contributed by Richard D. Palmiter, September 9, 1997

ABSTRACT **Zinc transporter-3 (ZnT-3), a member of a growing family of mammalian zinc transporters, is expressed in regions of the brain that are rich in histochemically reactive zinc (as revealed by the Timm's stain), including entorhinal cortex, amygdala, and hippocampus. ZnT-3 protein is most abundant in the zinc-enriched mossy fibers that project from the dentate granule cells to hilar and CA3 pyramidal neurons. We show here by electron microscopy that ZnT-3 decorates the membranes of all clear, small, round synaptic vesicles (SVs) in the mossy fiber boutons of both mouse and monkey. Furthermore, up to 60–80% of these SVs contain Timm's-stainable zinc. The coincidence of ZnT-3 on the membranes of SVs that accumulate zinc, and its homology with known zinc transporters, suggest that ZnT-3 is responsible for the transport of zinc into SVs, and hence for the ability of these neurons to release zinc upon excitation.**

Most of the zinc in the mammalian brain is associated with metalloproteins; however, there is also a pool of histochemically reactive zinc that exists in synaptic vesicles (SVs) of a subset of glutamatergic neurons, which has led to classification of these neurons as zinc-containing or zinc-ergic (1–4). Pathways utilizing this vesicular form of zinc have been mapped using histochemical stains such as the neo-Timm's sulfide-silver method (5), selenium stain (6, 7), and the fluorescent compound, TSQ (8). One of the best described zinc-ergic systems is found in the rodent hippocampal formation, where vesicular zinc can be detected in each component of the trisynaptic circuit that includes (*i*) perforant path projections from the entorhinal cortex to the outer molecular layer of the dentate gyrus, (*ii*) mossy fiber (MF) projections from granule cells in the dentate gyrus to hilar neurons and pyramidal cells in the CA3 region (4, 9–11), (*iii*) projections from CA3 pyramidal neurons to neurons in the CA1 region, and (*iv*) projections from CA1 to subiculum (3, 4). Electron microscopy (EM) has revealed that the Timm's stain precipitate is present within SVs in the giant axonal boutons of the MFs in the hilus and stratum (s.) lucidum (1, 2, 12). However, only ≈10–15% of the SVs within a given bouton have been shown to contain Timm's precipitate (2); thus, it has been difficult to ascertain whether zinc is present in a subset of vesicles or if it is present in the same vesicles as glutamate.

Accumulation of zinc within SVs presumably depends on the action of specific transporters, by analogy with the accumulation of other neurotransmitters in SVs (13). A gene, designated zinc transporter-3 (*ZnT3*), homologous to two established zinc transporters (14, 15) was recently cloned (16). ZnT-3 was shown by *in situ* hybridization to be expressed at high levels in hippocampus and neocortex. Immunocytochemical studies demonstrated its localization to the MFs, where the histochemical Timm's reaction has revealed zinc-containing SVs. This profile suggested that ZnT-3 might be the vesicular zinc transporter responsible for sequestration of zinc in MF SVs (16), but also raised questions regarding the ultrastructural localization of ZnT-3 relative to zinc and other neurotransmitters.

MATERIALS AND METHODS

Tissue Preparation. Eight mice (6 C57BL/6; 2 C57BL/6x129), ages 8–20 weeks, and five monkeys, (*Macaca nemestrina*), age 1 year were used for light microscopy and EM immunocytochemical localization of ZnT-3 and for histochemical localization of zinc within the MF system of the hippocampus.

Mice were anesthetized with Nembutal (100 mg/kg, i.p.), then perfused with isotonic saline with heparin (100 units/ml saline), followed by 4% paraformaldehyde in 0.1 M sodium phosphate buffer (PB), pH 7.4, or by a solution containing 4% paraformaldehyde, 0.1% glutaraldehyde, and 0.1% picric acid in PB. [The low level of glutaraldehyde was necessary to preserve immunoreactivity (IR) but resulted in suboptimal ultrastructure.] The brains were removed and placed in the same fixative for 4 hr at 4°C. Monkeys were anesthetized (Nembutal, 50–75 mg/kg) and perfused transcardially with 4% paraformaldehyde in PB. Tissue blocks from the temporal lobe, containing the hippocampus, were dissected and cut into 1.5-mm thick slices that were then placed in the same fixative for 24 hr at 4°C.

After postfixation, the brains (mice) or slices (monkey) were rinsed in PB, cryoprotected in 10% sucrose for 1 hr, followed by 30% sucrose for 8–12 hr at 4°C, then frozen on dry ice. Transverse serial sections, 30 μm for light microscopy and 80 μm for EM, were cut on a sliding microtome equipped with a freezing stage, and sections were selected for further processing.

EM Detection of ZnT-3. An affinity-purified rabbit antibody specific for ZnT-3 (16) was used to determine its ultrastructural localization. Sections were rinsed in PB, followed by 0.1 M Tris·HCl buffer (TB), pH 7.4; then endogenous peroxidases were inactivated by treatment with 0.5–1% H_2O_2 in TB for 2 hr. Sections were treated with 3% BSA, 3% goat serum, and 0.25% dimethyl sulfoxide in TBS (0.05 M TB/0.15 M NaCl, pH 7.4) for 1 hr to reduce nonspecific staining. Sections were rinsed in TBS for 30 min and incubated for 20 hr at 4°C in ZnT-3 antiserum, diluted 1:100 to 1:300 in TBS containing 1% goat serum, 2% BSA and 0.25% dimethyl sulfoxide. Following rinses for 2 hr in TBS, sections were incubated in biotinylated goat anti-rabbit IgG (diluted 1:500) for 24 hr at 4°C, rinsed 2 hr in TBS and then incubated in ABC (Elite ABC Kit; Vector

The publication costs of this article were defrayed in part by page charge payment. This article must therefore be hereby marked "*advertisement*" in accordance with 18 U.S.C. §1734 solely to indicate this fact.

Abbreviations: SV, synaptic vesicle; MF, mossy fiber; MFB, MF bouton; IR, immunoreactivity; ZnT-3, zinc transporter-3; EM, electron microscopy; s., stratum; GABA, γ-aminobutyric acid.

¶To whom reprint requests should be addressed. e-mail: palmiter@u.washington.edu.

Laboratories), diluted 1:500 in 1% goat serum, 2% BSA, 0.25% dimethyl sulfoxide and TBS for 24 hr at 4°C. Sections were rinsed in TB (pH 7.6), then incubated for 15 min in 0.025% 3,3'-diaminobenzidine in TB. After reaction for 5–10 min in fresh 3,3'-diaminobenzidine with 0.003% H_2O_2, sections were rinsed in TB, followed by PB. Specificity of the immunostaining was evaluated by omitting primary antibody.

Sections were further processed for EM by postfixation in 1% osmium tetroxide in PB for 1 hr at 22°C, followed by alcohol dehydration and flat embedding in Eponate 12 (Ted Pella, Redding, CA) between two aclar sheets for 24 hr at 60°C. Selected immunoreactive areas were cut from embedded sections and remounted with Eponate 12 on plastic blocks. Serial ultrathin sections were cut close to the tissue surface, stained with uranyl acetate and lead citrate, and examined on a Philips (Eindhoven, The Netherlands) 410 electron microscope.

Postembedding Detection of ZnT-3 and Glutamate. To investigate colocalization of ZnT-3 and glutamate in SVs of MFs, postembedding immunocytochemistry was performed as described by Wenzel *et al.* (17). Ultrathin sections from Timm's-stained sections or glutaraldehyde/paraformaldehyde-fixed tissue were etched with redox reagents (periodic acid, sodium metaperiodate) to reduce osmium staining and to expose antigenic sites. Sections were then incubated with the primary antibodies—rabbit anti-glutamate (Sigma) diluted 1:10,000 or affinity-purified ZnT-3 antibody, diluted 1:50 or 1:100—followed by goat-anti-rabbit IgG conjugated to gold (10 nm, Ted Pella), diluted 1:20.

Timm's Staining. For light microscopy detection in mouse and monkey brains, a Timm's-staining protocol described by Franck *et al.* (18) was adapted. Fixed hippocampal slices (1 mm) were immersed in 0.4% Na_2S for 30 min, then fixed ~16 hr in 1% paraformaldehyde and 1.25% glutaraldehyde. The fixed slices were cryoprotected, 30 μm sections were mounted and dried, and sections were immersed in developer [30 ml gum Arabic (50%), 5 ml citrate buffer (2 M, pH 3.7), 15 ml hydroquinone (5.67%) and 0.25 ml $AgNO_3$ (17%)] for at least 60 min. A brief staining period was used in most cases to focus on the densely reactive MF pathway; longer exposure times revealed typical laminar Timm's profile in the dentate molecular layer (not shown).

To increase the specific staining of zinc and improve visualization of the MF system by EM, a variant of the neo-Timm's stain (2, 5, 19, 20) was modified. After the initial fixation, the tissue was transferred to a solution containing 3–4% glutaraldehyde, 0.1% Na_2S, and 0.136 mM $CaCl_2$ in 0.12 M Millonig's buffer, pH 7.3, for 24 hr at 4°C. The tissue was transferred to cold 0.12 M Millonig's buffer with 0.136 mM $CaCl_2$ and sectioned with a vibratome at 80 μm. Sections containing the hippocampus were transferred to a fresh developing solution [60 ml gum Arabic (50%), 10 ml 2 M citrate buffer; 15 ml hydroquinone (5.67%) and 15 ml silver lactate (0.73%)] for 1 hr in the dark, with constant agitation (20), then washed for 10 min and postfixed in phosphate-buffered osmium tetroxide for 1 hr. The tissue was dehydrated through alcohols to propylene oxide, then flat-embedded in Eponate 12.

RESULTS

Morphological Characteristics of MF Boutons (MFBs) in Mouse and Monkey. MF axons of the dentate granule cells establish synaptic contacts with neurons in the dentate hilus and with pyramidal cells of the hippocampal CA3 region (see refs. 21 and 22 for reviews). MF axons ramify within the hilus, and form unmyelinated axon bundles in the CA3 region, forming a major band above the pyramidal cell bodies (s. lucidum) and ramifying within and below the pyramidal cell layer (s. pyramidale and s. oriens, respectively) see Figs. 1*A*; 2*A* and refs. 22 and 23. MF distribution is similar in monkey and rat hippocampus, although there are differences in MF trajectories between primates and rodents (24). The characteristic ultrastructural appearance of MF synaptic boutons is seen in both rat and monkey (24). In our study, features of MFs and their terminals in the mouse and monkey hippocampus were consistent with previous descriptions (see Figs. 1 and 2). The MFs form two types of boutons: some are relatively small terminals, whereas others are larger and more irregular in shape, with smaller vesicle-filled extensions arising from a large varicosity. Both types of boutons have regions filled with densely packed, clear, spherical SVs (35–45 nm in diameter); a few dense core vesicles (60–140 nm); mitochondria; tubules of the smooth endoplasmic reticulum; and occasional microtubules, neurofilaments, and large clear vesicles (60–200 nm) (23, 25). In both the mouse and the monkey, the large MFBs make two types of specialized contacts with CA3 pyramidal cells and hilar neurons: (*i*) symmetrical desmosome-like, nonsynaptic junctions (puncta adherentia), characterized by symmetrical densities in association with the proximal dendritic shafts of CA3 pyramidal cells in s. lucidum (Figs. 2*D*, 3 *B* and *C*); and (*ii*) asymmetrical synapses with complex branching and invaginating spines, called "thorny excrescences" by Cajal (26), arising from dendritic shafts and somata of CA3 and hilar neurons (Figs. 1 *E* and *F*; 2 *E* and *F*, and 3*A*). For comparison with the rat hippocampus, see ref. 25.

Localization of ZnT-3 and Zinc in MFBs from Mice. In sections of mouse hippocampus stained with antiserum to ZnT-3, intense IR was observed within the MF system (Fig. 1*B*). In particular, those regions where MFBs contact the somata and dendrites of hilar neurons and CA3 pyramidal cells stained intensely with the ZnT-3 antiserum. This pattern of ZnT-3 IR was identical to the histochemical localization of zinc by the Timm's reaction (Fig. 1*A*) and included suprapyramidal MFBs forming an immunoreactive band in the s. lucidum (arrow in Fig. 1*B*) reaching from the hilus to CA3a, and intrapyramidal and infrapyramidal MFBs, the latter primarily within the CA3c subregion (Fig. 1*B*). S. radiatum and s. oriens of CA1 also stained for ZnT-3, as did the dentate outer molecular layer; the dentate inner molecular layer showed only light staining with the antibody (Fig. 1*B*). Control sections not exposed to the primary ZnT-3 antibody showed no IR (Fig. 3*C*).

At the EM level, ZnT-3 IR was observed in MFBs within the hilus and the CA3 subregion (Figs. 1 *D* and *F*). The intense ZnT-3 IR corresponded exclusively to MFBs; SVs of interneurons in the same sections were not stained (Fig. 1*D*). Electron micrographs of MFBs at higher magnification (Fig. 1*F*) revealed that ZnT-3 IR was localized uniformly to the membranes of spherical, clear (agranular) SVs. ZnT-3 IR associated with round clear SVs was similar in both the small boutons on dendritic shafts (Fig. 3*B*), and large boutons associated with complex spines (Figs. 1*F* and 3*A*). MFBs sampled from different locations in the hilus and the CA3 subregion showed no difference in the pattern or intensity of ZnT-3 IR. In the outer molecular layer of the dentate gyrus, less intense ZnT-3 IR was observed on SVs in some axon terminals (Fig. 3*D*).

EM of Timm's-stained hippocampal sections revealed Timm's silver precipitate in regions corresponding to the MFBs (Fig. 1*C*). At higher magnification, it was apparent that up to 60–80% of the SVs of MFBs contain silver granules (Fig. 1*E*). In experiments in which immunocytochemical staining for ZnT-3 was carried out in Timm's-stained ultrathin sections (using postembedding techniques), the ZnT-3 associated gold particles were found exclusively over Timm's-positive MFBs (Fig. 3*G*). In addition, ultrathin sections reacted with an antibody against glutamate revealed glutamate IR in MFBs (Fig. 3*H*).

Localization of ZnT-3 and Zinc in Monkey Hippocampus. Using ZnT-3 immunocytochemistry, the pattern of MF collateral extension outside the hilar region was somewhat different in primates compared with mice (compare Figs. 1*B* and 2*B*). In the monkey, MFBs that stain with Timm's reaction product (Fig. 2*A*) and ZnT-3 antibody (Fig. 2*B*) occupy the hilus and entire CA3 region. Outside the MF system, ZnT-3 IR

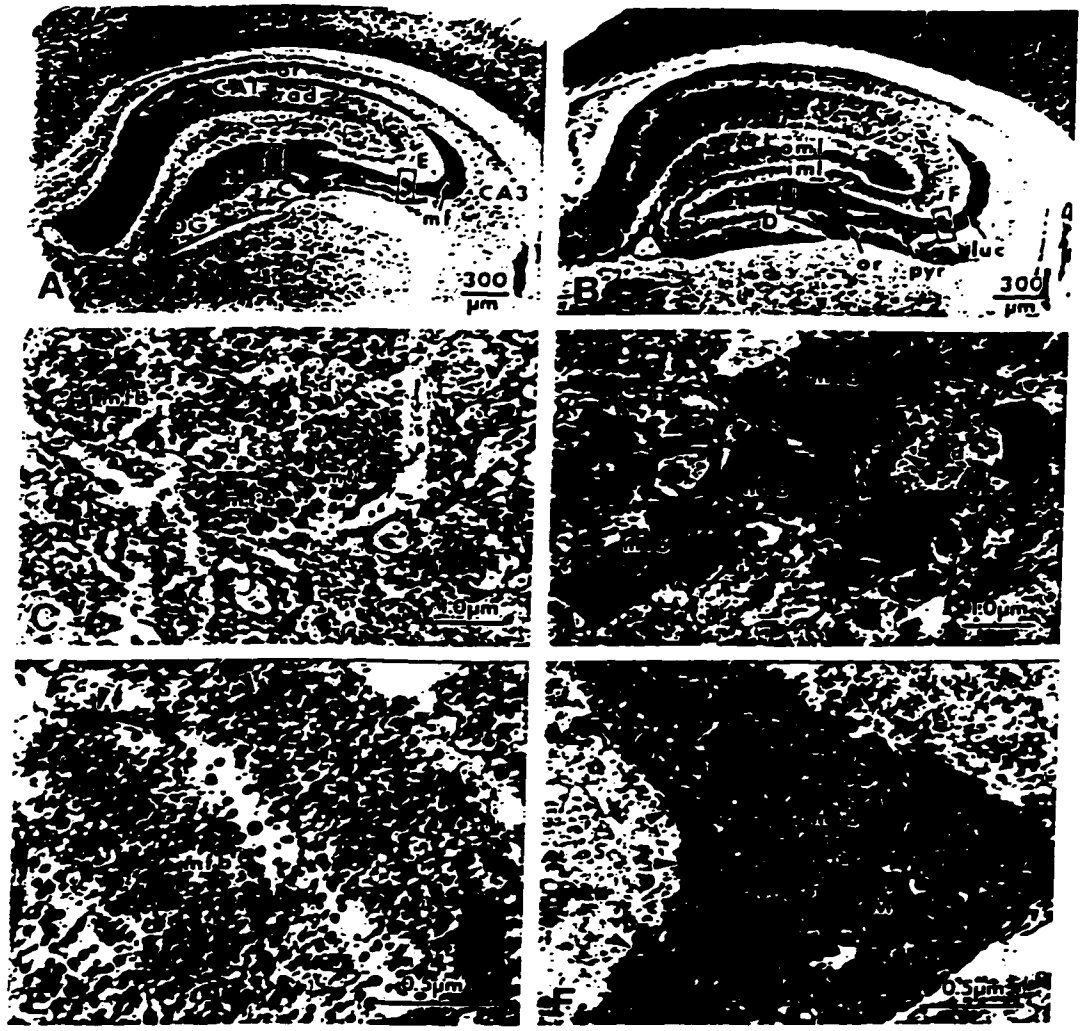

FIG. 1. Localization of histochemically reactive zinc (*A*, *C*, *E*) and IR for ZnT-3 protein (*B*, *D*, *F*) in the mouse hippocampus. (*A*) Transverse section of the hippocampus demonstrating intense reaction product in the mossy fiber (MF) system (dark band labeled "*mf*") after Timm's staining procedure; counterstained with cresyl violet. Note the lighter laminar staining in s. radiatum (rad) and oriens (or) of CA1. (*B*) Transverse section of the hippocampus reacted with an affinity-purified antiserum against ZnT-3 protein. IR is intense in the zinc-containing MF projections; arrows indicate ZnT-3 staining in s. lucidum (luc), pyramidale (pyr) and oriens (or) of CA3. The dentate outer (oml) and inner (iml) molecular layers, and s. radiatum (rad) and oriens (or) of CA1 also appear lightly immunoreactive for ZnT-3. (*C*) Electron micrograph from the dentate hilus (indicated area in *A*) showing MF boutons (mfb) with high density of silver granules. (*D*) Electron micrograph from the dentate hilus (indicated area in *B*) showing intense ZnT-3 IR in MFBs (mfb). Note the probable interneuron terminal (*A*) without ZnT-3 IR, making a symmetric synaptic contact (arrowhead) onto a dendrite (d). (*E*, *F*) Higher magnification of MFBs from CA3 s. lucidum (indicated areas in *A* and *B*) to demonstrate the vesicular localization of zinc (*E*) and ZnT-3 IR on synaptic vesicle membranes (*F*). Other abbreviations: CA1, CA3 hippocampal regions; DG, dentate gyrus; hi, hilus; M, mitochondrion; S, spine; arrowhead, synaptic contact.

was observed in a prominent band in the dentate inner molecular layer (but not the outer molecular layer); staining was also observed in s. radiatum and s. oriens of the CA1 region (Fig. 2*B*). At the EM level, the synaptic and nonsynaptic junctions between MFBs and dendritic shafts, somata, and thorny excrescences of CA3 pyramidal cells were similar to those seen in mice (Figs. 2 *D* and *F*; 3 *A* and *B*). Although MFBs were larger in size and exhibited more synaptic contacts per bouton in monkey than in mouse, there was no obvious difference in SV populations or in the localization of ZnT-3 IR to the vesicle membrane; the clear spherical SVs revealed ZnT-3 IR associated with vesicle membranes, irrespective of bouton size, location, or species (Figs. 1*F* and 2*F*). As in the mouse, EM of Timm's-stained sections of monkey hippocampus revealed silver precipitate in many SVs of MFBs, albeit less frequently than in mouse (Figs. 2 *C* and *E*).

DISCUSSION

This study reveals that ZnT-3 IR is localized to the membranes of all small, round, clear SVs of MFBs that have been shown

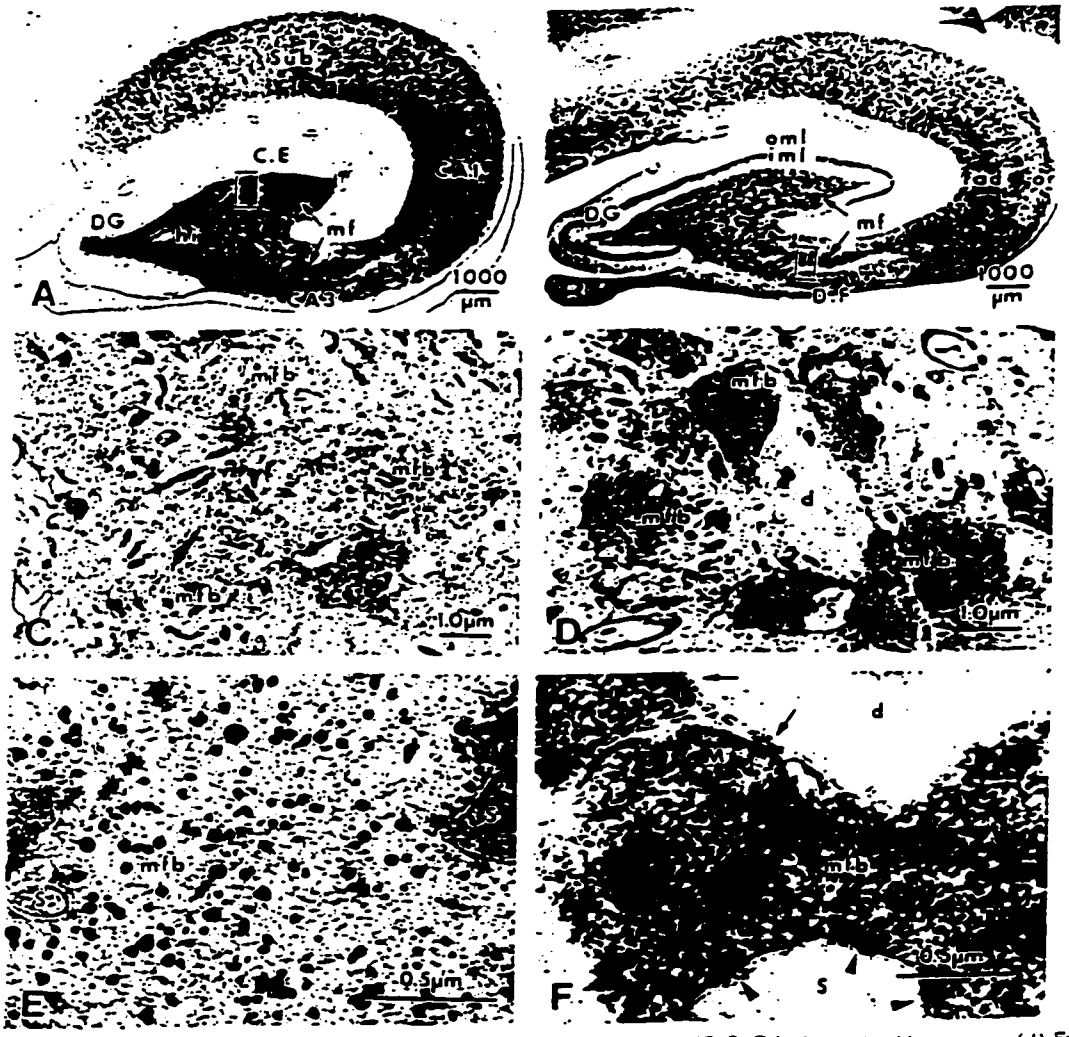

FIG. 2. Localization of histochemically reactive zinc (*A, C, E*) and IR for ZnT-3 protein (*B, D, F*) in the monkey hippocampus. (*A*) Frontal section of the hippocampus demonstrating intense Timm's stain for vesicular zinc in the MF projections (mf) within hilus and CA3. Lighter staining is seen in s. radiatum and oriens and subiculum (Sub). (*B*) Frontal section of the monkey hippocampus. ZnT-3 IR is present in the zinc-rich MF projections (mf) in hilus and CA3 region; lighter IR is seen in the dentate iml, in CA1 s. radiatum (rad) and oriens (or) and in subiculum. (*C*) Electron micrograph from the dentate hilus (indicated area in *A*) showing MFBs labeled with silver granules. (*D*) Electron micrograph from the s. lucidum (indicated area in *B*) demonstrating ZnT-3 IR in MFBs that surround a dendrite (d). (*E*) Higher magnification of part of a giant MFB in synaptic contact with spines in CA3 s. lucidum, showing dark silver granules located in the clear round SVs. (*F*) Higher magnification of a MFB in synaptic contact with a giant spine (arrowheads), also making nonsynaptic contacts onto a dendritic shaft (d, arrows). ZnT-3 IR is localized to the membranes of clear, round SVs within the bouton. Abbreviations as in Fig. 1.

previously to contain excitatory amino acids (17, 27). The majority (up to 60–80% in mouse MFBs) of these SVs also contain Timm's reaction product, indicative of vesicular zinc. The comparison of mouse to monkey revealed no species-related differences in the localization of ZnT-3 to SVs of MFBs, although there were differences in the general pattern of MF distribution. Synapses of nonglutamatergic local circuit neurons, e.g., hilar interneurons (Figs. 1*D*, 3 *E* and *F*), did not show ZnT-3 IR.

Recent studies demonstrate significant differences between rodents and primates with respect to dendritic length (28), the presence of basal dendrites (29), and basic ultrastructure (30). Our studies reveal another species difference in the pattern of MF projections to the pyramidal cells of the CA3 region. In mice, ZnT-3 and Timm's-positive MFBs were found in the hilus, s. lucidum, s. pyramidale between the CA3 pyramidal cells, and in s. oriens where MFBs were restricted to the CA3c subfield; in contrast, in the monkey hippocampus the MFBs that stain with Timm's reaction product and ZnT-3 antibody occupied the hilus and entire CA3 region. The appearance of large MFBs in s. lucidum and oriens in the monkey hippocampus is consistent with observations by Seress (24), who pointed out that large MFBs form synapses with both apical and basal parts of the dendritic tree in primates, whereas in rodents

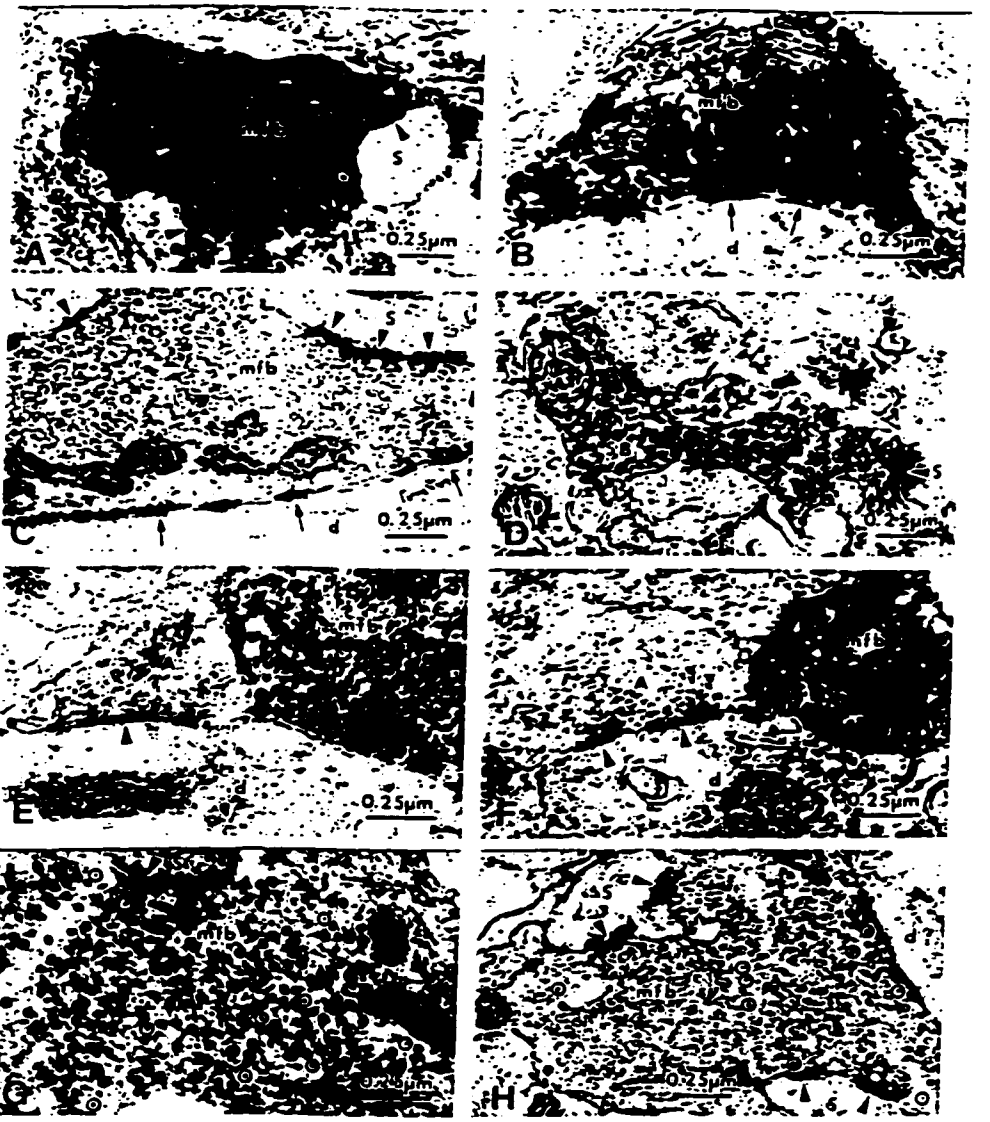

FIG. 3. Electron micrographs from the mouse and monkey (*E*) hippocampus showing ZnT-3 IR in terminals of glutamatergic projections. (*A*) ZnT-3 localization on clear, round SVs in a MFB in synaptic contact with spines (arrowheads). (*B*) ZnT-3 positive MFB making nonsynaptic contacts (arrows) onto a dendrite (d) in CA3 s. lucidum. (*C*) Control section of the CA3 s. lucidum in which the antibody against ZnT-3 protein was omitted: SVs in MFB (mfb) are devoid of ZnT-3 IR. The MFB forms synaptic contacts (arrowheads) with spines (s) and nonsynaptic contacts with a dendrite (d; arrows). (*D*) Synaptic bouton (SB) in the outer molecular layer of the dentate gyrus showing ZnT-3 IR on SV membranes. (*E*) and (*F*) Hilar dendrites (d) from the monkey (*E*) and mouse (*F*) hippocampus, contacted by MFBs with intense ZnT-3 IR. Adjacent presumably GABAergic terminals make symmetric synaptic contacts (arrowheads) and lack ZnT-3 IR on their SVs. (*G*) Part of a large MFB showing vesicular zinc (large silver granules) and ImmunoGold (Janssen) particles (10 nm, ⊃) corresponding to ZnT-3 protein labeled by a postembedding ImmunoGold procedure. (*H*) MFB with ImmunoGold-labeling for glutamate (10 nm particles, ⊃) demonstrating glutamate as the neurotransmitter of MF projections. Abbreviations as in Fig. 1.

synapses with large complex spines are seen only in s. lucidum. Another difference in the pattern of ZnT-3 IR (and Timm's) was observed in the dentate molecular layer. In mice, synapses of the perforant path showed ZnT-3 IR in the outer molecular layer, whereas in the monkey the inner molecular layer stained more intensely with the ZnT-3 antibody.

Evidence obtained from kinetic studies of zinc turnover and histochemical studies of zinc-containing boutons suggest that zinc is sequestered in SVs, and is released from boutons during normal activity by exocytosis of the zinc-filled vesicles (3). A zinc transporter localized to the SV membrane would provide an effective means of loading the SVs, and would be consistent with both light microscopy studies showing ZnT-3 staining pattern overlapping the MF distribution (16) and with the ultrastructural data showing its presence on SV membranes. Various brain regions containing zincergic neurons have been

examined using EM techniques after neo-Timm's or selenium staining, and in all cases the reaction product is restricted to the presynaptic boutons of neurons (3, 19, 31). In addition, Timm's-stainable zinc is also present in nonneuronal cells in the brain, e.g., in the choroid plexus. Earlier ultrastructural investigations demonstrated that the zinc in synaptic boutons is localized in the vicinity of presynaptic vesicles (1, 12) and more recent studies indicate that the zinc is within individual vesicles (2, 19). However, previous work indicated that only a small fraction of clear, round vesicles in MFBs were reactive for zinc (1–3), suggesting that a subclass of vesicles might contain zinc. In contrast, our study of Timm's-stained material demonstrates that the majority of SVs in MFBs contain zinc, consistent with the observation that all SVs were ZnT-3 positive, and thus presumably capable of facilitating zinc uptake. It seems likely that the lack of Timm's reaction product in individual SVs may represent vagaries of the methodology (e.g., rapidity of fixation), rather than absence of zinc. We suggest that all the SVs within MFBs contain both zinc and glutamate. In non-MFBs, e.g., boutons of entorhinal projections in the outer molecular layer of mouse (Fig. 3*D*), where both Timm's stainable zinc and ZnT-3 IR are less intense, all SVs still appear to react with the antibody. We suggest that the level of ZnT-3 expression may vary in different zinc-ergic neurons, but that all of their clear SVs are able to accumulate zinc, perhaps proportionally to the density of ZnT-3; thus, the amount of zinc in SVs would reflect ZnT-3 density. Clearly, zinc is not an obligatory component of SVs containing excitatory amino acids, because Timm's staining is not observed in many glutamatergic neurons (for review see Frederickson, ref. 3). It is not clear what signals direct ZnT-3 to SVs of MFBs. It is also not known whether ZnT-3 can associate with different types of SVs (e.g. clear vs dense core vesicles). Thus, it is possible that ZnT-3 expression in neurons that produce different kinds of vesicles could result in sequestration of zinc in one population of SVs but not another. When ZnT-3 that was tagged with green fluorescent protein was expressed in baby hamster kidney cells it was clearly associated with vesicles; however, ZnT-3 did not facilitate zinc sequestration in baby hamster kidney cells, unlike ZnT-2 expressed in these same cells (15, 16); thus, other components of SVs may be necessary for zinc transport by ZnT-3.

Zinc is capable of modulating a variety of voltage and ligand-gated ion channels at physiological concentrations (5–500 μM; ref. 32). Zinc inhibition of *N*-methyl-D-aspartate-type glutamate receptors has been reported by many authors (33–35), and variable effects of zinc have been observed on non-*N*-methyl-D-aspartate glutamate receptors (33, 34, 36, 37). Zinc has also been shown to exert a powerful modulatory inhibition of γ-aminobutyric acid $(GABA)_A$ receptors (38). The MF system is particularly interesting considering the role that zinc might play in modulating transmitter-mediated actions. First, the MFBs have presynaptic kainate receptors (39), and zinc modulation of kainate-induced currents appears to be sensitive to synaptic calcium levels, which may vary in an activity-dependent manner (40). Second, α-amino-3-hydroxy-5-methyl-4-isoxazolepropionic acid receptors are associated with synaptic contacts made by MF onto hilar mossy cells and CA3 pyramidal cells (41–43). Third, *N*-methyl-D-aspartate and GABA receptor-mediated inputs to CA3 pyramidal cells occur in s. radiatum and oriens, with strong $GABA_A$ inhibition associated with somatically localized receptors (42, 44, 45). Further, in various forms of hippocampal pathology (e.g., mesial temporal sclerosis associated with temporal lobe epilepsy), there is a sprouting of zinc-rich MFs back on to the granule cells of origin (18, 20, 46, 47). Their aberrant terminal localization and their proximity to GABA receptors have prompted investigators to postulate a role for zinc in the breakdown of inhibition that is associated with seizure generation in epileptic hippocampus (48). All of these receptors are probably within range of zinc diffusion, especially after high levels of activity that release large amounts of zinc. Given so many potential "targets," the role of zinc in modulating the receptor responses to transmitter release during normal synaptic transmission remains to be resolved. Inactivation of ZnT-3 by gene-targeting will help define the role of zinc in modulating synaptic activities in the central nervous system.

The authors thank Norma L. Anderson, Paul Schwartz, and Janet Schukar, for excellent technical assistance. We thank C. J. Frederickson for reviewing the manuscript. This work was supported in part by National Institutes of Health Grant NS18895 (P.A.S.) and U.S. Public Health Service National Research Service Award T32 GM07270 (T.B.C.).

1. Haug, F.-M. Š. (1967) *Histochemie* **8**, 355–368.
2. Perez-Clausell, J. & Danscher, G. (1985) *Brain Res.* **337**, 91–98.
3. Frederickson, C. J. (1989) *Int. Rev. Neurobiol.* **31**, 145–238.
4. Slomianka, L. (1992) *Neuroscience* **48**, 325–352.
5. Danscher, G. (1981) *Histochemistry* **71**, 1–16.
6. Danscher, G. (1984) in *The Neurobiology of Zinc*, eds. Frederickson, C. J., Howell, G. A. & Kasarskis, E. J. (Riva, New York), Vol. B, pp. 171–191.
7. Slomianka, L., Danscher, G. & Frederickson, C. J. (1988) *Neuroscience* **38**, 843–854.
8. Frederickson, C. J., Kasarskis, E. J., Ringo, D. & Frederickson, R. E. (1987) *J. Neurosci. Methods* **20**, 91–103.
9. Haug, F.-M. Š., Blackstad, T. W., Simonsen, A. H. & Zimmer, J. (1971) *J. Comp. Neurol.* **142**, 23–32.
10. Crawford, I. L. & Connor, J. D. (1972) *J. Neurochem.* **19**, 1451–1458.
11. Zimmer, J. & Haug, F.-M. Š. (1978) *J. Comp. Neurol.* **179**, 581–618.
12. Ihata, Y. & Otsuka, N. (1969) *J. Histochem. Cytochem.* **17**, 171–175.
13. Borowsky, B. & Hoffmann, B. J. (1995) *Int. Rev. Neurobiol.* **38**, 139–199.
14. Palmiter, R. D. & Findley, S. D. (1995) *EMBO J.* **14**, 639–649.
15. Palmiter, R. D., Cole, T. B. & Findley, S. D. (1996) *EMBO J.* **15**, 1784–1791.
16. Palmiter, R. D., Cole, T. B., Quaife, C. J. & Findley, S. D. (1996) *Proc. Natl. Acad. Sci. USA* **93**, 14934–14939.
17. Wenzel, H. J., Buckmaster, P. S., Anderson, N. L., Wenzel, M. E. & Schwartzkroin, P. A. (1997) *Hippocampus* **7**, in press.
18. Franck, J. E., Pokorny, J., Kunkel, D. D. & Schwartzkroin, P. A. (1995) *Epilepsia* **36**, 543–558.
19. Danscher, G. (1996) *Histochem. J.* **28**, 361–373.
20. Babb, T. L., Kupfer, W. R., Pretorius, J. K., Crandall, P. H. & Levesque, M. F. (1991) *Neuroscience* **42**, 351–363.
21. Frotscher, M., Soriano, E. & Misgeld, U. (1991) *Synapse* **8**, 148–160.
22. Amaral, D. G. & Witter, M. P. (1995) in *The Rat Nervous System*, ed. Paxinos, G. (Academic, San Diego), pp. 443–493.
23. Claiborne, B. J., Amaral, D. G. & Cowan, W. M. (1986) *J. Comp. Neurol.* **246**, 435–458.
24. Seress, L. (1992) in *The Dentate Gyrus and its Role in Seizures*, eds. Ribak, C. E., Gall, C. M. & Mody, I. (Elsevier, Amsterdam), pp. 3–28.
25. Amaral, D. G. & Dent, J. A. (1981) *J. Comp. Neurol.* **195**, 51–86.
26. Ramon y Cajal, S. (1893) *Ann. Soc. Esp. Hist. Nat.* **22**, 53–114.
27. Beaulieu, C., Dyck, R. & Cynader, M. (1992) *NeuroReport* **3**, 861–864.
28. Claiborne, B. J., Amaral, D. G. & Cowan, W. M. (1990) *J. Comp. Neurol.* **302**, 206–220.
29. Seress, L. & Frotscher, M. (1990) *J. Comp. Neurol.* **293**, 253–267.
30. Seress, L. & Ribak, C. E. (1992) *Brain Res.* **569**, 353–357.
31. Danscher, G., Howell, G., Pérez-Clausell, J. & Hertel, N. (1985) *Histochemistry* **83**, 419–422.
32. Smart, T. G., Xie, X. & Krishek, B. J. (1994) *Prog. Neurobiol.* **42**, 393–441.
33. Peters, S., Koh, J. & Choi, D. W. (1987) *Science* **236**, 589–593.
34. Westbrook, G. L. & Mayer, M. L. (1987) *Nature (London)* **328**, 640–643.
35. Christine, C. W. & Choi, D. W. (1990) *J. Neurosci.* **10**, 108–116.
36. Mayer, M. L., Vyklicky, L., Jr. & Westbrook, G. L. (1989) *J. Physiol. (London)* **415**, 329–350.
37. Huri, N., Galeno, T. & Carpenter, D. O. (1987) *Cell. Mol. Neurobiol.* **7**, 73–80.
38. Legendre, P. & Westbrook, G. L. (1991) *Mol. Pharmacol.* **39**, 267–274.
39. Bianchi, A., Nusser, Z., Molnar, E., Mellhuinney, R. A. & Somogyi, P. (1995) *Neuroscience* **69**, 1031–1055.
40. Dreixler, J. C. & Leonard, J. P. (1997) *Brain Res.* **752**, 170–174.
41. Schroder, H. (1993) *Hippocampus* **3**, 139–148.
42. Petralia, R. S., Wang, Y.-X. & Wenthold, R. J. (1994) *J. Neurosci.* **14**, 6102–6120.
43. Catania, M. V., Tolle, T. R. & Monyer, H. (1995) *J. Neurosci.* **15**, 7046–7061.
44. Siegel, S. J., Brose, N., Janssen, W. G., Gasic, G. P., Jahn, R., Heinemann, S. F. & Morrison, J. H. (1994) *Proc. Natl. Acad. Sci. USA* **91**, 564–568.
45. Johnson, R. R., Jiang, X. & Burkhalter, A. (1996) *J. Comp. Neurol.* **368**, 335–355.
46. Sutula, T., Cascino, G., Cavazos, J., Parada, I. & Ramirez, L. (1989) *Ann. Neurol.* **26**, 321–330.
47. Isokawa, M., Levesque, M. F., Babb, T. L. & Engel, J., Jr. (1993) *J. Neurosci.* **13**, 1511–1522.
48. Buhl, E. H., Otis, T. S. & Mody, I. (1996) *Science* **271**, 369–373.

APPENDIX C

Elimination of zinc from synaptic vesicles in the intact mouse brain by disruption of the *ZnT3* gene.

Cole, T.B., Wenzel, H.J., Kafer, K.E., Schwartzkroin, P.A., Palmiter, R.D., (1999) *Proc. Natl. Acad. USA* 96, 1716-1721.

Proc. Natl. Acad. Sci. USA
Vol. 96, pp. 1716–1721, February 1999
Neurobiology

Elimination of zinc from synaptic vesicles in the intact mouse brain by disruption of the *ZnT3* gene

TOBY B. COLE*, H. JÜRGEN WENZEL†, KATHY E. KAFER‡, PHILIP A. SCHWARTZKROIN†§, AND RICHARD D. PALMITER*‡¶

Departments of *Biochemistry, †Neurological Surgery, and §Physiology and Biophysics and ‡Howard Hughes Medical Institute, The University of Washington, Seattle, WA 98195

Contributed by Richard D. Palmiter, December 24, 1998

ABSTRACT **The mammalian protein ZnT3 resides on synaptic vesicle membranes of zinc-containing neurons, suggesting its possible role in vesicular zinc transport. We show here that histochemically reactive zinc, corresponding to the zinc found within synaptic vesicles, was undetectable in the brains of mice with targeted disruption of the *ZnT3* gene. Total zinc levels in the hippocampus and cortex of these mice were reduced by about 20%. The ultrastructure of mossy fiber boutons, which normally store the highest levels of vesicular zinc, was unaffected. Mice with one normal *ZnT3* allele had reduced levels of ZnT3 protein on synaptic vesicle membranes and had intermediate amounts of vesicular zinc. These results demonstrate that ZnT3 is required for transport of zinc into synaptic vesicles and suggest that vesicular zinc concentration is determined by the abundance of ZnT3.**

In the mammalian brain, 5–15% of total zinc is concentrated in synaptic vesicles in a subset of glutamatergic neurons (1–3), where it can be detected histochemically by using the neo-Timm sulfide silver method (4), with a selenium stain (5), or via the zinc-reactive fluorescent compound *N*-(6-methoxy-8-quinolyl)-*p*-toluene-sulfonamide (TSQ) (6). Histochemically reactive zinc is present in many regions of the central nervous system (7, 8) and is especially abundant in the hippocampus (7, 9, 10).

Despite the abundance of zinc in the brain (0.15–0.2 mM in gray matter) (8), little is known about the mechanisms controlling zinc homeostasis *in vivo*. Excess zinc may be sequestered by metallothioneins (11, 12), taken up into organelles (13), or transported out of the cell (14). Similarly, there are likely to be specific transport mechanisms regulating zinc influx. Under conditions of zinc toxicity, when extracellular zinc levels are high, zinc may enter into neurons via *N*-methyl-D-aspartate (NMDA) receptors, α-amino-3-hydroxy-5-methyl-4-isoxazolepropionic acid (AMPA)/kainate receptors, voltage-dependent calcium channels, or transporter-mediated exchange with intracellular sodium (15).

We recently identified a putative zinc transporter, ZnT3, that is expressed in zinc-containing neurons (16). ZnT3 belongs to a family of mammalian zinc transporters that includes ZnT1, a ubiquitously expressed zinc effluxer (14); ZnT2, which transports zinc into endosomal/lysosomal vesicles (13); and ZnT4, which is essential for regulating the zinc content of milk (17). ZnT3 is localized to the projections of zinc-containing neurons, producing an immunohistochemical staining pattern identical to that seen with the Timm stain for vesicular zinc (16, 18). ZnT3 immunoreactivity is evident on the membranes of zinc-rich (Timm-positive) synaptic vesicles (18). This localization, together with its homology to the vesicular zinc transporter, ZnT2 (16), suggested that ZnT3 might be responsible for the transport of zinc into synaptic vesicles. Here, we show that ZnT3 is required for zinc transport into synaptic vesicles and that vesicular zinc concentrations are sensitive to the amount of ZnT3 present on synaptic vesicle membranes.

The publication costs of this article were defrayed in part by page charge payment. This article must therefore be hereby marked "*advertisement*" in accordance with 18 U.S.C. §1734 solely to indicate this fact.

PNAS is available online at www.pnas.org.

MATERIALS AND METHODS

Generation of ZnT3 Knockout Mice. After isolating the *ZnT3* gene from a 129Sv mouse genomic library (16), a targeting vector was constructed by replacing a 4.3-kb *StuI-AflII* fragment encoding the first four exons with a cassette containing nuclear *lacZ* (*nlacZ*) and a neomycin-resistance gene (*neo*^{r}) driven by the *polII* promoter. Herpes simplex virus thymidine kinase (*TK*) genes were inserted 3 kb upstream at a *NotI* site and 1 kb downstream of the *neo*^{r} cassette at a *NarI* site. Electroporation and selection of AB1 embryonic stem cells were performed as described previously (19), using 2 μM gancyclovir. Three correctly targeted colonies were identified by PCR, using primers in the *polII* promoter and exon 7 of *ZnT3*. Genotype was assessed routinely by duplicate DNA dot hybridization of tail DNA with probes that lie within the *ZnT3* deletion and in *nlacZ*. In some cases, Southern blot analysis of DNA digested with *NheI* was used to confirm genotypes, using a 380-bp *TaqI/EcoRI* probe complementary to the 3′ untranslated region of *ZnT3*. C57BL/129Sv hybrid mice of the F2 generation were used in all experiments.

Temporal and Spatial Expression of *ZnT3*. Western blotting was performed as described (16), using a 1:1,000 dilution of ZnT3 antiserum. *ZnT3* mRNA levels were determined by solution hybridization essentially as described (20), using a riboprobe complementary to the 3′ untranslated region of *ZnT3*. Unhybridized RNA was digested with RnaseA/RnaseT1 instead of S1 nuclease. Values are presented as molecules of mRNA per cell, assuming 6.4 pg DNA per diploid cell ($n = 4$ for each data point). Expression of *nlacZ* was determined by staining tissues with 5-bromo-4-chloro-3-indolyl-β D-galactoside (X-gal), as described (21). Before staining, the vertebral column was decalcified by incubating 3 days in decalcification solution (0.34 M sodium citrate/22.5% formic acid) at room temperature, with three changes of solution, then rinsed in running tap water overnight.

Elemental Analysis. Dissected brain regions were weighed, placed in acid-washed glass flasks, digested in 2 ml of ultrapure nitric acid (J. T. Baker), evaporated to dryness, and resuspended in 2.5 ml of 2% (vol/vol) nitric acid. Twelve elements (Al, As, B, Ca, Cu, Fe, K, Mg, Na, P, Si, and Zn) were assessed by inductively coupled plasma emission spectroscopy, using a Jarrel-Ash 955 spectrophotometer. Ag, Ba, Cd, Co, Cr, Mn, Ni, Pb, Se, and V were below detectable levels.

Abbreviations: ZnT3, zinc transporter 3; $ZnT3^{+/+}$, wild-type; $ZnT3^{+/-}$, heterozygous mutant; $ZnT3^{-/-}$, homozygous mutant; TSQ, *N*-(6-methoxy-8-quinolyl)-*p*-toluene-sulfonamide; s, stratum; MFB, mossy fiber bouton.

¶To whom reprint requests should be addressed. e-mail: palmiter@u.washington.edu.

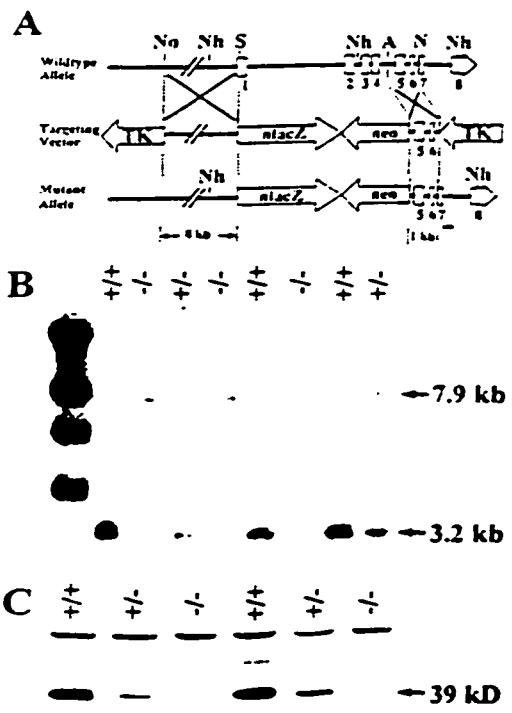

FIG. 1. Targeted disruption of the mouse *ZnT3* gene. (*A*) Diagram of the *ZnT3* wild-type allele, targeting vector, and predicted mutant allele. The targeting strategy placed *nlacZ* into the *ZnT3* locus, using *neo*^{r} for positive selection and herpes simplex virus thymidine kinase (*TK*) genes for negative selection. The eight numbered boxes represent exons. Homologous recombination in the regions indicated with an X should result in a mutant allele as shown at the bottom. The black bar represents the 380-bp *TaqI*/*Eco*RI probe used for Southern hybridization in *B*. A, *Afl*III; N, *Nar*I; Nh, *Nhe*I; No, *Not*I; S, *Stu*I. (*B*) Southern blot of *Nhe*I-digested genomic DNA from *ZnT3*$^{+/+}$, ZnT3$^{+/-}$, and ZnT3$^{-/-}$ mice. The probe detects a 7.9-kb mutant and 3.2-kb wild-type fragment. (*C*) Western blot of brain homogenates from 10-wk-old ZnT3$^{+/+}$, ZnT3$^{+/-}$, and ZnT3$^{-/-}$ mice. Equal amounts of total protein were loaded into each well. ZnT3 protein, which migrates as a 39-kD band, was undetectable in the brains of the mutants and reduced in the heterozygotes. The upper, nonspecific band controls for loading differences.

Tissue Processing for Timm Stain and Electron Microscopy. Brain tissue from 17 mice, ages 2–3 months, was processed for light microscopy and electron microscopy as described (18). The initial fixation was modified by using either 4% paraformaldehyde in 0.1 M sodium phosphate buffer, pH 7.4 (PB) (for immunocytochemistry), or 2% paraformaldehyde/2% glutaraldehyde in 0.1 M PB (for electron microscopy).

Immunocytochemistry. ZnT3 and dynorphin immunocytochemistry were performed as described (18, 22). To quantify ZnT3 immunoreactivity, film negatives of stained sections were analyzed by using IMAGETOOL (University of Texas Health Science Center, San Antonio, available at hyperlink ftp://maxrad6.uthscsa.edu) to measure average gray-scale values of selected regions. Data are presented as mean ± SEM of 16 sections for each genotype. For glutamate immunocytochemistry, a rabbit antiglutamate antibody (Sigma) was used (1:10,000 dilution), followed by goat-anti-rabbit IgG conjugated to gold (10 nm, Ted Pella, Redding, CA) (1:20 dilution).

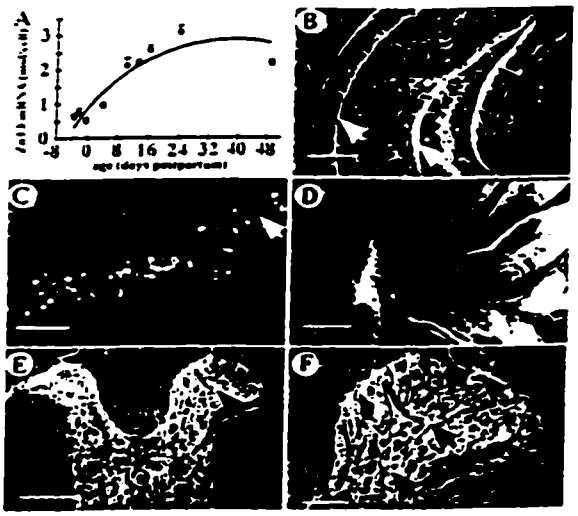

FIG. 2. ZnT3 is expressed in the central nervous system. (*A*) ZnT3 mRNA levels in developing mouse brain, assessed by solution hybridization. Data are presented as mean ± SEM. (*B–F*) Expression of *nlacZ* (under the control of the ZnT3 promoter) in the central nervous system of *ZnT3*$^{-/-}$ mice, as detected by 5-bromo-4-chloro-3-indolyl-β D-galactoside (X-gal) staining (white nuclei, indicated by black arrows). nlacZ is expressed in s granulosum of the dentate gyrus (*B*), the pyriform cortex (*C*), and the cochlear nucleus (*D*). *nlacZ* expression was not completely penetrant, as evident by the absence of staining (white arrows) in many areas where *ZnT3* is normally expressed. (*E* and *F*) *nlacZ* is expressed in laminae I, II, III, and IV of the spinal cord dorsal horn. Sections were photographed under dark-field illumination. [Bars = 500 μm (*B* and *D*); 200 μm (*C* and *E*); 100 μm (*F*).]

Timm Stain. Timm staining was performed by immersion in sulfide solution (18). The method described was modified slightly. After the initial perfusion with 4% paraformaldehyde in 0.1 M PB, brains were immersed in 3% glutaraldehyde/0.1% Na_2S/0.136 mM $CaCl_2$ in 0.12 M Millonig's buffer, pH 7.3 for 48 hr at 4°C. The tissue was transferred to cold 0.12 M Millonig's buffer with 0.136 mM $CaCl_2$, then cryoprotected, frozen on dry ice, cut into 30-μm sections, and mounted on gelatin-coated slides. Sections were immersed in developer [30 ml gum Arabic (50%)/5 ml citrate buffer (2 M, pH 3.7)/15 ml hydroquinone (5.67%)/0.25 ml $AgNO_3$ (17%)] for 60–90 min.

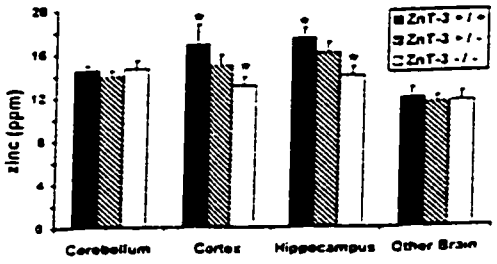

FIG. 3. Total zinc is reduced in the hippocampus and cortex of *ZnT3*$^{-/-}$ mice. Selected regions of the brain were dissected, and elemental analysis was performed for 22 elements, including zinc (see Materials and Methods). Total zinc was reduced by about 20% in the hippocampus and cortex of *ZnT3*$^{-/-}$ mice, and ZnT3$^{+/-}$ mice had a 10% reduction in total zinc in these same regions. Data are presented as mean ± SEM ($n = 4$).

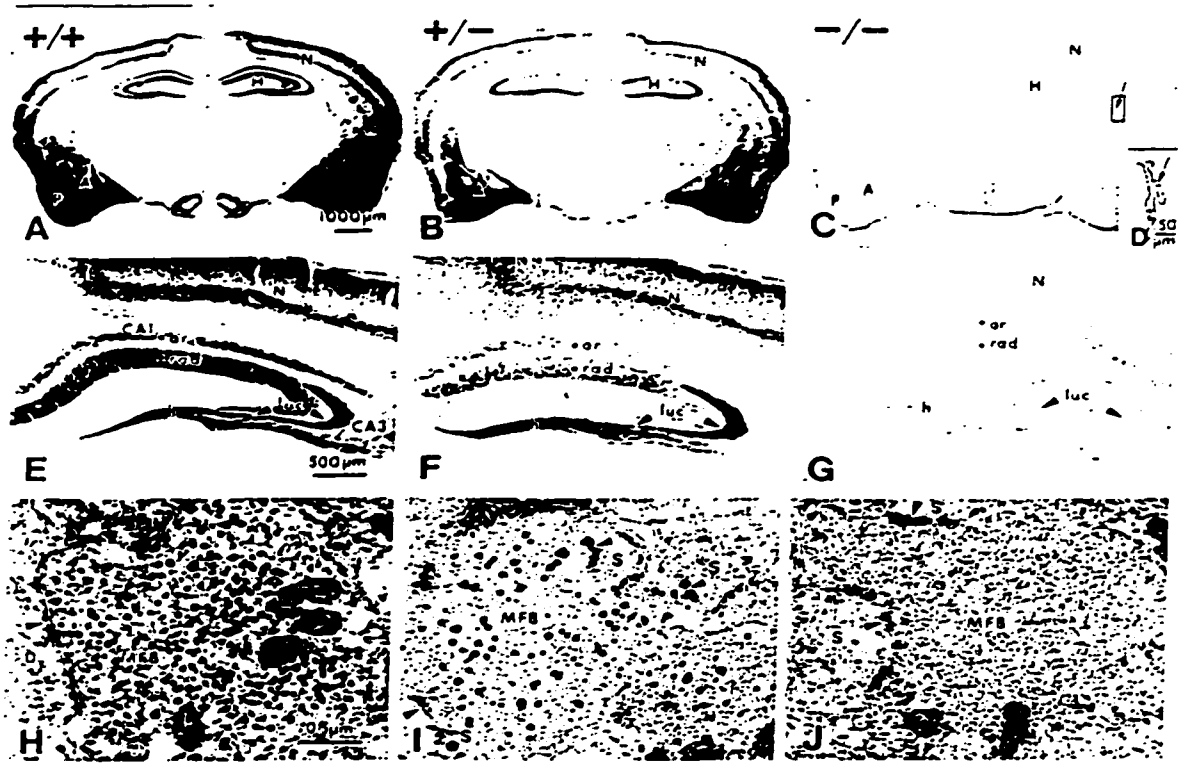

FIG. 4. Timm stain is undetectable in the brains of $ZnT3^{-/-}$ mice. Comparison of Timm stain between brains of $ZnT3^{+/+}$ (*A*, *E*, and *H*), $ZnT3^{+/-}$ (*B*, *F*, and *I*), and $ZnT3^{-/-}$ mice (*C*, *G*, and *J*). (*A–C*) Coronal sections through the midbrain. Timm stain in the hippocampus (*H*), piriform cortex (P), neocortex (N), and amygdala (A) was conspicuous in the $ZnT3^{+/+}$ brain (*A*), reduced in the $ZnT3^{+/-}$ brain (*B*), and undetectable in the brains of $ZnT3^{-/-}$ mice (*C*). (*D*) Higher magnification of the choroid plexus from the lateral ventricle (indicated area in *C*). Timm stain was unperturbed in the $ZnT3^{-/-}$ choroid plexus. (*E–G*) Higher magnification of Timm-stained hippocampi from $ZnT3^{+/+}$ (*E*), $ZnT3^{+/-}$ (*F*), and $ZnT3^{-/-}$ (*G*) mice. Timm stain was reduced ($ZnT3^{+/-}$) or absent ($ZnT3^{-/-}$) in the hilus (h), s lucidum (luc) of CA3, and s oriens (or) and s radiatum (rad) of CA1 and CA3. (*H–J*) Electron micrographs of Timm-stained MFBs in s lucidum of CA3, taken from a $ZnT3^{+/+}$ (*H*), a $ZnT3^{+/-}$ (*I*), and a $ZnT3^{-/-}$ (*J*) mouse. Timm-positive vesicles were abundant in $ZnT3^{+/+}$ MFBs, whereas fewer vesicles were Timm-positive in $ZnT3^{+/-}$ MFBs, and no Timm-positive vesicles were present in $ZnT3^{-/-}$ MFBs. Arrowheads represent synaptic contacts made with a dendrite (D) and dendritic spines (S).

For ultrastructural analysis, Timm staining was performed as described (18).

***N*-(6-Methoxy-8-quinolyl)-*p*-Toluene-Sulfonamide (TSQ) Histofluorescence.** A working solution of TSQ (Molecular Probes), prepared as described (6, 23), was pipetted onto unfixed frozen brain sections. Hippocampi were scanned under UV illumination (351–362 nm) with an ACAS 570 laser cytometer (Meridian Instruments, Lansing, MI). Emissions >370 nm were recorded, and images were analyzed on a DASY 9000 workstation (Meridian). Average fluorescence for selected regions was measured, then converted to percentage of maximal fluorescence, which was observed in the wild-type hilus. Regions selected for analysis included the hilus, CA3 [stratum (s) oriens and s lucidum], CA1 (s radiatum, s oriens, and s pyramidale), and a small section of the dorsomedial thalamus just beneath the dentate area of the hippocampus. Fluorescence was quantified from two coronal sections each of the left and right hippocampi of five mice. Frozen sections of mouse testis and pancreas were air-dried, fixed in ice-cold methanol, and stained with TSQ as above. Fluorescence was visualized and photographed with a Nikon Microphot FX microscope, using a UV-2A filter block (excitation, 330–380 nm; barrier, 420 nm).

RESULTS

Disruption of the Murine *ZnT3* Gene. The first four exons of *ZnT3* were replaced by a cassette that included *nlacZ* and *neo*^{r} (Fig. 1*A*). This construct was electroporated into embryonic stem cells. PCR analysis of 60 clones revealed three that were targeted correctly. One of these produced chimeras that transmitted the targeted allele through the germ line. F1 heterozygotes were generated by crossing the chimeras with C57BL/6 females. The F2 progeny from these mice, genotyped by duplicate DNA dot hybridization or by Southern blot analysis (Fig. 1*B*), were born in the expected Mendelian ratio. Mice heterozygous ($ZnT3^{+/-}$) or homozygous ($ZnT3^{-/-}$) for the disrupted allele showed no obvious phenotypic differences from their wild-type ($ZnT3^{+/+}$) littermates. Body weight, lifespan, fertility, and litter size were normal, and the mice showed no gross morphological abnormalities. ZnT3 protein, assessed by Western blot analysis of brain homogenates, was reduced in the brains of $ZnT3^{+/-}$ mice and undetectable in the brains of $ZnT3^{-/-}$ mice (Fig. 1*C*).

Insertion of *nlacZ* into the *ZnT3* locus confirmed the patterns of *ZnT3* expression seen previously by *in situ* hybridization (16), including expression in granule cells of the dentate gyrus, pyramidal cells of the CA3 and CA1 regions,

and the amygdala, neocortex, and piriform and entorhinal cortices (Fig. 2 *B* and *C*; data not shown for all regions). In addition, *nlacZ* expression was detected in the cochlear nucleus (Fig. 2*D*), laminae I–IV of the dorsal horn of the spinal cord (Fig. 2 *E* and *F*), and the testis, where ZnT3 mRNA is abundant but not translated into protein (16). ZnT3 mRNA, isolated from the brains of wild-type embryos or pups and quantified by solution hybridization, was negligible at birth, then increased linearly, reaching a maximum at about 3 weeks postpartum (Fig. 2*A*).

Vesicular Zinc Is Eliminated from Brains of *ZnT3*$^{-/-}$ Mice. To determine whether the levels of zinc or other metals were altered upon disruption of *ZnT3*, metal content was measured by plasma emission spectroscopy (Fig. 3). In the hippocampus and cortex, regions that contain abundant vesicular zinc (3), total zinc was reduced in the *ZnT3*$^{-/-}$ mice by 20% ($P < 0.001$, Student's *t* test) and 23% ($P < 0.01$), respectively, whereas the cerebellum and other (primarily thalamus and hypothalamus) regions without appreciable levels of vesicular zinc were unaffected (Fig. 3). Total zinc levels in the hippocampus and cortex of the *ZnT3*$^{-/-}$ mice were reduced by 10% ($P < 0.05$, Student's *t* test) (Fig. 3). None of the other 11 elements tested (see *Materials and Methods*) showed any change in abundance.

To test whether vesicular zinc is altered in these mice, we used two stains for histochemically reactive zinc, Timm stain and TSQ fluorescence. Timm stain was reduced in the brains of *ZnT3*$^{-/-}$ mice and eliminated from the brains of *ZnT3*$^{-/-}$ mice, including the staining normally seen in the hippocampus, neocortex, piriform cortex, amygdala (Fig. 4 *A–C*), entorhinal cortex, striatum, olfactory bulb, and cochlear nucleus (data not shown). In the hippocampus, Timm stain was reduced (*ZnT3*$^{-/-}$) or undetectable (*ZnT3*$^{-/-}$) in the mossy fibers projecting from dentate granule neurons to the hilus and s lucidum and s oriens of the CA3 region, and in projections to s radiatum and s oriens of the CA1 region (Fig. 4 *E–G*). Timm stain was undetectable in the *ZnT3*$^{-/-}$ brain even after long histochemical-development times (>90 min) that normally produce intense staining in CA1 and prominent staining in the inner and outer molecular layers of the dentate gyrus (data not shown). In contrast, Timm stain was readily detectable in the choroid plexus (Fig. 4*D*) and in convoluted tubule cells of the submaxillary gland (data not shown). At the ultrastructural level, Timm reaction product was present within synaptic vesicles of mossy fiber boutons (MFBs) in the *ZnT3*$^{+/+}$ brain (Fig. 4*H*), whereas the number of Timm-positive vesicles in *ZnT3*$^{+/-}$ MFBs was reduced (Fig. 4*I*), and no Timm-staining was detected within synaptic vesicles of *ZnT3*$^{-/-}$ MFBs (Fig. 4*J*), indicating that histochemically reactive zinc is eliminated from synaptic vesicles in the brains of *ZnT3*$^{-/-}$ mice.

Vesicular Zinc Content Is Determined by the Abundance of ZnT3 on Synaptic Vesicle Membranes. To investigate whether the amount of ZnT3 present on vesicle membranes was reduced in the *ZnT3*$^{+/-}$ brain, we assessed ZnT3 immunoreactivity in the brains of *ZnT3*$^{+/+}$, *ZnT3*$^{+/-}$, and *ZnT3*$^{-/-}$ mice at the light-microscopic and ultrastructural levels (Fig. 5). ZnT3 immunoreactivity in the *ZnT3*$^{+/+}$ brain was evident in the same areas reported previously (16, 18). In the corresponding regions of the mutant brain, ZnT3 immunoreactivity was reduced (*ZnT3*$^{+/-}$) or undetectable (*ZnT3*$^{-/-}$), including the amygdala, cortex, and hippocampus (for hippocampus, see Fig. 5 *A*, *C*, and *E*; other regions, data not shown). ZnT3 immunoreactivity in the hippocampi of *ZnT3*$^{+/+}$, *ZnT3*$^{+/-}$, and *ZnT3*$^{-/-}$ mice was quantified by computer-assisted gray-scale analysis of film negatives (low gray-scale values correspond to darker ZnT3 immunostaining). In the *ZnT3*$^{+/+}$ hippocampus, gray-scale values relative to the corpus callosum were intermediate in the hilus (*ZnT3*$^{+/+}$, 0.35 ± 0.03; *ZnT3*$^{+/-}$, 0.50 ± 0.02; *ZnT3*$^{-/-}$, 0.83 ± 0.05) and s lucidum of CA3 (*ZnT3*$^{+/+}$, 0.39 ± 0.04; *ZnT3*$^{+/-}$, 0.54 ± 0.02; *ZnT3*$^{-/-}$, 0.81 ± 0.05). At the ultrastructural level, ZnT3 immunoreactivity was present on all synaptic vesicles within *ZnT3*$^{+/+}$ MFBs, similarly as in the *ZnT3*$^{+/+}$ MFBs, but the intensity of ZnT3 immunoreactivity was reduced (compare Fig. 5 *B* and *D*). ZnT3 immunoreactivity was undetectable in MFBs of *ZnT3*$^{-/-}$ mice (Fig. 5*F*).

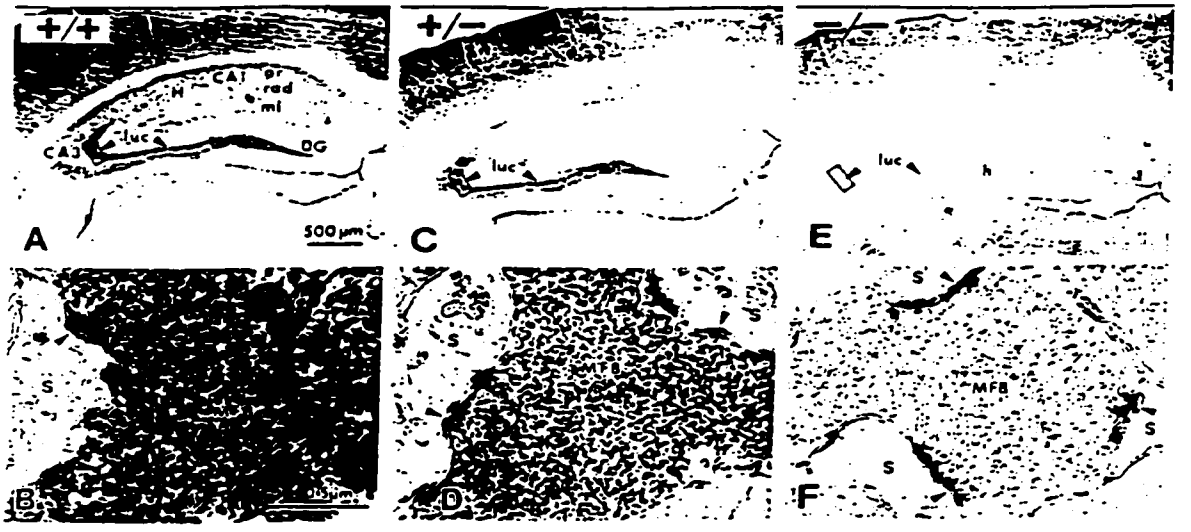

FIG. 5. ZnT3 immunocytochemistry in the *ZnT3*$^{+/+}$ (*A* and *B*), *ZnT3*$^{+/-}$ (*C* and *D*), and *ZnT3*$^{-/-}$ (*E* and *F*) hippocampus. Compared with the *ZnT3*$^{+/+}$ hippocampus (*A*), ZnT3 immunoreactivity was reduced in many areas of the *ZnT3*$^{+/-}$ hippocampus (*C*) and was undetectable in the *ZnT3*$^{-/-}$ hippocampus (*E*). (*B*, *D*, and *F*) Electron micrographs of MFBs in s lucidum (boxed area in *A*, *C*, and *E*). ZnT3 immunoreactivity was conspicuous on synaptic vesicle membranes of *ZnT3*$^{+/+}$ MFBs (*B*), reduced on vesicle membranes of ZnT3$^{+/-}$ MFBs (*D*), and undetectable on vesicle membranes of ZnT3$^{-/-}$ MFBs (*F*). The number of immunoreactive vesicles in the ZnT3$^{+/+}$ and ZnT3$^{+/-}$ MFBs was approximately the same. Arrowheads point to synaptic contacts made with dendritic spines (S). H, hippocampus; DG, dentate gyrus; h, hilus; luc, s lucidum; or, s oriens; rad, s radiatum; ml, molecular layer.

TSQ fluorescence, a specific indicator of vesicular zinc, was used to corroborate the results seen with Timm stain and to provide a quantitative comparison of vesicular zinc levels in the hippocampi of *ZnT-3*$^{+/+}$, *ZnT-3*$^{+/-}$, and *ZnT-3*$^{-/-}$ mice. TSQ fluorescence was undetectable in the *ZnT3*$^{-/-}$ hippocampus (Fig. 6*A*), but still abundant in differentiating spermatids in the testis and in β-islet cells of the pancreas (Fig. 6 *C* and *D*). TSQ fluorescence was quantified, using computer-assisted laser cytometry, from several regions of the hippocampus and a small region within the dorsomedial thalamus (Fig. 6*B*). Average fluorescence for each region was plotted as a percentage of the maximal fluorescence, which was seen in the wild-type hilus. TSQ fluorescence in the hilus and regions CA3 and CA1 was absent in the *ZnT3*$^{-/-}$ hippocampus ($P < 0.0001$, Student's *t* test), where it was even lower than the background fluorescence, i.e., that seen in the thalamus or corpus callosum (Fig. 6 *A* and *B*). TSQ fluorescence in the *ZnT3*$^{+/-}$ hippocampus was reduced by 47% in the hilus, 39% in region CA3, and 50% in region CA1 ($P < 0.0001$ for all regions, Student's *t* test) (Fig. 6*B*).

Ultrastructural Morphology of the *ZnT3*$^{-/-}$ Hippocampus Is Normal. Examination of the hippocampi of adult *ZnT3*$^{-/-}$ mice by light microscopy revealed no grossly aberrant morphology. Stratum granulosum of the dentate gyrus and strata pyramidale, oriens, and radiatum of the CA3 and CA1 regions were normal in appearance, and mossy fiber projections were evident in s lucidum and s oriens of CA3, as detected by dynorphin immunoreactivity (data not shown). Ultrastructural analysis revealed the *ZnT3*$^{-/-}$ hippocampus to be normal with respect to the relative number, distribution, and size of MFBs in the hilus and s lucidum, as well as the number of synaptic vesicles contained within the MFBs, the number of asymmetric synaptic contacts made with dendritic spines (Fig. 7), and the presence of glutamate immunoreactivity (data not shown). MFBs in the *ZnT3*$^{-/-}$ hippocampus showed normal characteristic ultrastructure, with densely packed clear, round synaptic vesicles, a few dense core vesicles, and numerous mitochondria (Fig. 7), lacking only histochemically reactive zinc within the synaptic vesicles (Fig. 4*J*).

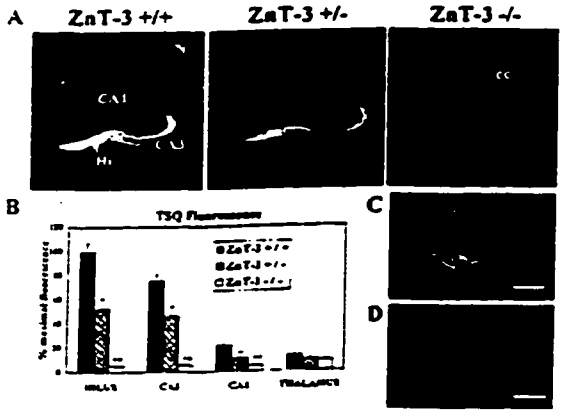

FIG. 6. TSQ fluorescence in the hippocampus. (*A*) Computer-generated images of TSQ fluorescence in the hippocampi of *ZnT3*$^{+/+}$ (*Left*), *ZnT3*$^{-/-}$ (*Center*), and *ZnT3*$^{+/-}$ (*Right*) mice. The bright fluorescence in the hilus (Hi), s oriens and s lucidum of CA3, and s oriens and s radiatum of CA1 was reduced in the *ZnT3*$^{+/-}$ hippocampus and undetectable in the *ZnT3*$^{-/-}$ hippocampus. TSQ staining was also reduced in the neocortex (N). TSQ fluorescence in the hippocampus of the mutants was less than the autofluorescence of the overlying corpus callosum (cc). (*B*) Quantification of TSQ fluorescence in regions within the hippocampus by computer-assisted laser cytometry. Data are expressed as mean ± SEM ($n = 5$). (*C*) TSQ-stained section of a single seminiferous tubule from the testis of a *ZnT3*$^{-/-}$ mouse. Spermatids poised at the lumen of the tubule fluoresced with TSQ, similar to wild-type spermatids (not shown). (*D*) TSQ-stained pancreas from a *ZnT3*$^{-/-}$ mouse, illustrating a single Islet of Langerhans, composed of beta cells that have an abundance of histochemically reactive zinc packaged in secretory granules. [Bars = 50 μm (*C*); 100 μm (*D*).]

DISCUSSION

Together with our previous observations (18), these studies indicate that zinc is taken up into synaptic vesicles by a transport mechanism that requires ZnT3 at the vesicle membrane. Histochemically reactive zinc was undetectable in the brains of *ZnT3*$^{-/-}$ mice, and there was a corresponding 20% reduction in total zinc in brain regions in which histochemically reactive zinc is usually detected. The remaining 80% of zinc in these regions represents zinc that is inaccessible to either sulfide or TSQ, presumably because of its tight association with metalloproteins in different parts of the cell. The results are consistent with previous studies suggesting that Timm stain and TSQ fluorescence throughout the brain correspond exclusively to zinc that is packaged into synaptic vesicles (8).

The *ZnT3*$^{-/-}$ brain had an intermediate level of both ZnT3 protein and histochemically reactive zinc, demonstrating that the amount of zinc in synaptic vesicles is limited by the abundance of ZnT3. This variation in ZnT3 immunoreactivity extended to the ultrastructural level, where the intensity of ZnT3 immunoreactivity on synaptic vesicle membranes in *ZnT3*$^{+/-}$ MFBs was reduced relative to that seen in *ZnT3*$^{+/+}$ MFBs, but the number of ZnT3 immunoreactive vesicles remained unchanged. The sensitivity of vesicular zinc levels to the amount of ZnT3 present on synaptic vesicle membranes is consistent with a steady-state model for the regulation of zinc content in synaptic vesicles. In such a model, vesicular zinc content is determined by steady-state balance between influx and efflux, rather than a predetermined "set point." Only steady-state mechanisms are predicted to be sensitive to the amount of transporter (ZnT3) present on the vesicle membrane (24). ZnT3 is similar to other synaptic vesicle transporters in this regard (25, 26).

ZnT3 transports zinc into vesicles against a high concentration gradient, but the driving force is not clear. ZnT3 may act as part of a complex of proteins that mediate zinc transport. ZnT3 appears to depend on the AP-3 vesicular chaperone complex for assembly into synaptic vesicles because *mocha* mice, which lack the δ-subunit of this complex, have reduced ZnT3 immunoreactivity in the hippocampus (27). Interestingly, the phenotype of *mocha* mice, which includes hypopigmentation, defects in hearing and neural activity, and platelet storage pool deficiencies, in addition to reduced vesicular zinc,

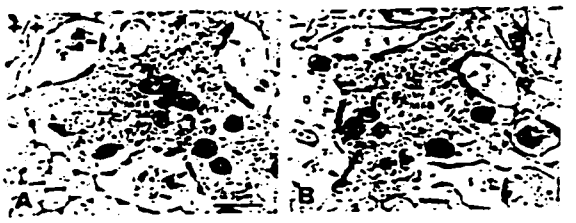

FIG. 7. MFBs in the *ZnT3*$^{-/-}$ hippocampus show normal ultrastructure. Electron micrographs of MFBs in s lucidum of CA3, taken from a *ZnT3*$^{+/+}$ (*A*) and a *ZnT3*$^{-/-}$ (*B*) mouse. *ZnT3*$^{-/-}$ MFBs were normal with respect to their size, the approximate number of small, clear synaptic vesicles contained within them, the numbers and types of synaptic contacts made with dendritic spines, and the presence of mitochondria. Note the asymmetric synaptic contacts (arrowheads) on dendritic spines (S) and a pyramidal cell dendrite (D).

is much more severe than that seen in *ZnT3*$^{-/-}$ mice, as would be expected if AP-3 is involved in the assembly of many vesicular components. The hypersynchronized theta rhythms, spontaneous bursts of epileptiform activity, and loss of hearing seen in *mocha* mice (27, 28) are not likely to be due exclusively to the loss of vesicular zinc, because *ZnT3*$^{-/-}$ mice can still hear more than a year after birth, and they manifest normal electroencephalographic activity (our unpublished observations).

ZnT3 is required for sequestration of zinc in synaptic vesicles of neurons, whereas removal of ZnT3 did not affect the histochemically reactive zinc found in secretory granules of pancreatic β-islet cells (29), salivary gland granular convoluted tubule cells (30), germ cells in the testis (31, 32), or cuboidal cells of the choroid plexus (8). Other members of the ZnT family are likely to be responsible for compartmentalization of zinc in these and other cells.

Zinc is found solely in synaptic vesicles of glutamatergic neurons, but not all glutamatergic neurons sequester zinc (8). This observation, as well as the results presented here, suggest that zinc is not required for utilization of glutamate as a neurotransmitter. Given the many potential neuromodulatory and neurotoxic roles of synaptically released zinc (33–35), it will be interesting to see whether neuronal activity or excitotoxic damage is altered in these mice. If zinc does act as a neuromodulator, we predict that there will be a mechanism for clearing zinc from the synapse (probably a reuptake transporter) and a mechanism for shuttling zinc back into synaptic vesicles. Members of the ZIP (36) family of metal ion uptake transporters and the zinc-binding protein metallothionein-III, which is expressed in zinc-containing neurons (11), are possible candidates for some of these processes.

We thank Norma Anderson for assistance with electron microscopy, Glenda Froelick for assistance with histology, Terrance Kavanaugh for assistance with laser cytometry, Jeff Noebels and Margit Burmeister for communication of results before publication, and members of the Palmiter and Schwartzkroin labs for valuable discussions. This work was supported in part by National Institutes of Health Grants DK53013 (R.D.P.) and NS18895 (P.A.S.) and a U.S. Public Health Service National Research Service Award (T32 GM07270 to T.B.C.).

1. Haug, F. M. (1967) *Histochemie* **8**, 355–368.
2. Pérez-Clausell, J. & Danscher, G. (1985) *Brain Res.* **337**, 91–98.
3. Frederickson, C. J. & Moncrieff, D. W. (1994) *Biol. Signals* **3**, 127–139.
4. Danscher, G. (1981) *Histochemistry* **71**, 1–16.
5. Danscher, G. (1984) in *The Neurobiology of Zinc*, eds. Frederickson, C. J., Kasarskis, E. J. & Howell, G. A. (Liss, New York), Vol. B, pp. 177–191.
6. Frederickson, C. J., Kasarskis, E. J., Ringo, D. & Frederickson, R. E. (1987) *J. Neurosci. Methods* **20**, 91–103.
7. Slomianka, L. (1992) *Neuroscience* **48**, 325–352.
8. Frederickson, C. J. (1989) *Int. Rev. Neurobiol.* **31**, 145–238.
9. Crawford, I. L. & Connor, J. D. (1972) *J. Neurochem.* **19**, 1451–1458.
10. Zimmer, J. & Haug, F. M. (1978) *J. Comp. Neurol.* **179**, 581–617.
11. Erickson, J. C., Hollopeter, G., Thomas, S. A., Froelick, G. J. & Palmiter, R. D. (1997) *J. Neurosci.* **17**, 1271–1281.
12. Maret, W. (1995) *Neurochem. Int.* **27**, 111–117.
13. Palmiter, R. D., Cole, T. B. & Findley, S. D. (1996) *EMBO J.* **15**, 1784–1791.
14. Palmiter, R. D. & Findley, S. (1995) *EMBO J.* **14**, 639–649.
15. Seni, S. L., Canzoniero, L. M. T., Yu, S. P., Ying, H., Koh, J. Y., Kerchner, G. A. & Choi, D. W. (1997) *J. Neurosci.* **17**, 9554–9564.
16. Palmiter, R. D., Cole, T. B., Quaife, C. J. & Findley, S. D. (1996) *Proc. Natl. Acad. Sci. USA* **93**, 14934–14939.
17. Huang, L. & Gitschier, J. (1997) *Nat. Genet.* **17**, 292–297.
18. Wenzel, H. J., Cole, T. B., Born, D. E., Schwartzkroin, P. A. & Palmiter, R. D. (1997) *Proc. Natl. Acad. Sci. USA* **94**, 12676–12681.
19. Thomas, S. A., Matsumoto, A. M. & Palmiter, R. D. (1995) *Nature (London)* **374**, 643–646.
20. Durnam, D. M. & Palmiter, R. D. (1983) *Anal. Biochem.* **131**, 385–393.
21. Masters, B. A., Quaife, C. J., Erickson, J. C., Kelly, E. J., Froelick, G. J., Zambrowicz, B. P., Brinster, R. L. & Palmiter, R. D. (1994) *J. Neurosci.* **14**, 5844–5857.
22. Houser, C. R., Miyashiro, J. E., Swartz, B. E., Walsh, G. O., Rich, J. R. & Delgado-Escueta, A. V. (1990) *J. Neurosci.* **10**, 267–282.
23. Erickson, J. C., Masters, B. A., Kelly, E. J., Brinster, R. L. & Palmiter, R. D. (1995) *Neurochem. Int.* **27**, 35–41.
24. Williams, J. (1997) *Neuron* **18**, 683–686.
25. Takahashi, N., Miner, L. L., Sora, I., Ujike, H., Revay, R. S., Kostic, V., Jackson-Lewis, V., Przedborski, S. & Uhl, G. R. (1997) *Proc. Natl. Acad. Sci. USA* **94**, 9938–9943.
26. Sung, H., Ming, G., Fon, E., Bellocchio, E., Edwards, R. H. & Poo, M. (1997) *Neuron* **18**, 815–826.
27. Kantheti, P., Qiao, X., Diaz, M. E., Peden, A. A., Meyer, G. E., Carskadon, S. L., Kapfhamer, D., Sufalko, D., Robinson, M. S., Noebels, J. L. & Burmeister, M. (1998) *Neuron* **21**, 111–122.
28. Noebels, J. L. & Sidman, R. L. (1989) *J. Neurogenet.* **6**, 53–56.
29. Toroptsev, I. V., Eschenko, V. A. & Troshkin, V. G. (1974) *Bull. Exp. Biol. Med.* **77**, 119–121.
30. Frederickson, C. J., Pérez-Clausell, J. & Danscher, G. (1987) *J. Histochem. Cytochem.* **35**, 579–583.
31. Danscher, G. & Zimmer, J. (1978) *Histochemistry* **55**, 27–40.
32. Andrews, J. C., Nolan, J. P., Hammerstedt, R. H. & Bavister, B. D. (1995) *Cytometry* **21**, 153–159.
33. Choi, D. W. & Koh, J. Y. (1998) *Annu. Rev. Neurosci.* **21**, 347–375.
34. Harrison, N. L. & Gibbons, S. J. (1994) *Neuropharmacology* **33**, 935–952.
35. Smart, T. G., Xie, X. & Krishek, B. J. (1994) *Prog. Neurobiol.* **42**, 393–441.
36. Eng, B. H., Guerinot, M. L., Eide, D. & Saier, M. H., Jr. (1998) *J. Membrane Biol.* **166**, 1–7.

APPENDIX D

Seizures and neuronal damage in mice lacking vesicular zinc.

Cole, T.B., Robbins, C.A., Wenzel, H.J., Schwartzkroin, P.A., Palmiter, R.D., (2000) *Epilepsy Res.* 39, 153-169.

ELSEVIER

Epilepsy Research 39 (2000) 153–169

Epilepsy Research

www.elsevier.com/locate/epilepsyres

Seizures and neuronal damage in mice lacking vesicular zinc

Toby B. Cole [a], Carol A. Robbins [b], H. Jürgen Wenzel [b], Philip A. Schwartzkroin [b,c], Richard D. Palmiter [a,d,*]

[a] *Department of Biochemistry, The University of Washington, Box 357370, Seattle, WA 98195, USA*
[b] *Department of Neurological Surgery, The University of Washington, Seattle, WA, USA*
[c] *Department of Physiology and Biophysics, The University of Washington, Seattle, WA, USA*
[d] *Howard Hughes Medical Institute, The University of Washington, Seattle, WA, USA*

Received 13 September 1999; received in revised form 29 November 1999; accepted 30 November 1999

Abstract

Synaptically released zinc has neuromodulatory capabilities that could result in either inhibition or enhancement of neuronal excitability. To determine the net effects of vesicular zinc release in the brain in vivo, we examined seizure susceptibility and seizure-related neuronal damage in mice with targeted disruption of the gene encoding the zinc transporter, ZnT3 (*ZnT3*$^{-/-}$ mice). *ZnT3*$^{-/-}$ mice, which lack histochemically reactive zinc in synaptic vesicles, had slightly higher thresholds to seizures elicited by the $GABA_A$ antagonist, bicuculline, and no differences in seizure threshold were seen in response to pentylenetetrazol or flurothyl. However, *ZnT3*$^{-/-}$ mice were much more susceptible than wild-type mice to limbic seizures elicited by kainic acid, suggesting that the net effect of hippocampal zinc on acute seizures in vivo is inhibitory. The hippocampi of *ZnT3*$^{-/-}$ mice showed typical seizure-related neuronal damage in response to kainic acid, demonstrating that damage to the targets of zinc-containing neurons can occur independently of synaptically released zinc. Mice lacking the neuronal zinc-binding protein metallothionein III (MT-III) are also more susceptible to kainic acid-induced seizures. Double knockout (*ZnT3* and *MT3*) mice show the same response to kainic acid as *ZnT3*$^{-/-}$ mice, suggesting that ZnT3 and MT-III function in the same pathway.

Keywords: Zinc; ZnT3; MT-III; Mouse; Kainic acid; Bicuculline

1. Introduction

In the mammalian brain, 5–15% of total zinc (Frederickson and Moncrieff, 1994) is concentrated in synaptic vesicles in a subset of glutamatergic neurons (Haug, 1967; Pérez-Clausell and Danscher, 1985; Frederickson, 1989), where it can be detected histochemically using the neo-Timm sulfide silver method (Danscher, 1981), with a selenium stain (Danscher, 1984), or via the zinc-reactive fluorescent compound *N*-(6-methoxy-8-quinolyl)-*p*-toluene-sulfonamide (TSQ) (Frederickson et al., 1987). Histochemically reactive zinc is present in many regions of the

* Corresponding author. Tel.: +1-206-5436090; fax: +1-206-5430858.
E-mail address: palmiter@u.washington.edu (R.D. Palmiter)

0920-1211/00/$ - see front matter
PII: S0920-1211(99)00121-7

CNS (Slomianka, 1992; Frederickson, 1989), and is especially abundant in the hippocampus (Crawford and Connor, 1972; Zimmer and Haug, 1978; Slomianka, 1992). Zinc levels within neurons and in the extracellular space are likely to be controlled by membrane-bound zinc transporters of the ZnT or ZIP families (Palmiter and Findley, 1995; Palmiter et al., 1996a,b; Huang and Gitschier, 1997; Eng et al., 1998), and by metal binding proteins such as metallothionein III (MT-III) (Erickson et al., 1997). Zinc is taken up into synaptic vesicles by a mechanism that requires the zinc transporter, ZnT3, at the vesicle membrane (Wenzel et al., 1997; Cole et al., 1999). Consequently, mice with only one normal *ZnT3* allele have reduced ZnT3 immunoreactivity and a corresponding decrease in vesicular zinc levels, and mice lacking both *ZnT3* alleles lack histochemically reactive zinc in synaptic vesicles throughout the CNS (Cole et al., 1999).

The function of vesicular zinc is not well understood. Zinc may facilitate storage of glutamate or macromolecules within synaptic vesicles (Frederickson, 1989), in a manner analogous to its role in the storage of insulin in pancreatic β cells (Epand et al., 1985) or NGF in the salivary gland (Pattison and Dunn, 1975). Alternatively, zinc could modulate neurotransmitter functions. Vesicular zinc is released with synaptic activity or depolarization (Assaf and Chung, 1984; Howell et al., 1984; Charton et al., 1985; Aniksztejn et al., 1987), and may reach concentrations of 100–300 μM in the synaptic cleft (Assaf and Chung, 1984). Upon release, it could modulate the activity of multiple ligand- and voltage-gated ion channels (Harrison and Gibbons, 1994; Smart et al., 1994). Potential roles for synaptically released zinc include inhibition of NMDA receptors (Peters et al., 1987; Westbrook and Mayer, 1987; Christine and Choi, 1990), potentiation of AMPA receptor responses (Rassendren et al., 1990), inhibition of $GABA_A$ receptors that lack γ subunits (Westbrook and Mayer, 1987; Draguhn et al., 1990; Celentano et al., 1991; Legendre and Westbrook, 1991; Smart et al., 1991), and antagonism of voltage-gated calcium channels (Winegar and Lansman, 1990). In hippocampal slices, zinc application causes giant depolarizing potentials (Xie and Smart, 1991; Ben-Ari and Cherubini, 1991), which are probably due to zinc-induced synchronization of GABA release (Xie and Smart, 1991; Lambert et al., 1992). Zinc also inhibits glutamate uptake by the glutamate transporter EAAT-1 (Spiridon et al., 1998; Vandenberg et al., 1998).

Thus, as a potential neuromodulator, zinc is capable of exerting effects that could either inhibit or promote neuronal excitability, suggesting the possibility of both pro- and anti-convulsant effects. Indeed, levels of cerebral zinc can be abnormal in epileptic animals (Chung and Johnson, 1983; Kasarskis et al., 1987; Fukahori et al., 1988). Intracerebral injection of zinc is epileptogenic in rabbits (Pei and Koyama, 1986) and rats (Itoh and Ebadi, 1982), and zinc application to cultured neurons results in high frequency bursts of action potentials (Mayer and Vyklicky, 1989). In a kindling model of epilepsy, zinc can block augmentation of GABAergic inhibition in dentate granule cells, suggesting that zinc release from sprouted mossy fibers reduces GABAergic inhibition in the epileptic hippocampus. (Buhl et al., 1996). However, zinc chelators (Mitchell and Barnes, 1993) and dietary (Fukahori and Itoh, 1990) or congenital (Feller et al., 1991) zinc deficiencies are also associated with increased seizure susceptibility. The mouse mutant, *mocha*, has reduced synaptic vesicle zinc and exhibits cortical hyperexcitability, characterized by brief epileptiform discharges and high voltage synchronization of theta rhythms (Noebels and Sidman, 1989; Kantheti et al., 1998).

Zinc may also mediate neuronal damage in response to brain insults (Choi and Koh, 1998). Exposure of neurons to high concentrations of zinc is toxic (Yokoyama et al., 1986; Choi et al., 1988; Lees et al., 1990), presumably due to intracellular accumulation of zinc after uptake through NMDA receptors (Koh and Choi, 1994), voltage-gated Ca^{2+} channels (Freund and Reddig, 1994; Sensi et al., 1997), AMPA/kainate receptors (Yin and Weiss, 1995; Yin et al., 1998), or via transporter-mediated exchange with intracellular sodium (Sensi et al., 1997). The translocation of zinc from presynaptic terminals to postsynaptic cell bodies may be responsible for much of the neuronal degeneration seen after prolonged

seizures (Sloviter, 1985; Frederickson et al., 1989; Weiss et al., 1993) or transient global ischemia (Tonder et al., 1990; Koh et al., 1996). In the gerbil hippocampus, transient ischemia is associated with increased expression of the zinc transporter, ZnT1, which is thought to protect cells against zinc toxicity by facilitating zinc efflux (Palmiter and Findley, 1995; Tsuda et al., 1997).

Mice deficient for the zinc-binding protein MT-III (*MT3*$^{-/-}$ mice) have decreased zinc levels in the hippocampus but no reduction in vesicular zinc (Erickson et al., 1997). These mice are more susceptible to seizures induced by kainic acid (KA) and exhibit increased neuron injury in the CA3 region (but not the CA1 region) of the hippocampus (Erickson et al., 1997). Conversely, mice that overexpress *MT3* show similar sensitivity to KA-induced seizures as wild-type mice, but exhibit less neuronal damage in the CA3 region (Erickson et al., 1997). The inhibitory effect of MT-III on seizure activity could be due to its possible role in the transport of zinc (an inhibitory neuromodulator) from sites of cellular uptake back to synaptic vesicles, which would serve to replenish vesicular zinc stores (Erickson et al., 1997), or its function could be unrelated to synaptically released zinc, e.g. as an oxygen radical scavenger (Coyle and Puttfarcken, 1993). If MT-III is important for recycling zinc, removal of MT-III from *ZnT3*$^{-/-}$ mice should not exacerbate their susceptibility to KA-induced seizures because there would be no synaptic zinc to recycle. However, if MT-III has functions that are independent of synaptic zinc release, then the seizure phenotype of double knockout mice might be more severe than either alone. Similarly, the apparent protective effect of MT-III on seizure-induced neuronal damage could be due to the zinc-binding properties of MT-III, or it could be due to other functions of MT-III. If MT-III protects against zinc-mediated damage by facilitating the clearance of zinc from the synaptic cleft, its neuroprotective capabilities would be ineffective in the absence of synaptically released zinc, and its removal from the brains of *ZnT3*$^{-/-}$ mice would not increase KA-induced damage to CA3 pyramidal cells. However, if the neuroprotective functions of MT-III are unrelated to vesicular zinc, double knockout mice might show increased neuronal damage.

To determine which functions of zinc are relevant for seizures and neuronal damage in vivo, we used several different drugs to induce seizures in *ZnT3*$^{-/-}$ mice, which lack vesicular zinc, and are thus incapable of releasing zinc into the synaptic cleft. We also address the question of whether the functions of MT-III and ZnT3 are inter-related with respect to their effects on seizures and seizure-related neuronal damage by examining the seizure phenotype of double knockout mice.

2. Materials and methods

2.1. *ZnT3*$^{-/-}$ and *MT3*$^{-/-}$ mice

Generation of *ZnT3*$^{-/-}$ and *MT3*$^{-/-}$ mice has already been described (Erickson et al., 1997; Cole et al., 1999). Wild-type (*ZnT3*$^{+/+}$), heterozygous (*ZnT3*$^{+/-}$) and mutant (*ZnT3*$^{-/-}$) C57Bl/6 × 129/svJ hybrid mice, 4–12 weeks old, were produced for this study by mating F1 or F2 mice that were heterozygous for the disrupted *ZnT3* allele. The offspring of these crosses were genotyped by dot blot hybridization or PCR analysis of tail DNA, as described (Erickson et al., 1997; Cole et al., 1999). Mice were age and sex-matched, and littermates were used as controls whenever possible. For experiments involving *MT3*$^{-/-}$ mice, all mice were produced by first crossing *ZnT3*$^{-/-}$ mice with *MT3*$^{-/-}$ mice, then mating the offspring (which were hemizygous for both *ZnT3* and *MT3*) to produce all possible genotypes. Genotypes were confirmed by Southern blot.

2.2. Seizure induction with kainic acid, bicuculline, pentylenetetrazol, and flurothyl

For kainic acid (KA), (+)-bicuculline, and pentylenetetrazol (PTZ), mice were injected intraperitoneally with stock solutions prepared as follows: 4 mg/ml KA (Sigma) in water, adjusted to pH 7.2 with NaOH; (+)-bicuculline (Sigma), dissolved in 0.1 M HCl, adjusted to pH 4.5 with NaOH, then adjusted to a final concentration of

0.5 mg/ml by adding normal saline; 18 mg/ml PTZ (Sigma) in phosphate buffered saline, pH 7.4. After i.p. injection, mice were observed in clear plastic cages for the entire duration of seizure (2 h for KA; 1 h for bicuculline; 30 min for PTZ), and the incidence and latency of behavioral seizures were recorded. The maximum behavioral seizure severity was scored as described (Racine, 1972)(see Table 1), with status epilepticus leading to death being scored as stage 6. Myoclonic jerks, which were more common and more pronounced with bicuculline than with kainic acid, were scored as stage 2 seizures. For mice implanted with electrodes, KA was injected subcutaneously. Flurothyl (2,2,2-trifluoroethyl ether, Aldrich) was administered by infusion (20 μl/min) onto a paper filter suspended 11.5" from the bottom of a 14 × 6 × 7.5" plexiglass chamber. The incidence and latencies of seizure behaviors (twitch, myoclonic jerk, tonic/clonic seizure, tonic extension) were recorded from the start of infusion until the onset of the second generalized seizure, at which time infusion was terminated and the chamber opened to room air.

2.3. Electroencephalography

Electrodes for monitoring electroencephalographic (EEG) activity were surgically implanted under ketamine/xylazine anesthesia. Microscrews (stainless steel), inserted into burr holes in the cranium (AP −2.0 mm, $L \pm 1.75$ mm), served as epidural recording electrodes, and were cemented in place with dental acrylic. A reference electrode was positioned 0.5 mm anterior to bregma and a ground was positioned over the cerebellum. A twisted pair of fine wires (76-μm diameter) was stereotaxically placed in the right hippocampus (AP −2.3 mm, L 2.0 mm, D 1.8 mm). Electrodes were attached to a microplug, which was cemented to the cranium. A DEEG/Video Monitoring System (Telefactor) was used to record EEGs and simultaneous video images of mouse behavior.

Table 1
Seizure severity scoring for kainic acid, bicuculline, and pentylenetetrazol

Score	Behavioral response
0	No response
1	Staring/unresponsive
2	Focal clonic convulsion (e.g. Head nod/twitch/myoclonic jerk/backing)
3	Forelimb clonus (tonic/clonic seizure)
4	Rearing
5	Loss of posture (e.g. jumping/rearing and falling)
6	Status epilepticus/death

2.4. Damage assessment

Three days after administration of KA, mice were killed by CO_2 asphyxiation then perfused with 4% paraformaldehyde in 0.1 M phosphate buffer, pH 7.4. Paraffin-embedded sections (7 μm) were stained with either cresyl violet or hematoxylin/eosin. Sections were examined and photographed on a Nikon Microphot FX microscope. Damage was assessed by determining the percentage of nuclei that were pyknotic, averaging the left and right hippocampus.

2.5. Statistical analysis

Maximum seizure severity scores did not usually follow the normal distribution, so the nonparametric Mann–Whitney U-test (two-tailed) was used to test for differences in the distribution of severity scores at each dose of convulsant. Incidence of myoclonic jerks and tonic/clonic seizures were analyzed by probit analysis (Finney, 1971), which allowed calculation of the estimated dose (ED) sufficient to produce seizures in 20% (ED_{20}), 50% (ED_{50}), or 90% (ED_{90}) of mice. χ^2 analysis revealed no significant heterogeneity of discrepancies between observed and expected values from the probit analysis, allowing assignment of 95% fiducial limits to the ED_{20}, ED_{50}, and ED_{90}. A two-tailed Student's t-test was used to test for differences in the mean for various parameters of electrographic seizures and for latencies to flurothyl-induced seizures. Data in all figures are presented as mean ± S.E.M.

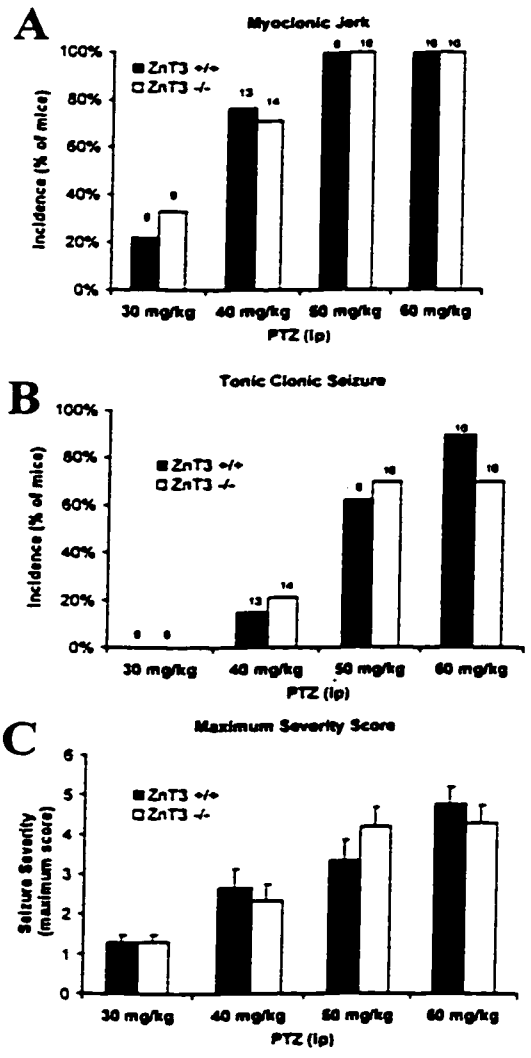

Fig. 1. $ZnT3^{-/-}$ mice show similar seizure sensitivities to PTZ as $ZnT3^{+/+}$ mice. (A) Dose response graph showing the percentage of mice responding with at least a stage-2 seizure (myoclonic jerk). (B) Percentage of mice responding with a stage-3 seizure (tonic/clonic seizure) or higher. (C) Maximum behavioral seizure severity score at various doses of PTZ. There were no significant differences in seizure severity in response to PTZ. Numbers above the bars represent n values.

3. Results

3.1. $ZnT3^{-/-}$ mice do not display spontaneous hyperexcitability

Under normal conditions $ZnT3^{-/-}$ mice are indistinguishable from wild-type mice. Tests of motor coordination, hearing, olfaction, anxiety, learning and memory have not yet revealed any abnormalities (Cole and Palmiter, unpublished observations). They are active and fertile, and the brain appears to have developed properly, including regions that are normally zinc-rich like the hippocampus (Cole et al., 1999). In contrast to other epileptic or seizure-prone lines of mice (Homanics et al., 1997; Kash et al., 1997; Smart et al., 1998), $ZnT3^{-/-}$ mice do not exhibit spontaneous seizures, nor were we able to induce seizures acoustically (115 dB for 60 s) or by handling (data not shown).

3.2. $ZnT3^{-/-}$ mice are similar to wild-type mice in their sensitivity to seizures elicited by pentylenetetrazol and flurothyl

The effects of removing zinc from synaptic vesicles may be most pronounced under conditions of high neuronal activity. To determine whether the net effect of zinc release during prolonged neuronal firing is excitatory or inhibitory, we tested seizure susceptibility of $ZnT3^{-/-}$ mice in a number of seizure-induction protocols.

$ZnT3^{-/-}$ and $ZnT3^{+/+}$ mice were tested for their sensitivity to seizures elicited by pentylenetetrazol (PTZ) and flurothyl, which act at least in part by reducing $GABA_A$-mediated inhibition. The progression of seizures was very rapid in response to intraperitoneal injection of PTZ; myoclonic jerks occurred within 3 min, clonus within 6 min, and seizures did not usually extend beyond 15 min post-injection. The incidence and latencies of myoclonic jerks and tonic/clonic seizures were similar for $ZnT3^{+/+}$ and $ZnT3^{-/-}$ mice (Fig. 1A and B; Table 2), as was overall seizure severity, based on the maximum behavioral severity score (Fig. 1C, Table 1).

Flurothyl, administered by inhalation, produces a well-defined series of behavioral seizures whose

Table 2
Seizure parameters

Treatment	Genotype	Dose (mg/kg)	Latency to myoclonic jerk (min)	Latency to clonus (min)	ED_{20}* (mg/kg) clonus	ED_{50}* (mg/kg) clonus	ED_{90}* (mg/kg) clonus
Kainic acid	+/+	15	n.d.	n.d.	12.0	14.7*	20.1*
		18	n.d.	36.7 ± 4.1	(10.5-13.7)	(13.6-16.0)	(17.4-23.2)
	−/−	15	n.d.	n.d.	10.6	12.3*	15.3*
		18	n.d.	30.7 ± 5.0	(9.6-11.8)	(11.5-13.1)	(14.0-16.7)
Bicuculline	+/+	4	5.5 ± 1.8*	8.7 ± 3.8	2.5	3.5	5.9
		5	2.3 ± 0.3	3.3 ± 0.9	(2.0-3.2)	(3.0-4.1)	(4.2-8.1)
	−/−	4	10.0 ± 3.2*	8.0 ± 3.4	3.4	4.4	6.5
		5	3.0 ± 0.4	3.2 ± 0.6	(3.0-4.0)	(3.8-5.1)	(4.7-8.9)
PTZ	+/+	50	2.1 ± 0.2	5.1 ± 1.2	39.5	46.7	60.2
		60	1.7 ± 0.2	2.3 ± 0.5	(33.1-47.2)	(41.7-52.2)	(50.1-72.2)
	−/−	50	2.3 ± 0.5	3.2 ± 0.7	41.8	50.2	66.3
		60	2.5 ± 0.5	3.0 ± 0.8	(35.5-49.1)	(45.0-55.9)	(53.0-83.0)

* The estimated doses necessary to produce tonic/clonic seizures in 20% (ED_{20}), 50% (ED_{50}), and 90% (ED_{90}) of mice were determined by probit analysis (Finney, 1971). Values in parentheses represent 95% fiducial limits.

* Significantly different among genotypes by either probit analysis (ED values) or Student's *t*-test (Latency to myoclonic jerk, $P<0.05$).

latencies depend on the rate of flurothyl infusion into the chamber (Prichard et al., 1969; Sperber and Moshe, 1988). *ZnT3*$^{+/+}$, *ZnT3*$^{+/-}$ and *ZnT3*$^{-/-}$ mice, in response to flurothyl administered at a rate of 20 μl/min, experienced numerous twitches and occasional myoclonic jerks, followed by a generalized tonic/clonic seizure at about 6 min from the start of infusion. After this first generalized seizure, about a third of the mice (4/11 *ZnT3*$^{+/+}$, 1/3 *ZnT3*$^{+/-}$, 4/9 *ZnT3*$^{-/-}$) immediately progressed into severe tonic extension, from which they could not be rescued. The rest of the mice experienced a post-ictal period following the first generalized seizure, followed by a second generalized seizure 4–6 min later. This second seizure invariably led to severe tonic extension and death. Thus, once an animal reached the tonic extension stage, there was 100% mortality. Latencies to twitch, myoclonic jerk, first tonic/clonic seizure, second tonic/clonic seizure and tonic extension were the same for *ZnT3*$^{+/+}$, *ZnT3*$^{+/-}$ and *ZnT3*$^{-/-}$ mice (Fig. 2).

3.3. ZnT3$^{-/-}$ *mice are somewhat less sensitive than ZnT3*$^{+/+}$ *mice to seizures elicited by low doses of bicuculline*

To test the *ZnT3*$^{-/-}$ mice in another seizure paradigm, we injected *ZnT3*$^{+/+}$ and *ZnT3*$^{-/-}$ mice with the competitive $GABA_A$ antagonist, bicuculline. *ZnT3*$^{-/-}$ mice were somewhat less susceptible to the seizure-inducing effects of bicuculline when it was administered at low doses. There was a trend (not statistically significant) towards lower incidence of myoclonic jerks and tonic/clonic seizures in the *ZnT3*$^{-/-}$ mice (Fig. 3A and B); ED_{50} values for tonic/clonic seizure were not significantly different (Table 2), presumably due to the obligatory inclusion of data from the higher doses of bicuculline, where there was clearly no difference. A G-test for differences in the incidence of tonic/clonic seizure revealed a significantly lower ($P < 0.05$) incidence of seizures in the *ZnT3*$^{-/-}$ mice at 2 mg/kg bicuculline, but not at the other doses. The maximum seizure severity score, used as a measure of the overall severity of seizures in response to bicuculline, was significantly reduced in the *ZnT3*$^{-/-}$ mice at lower doses of bicuculline (Fig. 3C). These doses of bicuculline produced twitches and myoclonic jerks in many of the *ZnT3*$^{+/+}$ mice, and limb clonus in a few *ZnT3*$^{+/+}$ mice. Most of the *ZnT3*$^{-/-}$ mice responded, if at all, with only staring or unresponsiveness. At the lowest dose tested (1 mg/kg bicuculline), very few mice exhibited any seizure behaviors besides unresponsiveness, regardless of genotype.

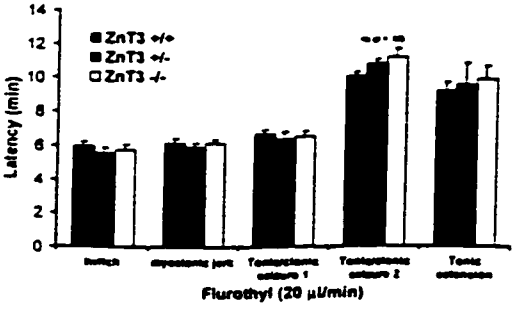

Fig. 2. *ZnT3*$^{-/-}$ mice show similar seizure sensitivities to flurothyl as *ZnT3*$^{+/+}$ mice. Mice of both genotypes progressed through the defined series of seizure behaviors listed on the abscissa. About a third of the mice of each genotype progressed immediately from the first tonic/clonic seizure to tonic extension. The remainder experienced a second tonic/clonic seizure. Latencies to twitch, myoclonic jerk, tonic/clonic seizure, and tonic extension were similar among genotypes. $n = 11$ (*ZnT3*$^{+/+}$), $n = 9$ (*ZnT3*$^{+/-}$), $n = 3$ (*ZnT3*$^{-/-}$).

3.4. ZnT3$^{-/-}$ *and ZnT3*$^{+/-}$ *mice are more susceptible than ZnT3*$^{+/+}$ *mice to kainic acid-induced seizures*

Seizures were induced in *ZnT3*$^{+/+}$, *ZnT3*$^{+/-}$ and *ZnT3*$^{-/-}$ mice by intraperitoneal injection of KA at doses ranging from 10 to 20 mg/kg. Seizures usually followed the progression described by Racine (1972)(Table 1), from milder seizure behaviors such as twitches, head nodding, and myoclonic jerks (twitches with whole body involvement), through forelimb clonus to behaviors indicative of more severe generalized seizures, such as loss of posture (jumping or rearing and falling). The incidence of myoclonic jerks and tonic/clonic seizures was higher in the *ZnT3*$^{-/-}$ mice than in *ZnT3*$^{+/+}$ mice (Fig. 4A and B), and

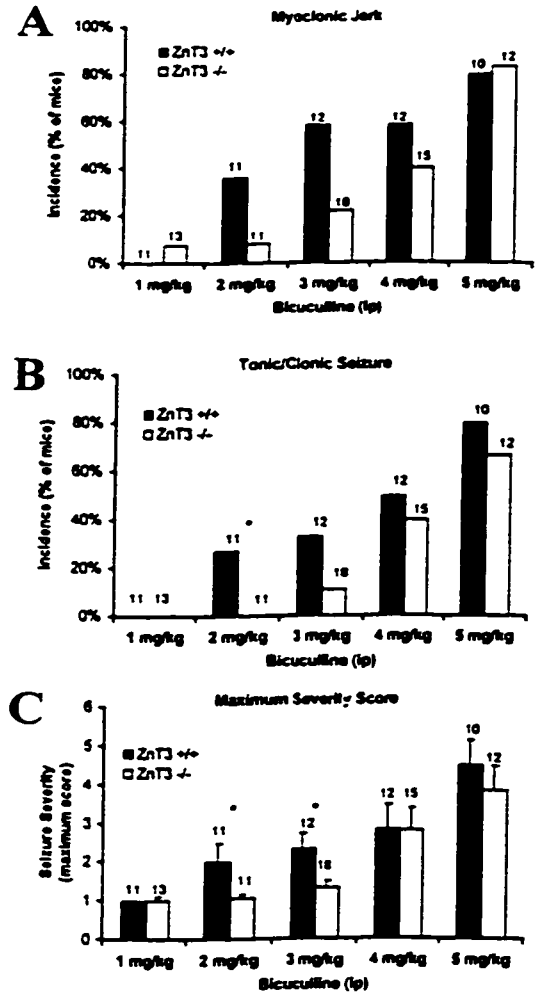

Fig. 3. $ZnT3^{-/-}$ mice are less susceptible to seizures induced by bicuculline. (A) Dose response graph showing the percentage of mice responding with at least a stage-2 seizure (myoclonic jerk). (B) Percentage of mice responding with a stage-3 seizure (tonic/clonic seizure) or higher. $ZnT3^{-/-}$ mice tended to have a lower incidence of both myoclonic jerks and tonic/clonic seizures, especially at lower doses. (C) Maximum behavioral seizure severity score at various doses of bicuculline. $ZnT3^{-/-}$ mice had significantly lower maximum seizure severity scores at the 2 and 3 mg/kg doses ($P < 0.05$, Mann–Whitney U-test). Numbers above the bars represent n values.

the ED_{50} for tonic/clonic seizure was significantly lower (Table 2). The maximum seizure severity observed during the 2-h period following KA administration was used as an indicator of the overall severity of seizures. $ZnT3^{-/-}$ mice had more severe seizures at most of the doses of KA tested (Fig. 4C). The maximum seizure severities in response to 18 mg/kg KA in the $ZnT3^{+/+}$ mice were widely distributed, with an average score of 3.33 ± 0.43 (corresponding to bilateral forelimb clonus)(Fig. 4D). In striking contrast, at this dose both $ZnT3^{+/-}$ and $ZnT3^{-/-}$ mice exhibited very strong convulsive seizures, with average severity scores of 4.89 ± 0.33 and 4.94 ± 0.34, respectively (corresponding to loss of posture). Frequently, seizures in the $ZnT3^{-/-}$ mice deteriorated into convulsive status epilepticus, followed by death. Seizures in the $ZnT3^{+/-}$ mice were intermediate in severity, occurring at a lower frequency than in the $ZnT3^{-/-}$ mice (data not shown), and with fewer of the mice progressing to convulsive status epilepticus or death (Fig. 4D). Latencies to bilateral forelimb clonus (Table 2) and loss of posture ($ZnT3^{-/-}$, 42.2 ± 9.0 min, $n = 16$; $ZnT3^{+/-}$, 29.1 ± 9.3 min, $n = 8$; $ZnT3^{+/+}$, 32.8 ± 6.9 min, $n = 6$) were not different among genotypes.

3.4.1. *Electroencephalographic activity during seizures elicited by kainic acid*

To characterize the seizures induced by KA in the $ZnT3^{-/-}$ mice, an electroencephalographic (EEG) activity/videomonitoring system was used. Video/EEGs were recorded from cortical epidural electrodes and hippocampal depth electrodes to correlate behaviorally scored seizure severity with electrographic activity in the hippocampus (Fig. 5A). These recordings were conducted for 10 min prior to, as well as 2 h following KA administration. No abnormalities in EEG patterns were observed in $ZnT3^{-/-}$ mice during the 10-min observation period prior to KA administration (Fig. 5A, see upper trace for each mouse). Likewise, no spontaneous behavioral or electrographic seizures were observed in these mice during 1-h recordings taken days to weeks after administration of KA.

Subcutaneous injection of 18 mg/kg KA into mice with implanted electrodes produced convulsive seizures with average behavioral severity scores of 3.50 ± 0.87 in the $ZnT3^{+/+}$ mice ($n = 5$) and 4.67 ± 0.88 in the $ZnT3^{-/-}$ mice ($n = 3$)(Fig. 5B). While the onset of electrical seizures in $ZnT3^{-/-}$ mice was similar to that observed in $ZnT3^{+/+}$ mice (Fig. 5A), $ZnT3^{-/-}$ mice responded more quickly to KA administration, with a latency of 2.0 ± 0.7 min to the first electrographic signs of epileptiform activity, compared to 12.4 ± 4.8 min for the $ZnT3^{+/+}$ mice (Fig. 5C). This initial electrical epileptiform activity was not associated with a behavioral seizure.

In striking contrast to $ZnT3^{+/+}$ mice, which spent $17.7 \pm 9.9\%$ of the time in electrographic seizure, $ZnT3^{-/-}$ mice spent $65.3 \pm 1.9\%$ of the observation time in electrical epileptiform discharge (Fig. 5D). Electrical seizures in the $ZnT3^{-/-}$ mice were longer in duration than in $ZnT3^{+/+}$ mice (Fig. 5E), with shorter interictal periods. Often, the electrical seizure episodes in

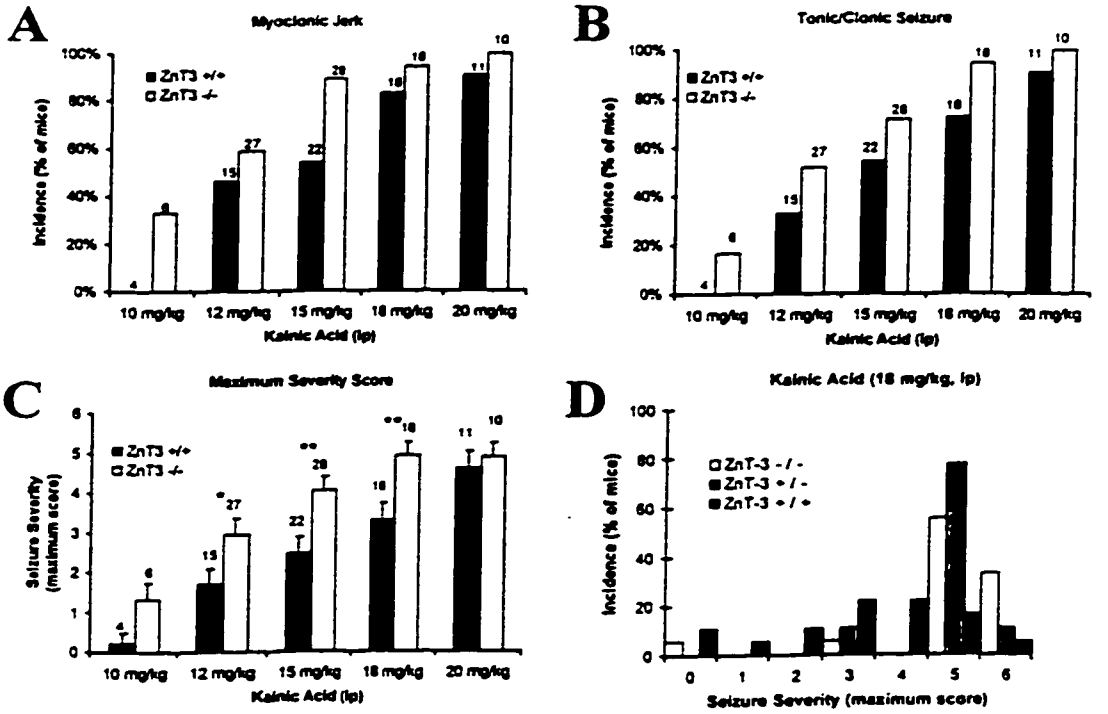

Fig. 4. $ZnT3^{-/-}$ mice are more susceptible to kainic acid-induced seizures. (A) Dose response graph showing the percentage of mice responding with at least a stage-2 seizure (myoclonic jerk). (B) Percentage of mice responding with a stage-3 seizure (tonic/clonic seizure) or higher. $ZnT3^{-/-}$ mice tended to have a higher incidence of both myoclonic jerks and tonic/clonic seizures at all doses tested. (C) Maximum behavioral seizure severity score at various doses of kainic acid. $ZnT3^{-/-}$ mice had significantly higher maximum seizure severity scores at the 12 mg/kg ($P < 0.05$, Mann–Whitney U-test), 15 mg/kg ($P < 0.01$), and 18 mg/kg ($P < 0.01$) doses. Numbers above the bars represent n values. (D) Histogram showing the percentage of mice of each genotype that exhibited a given maximum seizure severity score in response to 18 mg/kg KA, illustrating the skewed distribution of seizure severities in the $ZnT3^{-/-}$ mice at this dose. $ZnT3^{+/-}$ mice showed an intermediate response that was significantly higher in severity than that seen in the $ZnT3^{+/+}$ mice ($P < 0.01$, Mann–Whitney U-test). $n = 18$ each genotype.

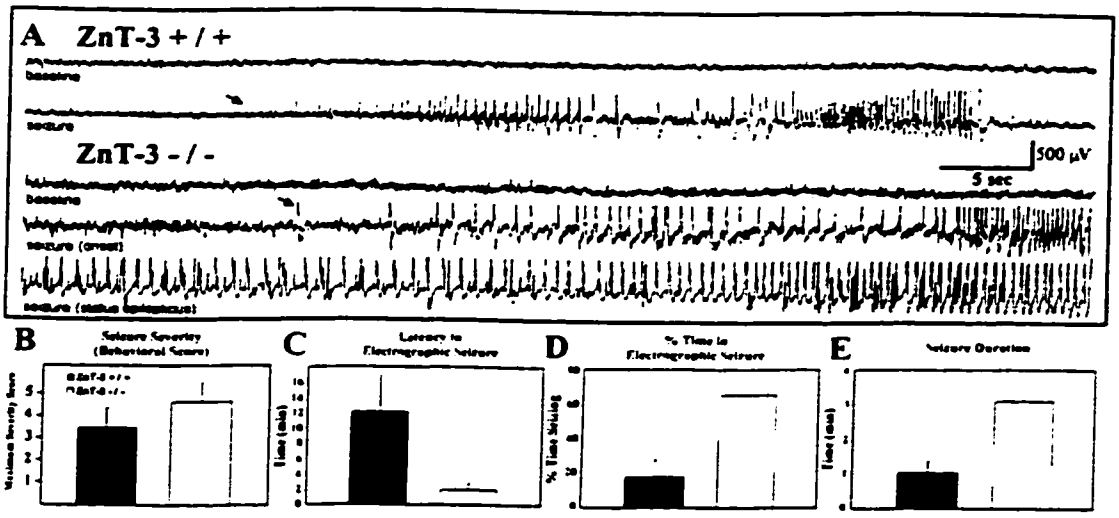

Fig. 5. $ZnT3^{-/-}$ mice have more severe electrographic seizures in response to kainic acid. (A) Representative EEGs recorded from cortical epidural electrodes implanted in $ZnT3^{+/+}$ (top two traces) and $ZnT3^{-/-}$ (bottom three traces) mice. Hippocampal depth electrodes showed similar patterns of activity. The upper traces represent 1 min of baseline recording before KA administration (18 mg/kg, sc). The bottom traces represent 1 min of recording taken during a severe convulsive (stage-5) seizure. The electrographic activity of seizures in $ZnT3^{+/+}$ mice typically had a discrete beginning and end ($ZnT3^{+/+}$, lower trace), with relatively long interictal periods. In $ZnT3^{-/-}$ mice, seizure onset (arrows) was similar to that seen in wild-type mice, but initial electrical seizure episodes frequently lengthened over time, reaching a stage of prolonged electrographic status epilepticus ($ZnT3^{-/-}$, lower trace). (B–E) Quantification of various aspects of seizure severity in $ZnT3^{+/+}$ and $ZnT3^{-/-}$ mice implanted with cortical electrodes. (B) Maximum behavioral seizure severity score. Because of high variability within groups, the difference in severity scores was not statistically significant. Latency to first electrographic seizure (C) was significantly shorter in $ZnT3^{-/-}$ mice than in $ZnT3^{+/+}$ mice ($P < 0.05$, Student's t-test). Percent time in electrographic seizure (D) was greater in $ZnT3^{-/-}$ mice than in $ZnT3^{+/+}$ mice ($P < 0.01$, Student's t-test). Average seizure duration (E) was greater in $ZnT3^{-/-}$ mice than in $ZnT3^{+/+}$ mice ($P < 0.001$, Student's t-test). $n = 5$ ($ZnT3^{+/+}$); $n = 3$ ($ZnT3^{-/-}$).

the $ZnT3^{-/-}$ mice progressed into a prolonged seizure characteristic of the merged stage of status epilepticus (Treiman et al., 1990) (see Fig. 5A, lower trace), that could last for hours. $ZnT3^{+/+}$ mice that exhibited status epilepticus were more likely to experience repeated discrete seizures (Fig. 5A), a less severe form of status epilepticus (Treiman et al., 1990). In both $ZnT3^{+/+}$ and $ZnT3^{-/-}$ mice, behavioral seizures were always associated with epileptiform electrical activity. Often, however, electrographic seizures occurred with little or no corresponding seizure behaviors. This was especially striking in the $ZnT3^{-/-}$ mice, some of which exhibited electrographic status epilepticus for 20 min or more without any outward behaviors indicative of the seizure activity detected by the EEG recordings.

3.4.2. Severe neuronal damage in the absence of synaptically released zinc

Zinc chelation has been shown to reduce damage in brain regions exposed to various insults (Choi and Koh, 1998). Therefore, we predicted that the $ZnT3^{-/-}$ brain might show less seizure-induced neuronal damage than the $ZnT3^{+/+}$ brain in regions where zinc is normally released, even though KA-induced seizures are more severe in $ZnT3^{-/-}$ mice. To test this hypothesis, mice were treated with KA doses that produced seizure activity of approximately equal intensity: 20 mg/

kg in $ZnT3^{+/+}$ mice and 15 mg/kg in $ZnT3^{-/-}$ mice. Animals were sacrificed 3 days after KA treatment and the percentage of pyknotic nuclei in various sub-regions of the hippocampus was determined. The hippocampi of both $ZnT3^{+/+}$ and $ZnT3^{-/-}$ mice showed some cell damage even in response to stage-3 seizures (data not shown). $ZnT3^{-/-}$ mice that experienced stage-5 seizures had severe damage in the dentate gyrus, hilus, and most strikingly in stratum (s.) pyramidale of the CA3 and CA1 regions (Fig. 6B, D, and F). Pyknotic nuclei were also conspicuous in the amygdala, neocortex, and entorhinal and piriform cortices (data not shown). The $ZnT3^{-/-}$ brains frequently displayed hemorrhages in the thalamus, and the choroid plexus was often swollen or broken and filled with erythrocytes (data not shown). $ZnT3^{+/+}$ mice that experienced stage-5 seizures showed pyknotic cells most conspicuously in the dentate gyrus, hilus, and s. pyramidale of CA3, with less damage to s. pyramidale of the CA1 region (Fig. 6G); they did not have appreciable damage to the thalamus or choroid plexus, and damage appeared to be less severe in the amygdala and cortex compared to the $ZnT3^{-/-}$ mice (although pyknotic nuclei were not quantified in those regions). Interestingly, the most severe damage in the $ZnT3^{-/-}$ hippocampus was in the CA1 region, which was spared in the $ZnT3^{+/+}$ mice. This more severe damage seen in the brains of $ZnT3^{-/-}$ mice may have been due to greater seizure severity and duration (even given attempts to equalize seizure severity by using different doses of kainic acid). The maximum seizure severity scores were identical for the two groups, but our EEG data suggest that this measure is an imprecise indicator of electrographic seizure activity.

3.5. The absence of MT3 does not enhance seizure sensitivity or neuronal damage in $ZnT3^{-/-}$ mice

To test whether ZnT3 and MT-III participate in the same pathways to reduce seizure sensitivity and affect neuronal damage, we generated $ZnT3^{-/-}$ mice that were either wild-type at the *MT3* locus ($MT3^{+/+}$), hemizygous for *MT3* ($MT3^{+/-}$), or homozygous mutant ($MT3^{-/-}$). These mice were injected intraperitoneally with KA at 12 mg/kg (the ED_{50} for tonic/clonic seizure; see Table 2), then the maximum seizure severity score was recorded. Three days later, the mice were sacrificed and neuronal damage was determined in the CA3 and CA1 regions of the hippocampus by measuring the percentage of nuclei that exhibited pyknotic morphology upon staining with cresyl violet. $ZnT3^{-/-}/MT3^{+/+}$ mice had an average seizure severity score of about 3.0, compared to a seizure severity score of about 2.0 for the $ZnT3^{+/+}/MT3^{+/+}$ mice (Fig. 7A), in agreement with previous results (Fig. 1). The double knockout mice ($ZnT3^{-/-}/MT3^{-/-}$) had similar seizure severity scores as $ZnT3^{-/-}/MT3^{+/+}$ mice (Fig. 7A). Neuronal damage tended to be higher in $ZnT3^{-/-}/MT3^{+/+}$ mice than in $ZnT3^{+/+}/MT3^{+/+}$ mice, especially in the CA1 region, probably reflecting the increased seizure severity seen in these mice (Fig. 7B). Removal of MT-III from the $ZnT3^{-/-}$ brain ($ZnT3^{-/-}/MT3^{-/-}$) did not increase the extent of neuronal damage in hippocampal subregions CA3 or CA1 (Fig. 7B) (compare to $ZnT3^{-/-}/MT3^{+/+}$). Unexpectedly, in the CA1 region of the hippocampus, removal of MT-III from the $ZnT3^{-/-}$ brain ($ZnT3^{-/-}/MT3^{-/-}$) significantly reduced the percentage of pyknotic nuclei compared to the $ZnT3^{-/-}/MT3^{+/+}$ mice, even though seizure severity was equivalent (Fig. 7B).

4. Discussion

4.1. Neuromodulatory effects of zinc

Histochemical localization of zinc in the mammalian brain reveals that it is most abundant in the mossy fiber terminals of hippocampal dentate granule cells; however, vesicular zinc is also abundant throughout the hippocampal structure, the neocortex, amygdala, striatum and olfactory bulb (Frederickson, 1989; Slomianka, 1992). The distribution of ZnT3 protein matches that of the Timm stain (Palmiter et al., 1996b; Wenzel et al., 1997) and both are completely gone after *ZnT3* gene disruption (Cole et al., 1999). Because $ZnT3^{-/-}$ mice are indistinguishable from wild-type littermates in all behavioral tests examined thus

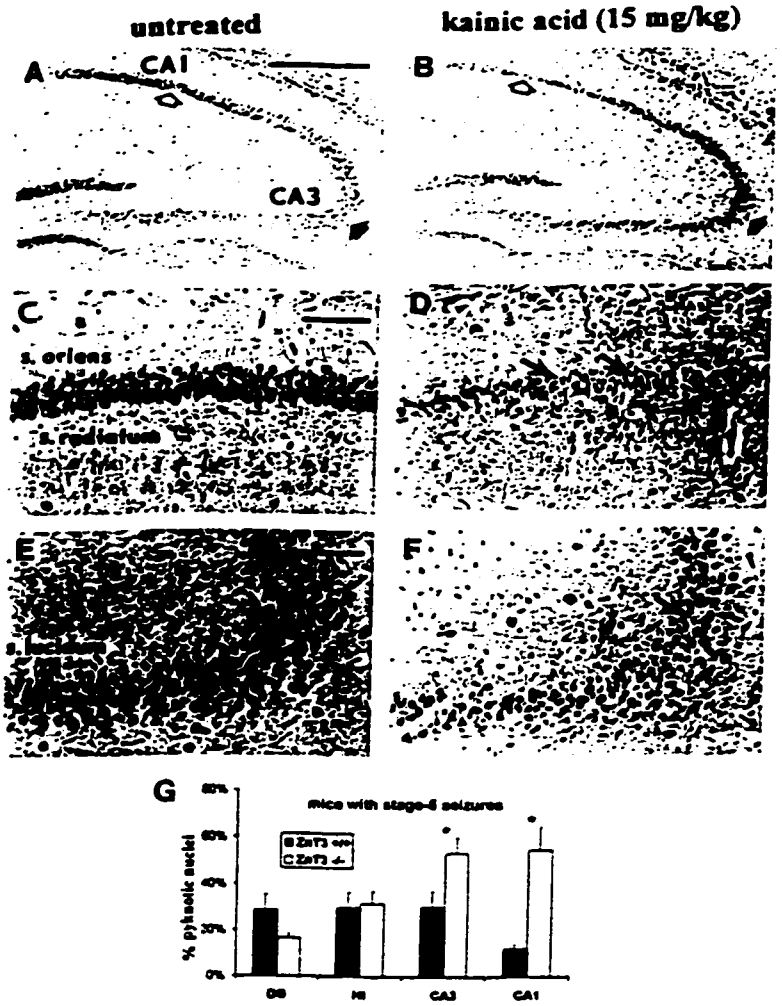

Fig. 6. Severe neuronal damage in the absence of the cytotoxic effects of synaptically released zinc. (A–F) Representative hematoxylin/eosin stained coronal sections of the dorsal hippocampus from a *ZnT3* $^{-/-}$ mouse, untreated (A,C,E), and 3 days after stage-5 seizures induced by KA administration (B,D,F). (C,D) and (E,F) Higher magnification images of the CA1 region (white arrow in A,B) and the CA3 region (black arrow in A,B), respectively. Arrows in D and F point to damaged (pyknotic) nuclei in s pyramidale of CA3 and CA1, which sustained particularly heavy damage in the *ZnT3* $^{-/-}$ mice. (G) Percentage of nuclei that were damaged (pyknotic) in different regions of the dorsal hippocampus in *ZnT3* $^{+/+}$ ($n = 6$) and *ZnT3* $^{-/-}$ ($n = 3$) mice that experienced stage-5 seizures. *ZnT3* $^{-/-}$ mice had significantly greater damage in the CA3 and CA1 regions ($P < 0.05$, student's *t*-test). Abbreviations: DG, dentate gyrus; Hi, hilus. Scale bars = 500 μm (A); 100 μm (C,E).

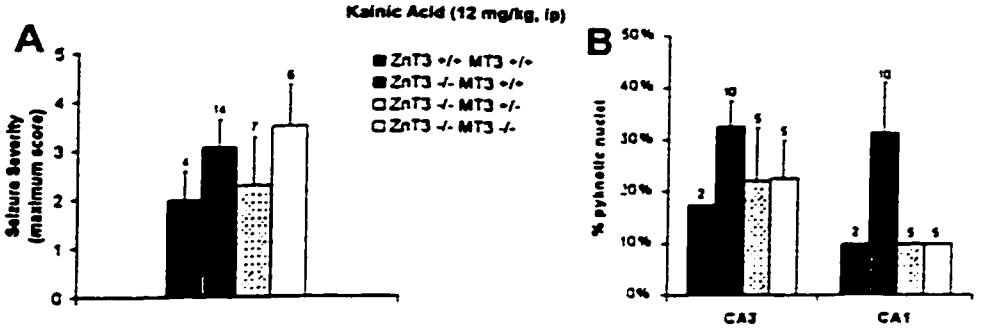

Fig. 7. The absence of MT-III does not increase seizure sensitivity or damage in the absence of ZnT3. $ZnT3^{+/+}/MT3^{+/+}$ mice or $ZnT3^{-/-}$ mice that were either $MT3^{+/+}$, $MT3^{+/-}$, or $MT3^{-/-}$ were injected with kainic acid (12 mg/kg, i.p.). (A) Maximum seizure severity score. Removal of MT-III had no effect on the severity of seizures in $ZnT3^{-/-}$ mice. (B) Seizure-related neuronal damage in the CA3 and CA1 regions of surviving mice. Damage was scored by estimating the percentage of cells in s. pyramidale that had pyknotic nuclear morphology. Removal of MT-III did not increase neuronal damage any further than that seen in the absence of ZnT3. Extensive damage to CA1 pyramidal cells in the $ZnT3^{-/-}$ hippocampus was significantly reduced upon removal of MT-III ($P < 0.05$, Student's t-test). Numbers above the bars represent n values. $ZnT3^{-/-}/MT3^{+/+}$ and $ZnT3^{-/-}/MT3^{-/-}$ mice that survived had average severity scores of 3.1 ± 0.6 and 3.0 ± 0.8, respectively.

far, and since these behaviors undoubtedly depend on glutamate neurotransmission, it seems unlikely that glutamate storage and release are altered greatly in the absence of vesicular zinc. This conclusion is consistent with our preliminary data from electrophysiological studies of hippocampal slices from $ZnT3^{-/-}$ mice (V. Lopantsev et al., our unpublished data). These observations, coupled with the fact that not all glutamatergic neurons sequester zinc in synaptic vesicles (Frederickson, 1989), argue that zinc is not essential for glutamate storage or release. Instead, it is more likely that released zinc modulates pre- or post-synaptic receptors and thereby influences neural transmission. The absence of spontaneous seizures, or any alteration in acoustic- or handling-induced seizures in $ZnT3^{-/-}$ mice suggests either that zinc is only important under extreme conditions of excessive excitability or that chronic absence of zinc leads to compensation under normal conditions.

Many previous studies have indicated neuromodulatory roles for zinc, either excitatory or inhibitory. The increased sensitivity of $ZnT3^{-/-}$ mice to KA-induced seizures suggests that the overall effect of zinc is to dampen excitability. $ZnT3^{-/-}$ mice had a higher incidence of seizures in response to KA, and their seizures were more severe. They spent a much higher percentage of the time (65 vs. 18%) in electrographic seizure (as revealed by monitoring EEG activity) than did $ZnT3^{+/+}$ mice. Strikingly, high voltage epileptiform activity often continued relentlessly for an hour or more (electrographic status epilepticus) in the $ZnT3^{-/-}$ mice, with only occasional behavioral indications that an electrical seizure was occurring. $ZnT3^{+/-}$ mice have intermediate levels of vesicular zinc and intermediate seizure severities (relative to $ZnT3^{-/-}$ and $ZnT3^{+/+}$ mice), indicating that enhanced seizure sensitivity is likely to be due to dose-dependent removal of zinc from synaptic vesicles.

The best described inhibitory effects of zinc are an antagonistic effect on NMDA receptors (Peters et al., 1987; Westbrook and Mayer, 1987; Christine and Choi, 1990) and an enhancement of GABA release (perhaps by blocking $GABA_B$ autoreceptors) that produces giant depolarizing potentials in the CA3 region (Ben-Ari and Cherubini, 1991; Xie and Smart, 1991). Multiple effects of zinc on glutamate and GABA receptors have been described primarily in isolated preparations (reviewed by Harrison and Gibbons, 1994; Smart et al., 1994), but it is not clear whether these receptors are exposed to physiologically relevant zinc concentra-

tions (i.e. those experienced in vivo). For example, the highest concentrations of vesicular zinc are found in the mossy fiber boutons of dentate granule cells, which synapse on complex spines of CA3 pyramidal cells. In this region, glutamate is thought to act predominantly on AMPA receptors, where zinc effects are small and potentiating (Rassendren et al., 1990). Potentiation of AMPA responses by zinc could result in an increased excitatory drive onto inhibitory interneurons. Alternatively, diffusion of zinc may provide a pathway to act at GABA or NMDA synapses. Heteromeric KA receptors are strongly inhibited by zinc in a subunit-dependent manner as the pH declines (D. Mott and R. Dingledine, personal communication). In the *ZnT3*$^{-/-}$ mice, loss of such zinc inhibition could result in enhanced KA-induced depolarization as synapses become relatively acidic during seizures. Finally, the effects of zinc may be mediated by undiscovered receptors, perhaps even dedicated zinc receptors. Our data do not directly address the question of whether this net inhibitory effect of zinc is due to direct antagonism of glutamate receptors, to enhancement of GABA-mediated inhibition, or to some other mechanism. Finally, it is unlikely that *ZnT3* is linked to a seizure susceptibility gene because the 129/svJ strain, which was used for gene targeting, is more resistant to KA-induced seizures than the C57Bl/6 strain (Erickson et al., 1997); moreover, experiments were performed with littermate controls to minimize differences in genetic background.

The response of *ZnT3*$^{-/-}$ mice to seizure-inducing drugs was highly dependent on the drug used to elicit seizures. The mice were susceptible to KA, but were similar to wild-type mice in their responses to PTZ or flurothyl, and they were less sensitive than wild-type mice to bicuculline-induced seizures. The differing sensitivities to epileptogenic drugs could reflect differential effects of zinc on its target receptors. *ZnT3*$^{-/-}$ mice were minimally sensitive to seizures elicited by drugs that block GABA-mediated inhibition (bicuculline, PTZ, and flurothyl), suggesting that functional $GABA_A$ receptors need to be present to reveal an effect of zinc on seizure susceptibility. Thus, the predominant action of zinc in the control of hyperexcitability may be enhancement of GABA-mediated inhibition, rather than direct inhibition of post-synaptic glutamate receptors on excitatory neurons. KA is thought to inhibit GABA release by inhibitory interneurons, and it may also act directly on post-synaptic or extrasynaptic glutamate receptors on pyramidal cells (Lerma, 1997). In the absence of zinc, which normally would enhance GABA release and antagonize NMDA receptors, these effects of KA would be even more pronounced.

It is possible that the mice have compensated for the lack of zinc by enhancing inhibition in some other way, such that the normal balance between excitation and inhibition is maintained. The possibility of compensatory changes in glutamate or GABA neurotransmission complicates assessment of the normal role of zinc as a neuromodulator. The resistance of *ZnT3*$^{-/-}$ mice to low doses of bicuculline is consistent with a compensatory upregulation of GABA neurotransmission. Alternatively, resistance to bicuculline-induced seizures may reflect differential effects of zinc on the mechanisms by which KA and bicuculline induce seizures, as discussed above. In either case, it is intriguing that these mice can be sensitive to one epileptogenic agent and resistant to another.

4.2. Zinc and neuronal damage

Synaptically released zinc may contribute significantly to the excitoxicity seen after a variety of brain insults, including seizures (Sloviter, 1985; Frederickson et al., 1989; Weiss et al., 1993) and transient global ischemia (Tonder et al., 1990; Koh et al., 1996; Choi and Koh, 1998). The presence of severe seizure-related neuronal degeneration in mice no longer capable of releasing zinc into the synaptic cleft demonstrates that mechanisms not involving zinc (but which probably involve Ca^{2+}) are sufficient to inflict severe damage on the targets of zinc-containing neurons. A rigorous determination of whether the lack of vesicular zinc ameliorates seizure-related neuronal damage requires that seizure severity be comparable among genotypes. We attempted to keep seizure severity the same for *ZnT3*$^{-/-}$ and

ZnT3$^{-/-}$ mice by using different doses of kainic acid for the two genotypes and comparing mice that had identical seizure severity scores. However, our EEG data demonstrate that the behavioral seizure severity score is an imprecise measure of the intensity of electrographic seizures. Thus, despite our efforts to keep seizure severity the same, the possibility remains that the higher neuronal damage seen in the brains of *ZnT3*$^{-/-}$ mice resulted from seizures that were more severe than those experienced by the *ZnT3*$^{+/+}$ mice. Alternatively, vesicular zinc may be neuroprotective in the hippocampus of wild-type mice, perhaps by sequestering presynaptic glutamate and thus limiting the amount of free glutamate release (Sloviter, 1985).

4.3. MT-III, seizures and neuronal damage

The absence of MT-III exacerbates seizures in wild-type mice (Erickson et al., 1997), but not in *ZnT3*$^{-/-}$ mice. The lack of MT-III also increases KA-induced neuronal damage in the CA3 region of the hippocampus in the wild-type background (Erickson et al., 1997), but not when ZnT3 is also removed. It seems likely, therefore, that the protective effects of MT-III on seizure activity and neuronal damage are related to vesicular zinc in some way. An attractive possibility is that MT-III facilitates recycling of zinc to synaptic vesicles and thus prevents depletion of zinc from axonal boutons. Our results are consistent with the possibility that the neuroprotective functions of MT-III are due to its ability to facilitate the removal of zinc from the synaptic cleft and thus protect against zinc neurotoxicity — a function that is irrelevant in the *ZnT3*$^{-/-}$ mouse, where vesicular zinc is completely absent.

Acknowledgements

We thank Glenda Froelick for assistance with histology. This work was supported in part by National Institutes of Health grants DK53013 (R.D.P) and NS18895 (P.A.S.), and a U.S. Public Health Service National Research Service Award (T32 GM07270 to T.B.C.).

References

Aniksztejn, L., Charton, G., Ben-Ari, Y., 1987. Selective release of endogenous zinc from the hippocampal mossy fibers in situ. Brain Res. 404, 58–64.

Assaf, S.Y., Chung, S.H., 1984. Release of endogenous Zn^{2+} from brain tissue during activity. Nature 308, 734–736.

Ben-Ari, Y., Cherubini, E., 1991. Zinc and GABA in developing brain. Nature 353, 220.

Buhl, E.H., Otis, T.S., Mody, I., 1996. Zinc-induced collapse of augmented inhibition by GABA in a temporal lobe epilepsy model. Science 271, 369–373.

Celentano, J.J., Gyenes, M., Gibbs, T.T., Farb, D.H., 1991. Negative modulation of the gamma-aminobutyric acid response by extracellular zinc. Mol. Pharmacol. 40, 766–773.

Charton, G., Rovira, C., Ben-Ari, Y., Leviel, V., 1985. Spontaneous and evoked release of endogenous Zn^{2+} in the hippocampal mossy fiber zone of the rat in situ. Exp. Brain Res. 58, 202–205.

Choi, D.W., Koh, J.Y., 1998. Zinc and brain injury. Annu. Rev. Neurosci. 21, 347–375.

Choi, D.W., Yokoyama, M., Koh, J., 1988. Zinc neurotoxicity in cortical cell culture. Neuroscience 24, 67–79.

Christine, C.W., Choi, D.W., 1990. Effect of zinc on NMDA receptor-mediated channel currents in cortical neurons. J. Neurosci. 10, 108–116.

Chung, S.H., Johnson, M.S., 1983. Divalent transition-metal ions (Cu^{2+} and Zn^{2+}) in the brains of epileptogenic and normal mice. Brain Res. 280, 323–334.

Cole, T.B., Wenzel, H.J., Kafer, K.E., Schwartzkroin, P.A., Palmiter, R.D., 1999. Elimination of zinc from synaptic vesicles in the intact mouse brain by disruption of the *ZnT3* gene. Proc. Natl. Acad. Sci. U.S.A. 96, 1716–1721.

Coyle, J.T., Puttfarcken, P., 1993. Oxidative stress, glutamate, and neurodegenerative disorders. Science 262, 689–695.

Crawford, I.L., Connor, J.D., 1972. Zinc in maturing rat brain: hippocampal concentration and localization. J. Neurochem. 19, 1451–1458.

Danscher, G., 1981. Histochemical demonstration of heavy metals. A revised version of the sulphide silver method suitable for both light and electron microscopy. Histochemistry 71, 1–16.

Danscher, G., 1984. Dynamic changes in the stainability of rat hippocampal mossy fiber boutons after local injection of sodium sulphide, sodium selenite, and sodium diethyldithiocarbamate. In: Frederickson, C.J., Kasarskis, E.J., Howell, G.A. (Eds.), The Neurobiology of Zinc, vol. B. A.R. Liss, New York, pp. 177–191.

Draguhn, A., Verdorn, T.A., Ewert, M., Seeburg, P.H., Sakmann, B., 1990. Functional and molecular distinction between recombinant rat $GABA_A$ receptor subtypes by Zn^{2+}. Neuron 5, 781–788.

Eng, B.H., Guerinot, M.L., Eide, D., Saier, M.H. Jr, 1998. Sequence analyses and phylogenetic characterization of the ZIP family of metal ion transport proteins. J. Membrane Biol. 166, 1–7.

Epand, R.M., Stafford, A.R., Tyers, M., Nieboer, E., 1985. Mechanism of action of diabetogenic zinc-chelating agents. Mol. Pharmacol. 27, 366–374.

Erickson, J.C., Hollopeter, G., Thomas, S.A., Froelick, G.J., Palmiter, R.D., 1997. Disruption of the metallothionein-III gene in mice: analysis of brain zinc, behavior, and neuron vulnerability to metals, aging, and seizures. J. Neurosci. 17, 1271–1281.

Feller, D.J., Tso-Olivas, D.Y., Savage, D.D., 1991. Hippocampal mossy fiber zinc deficit in mice genetically selected for ethanol withdrawal seizure susceptibility. Brain Res. 545, 73–79.

Finney, D.J., 1971. Probit Analysis. Cambridge University Press, London.

Frederickson, C.J., Moncrieff, D.W., 1994. Zinc-containing neurons. Biol. Signals 3, 127–139.

Frederickson, C.J., Kasarskis, E.J., Ringo, D., Frederickson, R.E., 1987. A quinoline fluorescence method for visualizing and assaying the histochemically reactive zinc (bouton zinc) in the brain. J. Neurosci. Methods 20, 91–103.

Frederickson, C.J., Hernandez, M.D., McGinty, J.F., 1989. Translocation of zinc may contribute to seizure-induced death of neurons. Brain Res. 480, 317–321.

Frederickson, C.J., 1989. Neurobiology of zinc and zinc-containing neurons. Int. Rev. Neurobiol. 31, 145–238.

Freund, W.D., Reddig, S., 1994. AMPA/Zn^{2+}-induced neurotoxicity in rat primary cortical cultures: involvement of L-type calcium channels. Brain Res. 654, 257–264.

Fukahori, M., Itoh, M., 1990. Effects of dietary zinc status on seizure susceptibility and hippocampal zinc content in the El (epilepsy) mouse. Brain Res. 529, 16–22.

Fukahori, M., Itoh, M., Oomagari, K., Kawasaki, H., 1988. Zinc content in discrete hippocampal and amygdaloid areas of the epilepsy (El) mouse and normal mice. Brain Res. 455, 381–384.

Harrison, N.L., Gibbons, S.J., 1994. Zn^{2+}: an endogenous modulator of ligand- and voltage-gated ion channels. Neuropharmacology 33, 935–952.

Haug, F.M., 1967. Electron microscopical localization of the zinc in hippocampal mossy fibre synapses by a modified sulphide silver procedure. Histochemie 8, 355–368.

Homanics, G.E., DeLorey, T.M., Firestone, L.L., Quinlan, J.J., Handforth, A., Harrison, N.L., Krasowski, M.D., Rick, C.E.M., Korpi, E.R., Mäkela, R., Brilliant, M.H., Hagiwara, N., Ferguson, C., Snyder, K., Olsen, R.W., 1997. Mice devoid of γ-aminobutyrate type A receptor β3 subunit have epilepsy, cleft palate, and hypersensitive behavior. Proc. Natl. Acad. Sci. U.S.A. 94, 4143–4148.

Howell, G.A., Welch, M.G., Frederickson, C.J., 1984. Stimulation-induced uptake and release of zinc in hippocampal slices. Nature 308, 736–738.

Huang, L., Gitschier, J., 1997. A novel gene involved in zinc transport is deficient in the lethal milk mouse. Nat. Genet. 17, 292–297.

Itoh, M., Ebadi, M., 1982. The selective inhibition of hippocampal glutamic acid decarboxylase in zinc-induced epileptic seizures. Neurochem. Res. 7, 1287–1298.

Kantheti, P., Qiao, X., Diaz, M.E., Peden, A.A., Meyer, G.E., Carskadon, S.L., Kapfhamer, D., Sufalko, D., Robinson, M.S., Noebels, J.L., Burmeister, M., 1998. Mutation of the AP-3 delta subunit in the mocha mouse links endosomal cargo transport to storage deficiency in platelets, melanosomes, and neurotransmitter vesicles. Neuron 21, 111–122.

Kasarskis, E.J., Forrester, T.M., Slevin, J.T., 1987. Amygdalar kindling is associated with elevated zinc concentration in the cortex and hippocampus of rats. Epilepsy Res. 1, 227–233.

Kash, S.F., Johnson, R.S., Tecott, L.H., Noebels, J.L., Mayfield, R.D., Hanahan, D., Baekkeskov, S., 1997. Epilepsy in mice deficient in the 65-kDa isoform of glutamic acid decarboxylase. Proc. Natl. Acad. Sci. U.S.A. 9, 14060–14065.

Koh, J.Y., Choi, D.W., 1994. Zinc toxicity on cultured cortical neurons: involvement of *N*-methyl-D-aspartate receptors. Neuroscience 60, 1049–1057.

Koh, J.Y., Suh, S.W., Gwag, B.J., He, Y.Y., Hsu, C.Y., Choi, D.W., 1996. The role of zinc in selective neuronal death after transient global cerebral ischemia. Science 272, 1013–1016.

Lambert, N.A., Levitin, M., Harrison, N.L., 1992. Induction of giant depolarizing potentials by zinc in area CA1 of the rat hippocampus does not result from block of $GABA_B$ receptors. Neurosci. Lett. 135, 215–218.

Lees, G.J., Lehmann, A., Sandberg, M., Hamberger, A., 1990. The neurotoxicity of zinc in the rat hippocampus. Neurosci. Lett. 120, 155–158.

Legendre, P., Westbrook, G.L., 1991. Noncompetitive inhibition of gamma-aminobutyric $acid_A$ channels by Zn. Mol. Pharmacol. 39, 267–274.

Lerma, J., 1997. Kainate reveals its targets. Neuron 19, 1155–1158.

Mayer, M.L., Vyklicky, L. Jr, 1989. The action of zinc on synaptic transmission and neuronal excitability in cultures of mouse hippocampus. J. Physiol. (London) 415, 351–365.

Mitchell, C.L., Barnes, M.I., 1993. Proconvulsant action of diethyldithiocarbamate in stimulation of the perforant path. Neurotoxicol. Teratol. 15, 165–171.

Noebels, J.L., Sidman, R.-L., 1989. Persistent hypersynchronization of neocortical neurons in the mocha mutant of mouse. J. Neurogenet. 6, 53–56.

Palmiter, R.D., Findley, S., 1995. Cloning and functional characterization of a mammalian zinc transporter that confers resistance to zinc. EMBO J. 14, 639–649.

Palmiter, R.D., Cole, T.B., Findley, S.D., 1996a. ZnT-2, a mammalian protein that confers resistance to zinc by facilitating vesicular sequestration. EMBO J. 15, 1784–1791.

Palmiter, R.D., Cole, T.B., Quaife, C.J., Findley, S.D., 1996b. ZnT-3, a putative transporter of zinc into synaptic vesicles. Proc. Natl. Acad. Sci. U.S.A. 93, 14934–14939.

Pattison, S.E., Dunn, M.F., 1975. On the relationship of zinc ion to the structure and function of the 7S nerve growth factor protein. Biochemistry 14, 2733–2739.

Pei, Y.Q., Koyama, I., 1986. Features of seizures and behavioral changes induced by intrahippocampal injection of zinc sulfate in the rabbit: a new experimental model of epilepsy. Epilepsia 27, 183–188.

Pérez-Clausell, J., Danscher, G., 1985. Intravesicular location of zinc in rat telencephalic boutons. A histochemical study. Brain Res. 337, 91–98.

Peters, S., Koh, J., Choi, D.W., 1987. Zinc selectively blocks the action of *N*-methyl-D-aspartate on cortical neurons. Science 236, 589–593.

Prichard, J.W., Gallagher, B.B., Glaser, G.H., 1969. Experimental seizure-threshold testing with flurothyl. J. Pharmacol. Exp. Ther. 166, 170–178.

Racine, R.J., 1972. Modification of seizure activity by electrical stimulation. II. Motor seizure. Electroencephalogr. Clin. Neurophysiol. 32, 281–294.

Rassendren, F.A., Lory, P., Pin, J.P., Nargeot, J., 1990. Zinc has opposite effects on NMDA and non-NMDA receptors expressed in *Xenopus oocytes*. Neuron 4, 733–740.

Sensi, S.L., Canzoniero, L.M., Yu, S.P., Ying, H.S., Koh, J.Y., Kerchner, G.A., Choi, D.W., 1997. Measurement of intracellular free zinc in living cortical neurons: routes of entry. J. Neurosci. 17, 9554–9564.

Slomianka, L., 1992. Neurons of origin of zinc-containing pathways and the distribution of zinc-containing boutons in the hippocampal region of the rat. Neuroscience 48, 325–352.

Sloviter, R.S., 1985. A selective loss of hippocampal mossy fiber Timm stain accompanies granule cell seizure activity induced by perforant path stimulation. Brain Res. 330, 150–153.

Smart, T.G., Moss, S.J., Xie, X., Huganir, R.L., 1991. GABAA receptors are differentially sensitive to zinc: dependence on subunit composition. Br. J. Pharmacol. 103, 1837–1839.

Smart, T.G., Xie, X., Krishek, B.J., 1994. Modulation of inhibitory and excitatory amino acid receptor ion channels by zinc. Prog. Neurobiol. 42, 393–441.

Smart, S.L., Lopantsev, V., Zhang, C.L., Robbins, C.A., Wang, H., Chiu, S.Y., Schwartzkroin, P.A., Messing, A., Tempel, B.L., 1998. Deletion of the K(V)1.1 potassium channel causes epilepsy in mice. Neuron 4, 809–819.

Sperber, E.F., Moshe, S.L., 1988. Age-related differences in seizure susceptibility to flurothyl. Brain Res. 467, 295–297.

Spiridon, M., Kamm, D., Billups, B., Mobbs, P., Atwell, D., 1998. Modulation by zinc of the glutamate transporters in glial cells and cones isolated from the tiger salamander retina. J. Physiol. 506, 363–376.

Tonder, N., Johansen, F.F., Frederickson, C.J., Zimmer, J., Diemer, N.H., 1990. Possible role of zinc in the selective degeneration of dentate hilar neurons after cerebral ischemia in the adult rat. Neurosci. Lett. 109, 247–252.

Treiman, D.M., Walton, N.Y., Kendrick, C., 1990. A progressive sequence of electroencephalographic changes during generalized convulsive status epilepticus. Epilepsy Res. 5, 49–60.

Tsuda, M., Imaizumi, K., Katayama, T., Kitagawa, K., Wanaka, A., Tohyama, M., Takagi, T., 1997. Expression of zinc transporter gene, ZnT-1, is induced after transient forebrain ischemia in the gerbil. J. Neurosci. 17, 6678–6684.

Vandenberg, R.J., Mitrovic, A.D., Johnston, G.A.R., 1998. Molecular basis for differential inhibition of glutamate transporter subtypes by zinc ions. Mol. Pharmacol. 54, 189–196.

Weiss, J.H., Hartley, D.M., Koh, J.Y., Choi, D.W., 1993. AMPA receptor activation potentiates zinc neurotoxicity. Neuron 10, 43–49.

Wenzel, H.J., Cole, T.B., Born, D.E., Schwartzkroin, P.A., Palmiter, R.D., 1997. Ultrastructural localization of zinc transporter-3 (ZnT-3) to synaptic vesicle membranes within mossy fiber boutons in the hippocampus of mouse and monkey. Proc. Natl. Acad. Sci. U.S.A. 94, 12676–12681.

Westbrook, G.L., Mayer, M.L., 1987. Micromolar concentrations of Zn^{2+} antagonize NMDA and GABA responses of hippocampal neurons. Nature 328, 640–643.

Winegar, B.D., Lansman, J.B., 1990. Voltage dependent block by zinc of single calcium channels in mouse myotubes. J. Physiol. (London) 425, 563–578.

Xie, X.M., Smart, T.G., 1991. A physiological role for endogenous zinc in rat hippocampal synaptic neurotransmission. Nature 349, 521–524.

Yin, H.Z., Weiss, J.H., 1995. Zn^{2+} permeates Ca^{2+} permeable AMPA/kainate channels and triggers selective neural injury. Neuroreport 6, 2553–2556.

Yin, H.Z., Ha, D.H., Carriedo, S.G., Weiss, J.H., 1998. Kainate-stimulated Zn^{2+} uptake labels cortical neurons with Ca^{2+}-permeable AMPA/kainate channels. Brain Res. 781, 45–55.

Yokoyama, M., Koh, J., Choi, D.W., 1986. Brief exposure to zinc is toxic to cortical neurons. Neurosci. Lett. 71, 351–355.

Zimmer, J., Haug, F.M., 1978. Laminar differentiation of the hippocampus, fascia dentata and subiculum in developing rats, observed with the Timm sulphide silver method. J. Comp. Neurol. 179, 581–617.

VITA

Toby Brian Cole was born in Wichita, Kansas on April 20, 1967 and attended high school in Neosho, Missouri. As an undergraduate at Stanford University, Toby worked with Dr. Corey Goodman. He received a Bachelor of Science degree in Biology from Stanford University in 1989. Following graduation, he worked with Dr. Dennis Powers at Stanford University's Hopkins Marine Station, conducting research on transgenic fish and shellfish. In 1991, Toby moved to Seattle and worked with Dr. William Hammond at the University of Washington, in the Hematology Division of the School of Medicine. In December of 1992, he married Jean Fowler, who gave birth to his son, Henry in 1997. Toby began his graduate studies in the Department of Biochemistry at the University of Washington in September, 1994.